# Proton Transfer and Molecular Logic Functions of a Few Azole Derivatives

*A dissertation*
*as partial fulfilment for the degree of*
*Doctor of Philosophy in Chemistry*

*by*

**Saugata Sahu**
**11612212**


**Department of Chemistry**
**Indian Institute of Technology Guwahati**
**Guwahati 781039**
**Assam, India**

# Statement

The work contained in this thesis entitled "**Proton transfer and molecular logic functions of a few azole derivatives**" is the outcome of the research work carried out by me under the supervision of Dr. G. Krishnamoorthy, Department of Chemistry, Indian Institute of Technology Guwahati, India.

In the present thesis the general practice of the scientific observations are reported and whenever needed, the work on the findings of other investigators are described and thus due acknowledgements have been made.

2nd July, 2016

Saugata Sahu
Department of Chemistry,
IIT Guwahati
Guwahati, Assam, India-781039

**Dr. G. Krishnamoorthy**
*Head, Central Instruments Facility*
*& Professor of Chemistry*

**INDIAN INSTITUTE OF TECHNOLOGY GUWAHATI**
**Guwahati 781 039, Assam, India**
**Tel: +91 – 0361 – 258 2315 (W), 258 4315 (H)**
**Fax: +91 – 0361 – 2582349**
E-mail: gkrishna@iitg.ernet.in, gkrishna_2000@yahoo.com

## Certificate

It is certified that the work contained in thesis entitled "**Proton transfer and molecular logic functions of a few azole derivatives**" by Saugata Sahu is an authentic record of the results obtained from the research work carried out under my supervision in the Department of Chemistry, Indian Institute of Technology Guwahati, India.

02 July 2016
Guwahati

G. Krishnamoorthy

***Dedicated to my elder brother Jayanta***

# ~Acknowledgements~

*I would like to appreciate all the peoples around me who have assisted and guided me throughout my academic journey. Without their contributions this thesis would not have been a reality.*

*First of all, I would like to express my sincere gratitude to my supervisor Dr. G. Krishnamoorthy for his constant guidance and support throughout my research work. I am indebted to him for inspiring me towards scientific research. I have a deep respect for his meticulous analyses of the research problems and results. He provided me all the freedom to pursue my own research interests with a proper guidance. I find myself privileged to have worked under his guidance.*

*I would like to acknowledge my doctoral committee members Prof. Anumita Paul, Dr. Bhubaneswar Mandal and Dr. Ashwini Kumar Sharma for their valuable suggestions and encouragements which helped a lot to improve my thesis.*

*I take the opportunity to thank CSIR for the fellowship. I am thankful to IIT Guwahati, Department of Chemistry and Central Instruments Facilities for providing research facilities and instrumental facilities. I will always remain thankful to scientific staff of CIF and department of chemistry.*

*I would like to thank Prof. S. S. Ghosh, Dr. S. Dutta, Dr. L. M. Kundu, Dr. M. Qureshi and Prof. G. Das for teaching me during the period of course work. I thank our collaborator Dr. M. Sathiyendiran, University of Hyderabad and his student Dr. Bhaskaran Shankar. I like to thank Debashisda for helping me in theoretical calculations. I really thank my former and present labmates, Dr. Francis A.S. Chipem, Dr. A. Mishra, Dr. N. Dash, Dr. S. Chatrarjee, Ashimda, Santosh, Minati, Himadree, Ila for their endless help and co-operation. I specially thank Francisda, Ashimda and Santosh for their motivation, encouragements and constant support. Their company and moral supports in all my good and bad situations always inspired me lot. I would like to thank all my PhD batch mates for making a friendly environment. I specially thank Sourav, Debasish, Sujit, Harikrishna, Supriyoda, Sujoyda, Somnathda who always accompanied me in my successes and failures.*

*My parents and elder brother always motivate and encourage me throughout my life. I would be grateful to them forever. I am thankful to Anupriya for her support, inspiration and for always being with me. I am always grateful to the almighty god who is the creator of everything.*

*Sincerely*

*Saugata Sahu*

# ~Synopsis~

Proton transfer is one of the fundamental reactions in many chemical and biological processes. The proton transfer may be intramolecular or intermolecular process. The thesis deals with different proton transfer processes of a few azole derivatives both in the ground and excited states. At the end of the thesis, construction of molecular logic gate is shown by perturbing the emission characteristics of the fluorophores. The thesis is divided into seven chapters. Chapter one begins with a brief introduction regarding different proton transfer processes. The second chapter provides the detail of material, methods and instrumentation used throughout the thesis. Chapter 3 discusses about the intermolecular proton transfer of some azole dyes and the formation of anions in the ground and excited state. The fourth and fifth chapter describe inter- and intra-molecular proton transfer of a few azole molecules to produce different proton transfer species like different tautomer, anion, cation, zwitter ion etc. Construction of molecular switches, keypad lock devices, molecular subtractor with different azole derivatives and various external stimuli are shown in chapter six. The thesis is concluded with the summary of the present work and the scope of the future work. An overview of the thesis is described below in brief.

## Chapter 1: Introduction

A brief introduction regarding the proton transfer and molecular switches are presented in this chapter. In the first section, the ground state and the excited state intra- and inter-molecular proton transfer are described with a few examples. The factor affecting the proton transfer process are also discussed. In the second section, a general overview of different logic functions and the constructions of different logic gates using molecular characteristics are described. The motivation for the thesis is presented at the end of this chapter.

## Chapter 2: Materials, Methods and Instrumentation

The detail of the different materials and the synthesis procedures of new fluorophores used in the present work are described in this chapter. The sample preparation methods, data analysis and the detail of theoretical calculations are also elaborated. The details of a few instruments like UV visible spectrometer, steady state and time resolved fluorescence spectrometers are provided in this chapter.

## Chapter 3: Intermolecular Proton Transfer of 2-(2'-hydroxyphenyl) benzimidazole and its Nitrogenous Analogues in Polar Aprotic Medium.

This chapter is divided in two sections. In the first section, the inter molecular proton transfer between 2-(2'-hydroxyphenyl)benzimidazole (HPBI) in presence of external anions has been investigated. The effect of nitrogen substitution on the process is presented in the next section of this chapter.

### 3.1. Switching between *cis*- and *trans*- anions of 2-(2'-hydroxyphenyl)benzimidazole: a molecular rotation perturbed by chemical stabilization

In the ground state, 2-(2′-hydroxyphenyl)benzimidazole (HPBI, Chart 1) predominantly present as the *cis*-conformer due to existence of intramolecular hydrogen bond. The intermolecular proton transfer leads to the formation of anion. On contrary to the neutral form, the prototropic study of the molecule revealed that upon deprotonation it only exists as trans-anion in aqueous solution. It was interpreted that the trans-anion is more stable than the *cis*-anion due to the intramolecular hydrogen bond between the phenoxide ion and the 'NH' proton. No existence of dianion was reported in the excited state.

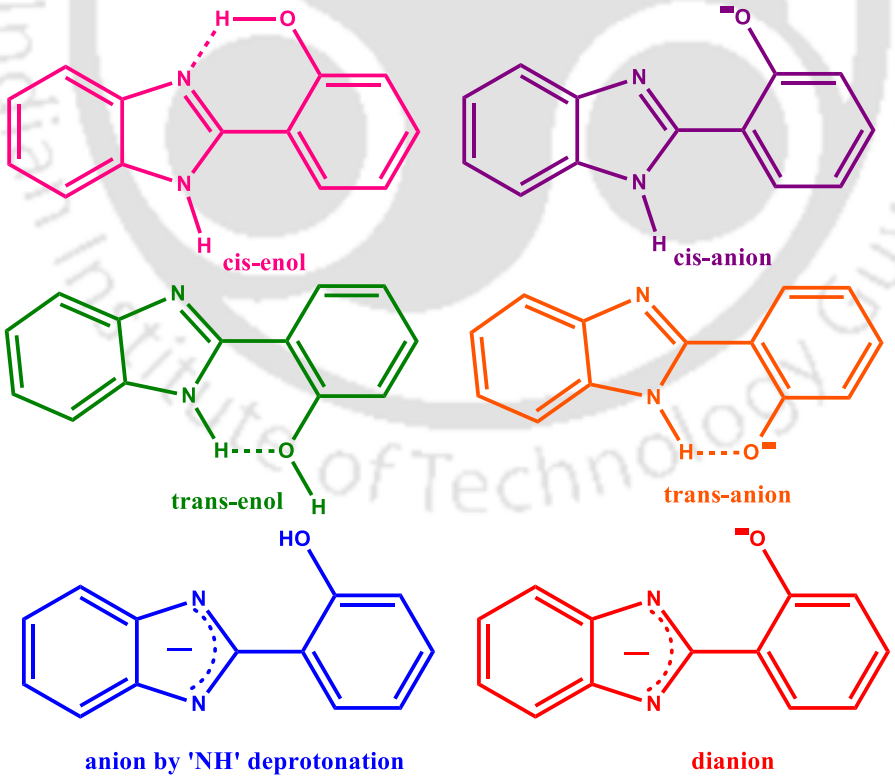


**Chart 1.** Conformers of 2-(2′-hydroxyphenyl)benzimidazole molecule (HPBI) and its different anions.

In the present work, it is shown that the *cis*-anion and dianion can be obtained upon proper stabilization in suitable environments. It is also demonstrated that the switching between *cis*- and *trans*- anion is possible by changing the environment (Scheme 1). Theoretical calculations have been performed to substantiate the existence of *cis*-anion and dianion. In converse to a literature report, it is also shown that not only in protic solvents but also in aprotic solvents the 'OH' group deprotonates before the 'NH' group to form monoanion.

The key factor in the existence of the *cis*- or *trans*- anion relies on the stabilization of the 'NH' proton. If the external anion forms strong hydrogen bond with the 'NH' proton of the initially formed *cis*-anion, the phenoxide unit does not rotate to produce the *trans*-anion. Otherwise, it forms the *trans*-anion. The solvation of the external anions in alkaline aqueous medium makes the anion inefficient to stabilize the 'NH' proton, and it results only the *trans*-anion.

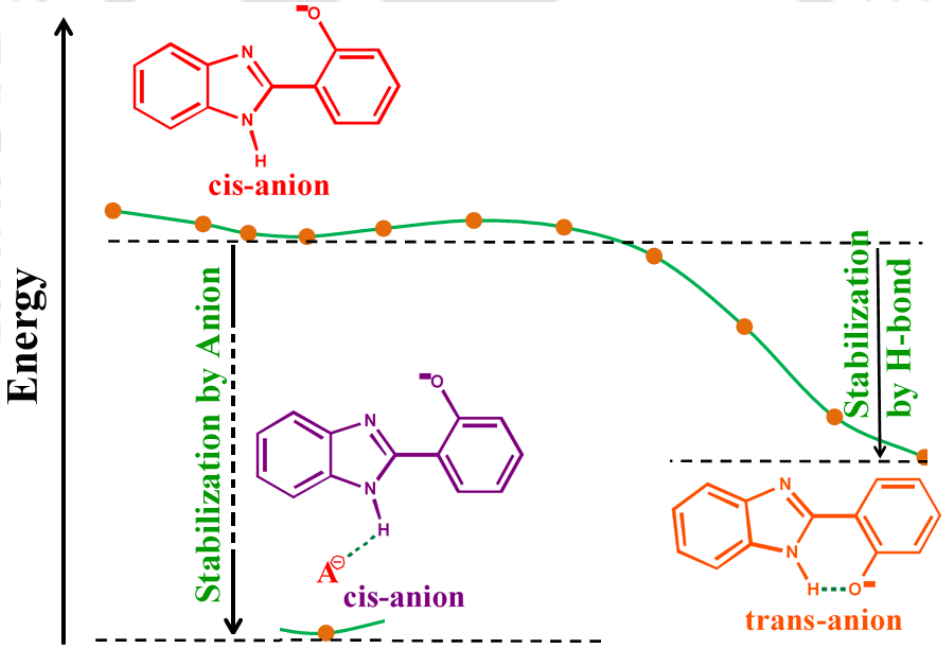


**Scheme 1.** Formation of stable *cis*-anion in ground state.

### 3.2. Effect of nitrogen substitution on anion sensitivity and deprotonation of HPBI

Nitrogen substitution on the benzene ring of the benzimidazole moiety of HPBI drastically changes the characteristics of the molecule. In this section, the effect of nitrogen substitution on the anion sensitivity and the deprotonation nature of the nitrogenous analogues of HPBI are described in polar aprotic medium. It is observed that the substitution of pyridyl nitrogen enhances the anion sensitivity (Chart 2).

However, despite the enhanced sensitivity of the nitrogenous analogues the deprotonation of these molecules in presence of strong anion is less favoured as compared to HPBI (Chart 2). This anomalous trend observed for the nitrogenous analogues is discussed and explained with the theoretical calculations and experimental findings. It is found that the sensitivity towards anion and the formation of anion depend also on the position of the pyridyl nitrogen.

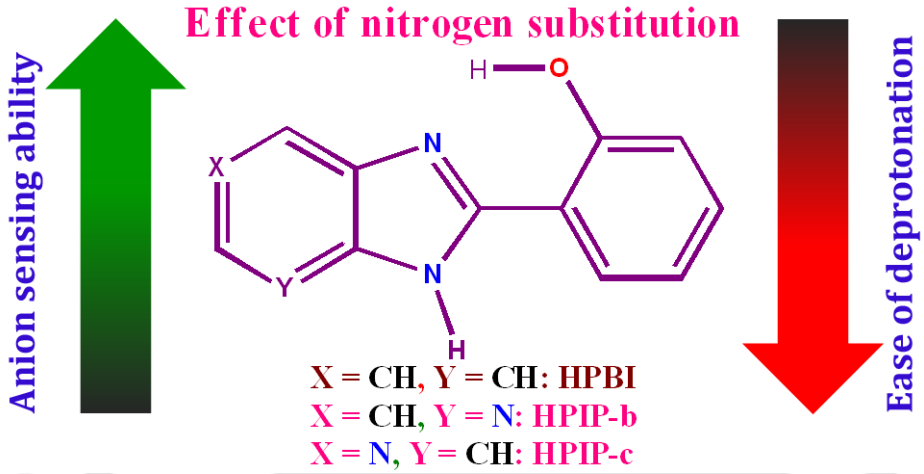


**Chart 2.** Effect of nitrogen substitution on anion sensitivity and ease of deprotonation of HPBI.

## Chapter 4: Intramolecular Proton Transfer and Conformer Specific Aggregation Induced Enhanced Emission of 1,4-bis(2-(2′-Hydroxyphenyl)benzimidazol-1-ylmethyl)-benzene

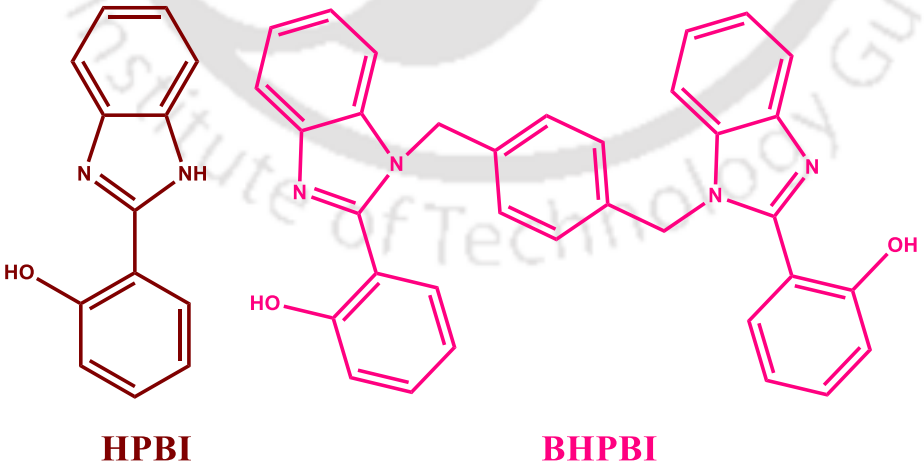


**Chart 3.** Comparison in molecular structure of HPBI and BHPBI.

In this chapter the photophysics and aggregation of a HPBI derivative, 1,4-bis(2-(2′-hydroxyphenyl)benzimidazol-1-ylmethyl)-benzene (BHPBI, Chart 3) are presented.

BHPBI possesses two HPBI units which are attached via a non-conjugating spacer at the azole nitrogen.

BHPBI also exists as two different conformers, twisted and quasi planar conformers. But the geometries of both the conformers are dissimilar from those of HPBI. The quasi planar conformer undergoes an excited state intra molecular proton transfer (ESIPT) to form a keto tautomer, which follows a torsional rotation to produce a new keto isomer. The twisted conformer does not undergo ESIPT, but experiences a photoinduced planarization. Controlling the molecular solubility and modifying the intra/inter molecular hydrogen bond, different aggregated structures have been obtained from different conformers (Scheme 2). Conformer specific enhanced emissions are observed from these aggregates. Upon varying the pH of the aqueous solution, the intermolecular proton transfer between BHPBI and the solvent takes place which results in different anionic and cationic species.

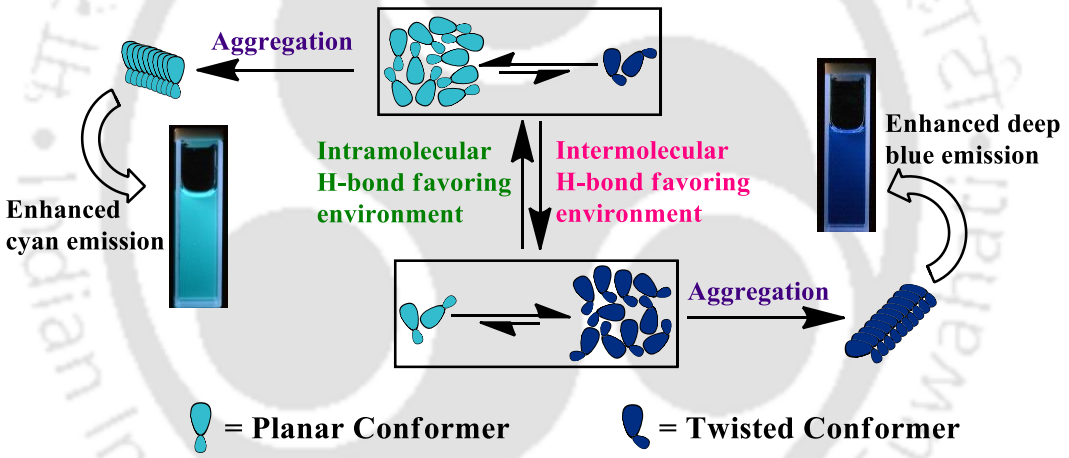


**Scheme 2.** different emission color from different aggregates of planar and twisted conformer of BHPBI.

**Chapter 5: Proton Transfer Induced Proton Transfer in (3,5-bis(2′-Hydroxyphenyl)-1H-1,2,4-triazole**

In this chapter, an azole derivative (3,5-bis(2′-hydroxyphenyl)-1H-1,2,4-triazole (Tz)) is investigated for possible consecutive proton transfers in the excited state. The studies reveal in solution Keto-I (K-I) and diketo (DK) are formed in the excited state (Chart 4). Whereas, in solid state Keto-II (K-II) is also formed by ESIPT (Chart 4). On the other hand, when one of the hydroxyl group is methylated (3-(2′-hydroxyphenyl)-5-(2′-methoxyphenyl)-1H-1,2,4-triazole (MTz))the molecule exhibits a single tautomer emission in solution. But, in solid state two tautomer emissions are observed. The probable reason for the difference in solution and solid phase are explained.

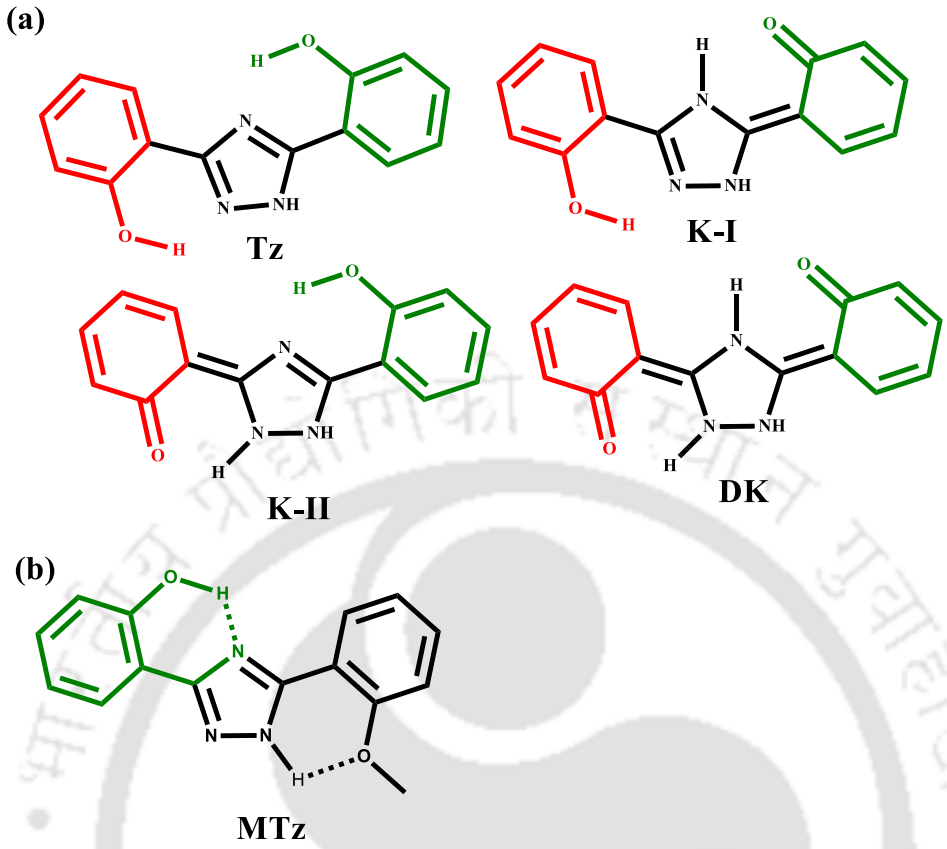


**Chart 4.** (a) Tz molecule and it different tautomers. (b) MTz molecule.

## Chapter 6: Construction of Molecular Logic Gates by Perturbing the Emission Characteristics s of a Few Azole Derivatives

Interactions of different analytes with molecules are used to develop molecular logic gates. In this chapter interaction with three different molecules are used to construct the logic gates and those are discussed in three different sections.

### 6.1. Specific site binding of metal ions in presence of anionic micelle and construction of molecular logic gates

2-(4′-N,N-dimethylaminophenyl)oxazolo[4,5-b]pyridine (DMAPOP) possesses three different metal ion binding sites. $Cu^{2+}$ and $Cd^{2+}$ ion bind to the molecule at more than one binding sites in non-aqueous solution. In the present work, the utility and effectiveness of surfactant in controlling the metal ion binding site on DMAPOP are demonstrated using sodium dodecyl sulfate (SDS), as surfactant. It is observed that both the metal ions bind at azole nitrogen which is in close proximity to the anionic head group of the micelle (Chart 4). The different interactions of $Cu^{2+}$, $Cd^{2+}$ in presence and in absence of micelle are exploited to develop different logic functions.

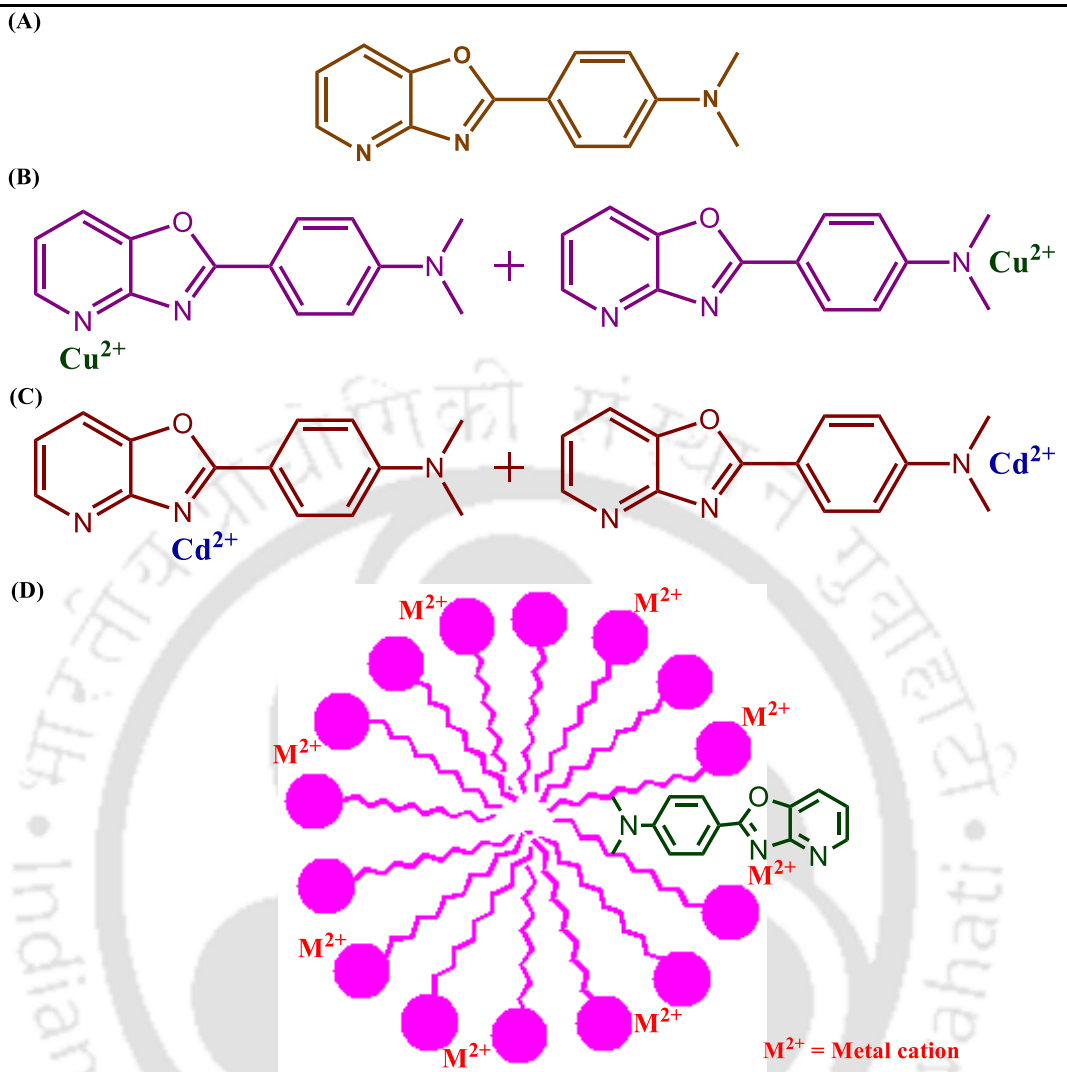


**Chart 4.** Molecular structure of DMAPO (A), and metal ions binding at different site of DMAPO in acetonitrile (B and C) and in micelle (D).

### 6.2. Construction of molecular logic gate and keypad lock system by inducing the inter molecular proton transfer

Upon photo-excitation, the acidity and the basicity of the functional group in an organic fluorophore are enhanced. Upon photoirradiation, BHPBI forms dication due to the proton transfer from the chloroform (solvent) to fluorophore. Consequently, the emission characteristics are altered. The interaction of the molecule with fluoride before and after the irradiations are different. This alters the emission characteristics of the molecule, and this is used to construct molecular INHIBT, IMPLICATION, TRANSFER, INVERTER logic gates. An input sequence dependent emission output is observed. This behavior is used to develop a highly secure molecular password entry system (Figure 1).

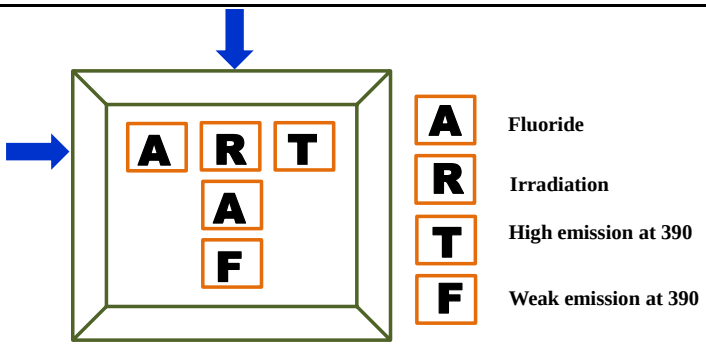


**Figure 1.** Molecular keypad lock system based on the sequence dependent output at 390 nm. The strong emission only appears for the input sequence ART.

### 6.3. Single fluorophore to address multiple logic gates

Now a day's research interest lies on the construction of multi-logic system on a single molecular platform. Rather than performing a simple logic operation, they are used to develop half adder, half subtracter, full adder, full subtractor to rationalize molecular arithmetic using a single molecule. In the present study, the interactions of $Fe^{3+}$ and fluoride with a biologically active molecule, 2-(4′-N,N-dimethylaminophenyl)imidazo [4,5-b]pyridine (DMAPIP-b) have been studied. The multiple complex forming ability of DMAPIP-b has been exploited to construct fluorescence On-Off based Boolean logic gates, molecular full-subtractor and molecular keypad lock system (Chart 5). Considering the switching phenomenon between different emission intensities ternary and infinite valued logic systems are implemented in molecular level. Fuzzy logic approach and neuro-computing are adapted in the construction of infinite valued logic system. A molecular attenuator and a molecular keypad lock device have also been proposed with the infinite valued fuzzy logic system.

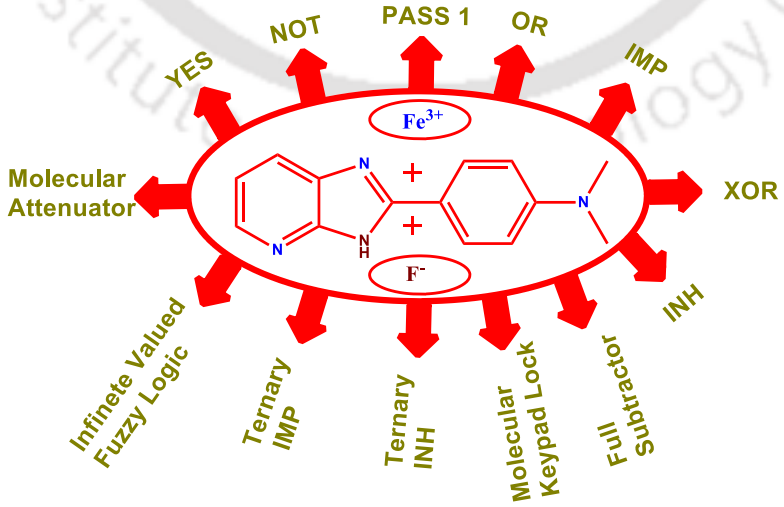


**Chart 5.** DMAPIP-b molecule to develop multiple logic system.

## Chapter 7: Summary and Scope for Future Work

The *cis*-anion of HPBI and its nitrogenous analogues can exist upon proper stabilization. The anion sensitivity of the nitrogen substituted molecule is more in comparison with HPBI. However, the extent of formation of anionic species is comparatively less for HPIP-b and HPIP-c. The BHPBI molecule equilibrates between a quasi-planar and twisted conformer in ground state. The equilibrium strongly depends on the solvent polarity and hydrogen bond factor. The quasi planar conformer undergoes ESIPT upon excitation. The separation of two conformers as nano-aggregates with enhanced emissions are achieved by controlling the molecular solubility, solvent polarity and hydrogen bond factor. The Tz molecule exhibit two consecutive ESIPT in the excited state. The construction of molecular logic gates with different azole systems are discussed in chapter six. The fuzzy interference system is developed to map the input data vector in scaler output. The scope for future work are described at the end of this chapter.

# Contents

# List of Abbreviations

| | |
|---|---|
| AIEE | Aggregation induced enhanced emission |
| ANFIS | Adapted neuro fuzzy interference system |
| AR | Analytical grade |
| BHPBI | 1,4-bis(2-(2′-hydroxyphenyl)benzimidazol-1-ylmethyl)-benzene |
| $CDCl_3$ | Deuterated chloroform |
| DMSO-$d_6$ | Deuterated dimethyl sulfoxide |
| DFT | Density Functional Theory |
| DMSO | Dimethyl- sulfoxide |
| DMF | Dimethyl-formamide |
| DMAPIP-b | 2-(4′-N,N-dimethylaminophenyl)imidazo[4,5-b]pyridine |
| DMAPOP | 2-(4′-N,N-dimethylaminophenyl)oxazolo[4,5-b]pyridine |
| DK | Diketo |
| ESIPT | Excited state intramolecular proton transfer |
| FESEM | Field emission scanning electrode microscope |
| FIS | Fuzzy interference system |
| HPBI | 2-(2’-hydroxyphenyl)benzimidazole |
| HPIP-b | 2-(2′-hydroxyphenyl)imidazo[4,5-b]pyridine |
| HPIP-c | 2-(2′-hydroxyphenyl)imidazo[4,5-c]pyridine |
| HPLC | High performance liquid chromatography |
| IEF-PCM | Integral equation formalism-polarizable continuum model |
| INH | INHIBIT |
| IMP | IMPLICATION |
| LED | Light emitting diode |
| MTz | 3-(2′-hydroxyphenyl)-5-(2′-methoxyphenyl)-1H-1,2,4-triazole |
| NaOH | Sodium hydroxide |
| NMR | Nuclear magnetic resonance |
| $pK_a$ | Acidity constant |
| $pK_a^*$ | Excited state acidity constant |
| SDS | Sodium dodecyl sulfate |
| TAC | Time to amplitude converter |
| TBAF | Tetrabutylammonium fluoride |
| TCSPC | Time correlated single photon counting |
| TDDFT | Time dependent density functional theory |
| THF | Tetrahydro furan |
| TRANES | Time resolved area normalized emission spectra |
| Tz | 3,5-bis(2′-hydroxyphenyl)-1H-1,2,4-triazole |
| UV | Ultraviolet |
| UV-Vis | Ultraviolet-Visible |
| XRD | X-Ray diffraction |
| $\lambda_{max}^{abs}$ | Absorbance maximum |
| $\lambda_{max}^{ex}$ | Excitation maximum |
| $\lambda_{max}^{em}$ | Emission maxima |
| $\lambda_{ex}$ | Excitation wavelength |
| $\lambda_{em}$ | Monitoring wavelength |
| $\phi$ | Quantum yield |
| $\tau$ | Excited state lifetime |

# List of Charts

# List of Figures

## Chapter 2



## Chapter 3

## Chapter 6

**Figure 6.3.12.** Schematic diagram of ANFIS using Sugeno's method to map the normalized intensity of DMAPIP-b with [$Fe^{3+}$] and [$F^-$].

# List of Schemes

# List of Tables

# Chapter 1

# Introduction

## 1.1. Proton transfer

Proton transfer is a fundamental and important phenomenon in several chemical and biological processes.[1-5] The release or uptake of a proton depends on the distribution of the electron charge density inside the molecule, and the determining factor is the acid dissociation constant ($pK_a$). A lower $pK_a$ indicates a higher dissociation ability of an acidic substance. It is well established that upon photoexcitation, the electron cloud is reoriented within the molecular orbital. Thus, the $pK_a$ of a molecule is also affected upon photoexcitation.

In 1931, Weber reported for the first time that the fluorescence of 1-naphthylamine-4-sulphonate is drastically changed with pH, whereas the changes are little for the absorption spectra.[6] It clearly indicates that the molecule is more sensitive towards the pH in the excited state as compared to the ground state. Based on the Weber's observation, in 1949, Förster provided a proper explanation for the phenomenon and initiated a new field, excited state inter molecular proton transfer.[7] He proposed a valuable method to find out the excited state acid dissociation constant ($pK_a^*$) from the ground state $pK_a$ value based on the absorption and emission maxima of an organic molecule. Later on, it was established that in excited state $RNH_2$, $R_2NH$, $RNH_3^+$, ROH become more acidic and RCOOH, $R_2COH^+$, $RSO_3H_2^+$, $RPO_3H_3^+$ become stronger base.[8] In general, the basicity of a proton accepting group and the acidity of a proton donating group of an aromatic molecule is enhanced upon photo excitation. For example, the enhanced basicity of the ring carbon in 1,3-dimethoxy benzene upon photo excitation leads to a regioselective deuterium exchange at C2 in 10% $D_2SO_4/D_2O$ medium (Scheme 1.1.1). The exchange process needs high acid concentration to go on thermally, and it results the deuterium exchange predominantly at C4 position. It was explained that the electron density at C4 is higher than C2 in HOMO of the molecule. But in LUMO it is just opposite. As a consequence, upon photo excitation, deuteration occurs at C2 position where the charge density is higher. Similarly, deprotonation may also take place in the excited state due to the proton transfer in a reverse manner i.e. from molecule to the solvent. Upon laser excitation of aqueous solution of 2-hydroxynapthene-6-sulfonate (pH 7) a rapid equilibrium reaches between the neutral and anionic form in the excited state ($k_f = 1.02 \times 10^9\ s^{-1}$, $k_b = 9 \times 10^{10}\ s^{-1}$, scheme 1.1.2). Within the excited state lifetime, the $H_3O^+$ concentration was found to increase by $> 10^{-4}$ times. It indicates the proton transfer to the water molecule due to the enhanced acidity of the hydroxyl group in the excited state.

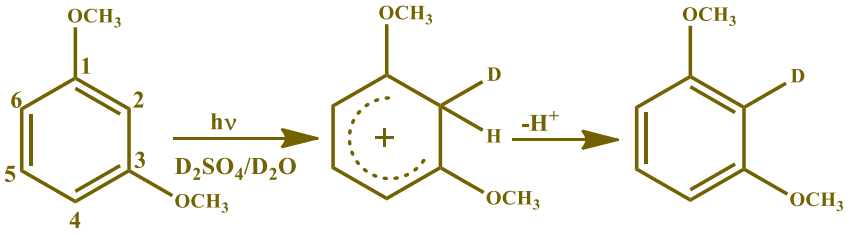


**Scheme 1.1.1.** Enhanced basicity of $sp^2$ carbon in the excited state.

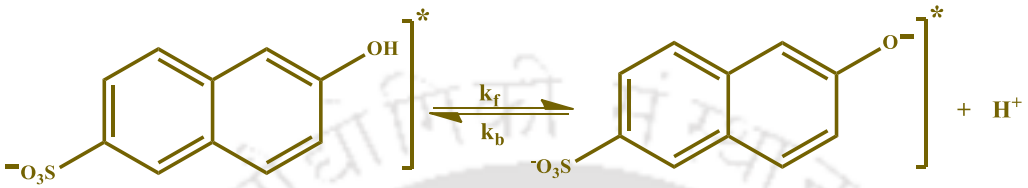


**Scheme 1.1.2**. Enhanced acidity of hydroxyl proton in the excited state.

### 1.1.1. Intermolecular proton transfer

There are several different donor-acceptor pairs, where intermolecular proton transfer can take place. It may be between two organic molecules of same kind, or two different kind of organic molecules, or a duos of solvent and organic molecule. 2-(2'-pyridyl)benzimidazole exhibits a normal Stokes' shifted strong emission in cyclohexane.[9] However in cyclohexane-ethanol binary solvent mixture, the emission intensity wanes with gradual increase of ethanol fraction.[9, 10] It was demonstrated that in the ground state, the 'NH' of the imidazole ring is bridged to the $sp^2$ nitrogen of the pyridyl ring through intermolecular hydrogen bond with ethanol molecule. In the excited state, the basicity of the pyridine nitrogen increases ($pK_a^* = 10$)[11, 12] and the proton transfer occurs from the imidazole nitrogen to the pyridine nitrogen. Due to the non-emissive nature of the tautomer species the fluorescence intensity gradually decreases (Scheme 1.1.3).

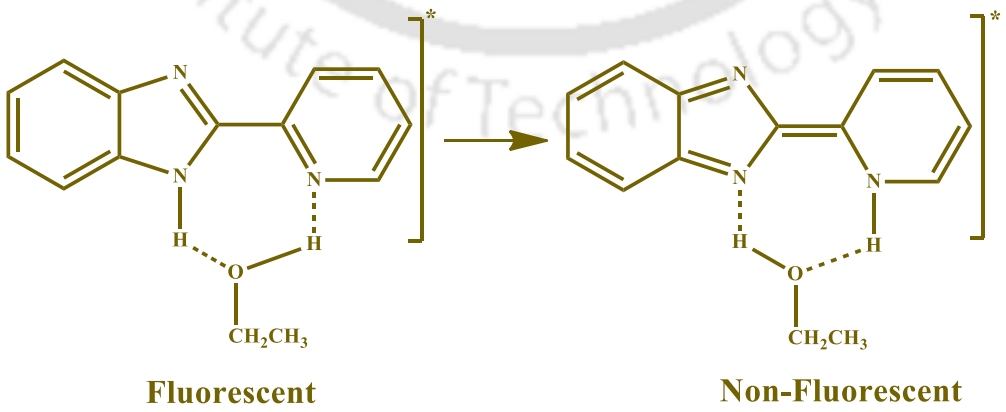


**Scheme 1.1.3.** Excited state intermolecular proton transfer of 2-(2'-pyridyl)benzimidazole in ethanol.

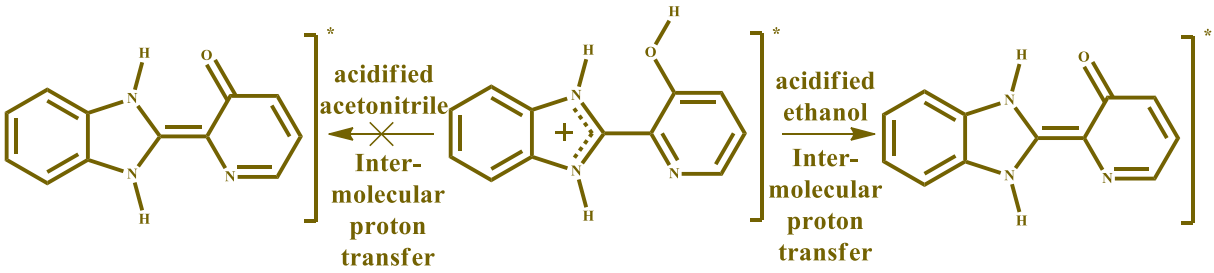


**Scheme 1.1.4.** Ability of excited state intermolecular proton transfer of protonated 2-(3′-Hydroxy-2′-pyridyl)benzimidazole in different solvents.

An excited state inter molecular proton transfer process may lead to the formation of neural tautomer via the deprotonation of a cationic species in the excited state in a proper solvent. 2-(3′-Hydroxy-2′-pyridyl)benzimidazole shows predominant cationic emission in acidified acetonitrile.[13] Whereas, in acidified ethanol solution, a highly Stokes' shifted tautomer emission is mainly observed along with a weak cationic emission.[13] The existence of different emitting states in different solvents depend on the proton accepting nature of the solvents from the excited cationic species (Scheme 1.1.4). The proton transfer in excited state is failed to occur in acidified acetonitrile due to the inability of the solvent to accept the proton.

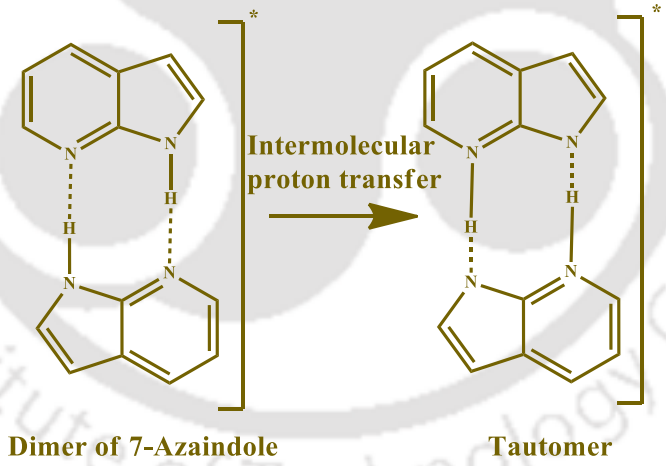


**Scheme 1.1.5.** Excited state intermolecular proton transfer of 7-azaindole dimer in 3-methylpentane.

7-Azaindole undergoes intermolecular proton transfer within two same molecular unit. The molecule produces a violet emission in etherial solution in ambient temperature. However, it emits a green emission in 3-methyl pentane.[14] The former emission comes from the normal species and the later one appears from a different tautomer. In 3-methyl pentane, the molecule exists in dimer form. Whereas, in ether solution, it exist in monomer form. A concerted double proton transfer in the excited state resulted in the low lying tautomer state from the dimer species (Scheme 1.1.5).[14-19]

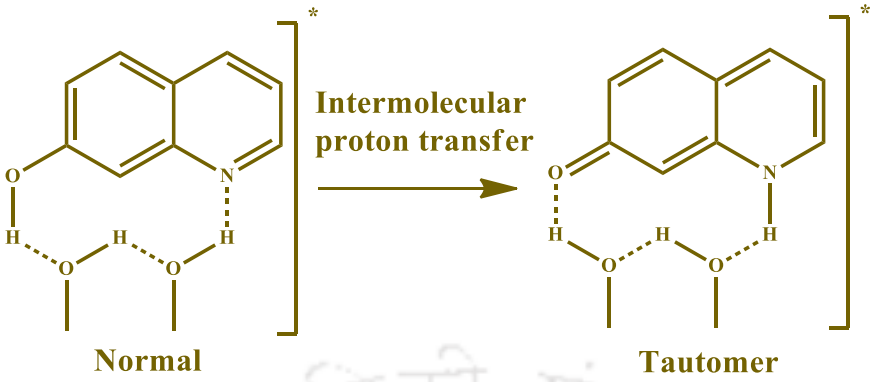


**Scheme 1.1.6.** Solvent assisted excited state intermolecular proton transfer in 7-hydroxyquinoline.

The proton transfer process can take place through multiple solvent molecules also. When the proton donating and proton accepting groups remain far from each other, more than one solvent molecules participate to transfer the proton from the donor group to the acceptor moiety in a relay method. 7-hydroxyquinoline does not exhibit any fluorescence in nonpolar hexane medium.[20] However, the addition of a little amount of methanol in solution switches on its emission nature.[20, 21] A high Stokes' shifted band is observed due to the excited state solvent assisted proton transfer. Two methanol molecules take part in the relay transfer (Scheme 1.1.6).[20-22]

### 1.1.2. Intramolecular proton transfer

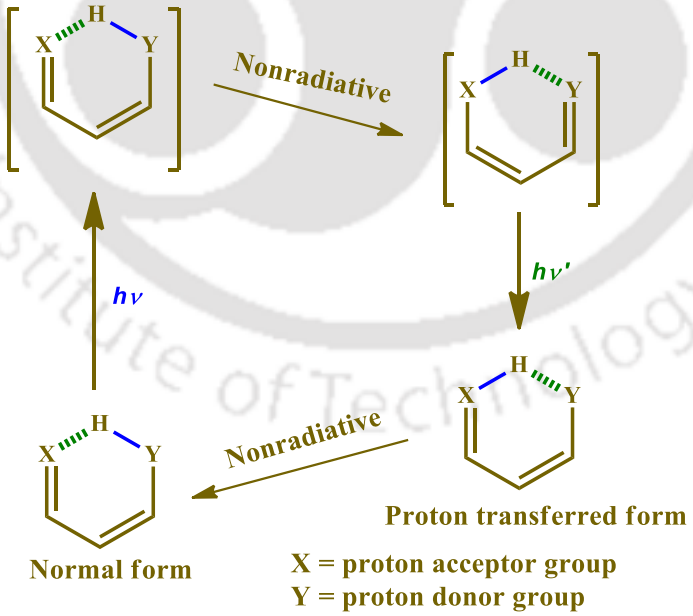


**Scheme 1.1.7.** A general scheme for excited state intramolecular proton transfer.

The proton transfer phenomena which are discussed so far are intermolecular processes. In cases where the donor and the acceptor are in close proximity and form

intramolecular hydrogen bond, the proton transfer can be an intramolecular process. In 1955, Weller first reported the intramolecular proton transfer process.[23] He found an unusually Stokes' shifted emission from methyl salicylate. When the alcoholic proton was methylated only a normal Stokes' shifted emission appeared as a mirror image of the absorption spectra. It was established that the longer wavelength emission appears from a tautomer which was generated due to the excited state intramolecular proton transfer (ESIPT). Upon photoexcitation, the acidity of the phenolic 'OH' and the basicity of the 'C=O' enhances, and the intramolecular proton transfer between the two groups generates the excited tautomeric species (Scheme 1.1.7). The methoxy derivative cannot undergo ESIPT due to the absence of the acidic 'OH' proton.

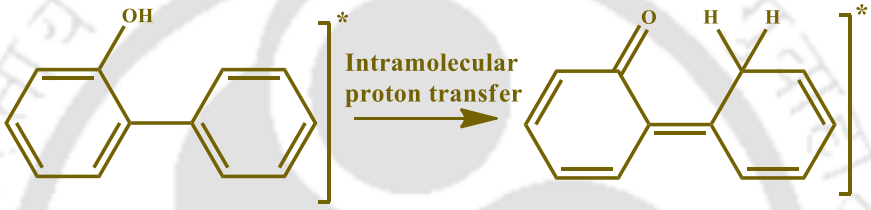


**Scheme 1.1.8.** Excited state intramolecular proton transfer from phenolic 'OH' to $sp^2$ carbon in 2-phenylphenol.

There are several acid base coupled neutral molecules which undergo ESIPT. The most common is an enol-keto system. The ground state enol-keto system produces a keto-enol tautomeric species due to photoinduce proton transfer in the excited state. ESIPT process also takes place in imine-amine system, imine-enol system and keto-amine system. Recently, the ESIPT was also observed between $sp^2$ ring carbon and phenolic 'OH' (Scheme 1.1.8).[24, 25]

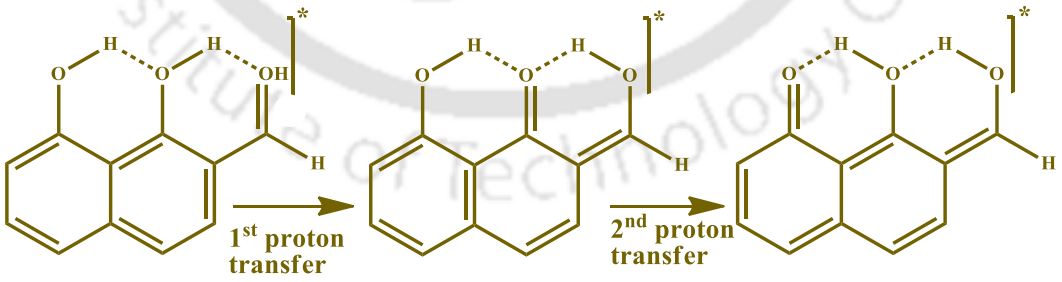


**Scheme 1.1.9.** Stepwise excited state intramolecular double proton transfer in 1,8-Dihydroxy-2-naphthaldehyde.

In most of the cases, the proton transfer process is executed within a single six-membered ring structure which is formed by a strong intramolecular hydrogen bond. A relay type proton transfer was described for 1,8-dihydroxy-2-naphthaldehyde where

the terminal donor and acceptor atoms are not directly connected through a hydrogen bond.[26] A step wise mechanism involving two six-membered rings was demonstrated, where dual proton transfer process occurs in a consecutive way (Scheme 1.1.9).

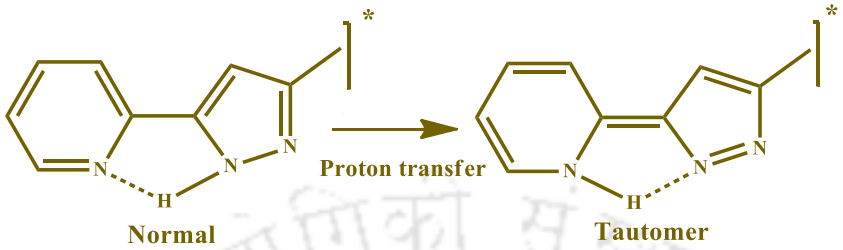


**Scheme 1.1.10.** Excited intramolecular proton transfer in five member H-bonded ring system.

ESIPT processes with five or less than five membered ring are rare. 2-pyridylpyrazole was reported to execute an ESIPT process inside a five-membered hydrogen bonded ring system (Scheme 1.1.10).[27] Rather than the tautomeric structure, ESIPT may also produce a Zwitterion structure. ESIPT from a pyrrole 'NH' to a tertiary amine, embedded inside a flexible alkyl chain was observed in boryl-substituted dithienylpyrrole skeleton.[28] The tertiary nitrogen acts as a proton acceptor in excited state, and the generated negative charge on pyrrole nitrogen is transduced to the terminal boryl group (Scheme 1.1.11).

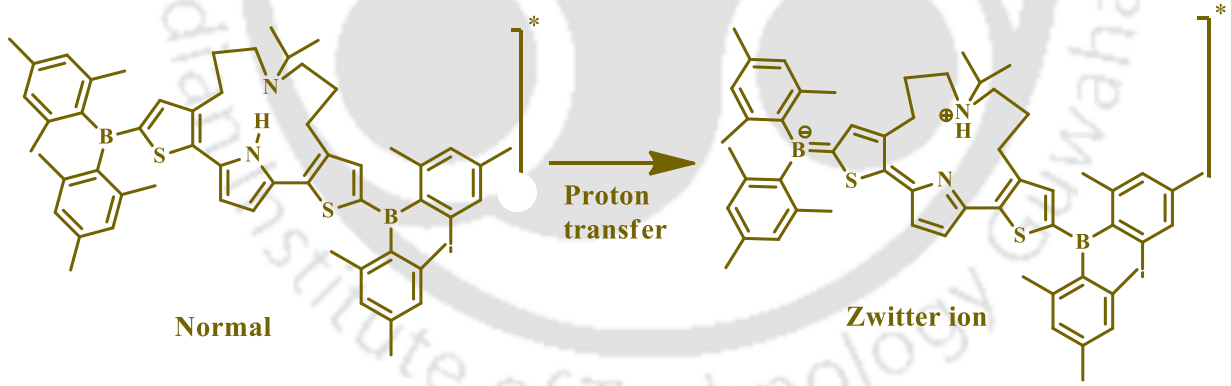


**Scheme 1.1.11.** Excited intramolecular proton transfer to generate a Zwitter ionic state.

### 1.1.3. Factors affecting the proton transfer

The proton transfer processes, either in the ground or in the excited state are basically acid-base phenomena. But, it depends not only on the strength of the proton donating and accepting moieties but also on several other factors such as molecular planarity, polarity and hydrogen bonding ability of the solvent, external analytes, intermolecular interaction etc. However, the effects are different for inter- and intra- molecular proton transfer processes.

### 1.1.3.1. Molecular structure

A conjugated planar system can stabilize a charge more efficiently than a non-planar system and facilitates the formation of the proton transferred species. For example, fluoradene molecule is more acidic than its analogous 9-phenylfluorene (Chart 1.1.1). This completely depends on the stabilization of the resultant negative charge in their conjugate bases. Upon deprotonation, 9-phenylfluorene generates a nonplanar conjugate base where the negative charge cannot be delocalized completely over the whole molecule. The $pK_a$ value of the molecule is also high, 18.[29] On the other hand, fluoradene is a fused cyclopentano ring system. It generates a planar deprotonated species where the negative charge easily delocalizes over the whole system. As a result, the conjugate base of fluoradene is very much stable and the $pK_a$ value is also lower (11) than 9-phenylfluorene.[30]

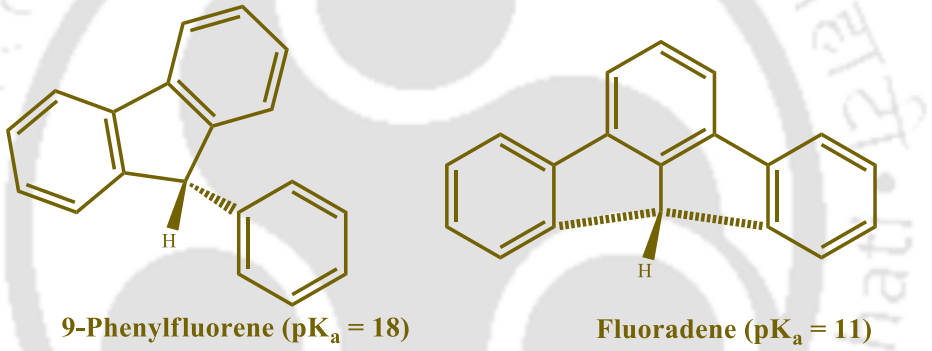


**Chart 1.1.1.** Molecular structure of 9-phenylfluorene and fluoradene.

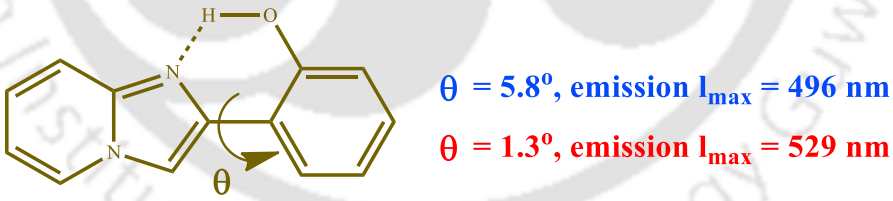


**Chart 1.1.2.** The polymorphs of 2-(2′-hydroxyphenyl)imidazo[1,2-a]pyridine exhibit different ESIPT emissions.

Molecular planarity plays a major role in intramolecular proton transfer process. The primary requisition is the formation of a cyclic hydrogen bonded ring structure connecting the donor and acceptor atoms. The planar structure is the ideal one. With increasing the dihedral angle between the donor and acceptor moiety the ease of the proton transfer is reduced. 2-(2′-hydroxyphenyl)imidazo[1,2-a]pyridine produces a Zwitterion upon ESIPT (Chart 1.1.2).[31] Two different crystal polymorphs of the molecule were obtained with different dihedral angles between the imidazopyridine ring and the

phenol moiety. The enol species with higher dihedral angle exhibits a blue-green emission. On the other hand, the more planar enol species shows a longer wavelength yellow emission.

The non-planarity of the cyclic hydrogen bond ring structure in the ground state may also cause to higher non-radiative decay rate of an ESIPT species. The radiationless decay process decreases the fluorescence lifetime of the ESIPT state. 1-methyl-2-(2′-hydroxyphenyl)-benzimidazole possesses a non-planar *cis*-enol structure in the ground state (Chart 1.1.3). The excited state lifetime of its keto tautomer is very low (one tenth) as compared to the keto tautomer of analogous 2-(2′-hydroxyphenyl)-benzimidazole (HPBI) molecule.[32] It was reported that the excited keto tautomer of HPBI and similar molecules undergo a torsional rotation induced nonradiative decay pathway. In 1-methyl-2-(2,-hydroxyphenyl)-benzimidazole the non-radiative path is much faster because of the non-planarity of the molecule.

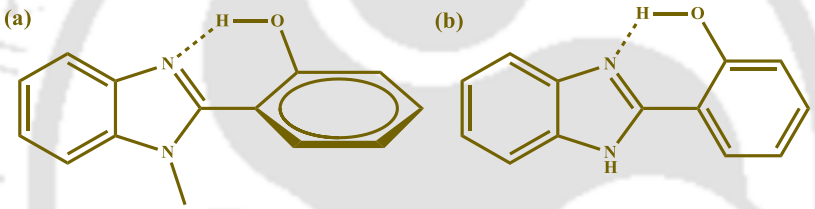


**Chart 1.1.3.** Molecular structure of (a) 1-methyl-2-(2′-hydroxyphenyl)-benzimidazole and (b) 2-(2′-hydroxyphenyl)-benzimidazole.

### 1.1.3.2. Solvent effect on proton transfer

Solvent molecules have an important role in inter- as well as intra- molecular proton transfer. The polarity, dielectric constant, hydrogen bonding ability are the key factors to stabilize or destabilize the proton transferred species. For example, the $pK_a$ difference of picric acid and p-nitro phenol is 6.4, 7.4 and 11.8 in water, methanol and dimethyl sulfoxide (DMSO), respectively (Chart 1.1.4).[33] Basically, the dissociation of an acid or base depends on the stabilization of the counter ions. The solvation of the counter parts provides an extra stabilization. The charged species obtained by the intermolecular proton transfer can be stabilized more in polar protic solvents due to the strong hydrogen bond interaction and dipole-dipole interaction. The whole equilibrium of a system may be shifted by differing the solvents factors. For instance, the equilibrium of fluorene and methoxide ion lies towards the neutral fluorene in methanol (Scheme 1.1.12). But in dimethyl sulphoxide (DMSO), it shifts toward the fluorene ion.[34] This is due to the hydrogen bond accepting ability of the anionic substances and the dipolar interaction with the solvent molecules. In methoxide anion, the negative charge is

localized. Methanol (solvent) can stabilize the anion by forming strong hydrogen bond. Whereas, due to the lack of hydrogen bond donating ability in DMSO, methoxide anions cannot be stabilized effectively. On the other hand, the negative charge in the fluorene anion can delocalize over the whole molecule, and the anion is significantly stabilized by the dipolar interaction in DMSO. A similar explanation also substantiates why deprotonation of organic acids by external anions like fluoride, acetate, phosphate is more efficient in polar aprotic solvent but not in polar protic solvents. Some molecules exist in a neutral-anion equilibrium in DMSO and dimethylformamide (DMF), though in polar protic solvents only the neutral species does exist.[35]

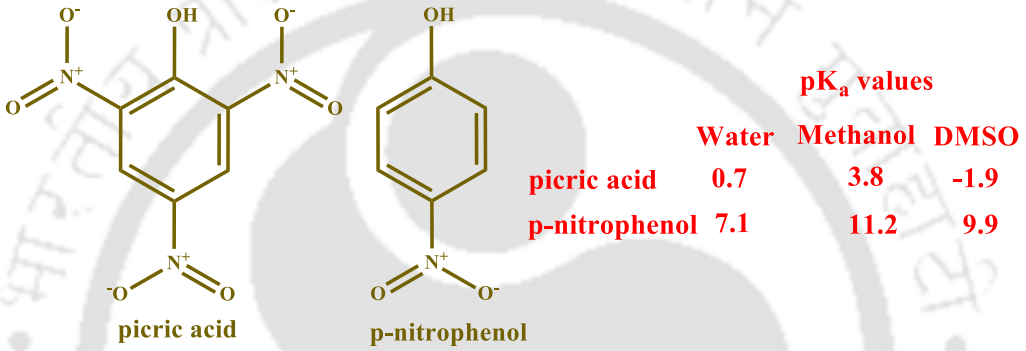


**Chart 1.1.4.** Solvent dependent pK$_a$ values of picric acid and p-nitrophenol.

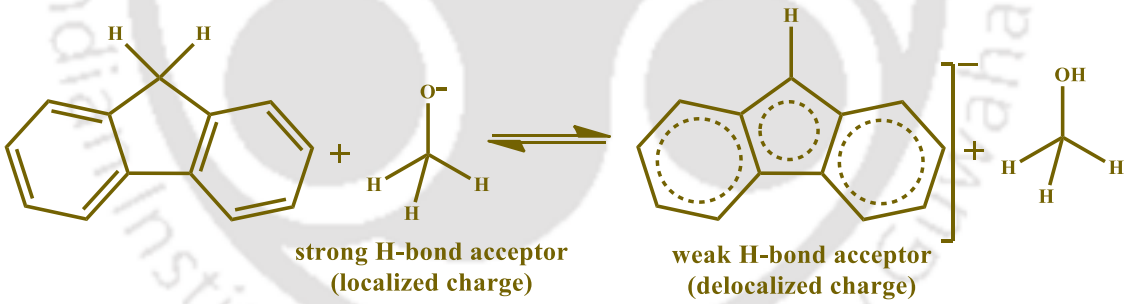


**Scheme 1.1.12.** Intermolecular proton transfer between fluorene and methoxide anion.

The intramolecular proton transfer is also affected to a great extent by the nature of solvents. An intramolecular hydrogen bond between the acidic proton and the receptor assists the molecule to build the planar cyclic ring structure. In polar protic solvent the intramolecular hydrogen bond is weakened and replaced by the intermolecular hydrogen bond of the solvent molecules. Upon photoexcitation the hydrogen bond complex cannot undergo intramolecular proton transfer and produces only normal emission. In cyclohexane, methyl salicylate produces a single emission at visible range due to the ESIPT. However, in polar protic solvent it produces the tautomer emission along with a normal emission. Eventually, the strong intermolecular hydrogen bond

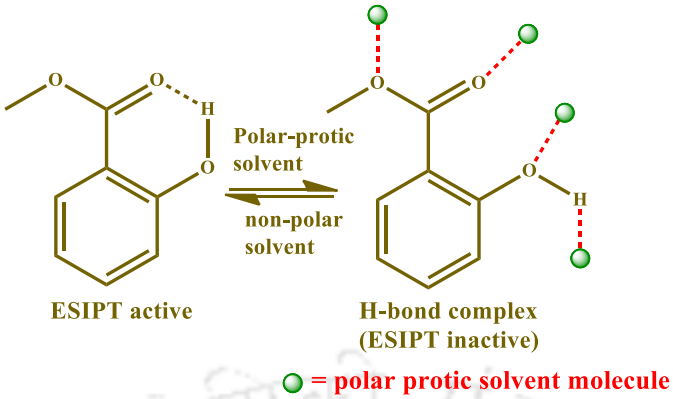


**Scheme 1.1.13.** Formation of non ESIPT H-bond complex of methyl salicylate in polar protic solvent.

with solvents prevents the molecule to take part in ESIPT (Scheme 1.1.13).[36] It is also possible for a molecule to have another ground state conformer where the proton donor and acceptor groups remain far from each other without any interlinking hydrogen bond. The later conformer must be ESIPT inactive and would exhibit only normal emission. The intensity ratio of normal and tautomer emission directly depends on the ground state equilibrium of the two conformers. In nonpolar solvent the conformer with intramolecular hydrogen bond predominates. Whereas, with increasing solvent's hydrogen bond ability the population of other conformer increases. For example, in dry nonpolar solvents, 4,5-dimethyl-2-(2'-hydroxyphenyl)imidazole exhibits a single blue-green tautomer emission from its *cis*- conformer. In polar protic solvent the population of trans-conformer enhances and the intensity of the normal emission also enhances (Scheme 1.1.14).[37] The solvent polarity also alters the relative population of the conformers. The conformer with higher dipole moment is more stable in polar solvents due to the high dielectric constant of the solvent. Therefore, the population of *trans*-enol increases with the increase of solvent polarity.[37]

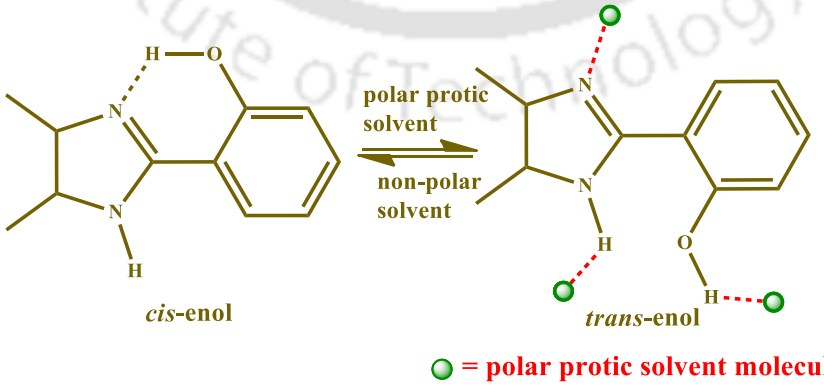


**Scheme 1.1.14.** Equilibrium between *cis*- and *trans*- enol conformer of 4,5-dimethyl-2-(2'-hydroxyphenyl)imidazole.

### 1.1.3.3. Effect of external analytes

External analytes can catalyze or inhibit the proton transfer process. It may be a solvent molecule or a base moiety or an acidic substance which may have a strong or weak interaction with the molecule to undulate the proton transfer process. The intermolecular proton transfer in 2-pyridinamine is observed in isooctane/acetic acid mixture.[38] The acetic acid forms an eight membered hydrogen bonded ring structure with the molecule (Scheme 1.1.15). An excited state double proton exchange results a high Stoke's shifted emission from 2-pyridinimine tautomer. In isooctane/ethanol solvent mixture the molecule forms a similar six member hydrogen bonded structure with ethanol. But this complex does not undergo excited state double proton transfer, and it exhibits a little red shifted normal emission. Here, the higher proton donating ability of acetic acid enables the stepwise double proton transfer process by generating an ion-pair intermediate in the excited state.[39, 40]

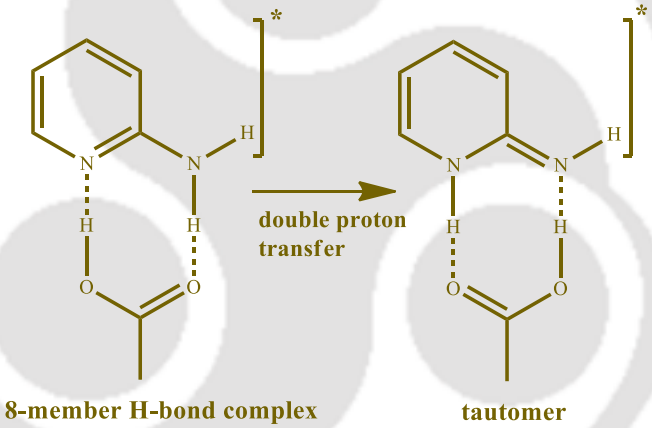


**Scheme 1.1.15.** Excited state double proton transfer of 2-pyridinimine in presence of acetic acid.

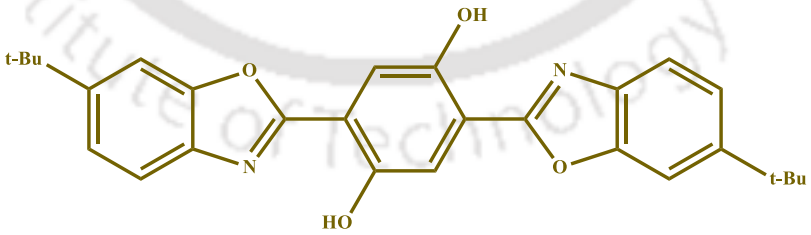


**Chart 1.1.5.** Enhanced ESIPT in presence of anion.

The proton transfer may also be provoked in presence of an external anion. A benzoxazole derivative (Chart 1.1.5) exhibits the proton transfer emission at 607 nm in THF/Ethanol (50:1) medium.[41] The quantum yield (ϕ) of the tautomer emission is very

low, 0.02. However, in presence of fluoride the quantum efficiency of the tautomer emission enhances to 0.40. The intermolecular proton transfer from one of the two hydroxyl group to the external anion generates the anion, and it significantly affects the radiative decay of the tautomer.

An external ion can also inhibit the proton transfer process. The intramolecular proton transfer process is strongly affected by presence of external ions. The electronegative proton donor may form chelate complex with the metal ion. On the other hand, the proton donor part can easily donate the proton to some external stronger base rather than the internal acceptor. In all of the cases, the intramolecular proton transfer is averted.[42-46] Rather than direct deprotonation of the particular acidic proton, the external anion may abstract some other more acidic proton or it can form an anionic complex with the molecule. 2-(2'-phenyl-ureaphenyl)-benzoxazole possesses two acidic protons, $H_a$ and $H_b$ (Scheme 1.1.16). The ESIPT of the molecule is prevented in presence of acetate and fluoride anions. However, both the anions follow different inhibiting mechanisms. The acetate anion forms hydrogen bond complex with the urea unit and prevents the excited state proton transfer process.[47] Whereas, the fluoride anion which is a stronger base than acetate, deprotonates the $H_a$ proton and makes the proton transfer energy barrier too high for the proton transfer.[48]

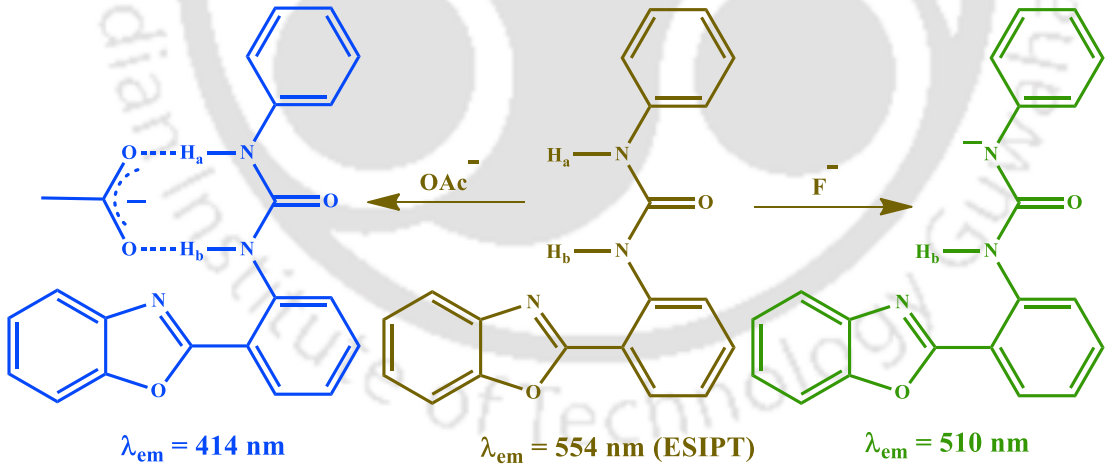


**Scheme 1.1.16.** Different ESIPT inhibition processes of 2-(2'-phenyl-ureaphenyl)-benzoxazole in presence of acetate and fluoride anion.

### 1.1.3.4. Substituent effect on proton transfer

Substitution of electron withdrawing group enhances the acidity of a proton donor by increasing the stability of the conjugate base. On the other hand, an electron donating group makes the conjugate base more unstable. As a consequence, the acidity of the molecule decreases in presence of electron donating group. For example, 2-(2′-

hydroxyphenyl)imidazo[4,5-b]pyridine (HPIP-b) and 2-(2′-hydroxyphenyl)imidazo [4,5-c]pyridine (HPIP-c), the nitrogen substituted analogues of HPBI have lower neutral-anion $pK_a$ value than HPBI in aqueous medium. The enhanced acidity in nitrogenous analogues is observed due to the strong electron withdrawing nature of pyridylimidazole moiety than the benzimidazole unit (Chart 1.1.6).

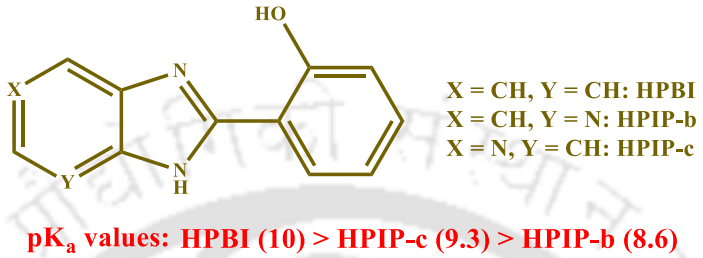


**Chart 1.1.6.** Neutral-anion $pK_a$ value of HPBI and its nitrogenous analogues in aqueous medium.

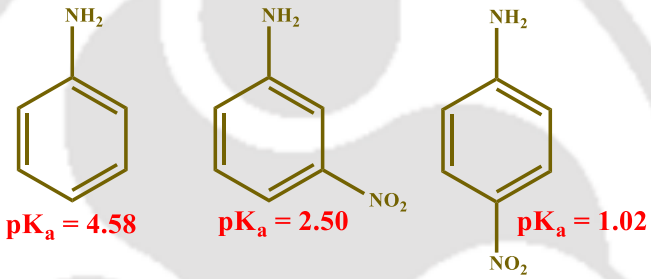


**Chart 1.1.7.** $pK_a$ values (of conjugate base) of substituted anilines.

The substituent effect is reversed for a proton acceptor. The basicity of the acceptor decreases by electron withdrawing substituents and increases by electron donating substituents. The lone pair electron of amine in aniline behaves as a proton acceptor. The $pK_a$ of the conjugate base of aniline is 4.58 (Chart 1.1.7).[49] For meta-nitro and para-nitro substituted derivatives the $pK_a$ decreases to 2.50 and 1.02, respectively (Chart 1.1.7).[49] The significant difference in the $pK_a$ values entirely depends on the ability of delocalization of the lone pair over the whole molecule. In meta-nitro aniline the inductive effect of the nitro group enhances the delocalization as compared to aniline. When it is substituted at para position, the inductive effect as well as resonance effect delocalize the lone pair. Thus, the intermolecular proton transfer process depends not only on the substituents but also on the position of substitution.

The substitution not only affects the proton transfer process but also alters the emission characteristics. Depending on the position of donor and acceptor, two different situations may arise. Some proton transfer molecules like o-hydroxybenzaldehyde possesses the donor and acceptor group attached to the same aromatic ring. The stability

of the proton transferred species of o-hydroxybenzaldehyde derivatives in its first excited state depends on the electron donating and withdrawing nature of the substituents (Chart 1.1.8).[50] An electron withdrawing group at C0 or C5 stabilizes the excited state more as compare to the ground state. Accordingly, the energy gap (ΔE) decreases, and a red shift appears in the emission spectra. The fluorescence quantum yield also decreases. On the other hand, an electron donating substituent at C0 or C5 results in the reverse stability and generates a hypsochromic shift as compared to the unsubstituted molecule.

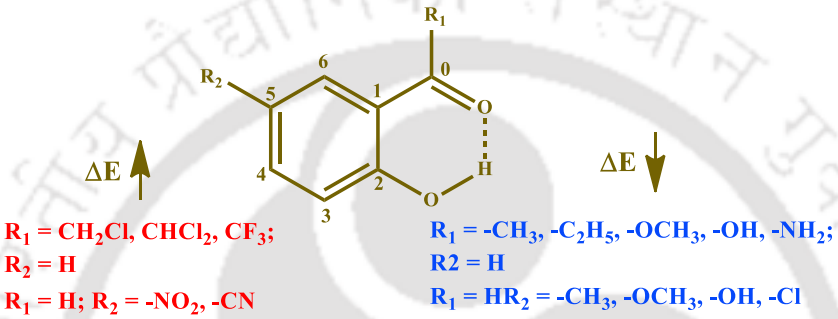


**Chart 1.1.8.** Effect of substitution on the emission energy (ΔE) of intramolecular proton transferred species.

In a few molecules, the donor and acceptor groups are situated in different aromatic rings which are interconnected with a spacer unit or a single bond. Upon photo excitation, 2-(2′-hydroxyphenyl)imidazo[1,2-a]pyridine undergoes proton transfer and produces a Zwitterion.[51] The pyridylimidazole group and the phenol group act separately as proton acceptor and donor, respectively. Substitution of electron donor at C5′ position causes a red shift in the emission spectrum of the Zwitter ion. Whereas, the substitution of electron acceptor group at C5′ produces a blue shift. On the other hand, the insertion of such groups at C6 position shows a reverse effect. The shift in emission spectrum depends on the stabilization of HOMO and LUMO of the Zwitterion after the substitution. The theoretical calculation reveals that the HOMO and the LUMO localize on the phenyl and imidazo[1,2-a]pyridine ring, respectively (Chart 1.1.9). An electron withdrawing group at C5′ makes the HOMO more stable than that of the LUMO. This increases the energy separation between the orbitals. Substitution of an electron donor at C5′ raises the HOMO more relative to the LUMO, which decreases the energy gap. On the other hand the introduction of an electron acceptor at C6 destabilizes the LUMO more as compare to the HOMO. It produces a hypsochromic shift in the emission spectrum. An opposite situation arises upon substitution of electron donor at C6 position.

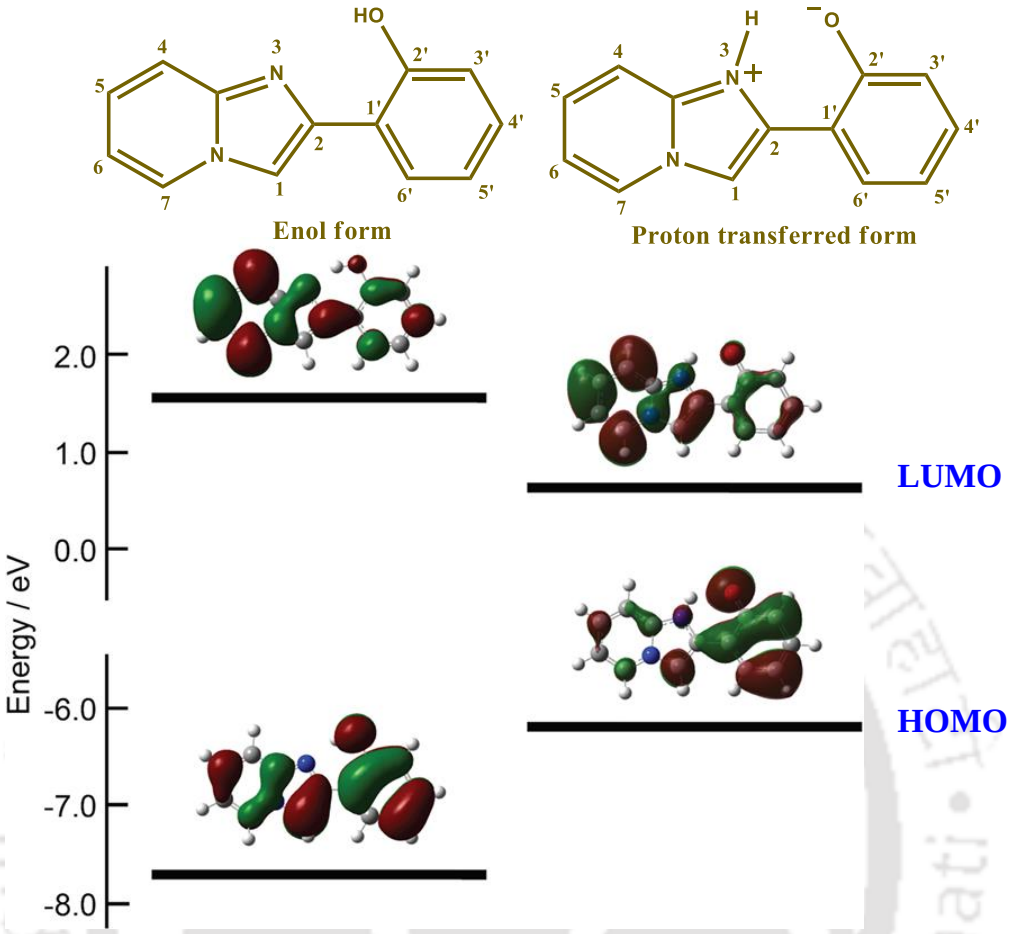


**Chart 1.1.9.** Molecular orbital of enol and proton transferred form of 2-(2′-hydroxyphenyl)imidazo[1,2-a]pyridine.

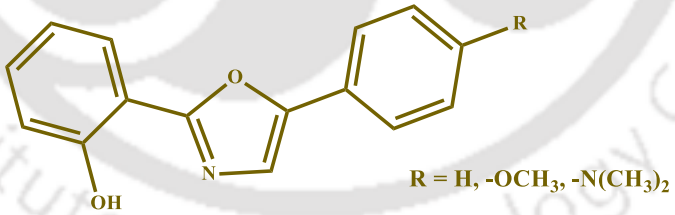


**Chart 1.1.10.** 2-(2′-hydroxyphenyl)-5-(4′-methoxyphenyl)oxazole and its derivatives.

The redistribution of charge with different substituents may also have a strong influence on the ESIPT reaction rate. Upon photoexcitation 2-(2′-hydroxyphenyl)-5-phenyloxazole (Chart 1.1.10) may produce a dual emission, from normal enol and proton transferred tautomer.[52] The tautomer emission is 210 times higher than that of the normal emission in octane medium. The proton transfer significantly diminishes in 2-(2′-hydroxyphenyl)-5(4′-methoxyphenyl)oxazole. The tautomer to normal emission intensity ratio reduces to 5. Only normal emission is observed upon substitution of stronger electron donating N,N-dimethyl amino group. The results elucidate that the

charge flow from donor 2′-hydroxyphenyl to the acceptor heterocycle is inhibited in presence of a strong electron donor on the other phenyl ring, and it prevents the ESIPT.

### 1.1.3.5. Effect of molecular aggregation

The torsional rotations and internal vibrations increase the non-radiative decay of the tautomer and decrease the fluorescence intensity. An aggregated structure can restrict this motions and reduces the non-radiative decay processes.[53-56] N-(4-(benzo[d]thiazol-2-yl)-3-hydroxyphenyl)-benzamide (Chart 1.1.11) an ESIPT exhibiting molecule shows 15 times enhanced emission in water as compared to cyclohexane medium.[57] It was reported that due to the J-aggregation and restriction of intermolecular rotation the molecule produces the enhanced emission in water.

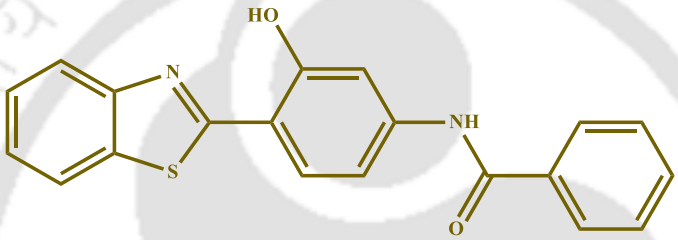


**Chart 1.1.11.** Molecular structure of N-(4-(benzo[d]thiazol-2-yl)-3-hydroxyphenyl)benzamide.

## 1.2. Molecular logic gates

Logic gates are the elementary building blocks of modern digital circuits. In every aspect of information processing, data storing or transmission of signal the modern digital circuits entirely depend on the logic gates. All of these processes depend on the encoding of a series of zeros and ones. 1 indicates a higher potential value and 0 denotes a lower potential value.

### 1.2.1. Classification of logic gates

**Table 1.2.1.** Single input logic gates.

| Input | 0 | 1 |
|---|---|---|
| Output PASS 0 | 0 | 0 |
| Output NOT | 1 | 0 |
| Output YES | 0 | 1 |
| Output PASS 1 | 1 | 1 |

Based on the number of inputs, logic gate can be classified as single input and double input system. There are only four different types of single input logic functions, named

as PASS 0, NOT, YES and PASS 1 (Table 1.2.1). A PASS 0 logic gate generates only low output irrespective of input values. A NOT gate inverses the input values in output. This logic gate is also called INVERTER logic gate. A YES gate maintains an identical input value in output. That's why, it is also called an IDENTICAL logic gate. Similar to PASS 0 gate, PASS 1 also behaves irrespective of inputs but it always produces a high output. For an input variable A, the outputs of PASS 0, NOT, YES and PASS 1 logic gates can be expressed as 0, $\bar{A}$, A and 1. $\bar{A}$ denotes the opposite value of A.

**Table 1.2.2.** Double input logic gates.

| **Input 1** | **0** | **1** | **0** | **1** |
|---|---|---|---|---|
| **Input 2** | **0** | **0** | **1** | **1** |
| Output PASS 0 | 0 | 0 | 0 | 0 |
| Output PASS 1 | 1 | 1 | 1 | 1 |
| Output OR | 0 | 1 | 1 | 1 |
| Output AND | 0 | 0 | 0 | 1 |
| Output XOR | 0 | 1 | 1 | 0 |
| Output NOR | 1 | 0 | 0 | 0 |
| Output NAND | 1 | 1 | 1 | 0 |
| Output XNOR | 1 | 0 | 0 | 1 |
| Output TRANSFER (input 1) | 0 | 1 | 0 | 1 |
| Output TRANSFER (input 2) | 0 | 0 | 1 | 1 |
| Output NOT-TRANSFER (input 1) | 1 | 0 | 1 | 0 |
| Output NOT-TRANSFER (input 2) | 1 | 1 | 0 | 0 |
| Output INHIBIT (input 1) | 0 | 0 | 1 | 0 |
| Output INHIBIT (input 2) | 0 | 1 | 0 | 0 |
| Output IMPLICATION (input 1) | 1 | 1 | 0 | 1 |
| Output IMPLICATION (input 2) | 1 | 0 | 1 | 1 |

On the other hand, sixteen different types of input-output combinations are possible for the double input system (Table 1.2.2). In the beginning of the Table 1.2.2, input independent PASS 0 and PASS 1 logic gates are shown. Next six logic gates are called commutative logic gates. The output patterns of those logic gates do not change with swapping of the inputs. However, last eight logic gates behave in a non-commutative manner. An OR gate computes a high output if any of the input values is high. An Exclusive-OR (XOR) logic gate functions in a similar manner of OR gate but simultaneous high values of both the inputs results a low output. An AND logic operation produces a high output only when both of the inputs hold the high value. NOR, NAND and XNOR gates are basically a NOT gate concatenated OR, AND and XOR gate respectively, to produce an inversed output. A TRANSFER logic gate transfers the values of a particular input in the output irrespective of the other input. It is similar to a single input YES logic gate considering the other input is left unconnected

to the device. A NOT-TRANSFER gate generates an inverted output compared to that of TRANSFER gate. In an INHIBIT (INH) gate, the high output due to a high value of a particular input is inhibited by the high value of the other input. An IMPLICATION (IMP) logic gate produces an inversed result of the INH gate. It is just a NOT-INH operation.

### 1.2.2. Implementation of logic gates in molecular scale

Any molecular system which can exist in two quasi stable states of different physical or chemical properties can be considered as a molecular switch. One state can be considered as ON state or logical 1 state and the other state can be regarded as OFF state or logical 0 state. The switching of two states can be achieved by the means of proton transfer, charge transfer, oxidation/reduction, fluorescence quenching etc.[58-62] Their privileges over the silicon chip based logic gate are less power consumption and smaller size. Above all they are simple and easy to construct and operate. Another advantage of the molecular logic system is the ability to increase the radix number. Information density also increases with increasing the radix number.[63, 64] However, Boolean logic system can only deals with binary radix. In contrary, any single change in molecular system by an external stimulus can be considered as a change of logical state. This way a molecular logic can deals with higher radix system.[65]

Generally molecular switch contains three different units – receptor moiety, reporter moiety and a spacer part.[66, 67] Receptor moiety works to bind with the trigger or the external stimuli. The reporter moiety exhibits the changes of state due to the external stimuli. In most of the cases, fluorophore molecules are chosen as a reporter moiety. It is because the electronic spectral properties of a molecule are very much sensitive towards the environment and also it is easy to monitor the changes. The spacer part connects the receptor moiety and the reporter moiety. The construction of a few different type of molecular logic gates are discussed below.

Tucker et al. reported an anthracene based ditopic ligand (L1) as a metal ion sensor (Scheme 1.2.1).[68] The 2,2′-bipyridyl unit can bind with $Hg^{2+}$ metal ion and the ethereal oxygen can host a $Na^{+}$ metal ion. The anthracene units of L1 undergo [4π+4π] pericyclic addition in presence of UV irradiation. Binding of the ligand with either of the metal ions enforces the conformational change and the photoinduced cyclization is catalyzed in presence of metal ions. The change in emission spectra from the cyclized product in the absence and in the presence of metal ions can be correlated with a molecular OR logic gate.

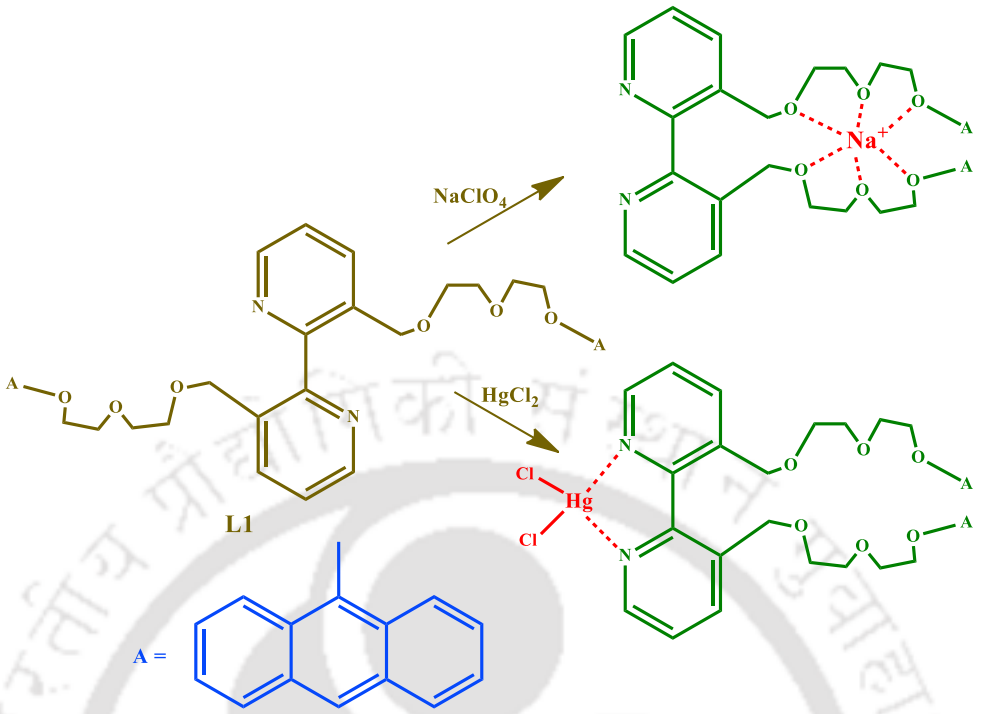


**Scheme 1.2.1.** Binding of $Na^+$ and $Hg^{2+}$ with L1.

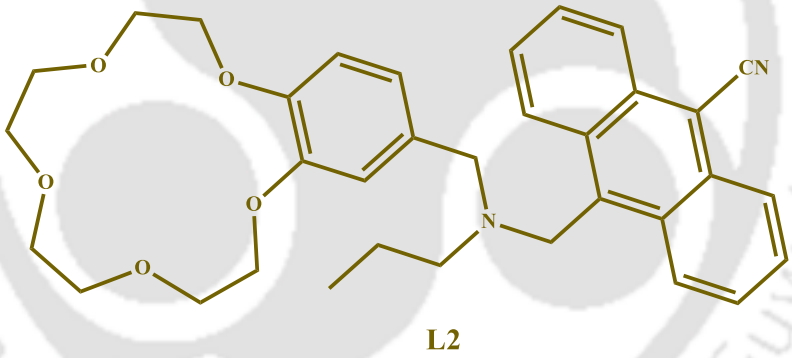


**Chart 1.2.1.** Ligand L2 can function as molecular AND logic gate in presence of proton and $Na^+$.

de Silva et al. first reported a molecular AND logic gate based on the change in emission properties of a cyanoanthryl fluorophore (Chart 1.2.1).[69] Due to the photo induced electron transfer from the electron rich crown ether and triethylamine L2 exhibits a weak fluorescence. The azacrown receptor is suitable to host a $Na^+$ cation and the tertiary amino group acts as a proton receptor. Simultaneous occurrence of $Na^+$ and proton in the system causes a strong emission from the complex. However, individual presence of the analytes is not sufficient to produce a high emission from the reporter fluorophore.

A molecular XOR operation was first reported by Balzani et al. with a pseudo-rotaxane system (L3).[70] The macrocycle unit contains an electron donor moiety

dinaptho-30-crown-10, and the thread is consisted with an electron accepting 2,7-diazapyrenium unit (Chart 1.2.2). In interlocked condition, both units exhibit very weak emission. The addition of trifluoroacetic acid protonates the crown ether moiety and disassembles the rotaxane system. The thread part comes out of the macrocycle, and both the moieties produce strong emission individually. On the other hand, tributyl amine also efficiently dislodges the diazapyrenium cation by forming a strong charge transfer complex. Consequently, the system moves to the 'switched on' emission state. However, the concomitant addition of acid and amine forms tributylammonium trifluoroacetate and the fluorescence intensity does not increase. The emission behavior of the individual units follows a XOR logic operation with addition of the analytes.

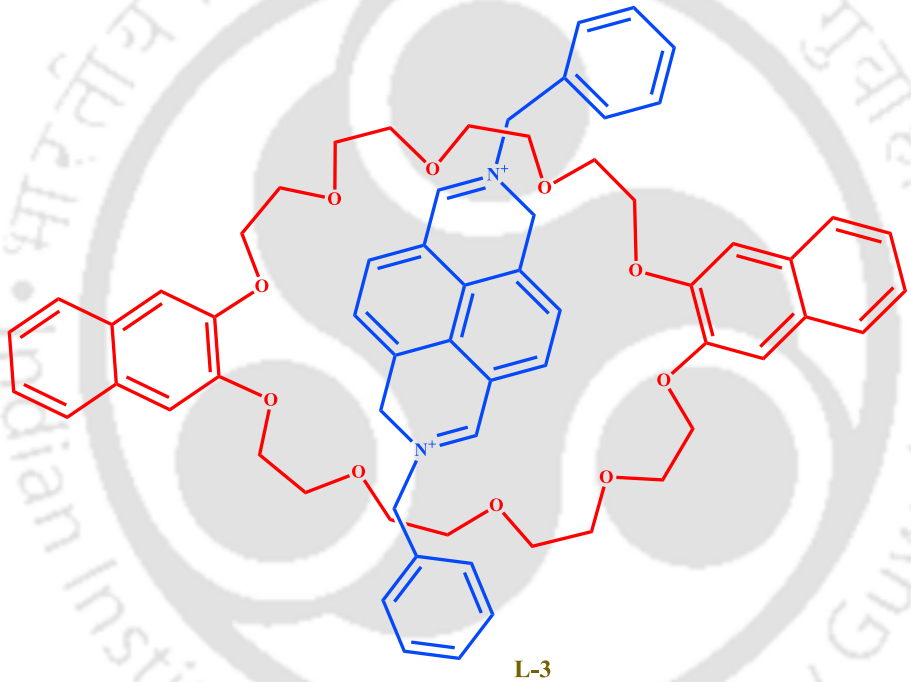


**Chart 1.2.2.** L3 can function as molecular XOR gate in presence of trifluoroacetic acid and tributyl amine.

Recently, Pischel et al. reported a ternary NOR logic system based on a 1,8-naphthalimide derivative(L4).[71] The monocationic species of L5 shows three different emission intensities at a particular wavelength (520 nm) in presence of low, medium and high fluoride anion concentration. Different deprotonated species in presence of different fluoride concentration produce different emission intensities (Scheme 1.2.2). A photoinduced electron transfer between the tertiary amine and unsubstituted 1,8-naphthalimide unit, and an electronic energy transfer between the unsubstituted to substituted 1,8-naphthalimide unit are the key factors for the molecule to behave as ternary NOR logic system.

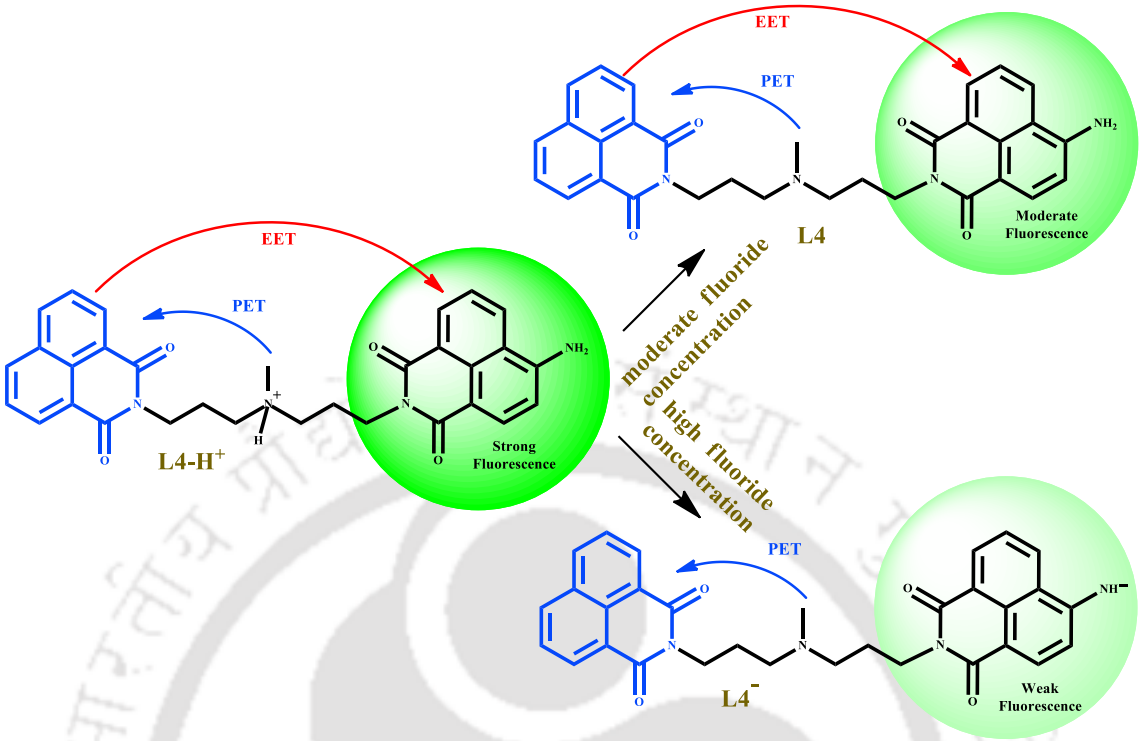


**Scheme 1.2.2.** Functioning of L4 as a ternary molecular logic system.

## 1.3. Motivation of the present work

In nonpolar solvent such as cyclohexane HPBI emits only tautomer emission due to existence of *cis*-enol.[72] Though, it present in *cis-trans* equilibrium in high polar protic solvents, the *cis*-enol is the major conformer.[73] However, Dogra et al. reported that the anion which is generated by an intermolecular proton transfer in basic aqueous solution exist only as *trans* conformer.[72] Therefore, the intermolecular proton transfer between HPBI and different anions has been investigated in non-aqueous solvents. Since, the nitrogen substitution affects the *cis-trans* equilibrium, the intermolecular proton transfers between both HPIP-b and HPIP-c with different anions have been investigated in non-aqueous solvents. (Chapter 3).

Lots of the ESIPT molecules exist in *cis-trans* equilibrium. While the *cis*-enol undergoes ESIPT to produce highly Stokes' shifted tautomer emission, the *trans*-enol exhibits normal emission which is less Stokes' shifted. Though aggregation induced enhanced emission (AIEE) was observed with ESIPT exhibiting molecules both the emission appear together upon aggregation. The photophysics of a derivative of HPBI, 1,4-bis(2-(2'-hydroxyphenyl)benzimidazol-1-ylmethyl)-benzene (BHPBI) has been studied. Different conformer specific AIEE have been acquired by strategic designing and controlling the intra and inter molecular hydrogen bonding.

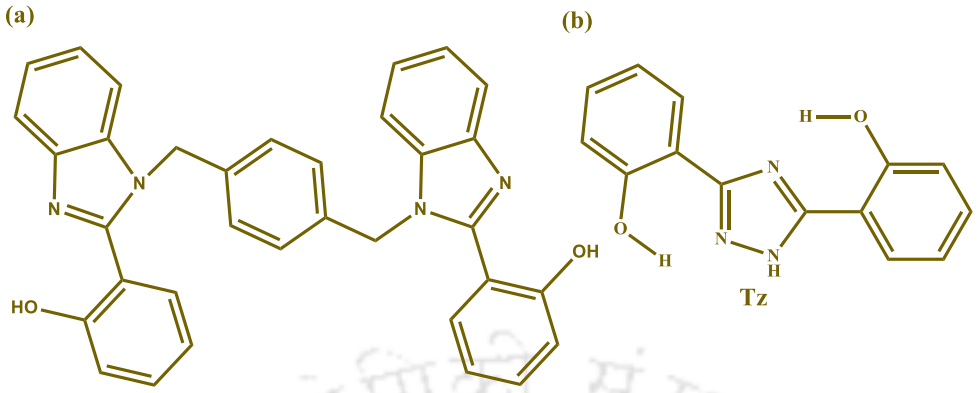


**Chart 1.3.1.** Molecular structure of (a) BHPBI and (b) Tz.

The *cis*-conformer of 2-(2′-hydroxyphenyl)azole derivatives possesses intramolecular hydrogen bond between the donor and the acceptor. This is a fundamental requirement for ESIPT. However, the existence of more than one intramolecular hydrogen bonded acid-base pair does not always lead to multiple proton transfer from a single molecule in the excited state.[50, 74] The feasibility of more than one intramolecular proton transfer has been investigated by strategically designing and synthesizing an azole derivative, 3,5-bis(2′-hydroxyphenyl)-1H-1,2,4-triazole (Tz) to gain more insight.

As discussed in the last section that the emission and absorption characteristics of the molecules strongly depend on the external stimuli. Based on the different emission and absorption behavior of the molecule in presence of external analyte, different molecular logic gates can be constructed. Azole derivatives, containing more than one electrophilic and nucleophilic centers can be exploited to mimic multiple logic operations by altering the spectral properties in presence of different outputs. Further, construction of fuzzy interference system can produce a detail of input-output correlation.

# Chapter 2

# Materials, Methods and Instrumentations

## 2.0. Introduction

The chapter provides the details of the materials used in the present work and the procedures followed in the syntheses of the fluorophores. Methods used for the analysis, calculations and sample preparation are also described. The quantum mechanical methods used for different theoretical calculations are explained in detail. In addition, a brief descriptions of the instrumentations used in the present thesis such as UV-Visible absorption spectrophotometer, and Steady-state and time-resolved fluorimeters are provided.

## 2.1. Materials

Details of the materials utilized in the present work are given below.

### 2.1.1. Solvents

- Acetonitrile, $CH_3CN$ (HPLC grade, Spectrochem India)
- 1-Butanol, $CH_3CH_2CH_2CH_2OH$ (HPLC grade, Spectrochem India)
- Chloroform, $CHCl_3$ (HPLC grade, Spectrochem India)
- Cyclohexane, $C_6H_{12}$ (HPLC grade, Spectrochem India)
- Dichloromethane, $CH_2Cl_2$ (HPLC grade, Spectrochem India)
- Diethyl ether, $(C_2H_5)_2O$ (AR grade, Merck India)
- *N*,*N*-Dimethylformamide, $N(CH_3)_2CHO$ (HPLC grade, Spectrochem India)
- Dimethylsulfoxide, $(CH_3)_2SO$ (HPLC grade, Spectrochem India)
- 1, 4-Dioxane, $C_4H_8O_2$ (AR grade, Spectrochem India)
- Ethyl acetate, $CH_3COOCH_2CH_3$ (HPLC grade, Spectrochem India)
- Glycerol, $CH_2OHCHOHCH_2OH$ (AR grade, Rankem India)
- Methyl alcohol, $CH_3OH$ (HPLC grade, Spectrochem India)
- Methyl tetrahydrofuran, $C_5H_{10}O$ (AR grade, Spectrochem India)
- Tetrahydrofuran, $C_4H_8O$ (HPLC grade, Spectrochem India)
- Toluene, $C_6H_5CH_3$ (HPLC grade, Rankem India)
- Polyethylene Glycol, $C_{2n}H_{4n+2}O_{n+1}$ (AR grade, Rankem India)
- 1-Propanol, $CH_3CH_2CH_2OH$ (HPLC grade, Spectrochem India)
- 2-Propanol, $CH_3CH_2CH_2OH$ (HPLC grade, Spectrochem India)
- Water, $H_2O$ (Millipore water)

### 2.1.2. Salts of different metal ions and anions

- Copper perchlorate hexahydrate, $Cu(ClO_4)_2.6H_2O$, (98.0%, Sigma Aldrich)

- Cadmium nitrate tetrahydrate, $Cd(NO_3)_2.\ 4H_2O$, (98.0%, Sigma Aldrich)
- Iron chloride hexahydrate, $FeCl_3.6H_2O$ (97.0%, Sigma Aldrich)
- Tetrabutyl ammonium fluoride hydrate, $[CH_3(CH_2)_3]_4NF{\cdot}xH_2O$, (98.0%, Sigma Aldrich)
- Tetrabutylammonium acetate, $(CH_3CH_2CH_2CH_2)_4N(COOCH_3)$, (97.0%, Sigma Aldrich)
- Tetrabutylammonium chloride, $(CH_3CH_2CH_2CH_2)_4NCl$, (97.0%, Sigma Aldrich)
- Tetrabutylammonium bromide, $(CH_3CH_2CH_2CH_2)_4NBr$, (≥ 98.0%, Sigma Aldrich)
- Tetrabutylammonium iodide, $(CH_3CH_2CH_2CH_2)_4NI$, (≥ 98.0%, Sigma Aldrich)
- Tetrabutylammonium bisulphate, $(CH_3CH_2CH_2CH_2)_4N(HSO_4)$, (≥ 99.0%, Sigma Aldrich)
- Tetrabutylammonium phosphate monobasic, $(CH_3CH_2CH_2CH_2)_4NH_2PO_4$, (≥ 99.0%, Sigma Aldrich)
- Tetrabutylammonium rhodanide, $(CH_3CH_2CH_2CH_2)_4N(SCN)$, (98.0%, Sigma Aldrich)
- Tetrabutylammonium nitrate, $(CH_3CH_2CH_2CH_2)_4N(NO_3)$, (97.0%, Sigma Aldrich)

### 2.1.3. Other chemicals

- 2-Amino-3-hydroxypyridine, $(C_5H_6N_2O)$, (98%, Sigma Aldrich)
- Benzene-1,2-diamine, $(C_6H_8N_2)$, (98%, Merck)
- Chloroform-d, $(CDCl_3)$, (Sigma Aldrich)
- 2,3-Diaminopyridine, $(C_5H_7N_3)$, (98%, Sigma Aldrich)
- 4-(Dimethylamino)benzoic acid, $(C_9H_{11}NO_2)$ (98%, Sigma Aldrich)
- Dimethylsulfoxide-$d_6$, $(C_2D_6OS)$, (Sigma Aldrich)
- Diphosphorous pentoxide, $(P_2O_5)$, (97%, Merck)
- Hydrazin hydrate, $(N_2H_4{\cdot}H_20)$ (80% solution in water) (Merck)
- 2-Methoxybenzoic acid, $(C_8H_8O_3)$ (98%, Sigma Aldrich)
- ortho-Phosphoric Acid, $(H_3PO_4)$, (AR grade, Rankem India)
- Potassium Carbonate, $(K_2CO_3)$, (Rankem India)
- Potassium hydroxide, (KOH), (Merck)
- Salicylic Acid, $(C_7H_6O_3)$, (98%, Merck)
- Salicylamide, $(C_7H_7NO_2)$, (99%, Sigma Aldrich)
- Silica gel, $(SiO_2)$ (60-120 mesh) (Merck India)

- Silica gel, (TLC) ($SiO_2$), (Merck India)
- Silica gel GF254 (Merck India)
- Sodium dodecyl sulfate, ($C_{12}H_{25}NaO_4S$), (SDS, Sigma Aldrich)
- Sodium hydrogen carbonate, ($NaHCO_3$), (Merck)
- Sodium hydroxide, (NaOH), (Merck)
- Sodium sulphate anhydrous, ($NaSO_4$), (Merck India)
- Sulphuric Acid, ($H_2SO_4$), (AR grade, Rankem India)

### 2.1.4 Synthesis of 2-(2'-hydroxyphenyl)benzimidazole, 2-(2'-hydroxyphenyl)-3*H*-imidazo[4,5-*b*]pyridine and 2-(2'-hydroxyphenyl)-3*H*-imidazo[4,5-*c*]pyridine

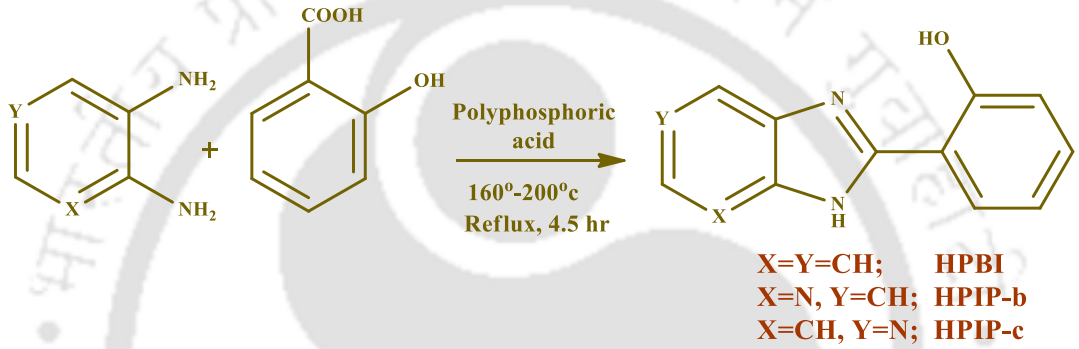


**Scheme 2.1.1.** Synthetic procedure of HPBI, HPIP-b and HPIP-c.

HPBI, HPIP-b and HPIP-c were synthesized by following the reaction scheme shown in Scheme 2.1.1.[75-77] Equimolar mixture of appropriate diamine and salicylic acid was heated in polyphosphoric acid solution at 160-200 °C for 4.5 hours until the reaction was completed. The reaction was monitored with GF254 silica gel thin layer chromatography (TLC) plate. The reaction mixture was cooled to room temperature. Ice cold water was poured to the reaction mixture and stirred well to obtain a complete slurry. The slurry was neutralized with aqueous KOH solution to neutral pH at which the product precipitated out. The precipitate was vacuum suctioned and dried by keeping overnight in a desiccator. The dried precipitate was dissolved in methanol by heating. The solution was filtered and the filtrate was kept for recrystallization. The recrystallization was performed in methanol for at least three times until the pure product was obtained. The identities and purity of the synthesized compounds were confirmed by NMR and TLC. The NMR spectra of HPBI, HPIP-b and HPIP-c are shown in Annexure-A. The spectral data match with the literature reports.[35]

**HPBI:** white solid; $^1$H NMR (600 MHz, DMSO-$d_6$) δ 13.21 (s, 1H), 13.17 (s, 1H), 8.06 (dd, *J* = 7.8, 1.5 Hz, 1H), 7.72 (d, *J* = 6.8 Hz, 1H), 7.61 (d, *J* = 6.8 Hz, 1H), 7.43 – 7.35 (m, 1H),

7.28 (d, *J* = 6.4 Hz, 2H), 7.07 – 7.00 (m, 2H).

**HPIP-b:** light green solid; 1H NMR (600 MHz, DMSO-$d_6$) δ 8.39 (s, 1H), 8.08 (t, *J* = 31.6 Hz, 2H), 7.41 (t, *J* = 7.4 Hz, 1H), 7.33 – 7.25 (m, 1H), 7.08 – 6.94 (m, 2H).

**HPIP-c:** white solid; $^1$H NMR (600 MHz, DMSO-$d_6$) δ 8.98 (s, 1H), 8.32 (d, *J* = 5.7 Hz, 1H), 8.16 (dd, *J* = 7.8, 1.6 Hz, 1H), 7.68 (d, *J* = 5.7 Hz, 1H), 7.40 (t, *J* = 7.7 Hz, 1H), 7.05 (d, *J* = 8.2 Hz, 1H), 7.02 (t, *J* = 7.5 Hz, 1H).

### 2.1.5 Synthesis of 1,4-bis(2-(2′-hydroxyphenyl)benzimidazol-1-ylmethyl)-benzene (BHPBI)

The molecule, 1,4-bis(2-(2′-hydroxyphenyl)benzimidazol-1-ylmethyl)-benzene (BHPBI) was obtained from Dr. M. Sathiyendiran's Laboratory, Department of Chemistry, University of Delhi, India (presently at School of Chemistry, University of Hyderabad). The synthesis procedure of the molecule was reported elsewhere.[78]

### 2.1.6 Synthesis of 3,5-bis(2′-hydroxyphenyl)-1H-1,2,4-triazole (Tz) and 3-(2′-hydroxyphenyl)-5-(2′-methoxyphenyl)-1H-1,2,4-triazole (MTz)

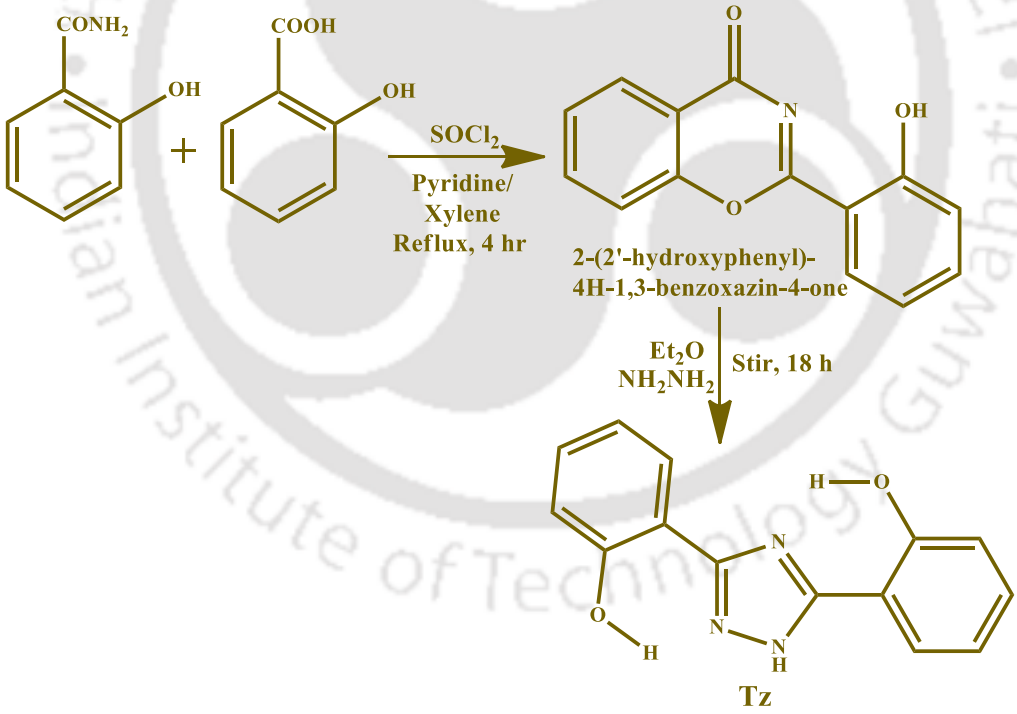


**Scheme 2.1.2.** Synthesis procedure of Tz.

The synthesis of Tz was carried out in two steps by following the procedure reported by Hegetschweiler et al.[79] In the first step 2-(2′-hydroxyphenyl)-4H-1,3-benzoxazin-4-one was synthesized, which was used as starting material to obtain the Tz molecule (Scheme 2.1.2).

**Step I**

Equimolar amount of salicylic acid and salicylamide and catalytic amount of pyridine (1/10) were dissolved in xylene. The solution was stirred vigorously under reflux condition and two equivalents of thionylchloride was added slowly to the solution over a period of 4 hours. A yellow solid precipitate appeared at the end of the reaction. Stirring of the reaction mixture was continued for 30 more minutes without heating. The solvent was removed by evaporation under reduced pressure. Ethanol and a little amount of acetic acid were added to the semi-dried solution. The suspension was heated at the boiling temperature of ethanol and cooled at room temperature. The resulting precipitation was filtered and purified using column chromatography.

**Step II**

Equivalent amount of hydrazine monohydrate and 2-(2′-hydroxyphenyl)-4H-1,3-benzoxazin-4-one were dissolved in diethylether in a closed round bottom flask. The solution was stirred for 12 hrs. The resultant white precipitated was isolated by filtration. Pure Tz compound was obtained by washing the crude product with solvents like chloroform, THF, methanol. The NMR spectra of Tz is shown in Annexure-A.

**Tz:** white solid; $^1$H NMR (600 MHz, DMSO) δ 11.46 (s, 2H), 8.02 (dd, *J* = 7.8, 1.6 Hz, 2H), 7.35 (t, *J* = 7.7 Hz, 2H), 7.03 (d, *J* = 8.1 Hz, 2H), 7.00 (t, *J* = 7.5 Hz, 2H).

The mono-methoxy derivative of the Tz molecule, 3-(2′-hydroxyphenyl)-5-(2′-methoxyphenyl)-1H-1,2,4-triazole (MTz) was synthesized as follow. First, 2-hydroxy-N-(2-methoxybenzoyl)benzamide (HMB) was synthesized following the Step-I procedure (Scheme 2.1.3). It was purified by column chromatography. 1 mmole of the benzamide obtained from the earlier step was taken in 3 ml of 30% acetic acid/water mixture.[80] 1 mmole of hydrazine hydrate was added to the solution and refluxed at 118° C for 24 hours. A clear solution was observed at the end of the reaction. It was partially neutralized with sodium bicarbonate solution and the product was extracted with chloroform. The NMR spectra of HMB and MTz are displayed in Annexure-A.

**HMB:** pale yellow solid; $^1$H NMR (600 MHz, DMSO-$d_6$) δ 7.89 (d, *J* = 7.9 Hz, 1H), 7.83 (d, *J* = 7.7 Hz, 1H), 7.58 (t, *J* = 7.8 Hz, 1H), 7.44 (t, *J* = 7.7 Hz, 1H), 7.21 (d, *J* = 8.4 Hz, 1H), 7.10 (t, *J* = 7.5 Hz, 1H), 7.03 (d, *J* = 8.2 Hz, 1H), 6.96 (t, *J* = 7.5 Hz, 1H).

**MTz:** white solid; $^1$H NMR (600 MHz, $CDCl_3$): δ 12.21 (s, 1H), 11.28 (s, 1H), 8.28 (d, *J* = 7.7 Hz, 1H), 8.10 (d, *J* = 7.7 Hz, 1H), 7.46 (t, *J* = 7.8 Hz, 1H), 7.30 (t, *J* = 7.6 Hz, 1H), 7.17 (t, *J* = 7.5 Hz, 1H), 7.04 (d, *J* = 8.2 Hz, 1H), 6.99 (d, *J* = 8.3 Hz, 1H), 6.92 (t, *J* = 7.4 Hz, 1H), 3.94 (s, 3H).

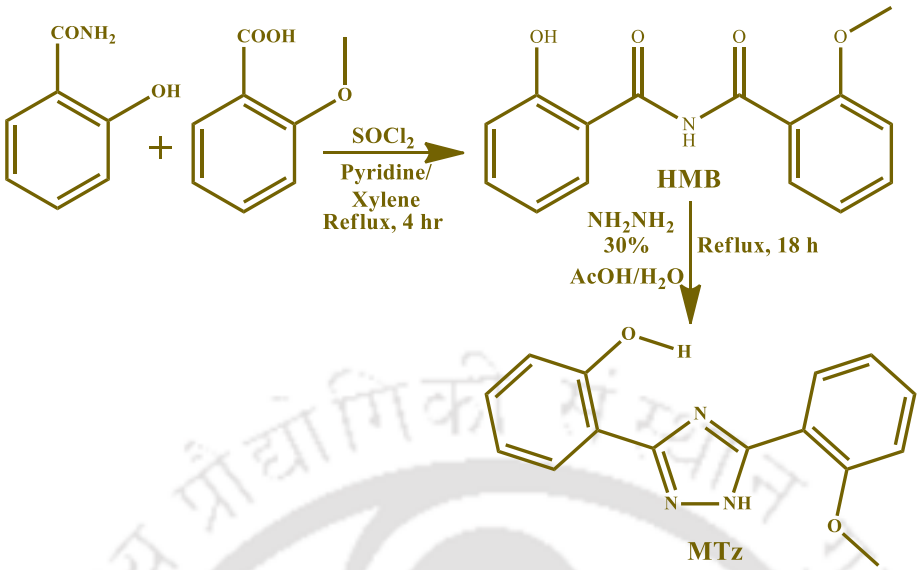


**Scheme 2.1.3.** Synthesis procedure of MTz.

### 2.1.7 2-(4′-*N*,*N*-dimethylaminophenyl)oxazolo[4,5-b]pyridine (DMAPOP) and 2-(4′-*N*,*N*-dimethylaminophenyl)imidazo[4,5-b]pyridine (DMAPIP-b)

DMAPOP and DMAPIP-b in pure form were available in our laboratory. The synthesis procedure of the molecules were reported elsewhere.[81, 82]

## 2.2. Sample preparation

### 2.2.1. Fluorophore solutions

A stock solution of the fluorophore of 1 mM concentration was prepared in methanol or methanol-THF mixture. 50-100 μL of the solution was pipetted out to a 10 ml volumetric flask. The solution was dried by blowing nitrogen gas. After complete removal of solvent, 10 ml of required solvent or solution was added to each volumetric flask containing the dried compound. The flask was shaken well to dissolve the compound completely. The final concentration of the fluorophore was 5-10 μM.

### 2.2.2. Metal ion, anion and pH titration

Salts of metal ions and anions were dissolved in required solvents. The appropriate amount of the salt solution was added to the fixed amount of fluorophore. For pH titrations, a small amount of $H_2SO_4$ or $H_3PO_4$ or NaOH solution was added gradually to obtain the desired pH.

### 2.2.3. Micellar solution

The stock solutions of surfactant was prepared in 100 ml volumetric flask by adding appropriate quantity of SDS in millipore water. The appropriate amount of the

fluorophore solutions were taken in the volumetric flasks and dried by blowing nitrogen. The surfactant solutions were added to the volumetric flasks. The pH of the solutions were adjusted by adding small amount of dilute sulfuric acid or sodium hydroxide solution.

### 2.2.4. Aggregates of fluorophores

5 μM of BHPBI solution was prepared in THF and water medium. Two solution were mixed in different ratios, and the final solution was sonicated for five minutes to obtain the aggregated structures.

## 2.3. Methods

### 2.3.1. Quantum yield

The excited molecules after absorption of light dissipate their absorbed energy by emission or nonradiative de-excitation. The efficiency with which these processes take place is called the quantum efficiency. Quantum yield of fluorescence ($\phi$) is defined as the ratio of the number of photons emitted to the number of photons absorbed as given by the following equation.

$$\phi = \frac{\text{Number of photon emitted}}{\text{Number of photon absorbed}} \qquad \textbf{(eq. 2.1)}$$

The fluorescence quantum yield of a sample ($\phi_s$) is determined with respect to that of a standard ($\phi_r$) known fluorophore using the **Equation 2.2** given below

$$\phi_s = \frac{I_s A_r n_s^2}{I_r A_s n_r^2} \phi_r \qquad \textbf{(eq. 2.2)}$$

where $I_s$ and $I_r$ are the integrated fluorescence area, and $A_s$ and $A_r$ are the absorbances for the sample and reference, respectively. $n_s$ and $n_r$ are the refractive indices for the sample and reference solutions, respectively. Quinine sulphate in 1N sulphuric acid solution ($\phi_r$ = 0.546) was used as the reference for fluorescence quantum yield determination.[83] The dielectric constants and refractive indices of different solvents at different temperatures for the determination of fluorescence quantum yields were taken from the literature.[84, 85]

### 2.3.2. Time-resolved area normalized emission spectra

Evolution of fluorescence spectra during the excited state lifetime of the fluorophores were obtained by time correlated single photon counting method.[86] The fluorescence spectra at various times were constructed from the fluorescence decays recorded at

several wavelengths. The details of fluorescence decay acquisition was described in section 2.4.4. Each of the different decays were deconvulated from the instrument response function and fitted with multi-exponential function using standard method of non-linear least square and iterative reconvulation method. A three- or four-exponential function was used to obtain a decent fitting of the fluorescence decays. A corrected Steady-state fluorescence spectra was recorded by excitation at same wavelength, and it was used to obtain different fluorescence emission at different times. Time resolved emission spectra at different wavelengths were constructed using the equation 2.3.

$$I(\nu, t) = I_{ss}(\nu)\frac{\sum_j \alpha_j(\nu) e^{-t/\tau_j(\nu)}}{\sum_j \alpha_j(\nu)\tau_j(\nu)} \qquad \textbf{(eq. 2.3)}$$

where $I_{ss}(\nu)$ is the Steady-state fluorescence intensity at $\nu$, $\alpha_j(\nu)$ and $\tau_j(\nu)$ are the fit parameters. Time-resolved area normalized emission spectra were constructed by normalizing the area of each emission spectra at different times.

### 2.3.3. Quantum mechanical calculations

Theoretical calculations were performed using Gaussian 09W program to obtain the molecular parameters.[87] GaussView 5.0 was used for drawing the molecules, to obtain the coordinates and to feed the inputs.[88] The density functional theory (DFT)[89, 90] and the time dependent DFT (TDDFT) were used to optimize the ground and the excited state geometries, respectively.[91] A 6-31+G(d,p) basis set with Becke's three-parameter exchange functional along with Lee-Yang-Parr nonlocal correlation functional (B3LYP) was used for the geometry optimization.[92, 93] The minimum energy nature of a fully optimized geometry was confirmed by vibration frequency calculations performed on the optimized geometries and using the same basis set 6-31+G(d,p).[196,197] The excitation and the emission energies were calculated from the optimized ground state and excited state geometries, respectively using TDDFT/B3LYP/6-31+G(d,p) calculations.[94, 95] The solvent stabilization of the molecule was included by considering integral equation formalism-polarizable continuum model (IEF-PCM) and choosing specific solvent.

## 2.4. Instruments

### 2.4.1. pH meter

The pH of different solutions were measured using Jenway pH meter (Model No. 3510). The pH meter was calibrated by using three different standard buffer solutions (pH 4.00, pH 7.00 and pH 10.00) within a range of ± 0.01-0.02 pH units.

### 2.4.2. Absorption spectrophotometer

Absorption spectroscopy is the most widely used spectroscopic tool which provides the wavelength of a transition and the corresponding molar extinction coefficient ($\varepsilon_\lambda$) of a chromophore under investigation. The modern Ultraviolet-Visible (UV-Vis) spectrometer consists of light source, monochromator, detector, amplifier and recording devices. Quartz cells are used for the measurement of the absorption spectra.

In the present work, the absorption spectra were recorded with Varian-Cary 100, Perkin Elmer Lambda 25, and Perkin Elmer Lambda 750 double beam UV-Vis spectrometer. All these instruments use deuterium and tungsten lamps as light sources. Perkin Elmer and Varian-Cary instrument have diode and photomultiplier tube (PMT) as detector, respectively.

### 2.4.3. Steady-state fluorimeter

Steady-state fluorescence spectra were recorded on Edinburgh Instruments FSP 920, Jobin Yvon Spex Fluoromax 4 and Cary Eclipse spectrophotometers. As an illustration for the instrumentation of spectrofluorimeter, a diagram of FSP 920 instrument is shown in Figure 2.4.1.

**Optical system**

The most common light source for fluorimeters is xenon arc lamp. These lamps provide a relatively uniform intensity over a broad spectral range from UV to near infra-red. An excitation monochromator is used to select the excitation wavelength. Fluorescence is collected at the right angle with respect to the incident beam through a monochromator by using a PMT. A motorized monochromator is used for the automatic scanning of wavelengths. The monochromators are controlled by the electronic devices and computer. The optical module contains various parts, a sample holder, shutters, polarizers if necessary, and a beam splitter consisting of a quartz plate reflecting a fraction of the exciting light towards a quantum counter or a photodiode.

The emission spectrum reflects various fluorescence intensities as a function of $\lambda_{em}$ (the wavelength at which the fluorescence is observed) when the excitation wavelength ($\lambda_{ex}$) is fixed. The excitation spectrum shows the variation of fluorescence intensity as a function of $\lambda_{ex}$ with fixed $\lambda_{em}$. The spectra are recorded as a function of wavelength and not wavenumber because the monochromators of spectrofluorimeter are equipped with gratings, so that for a given width of the input and output slits, the monochromators operate at a constant band pass expressed in wavelength. The fluorescence spectra are

needed to be corrected for the distortion by the wavelength dependence of several components of the instrument.

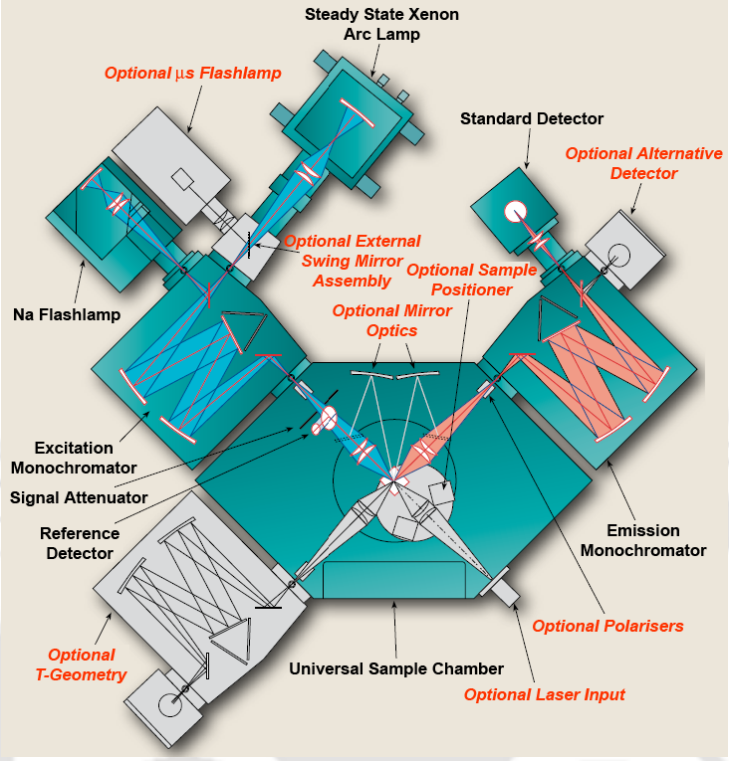


**Figure 2.4.1.** Block diagram of FSP 920 Steady-state fluorescence spectrophotometer from Edinburgh Instruments. Diagram was obtained from the catalogue of Edinburgh instruments FSP 920.

### Correction for emission spectra

The emission spectrum is distorted by the wavelength dependence of the emission monochromator efficiency and the photomultiplier response. In general, the correction factors are measured using a calibrated tungsten lamp or by a standard fluorescent dye whose corrected emission spectrum has been reported earlier. Emission correction factors are provided by the manufacturer in all the three instruments used.

### Correction for excitation spectra

The excitation spectrum is distorted by the variations of the intensity of the exciting light. These variations are due to the wavelength dependence of the lamp intensity and of the transmission efficiency of the excitation monochromator. Because the quantum counter circumvents the wavelength dependence of the sensitivity of the sample and the reference photomultiplier, the ratio of the fluorescence signal from the sample to that from the quantum counter or photodiode (as a function of the excitation wavelength) provides the corrected excitation spectra. However, such correction

procedures may be insufficient when very accurate measurements are needed (for instance when information is expected for the comparison of the absorption and excitation spectra). In fact, the optical geometry of the reference channel is not identical to that of the main channel, and the wavelength dependence of optical parts (e.g. focal length of lenses) may introduce some distortion into the excitation spectrum. It is then recommended to use correction factors obtained by using a fluorescent compound which absorbs in the same wavelength range as that of the sample to be studied, and whose absorption spectrum is identical to its excitation spectrum. The ratio of the measured excitation spectrum of this reference compound (as described above using the quantum counter) to the absorption spectrum provides the correction factors that can be stored in the computer. Spectrofluorometers equipped with a photodiode instead of a quantum counter provide excitation spectra that should be further corrected because, in addition to the reasons explained above, the wavelength response of the photodiode is not strictly flat, over the whole wavelength range available. It should be noted that most commercially available instruments are delivered with a file containing the correction factors and the manufacturer provided the correction file for all three molecules.

FSP 920 is equipped with double excitation monochromator and the other instruments used for the measurement have single excitation monochromator. FSP 920 and Fluoromax 4 have 450 W and 150 W Xe arc lamps, respectively as light source. But Cary Eclipse employs 75 W pulsed Xe lamp as light source. All three instruments use Hamamatsu red sensitive PMT as detector.

### 2.4.4. Time resolved fluorimeter

The decay of a photoexcited fluorophore molecule to the ground state can be expressed as

$$I(t) = I_0 e^{-\frac{t}{\tau}} \qquad \textbf{(eq. 2.4)}$$

where $I_0$ is the fluorescence intensity at time zero after the photoexcitation. $\tau$ is the excited state lifetime of the molecule. It is basically the time that is needed to drop the emission intensity by 1/e (~37%). $I(t)$ is the emission intensity after the time $t$. In term of radiative ($k_r$) and non-radiative ($k_{nr}$) rate constant, the fluorescence lifetime can be expressed as

$$\tau = \frac{1}{k_r + k_{nr}} \qquad \textbf{(eq. 2.5)}$$

Fluorescence lifetime is an intrinsic property of a fluorophore and is independent of how it is measured. It is considered as a state function as it is independent of the initial perturbation conditions like excitation wavelength, one- or multiphoton excitation, duration of light exposure, fluorescence intensity and fluorophore concentration. Moreover, it is not affected by photobleaching. Since fluorescence occurs from an energetically unstable state, fluorescence lifetime is sensitive to internal and external factors. The internal factor comprises of the fluorophore structure and the external factors include temperature, polarity, viscosity and the presence of fluorescence quenchers.

There are two ways to determine the fluorescence lifetime of fluorophores, frequency-domain and time-domain.[96, 97] They have different instrumentation setups and follow different data acquisition methods, however, both approaches are mathematically equivalent and their data can be interconverted by Fourier transformation. In frequency domain, the incident light is sinusoidally modulated at high frequencies such that the emission occurs at the same frequency as the incident light. The difference between the incident and emitted light is that the emitted light experiences a phase delay, and the amplitude of the emitted light is changed relative to the excitation light (demodulation). Data are acquired with photomultipliers or charge-coupled devices (CCD) equipped with a gain modulator.

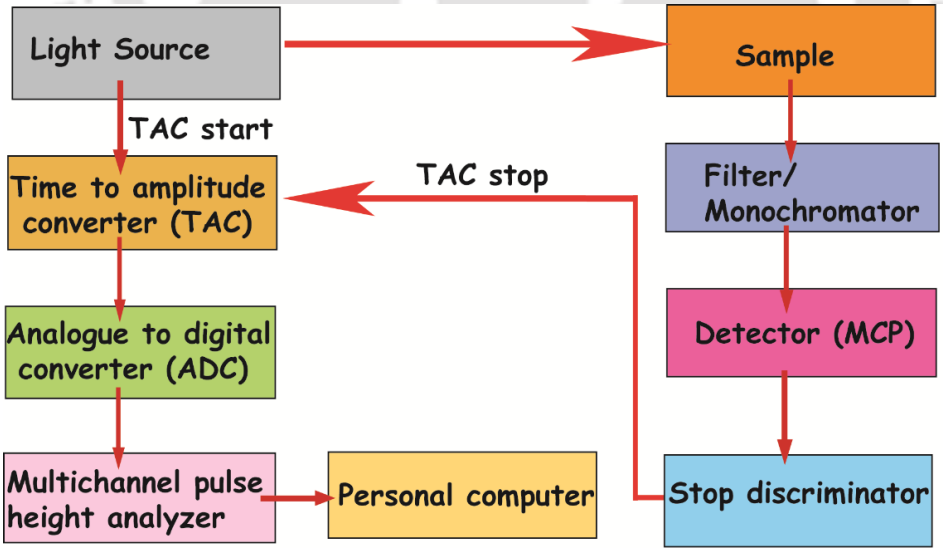


**Figure 2.4.2.** Block diagram of a TCSPC instrument.

In time-domain, the sample to be analyzed is excited with a short light pulse from a light source with sufficient delay between pulses. The light source can be flash lamp,

pulsed laser, laser diode, or LED. Various methods are available for data collection. The most common technique is the time-correlated single photon counting (TCSPC) which is applied in this work.[96, 97] Figure 2.4.2 explains schematically the working principle of a TCSPC instrument. In TCSPC method, the source light beam is split into start and stop signal pulses. The start signal pulse travels to a PMT or micro-channel plate (MCP) photomultiplier tube which activates the time-to-amplitude converter (TAC). The stop signal pulse travels through the sample. The growth of ramp signal in TAC is stopped by this pulse. The TAC output can be amplified by an amplifier, and this analogue pulse of height corresponding to a measured time of the signal goes through further processing to convert to digital pulse through the analogue to digital converter (ADC).

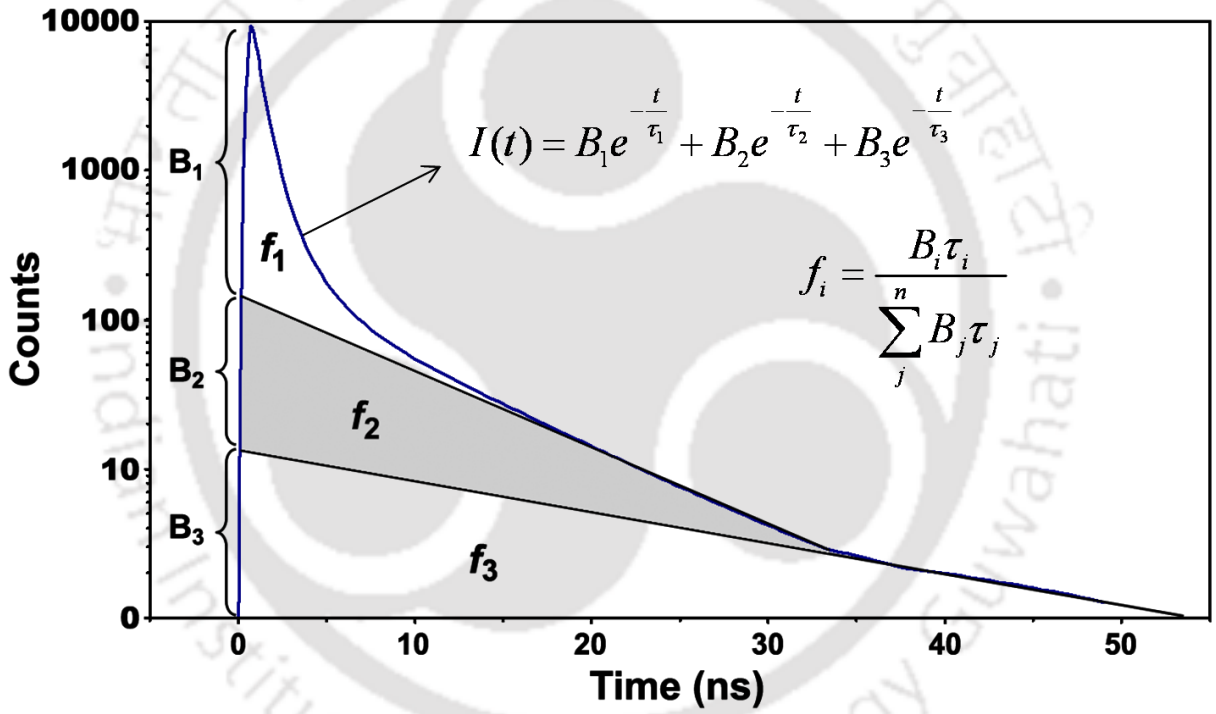


**Figure 2.4.3.** Exponential decay model for three components.

Since the fluorophores emit photons at different relaxation times following their excitation by radiation, the decay time of a single molecule must have a certain rate rather than occurring at a specific time. The principle of TCSPC is the detection of single photons and the measurement of their arrival times with respect to a reference signal from the light source. The TCSPC method needs a high repetitive light source to accumulate the sufficient number of photons. Since this is a statistical method, it requires a large numbers of statistical data precision. The time measurement of the start and stop sequence is represented by an increase of a memory value in a histogram. Thus,

this experiment must be repeated many times to gather sufficient photons in the full range of delays between excitation and emission. The resulting histogram counts versus the time channels on the x-axis represents the curve of fluorescence decay profiles. A typical emission decay of a fluorophore consisting of three components obtained from TCSPC method is shown in Figure 2.3.

In the entire work, fluorescence lifetimes were measured with LifeSpec II instrument from Edinburgh Instruments. LifeSpec II employs Hamamatsu MCP detector that has response time of 50 ps. The light sources used to excite the sample were 290 nm, 308 nm and 336 nm LED from PicoQuant and 375 nm laser diode from Edinburgh. Time-resolved data were analyzed with reconvolution method based on discrete components analysis model using the FAST software developed by the Edinburgh Instruments Ltd.

### 2.4.5. Other instruments

Fourier transformed infra-red (FT-IR) spectra in the range 450-4000 $cm^{-1}$ were recorded on Nicolet Impact-410 in KBr pellets. Fourier transform nuclear magnetic resonance (FT NMR) spectra were recorded in $CDCl_3$ or DMSO-$d_6$ with tetramethylsilane as the standard for $^1H$ nuclei on Varian Mercury plus 400 MHz or Bruker Avance III 600 MHz NMR spectrometers. The chemical shifts were recorded in parts per million (ppm) on the scale using tetramethylsilane (TMS) or residual solvent peak as the reference. The images of micro particles (aggregates) were recorded with Carl Zeiss, SIGMA VP field emission scanning electrode microscope.

For single crystal structure determination, the intensity data were collected using Bruker SMART APEX-II CCD diffractometer equipped with a fine focus 1.75 kW sealed tube graphite monochromated Mo-$K_\alpha$ radiation ($\lambda$ = 0.71073 Å) at 298(3) K with increasing $\omega$ (width of 0.3$^o$ per frame) at a scan speed of 5 second per frame. Cell parameters were retrieved using SMART software[98] and refined with SAINT software on all observed reflections. Data reduction was performed with SAINT software and corrected for Lorentz and polarization effects. Absorption corrections were applied with the program SADABS.[99] The structure was solved by direct methods implemented in SHELXS-97 program and refined by full-matrix least-squares methods on $F_2$ using SHELXL-97.[100] All non-hydrogen atomic positions were located in difference Fourier map and refined anisotropically. The hydrogen atoms were placed in their geometrically generated positions. The positional and temperature factors were refined isotropically. Structural illustrations were drawn with MERCURY-3.6 for Windows.[101]

# Chapter 3

# Intermolecular Proton Transfer of 2-(2'-Hydroxyphenyl)benzimidazole and its Nitrogenous Analogues in Polar Aprotic Medium

## 3.0. Introduction

The intermolecular proton transfer may lead to the formation of ions. The acidic proton of a fluorophore can be transferred to a base. The process generates anion. The proton transfer efficiency depends on the acidity of the donor and the proton accepting ability of the base. Since, the acidity of the proton donor group is enhanced in the excited state, the proton transfer is more effective in the excited state. The proton accepting ability of a base can be tuned by changing its solubility, dissociation constant, counter ion etc.

The present chapter demonstrates the formation of anion of HPBI and its nitrogenous analogues by intermolecular proton transfer and the perturbation of their existence by chemical stabilization. The chapter is divided into two sections. The first section describes the ground and excited state proton transfer of HPBI in presence of different bases and the stabilization factors of different anionic conformers of HPBI. The second section explains the effect of nitrogen substitution on the anion sensing ability and the efficiency of proton transfer.

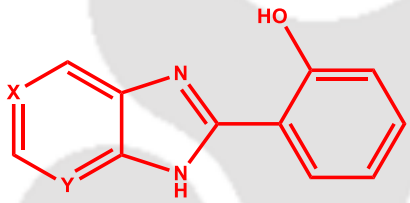


**X = CH, Y = CH: HPBI**
**X = CH, Y = N: HPIP-b**
**X = N, Y = CH: HPIP-c**

**Chart 3.0.** Structures of HPBI and its nitrogenous analogues.

## 3.1. Switching between *cis*- and *trans*- anions of 2-(2'-hydroxyphenyl) benzimidazole: a molecular rotation perturbed by chemical stabilization

The ESIPT can be prevented with a strong base due to the abstraction of the phenolic proton responsible for the proton transfer. The prototropic study of HPBI in aqueous medium was carried out by Dogra et al.[72] Despite the fact that the *cis*-enol is the predominating conformer in the ground state, they found that in basic pH, the *cis*-anion was completely absent and HPBI existed only as *trans*-anion (Chart 3.1.1). Mosquera et al. also reported that the *trans*-enol in aqueous solution is deprotonated to form the *trans*-anion.[73] They showed the formation of the same anion in basic ethanol as well. Most recently, Wang et al. investigated the anion sensing ability of HPBI in DMSO and suggested the formation of anion in presence of fluoride ion.[102] However, they hypothesized that the anion is formed by the deprotonation of 'NH' proton (instead of 'OH' proton, Chart 3.1.1). In the pyridyl nitrogen substituted analogue, Mosquera et al.

also reported the presence of two neutral forms (*cis*- and *trans*-) but one anion.[12] The oxazole derivative of HPBI, 2-(2′- hydroxyphenyl)benzoxazole was reported to form only one anion in alkaline aqueous medium and two anions (normal and twisted) in zeolites.[103, 104] On the other hand in thiazole derivatives of HPBI and related molecules, only one anion formation was reported. However, clear distinction was not made between the conformers of the anion.[105, 106] Unlike the oxazole and thiazole derivatives, HPBI has 'NH' proton that provides extra stabilization to the *trans*-anion by intramolecular hydrogen bonding (Chart 3.1.1). Thus, the objectives of the present study are (i) to ascertain whether it is feasible to obtain the *cis*-anion of HPBI and clearly distinguish the spectral characteristics of the *cis*-anion and the *trans*-anion and (ii) to establish the precedency of deprotonation between the 'OH' and the 'NH' protons in aprotic environment.

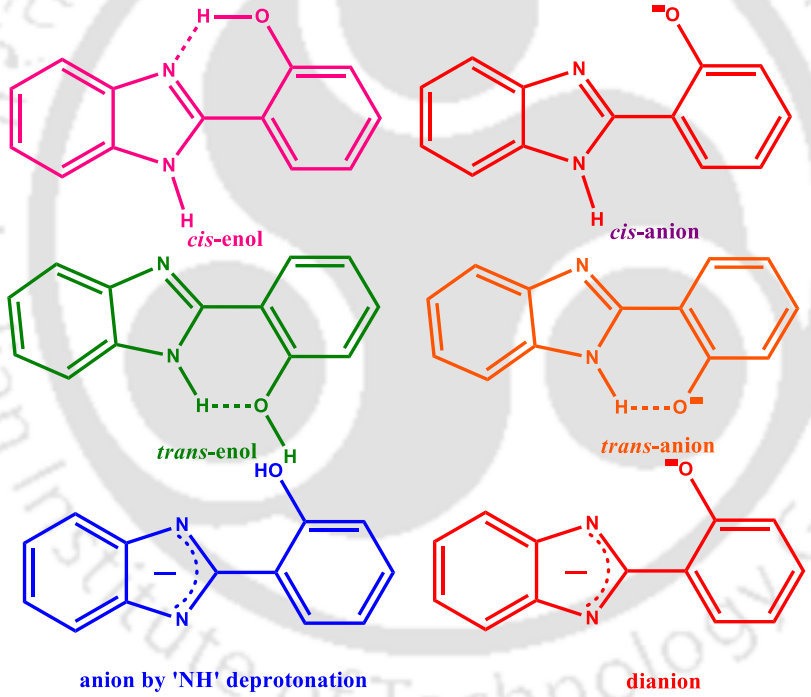


**Chart 3.1.1** Conformers of HPBI and its different anions.

### 3.1.1 Quantum chemical calculation

The *cis*-enol conformer possesses a planar geometry in the ground state in acetonitrile.[107] On the other hand, the ground state optimization of the *cis*-anion provides a twisted geometry with a dihedral angle 43° between the benzimidazole and the phenolate moiety (Annexure-B). The *trans*ition energy for the *cis*-anion is 3.28 eV ($\lambda_{max}^{abs}$ = 378 nm) with 0.32 oscillator strength. The possibility of rotation of the anionic species from the

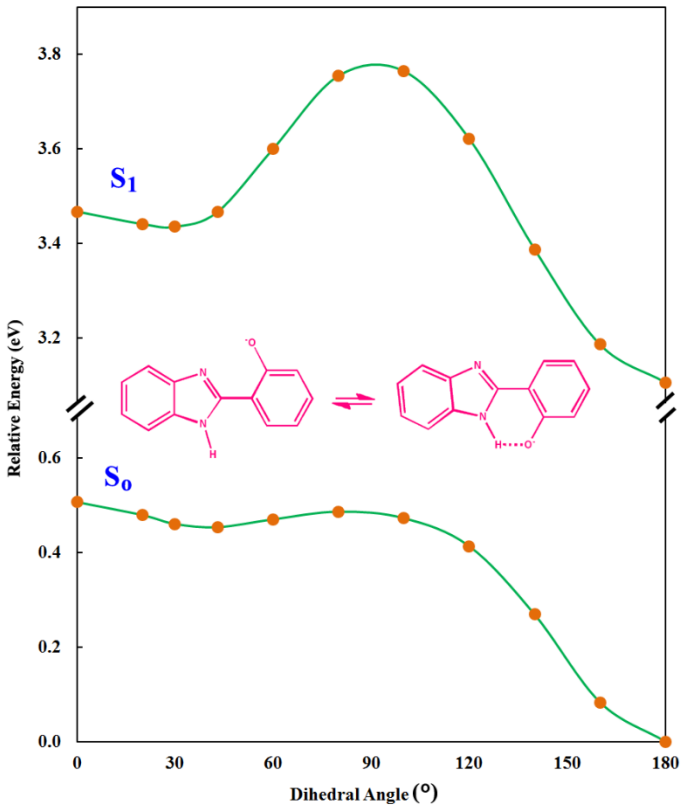


**Figure 3.1.1.** Potential energy diagram for the conversion of *cis*-anion to *trans*-anion in the ground and the excited state with acetonitrile as medium. The relative energy has been plotted with respect to the ground state *trans*-anion energy (-18660.1032 eV).

*cis* to the *trans* conformer were studied theoretically by optimizing different geometries of preset torsional angles between the benzimidazole and the phenolate moiety (Figure 3. 1.1). A very low energy barrier is observed for the conversion of the *cis*-anion to the *trans*-anion whereas, the barrier for the reverse process is very high. A fully optimized *trans*-anion in ground state holds a planar structure (Annexure-B) and is more stable than the *cis*-anion. As mentioned earlier, this is due to the formation of intramolecular hydrogen bond between the 'NH' proton and the deprotonated phenolate ion. The longer wavelength transition for the *trans*-anion is 364 nm with 0.47 oscillator strength. In both conformers the lowest energy transition is a $\pi$-$\pi^*$ transition from HOMO to LUMO. The ground state dipole moment for the *cis*- and the *trans*- anions are 12.9 D and 5.0 D, respectively. The energy difference between the *cis* anion and the *trans*-anion decreases in the excited state with respect to the ground state. However, the rotation barrier increases considerably for both the rotamers in the excited state. The calculated emission maxima for the *cis* and the *trans*-anions are 439 nm and 421 nm, respectively. The ground state optimized structure of the dianion has a twisted geometry with a

dihedral angle of 74° between the deprotonated benzimidazole and phenolate moiety (Annexure B). The calculated excitation maximum of dianion is 324 nm and its dipole moment is 7.8 D.

### 3.1.2. Interaction of the fluoride anion with HPBI in acetonitrile

In acetonitrile, HPBI shows an absorption spectrum with well resolved vibrational structures. For the initial addition of TBAF, only a small decrease is observed in absorbance without any spectral shift. However an additional hump emerges at the longer wavelength region. Upon further addition of TBAF, the absorption band (at 316, 330 nm) undergoes a bathochromic shift without any change in the vibrational pattern (Figure 3.1.2.A). The additional hump appears clearly in the longer wavelength region at 375 nm. At higher concentration a new band emerges at 358 nm. With further increase in fluoride concentration a little increment in absorbance around 358 nm and a small decrease in absorbance around 375 nm are found. An absorbance ratio plot is shown in Figure 3.1.2.B.

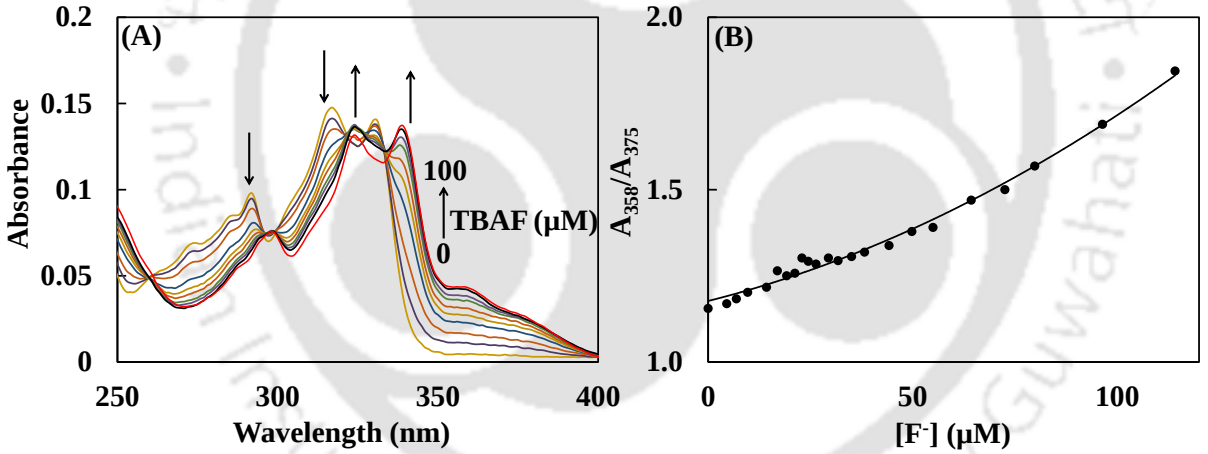


**Figure 3.1.2.** (A) Absorption spectra of HPBI at different TBAF concentrations in acetonitrile. (B) The ratio of absorbance at 358 nm and 375 nm ($A_{358}/A_{375}$) with increasing fluoride concentration.

First, the emission nature of the new species were followed by exciting at 360 nm (Figure 3.1.3.A). Like the absorption spectra different emission spectra are observed at low and high fluoride concentrations. Up to 12 μM of TBAF, a band arises at 412 nm with addition of TBAF. With further addition of TBAF, the band maximum shifts from 412 nm to 421 nm. The excitation spectra recorded at 412 nm in 12 μM of TBAF and 421 nm in 100 μM of TBAF exhibit longer wavelength absorption band at 365 nm and 375 nm, respectively (Figure 3.1.3.B). When excited at 325 nm before the addition of TBAF, the molecule exhibits a strong tautomer emission at 460 nm with a very weak normal

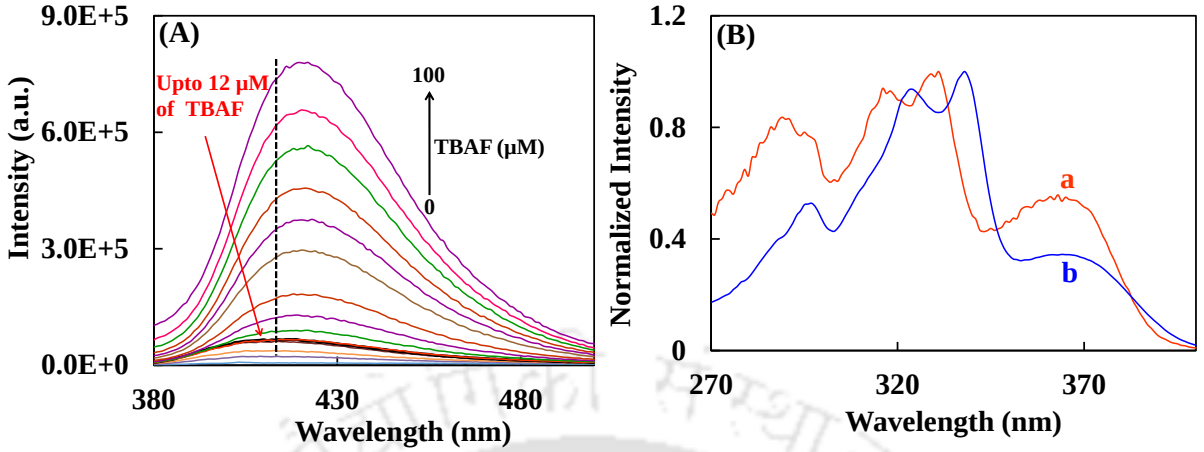


**Figure 3.1.3.** (A) Emission spectra of HPBI at different TBAF concentrations in acetonitrile, $\lambda_{ex}$ = 360 nm. (B) Normalized excitation spectra of HPBI in presence of (a) 12 μM of TBAF and (b) 100 uM of TBAF, $\lambda_{em}$ = 420 nm.

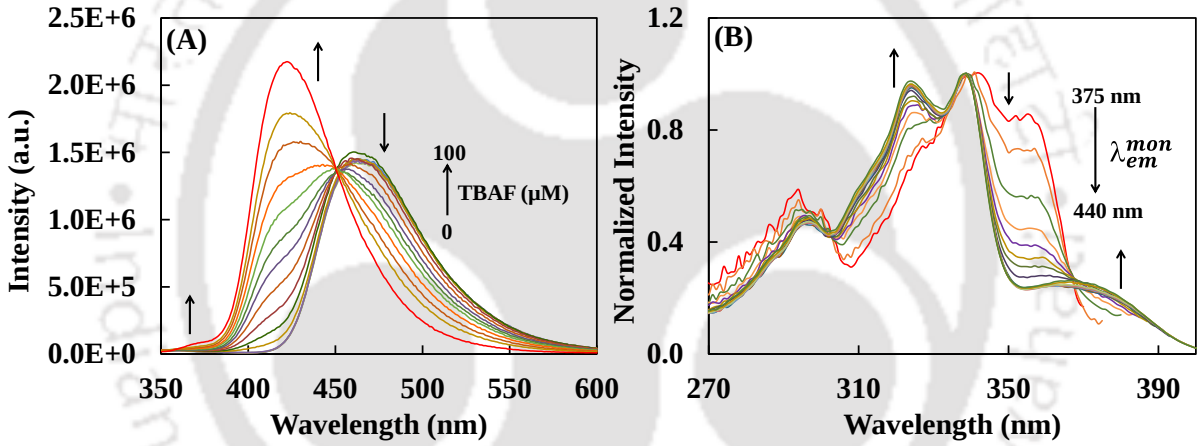


**Figure 3.1.4.** (A) Emission spectra of HPBI at different TBAF concentrations in acetonitrile, $\lambda_{ex}$ = 325 nm. (B) Normalized excitation spectra of HPBI in acetonitrile in the presence of 100 μM of TBAF monitored at different emission wavelengths.

emission at 350 nm. For the initial addition of TBAF, the tautomer emission slowly decreases and at higher concentration, the 421 nm band gradually increases (Figure 3.1.4.A). At very high concentration another low intensity emission is observed at 380 nm along with the 421 nm emission (Figure 3.1.4.A). The excitation spectra in 100 μM of TBAF solution, monitored at different wavelength are shown in Figure 3.1.4.B. When monitored at longer wavelengths, the excitation spectra appear almost similar to the absorption spectrum with maxima at 322 nm, 338 nm along with a hump at 375 nm. When monitored at shorter wavelengths, the excitation spectra seem different with maxima at 295 nm, 340 nm and 358 nm (Figure 3.1.4.B). To further investigate the emitting species, the fluorescence decays are monitored at 421 nm by excitation at 336

nm and 375 nm. Both decays fit mono-exponentially with an emission lifetime 3.0 ns. But a different lifetime, 1.0 ns is obtained for the 380 nm emission.

### 3.1.3. Interaction of hydroxyl anion with HPBI in aprotic solvents

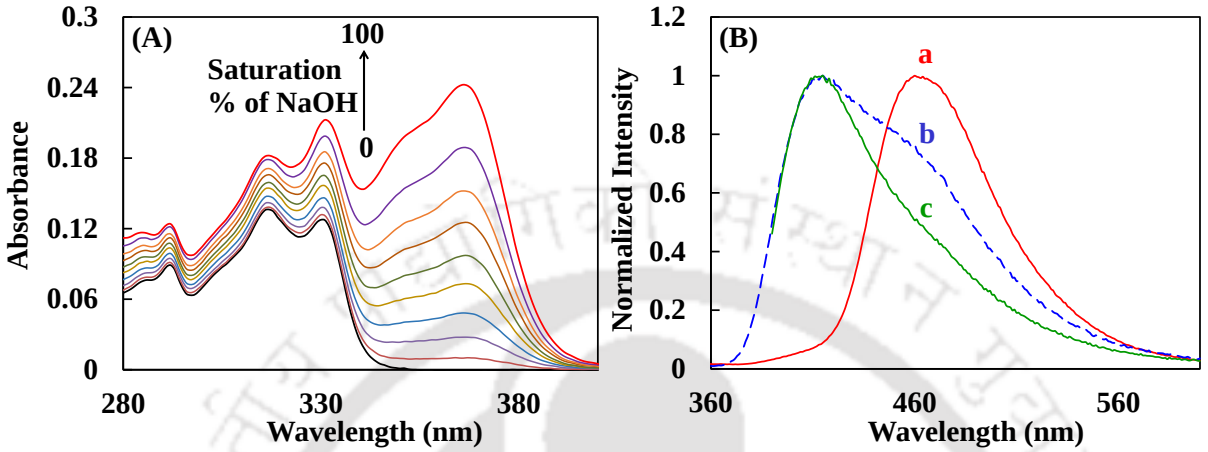


**Figure 3.1.5**. (A) Absorption spectra of HPBI in acetonitrile at different NaOH concentrations. (B) Normalized emission spectra of HPBI in NaOH saturated acetonitrile, (a) $\lambda_{ex}$ = 320 nm, (b) $\lambda_{ex}$ = 375 nm, (c) $\lambda_{ex}$ = 350 nm.

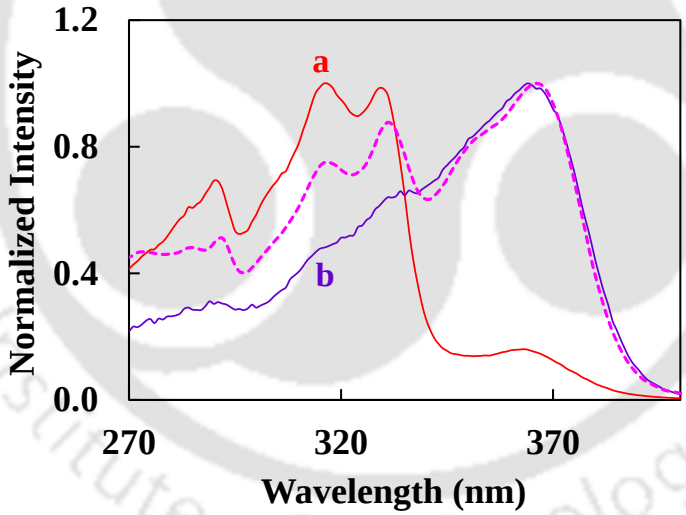


**Figure 3.1.6.** Normalized excitation spectra of HPBI in NaOH saturated acetonitrile (a) $\lambda_{em}$ = 460 nm and (b) $\lambda_{em}$ = 420 nm along with the absorption spectrum (dotted line) of the solution.)

With addition of sodium hydroxide, a hyperchromic effect is observed without any shift in the absorption spectrum of HPBI in acetonitrile (Figure 3.1.5A). In addition, a new band also appears at longer wavelength (365 nm) along with a small hump at 355 nm. The emission spectra of HPBI in NaOH saturated acetonitrile are recorded at different excitation (Figure 3.1.5B). When excited at 320 nm, like the absorption maxima the emission maximum remains unaffected and the 460 nm tautomer emission is observed. The excitation at longer wavelength results in a new emission band at 412 nm. The band

maximum matches with the band maximum observed for HPBI at low fluoride concentration (Figure 3.1.3.A). The excitation spectra monitored at 460 nm and 420 nm are compared with the absorption spectrum in Figure 3.1.6.

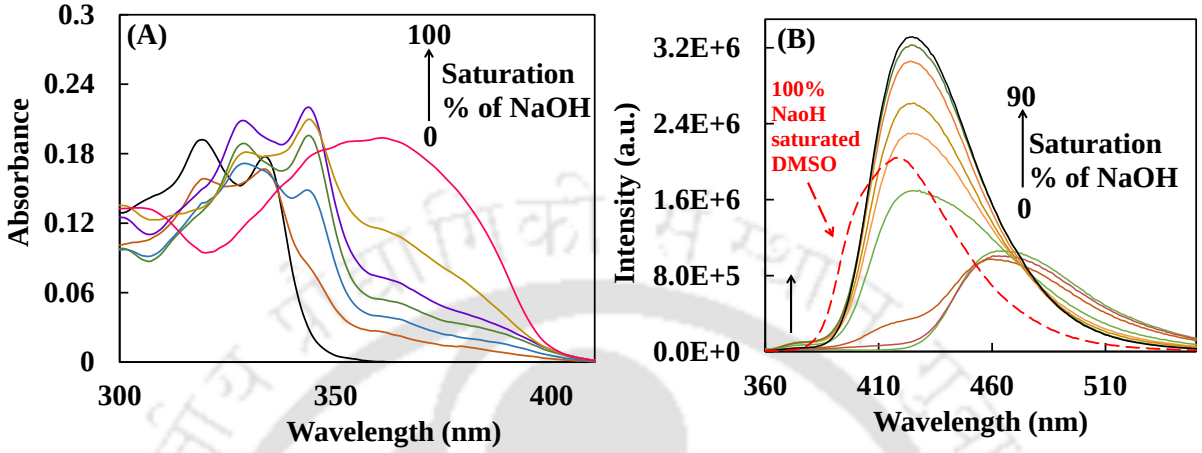


**Figure 3.1.7** (A) Absorption spectra of HPBI in DMSO with increasing NaOH concentration. (B) Emission spectra of HPBI in DMSO with increasing NaOH concentration. $\lambda_{ex}$ = 340 nm.

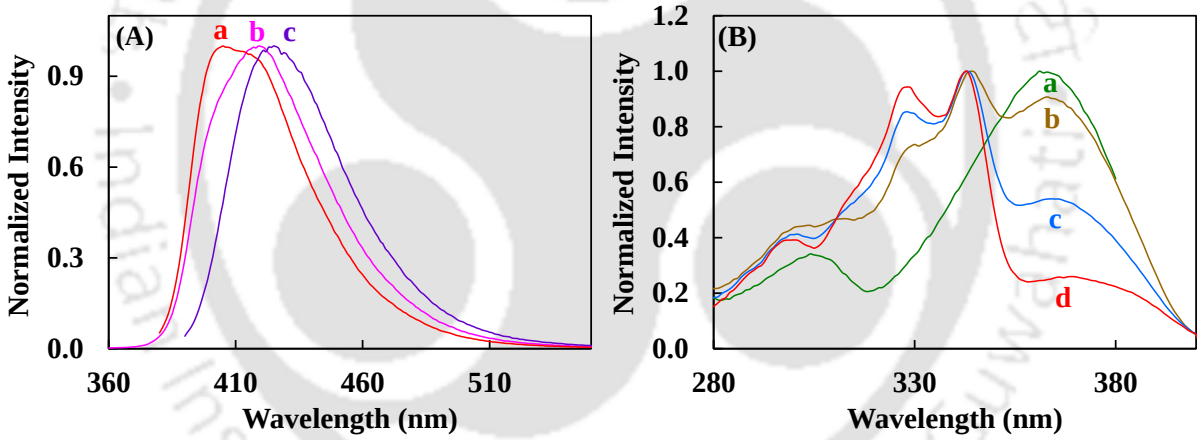


**Figure 3.1.8** (A) Normalized emission spectra of HPBI in NaOH-saturated DMSO upon excitation at (a) 360 nm, (b) 340 nm, (c) 375 nm. (B) Normalized excitation spectra of HPBI in NaOH-saturated DMSO, (a) $\lambda_{em}$ = 390 nm, (b) $\lambda_{em}$ = 420 nm, (c) $\lambda_{em}$ = 430 nm, (a) $\lambda_{em}$ = 460 nm.

A similar study was also performed in DMSO medium which has higher dielectric constant (ε = 46.7) than acetonitrile (ε = 37.5). The absorption spectra of HPBI in DMSO with gradual increase of NaOH strength (Figure 3.1.7.A) are different from the absorption spectra observed in alkaline acetonitrile (Figure 3.1.5.A). But the result is parallel with the observation in presence of TBAF in acetonitrile medium (Figure 3.1.2.A). The emission spectra are also found to be similar (Figure 3.1.7.B and Figure 3.1.4.A), i.e. the tautomer emission is replaced by a new blue shifted emission (422 nm) upon addition of alkali, and at higher concentration an additional small band is found

at 380 nm. The excited state lifetimes observed for 422 nm and 380 nm emissions are 3.3 ns and 1.0 ns, respectively. However, both absorption and emission spectra in NaOH saturated DMSO are different from those at lower concentrations. A very broad absorption spectrum is observed with wavelength maximum at around 365 nm (Figure 3.1.7.A). The emission spectra of HPBI in this solution are also found to be excitation wavelength dependent (Figure 3.1.8.A). Excitation at 340 nm produces a band with maximum at 420 nm whereas excitations at 360 nm and 375 nm yield emission bands with maxima at 404 nm and 422 nm, respectively. The excitation spectra monitored at different wavelengths suggest that a species with excitation band maximum at 365 nm is responsible for the emission in the 404 nm region (Figure 3.1.8.A). In contrast, the longer wavelength emission is found to be same as that observed at unsaturated alkali solution (422 nm band) and the 421 nm emission band of HPBI in presence of TBAF in acetonitrile. The fluorescence decays monitored at different emission maxima using different light sources (336 nm and 375 nm) are monoexponential with fluorescence lifetime of 3.3 ns. In NaOH saturated DMSO solution, the 380 nm band completely vanishes. The absence of 1.0 ns decay further substantiates the disappearance of 380 nm band.

### 3.1.4. NMR titrations

Wang et al. demonstrated the NMR spectral changes of HPBI with addition of TBAF.[102] But they did not report the spectrum at high TBAF concentration. Due to low solubility of HPBI in acetonitrile-$d_3$, the NMR experiments was carried out only in DMSO-$d_6$. The NMR peaks assignment for HPBI in DMSO was reported elsewhere.[35, 102] The NMR peaks of both the 'NH' and 'OH' disappear with addition of TBAF (Figure 3.1.9.b). In 1:1 equivalent (HPBI:TBAF) solution, the peak of H-6' proton is significantly shifted downfield ($\Delta\delta$ = 0.172 ppm) and all the other peaks of protons shift to upfield. NMR peaks of H-4 and H-7 merge after addition of TBAF. Similarly the peaks of H-5 and H-6 protons merge with each other. The H-3' and H-5' proton peaks which were closer to each other before addition of TBAF, move apart from each other after addition of TBAF. However, with further addition of TBAF all the peaks including that of H-6' proton exhibit an up field shift (Figure 3.1.9.c). A little different type of spectral pattern is observed with the addition of NaOH (Figure 3.1.9.d). A very little downfield shift ($\Delta\delta$ = 0.004 ppm) is noticed for the peak of H-6' proton. The upfield shift in peaks of other protons in NaOH saturated DMSO (Figure 3.1.9.e) are more than those observed in presence of TBAF. However changes appear for peaks of H-4, H-7 proton and H-5, H-6

are similar to the changes observed with TBAF addition. The relative spectral shift observed for H-3′ and H-5′ proton are also parallel.

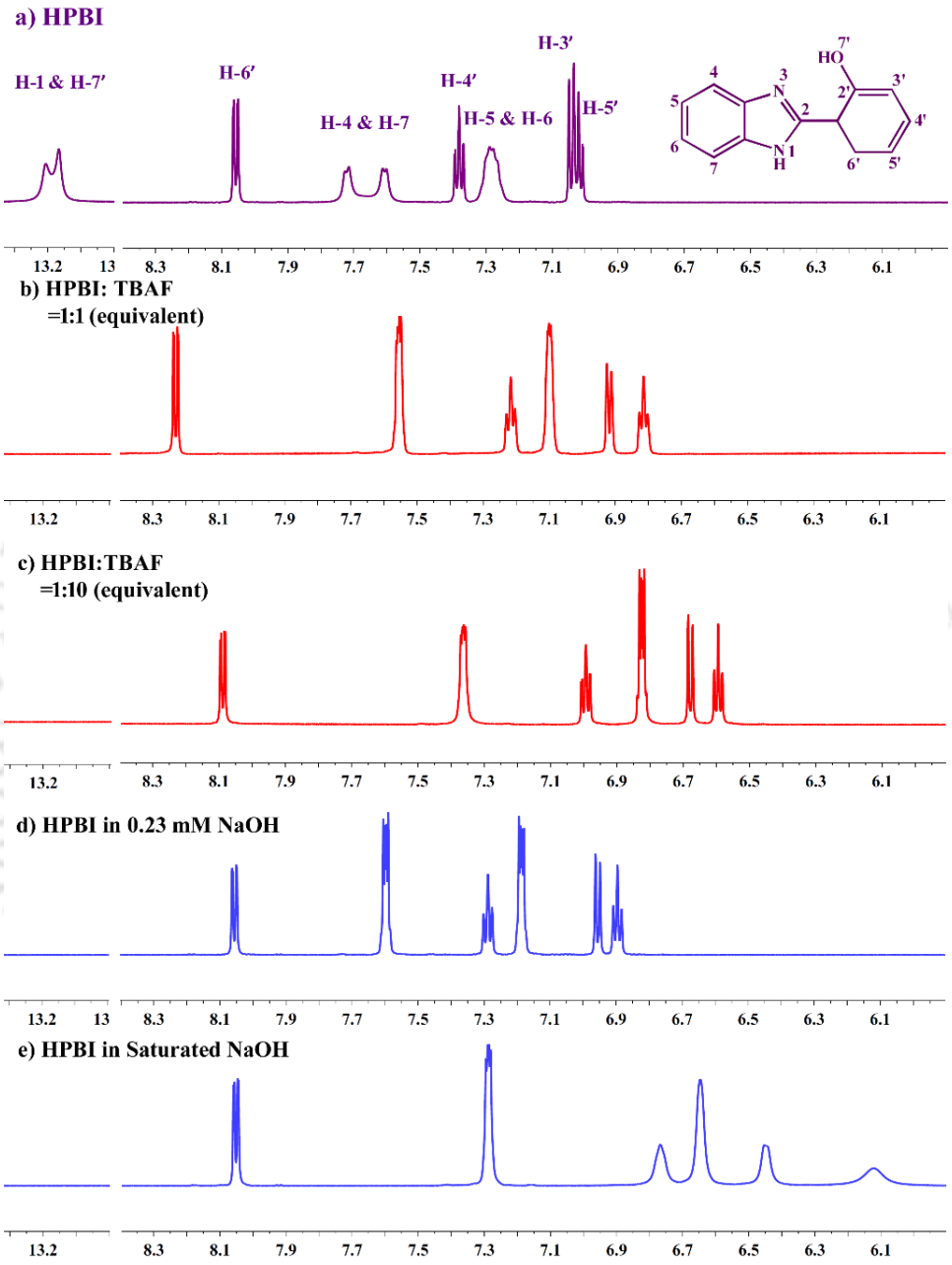


**Figure 3.1.9.** $^{1}$H NMR spectra of HPBI in (a) absence of base, (b) presence of 1 : 1 equivalent of TBAF, (c) presence of 1 : 10 equivalent of TBAF, (d) presence of 0.23 mM NaOH and (e) in NaOH-saturated DMSO-$d_6$.

### 3.1.5. Existence of *cis*-anion and dianion

The excitation and emission spectral band maxima of HPBI in different environment aresummarized in Table 3.1.1. In the ground state, the *cis*-enol and the *trans*-enol of

HPBI equilibrate with each other in acetonitrile. The *cis*-enol is more stable than the *trans*-enol in the ground state.[72, 108] The well resolved vibrational structures (316, 330 nm) present in the absorption spectrum of HPBI correspond to the predominating *cis*-enol conformer.[72] A small red shift in the absorption and the excitation spectra (324, 338 nm) in 100 μM of TBAF suggests a hydrogen bonding interaction between the fluoride ion and the *cis*-enol. The species was labelled as *cis* H-bond complex (Scheme 3.1.1). The additional large red shifted band (375 nm) in presence of TBAF suggests the complete deprotonation of HPBI by intermolecular proton transfer to the fluoride ion. HPBI has two acidic centers the 'OH' group and the 'NH' group. Deprotonation of either of the proton would generate an anion. The deprotonation of the 'NH' proton will produce one anion, but the deprotonation of the 'OH' group may generate either the *cis*-anion or the *trans*-anion (Chart 3.1.1). Dogra et al. reported that in aqueous medium, only the *trans*-anion exists due to the stabilization by intramolecular hydrogen bond between the oxygen of the phenolate ion and the 'NH' proton (Chart 3.1.1.).[72] Wang et al. suggested that in DMSO, in presence of fluoride ion, the 'NH' proton was deprotonated to form the anion (Chart 3.1.1.).[102] It is well known that in HPBI, the benzimidazole is the charge acceptor moiety and the phenolic ring is the charge donor moiety.[35] The deprotonation of the 'NH' proton would resist the charge flow from the phenyl ring to the benzimidazole ring which reduces conjugation. Therefore, it must produce a blue shift in compare to the neutral molecule. Such a blue shift upon deprotonation of the azole 'NH' proton is reported in several other 2-phenyl benzimidazole derivatives and related molecules.[82, 109, 110] On the other hand, the deprotonation of the 'OH' group increases

**Table 3.1.1.** Excitation maxima ($\lambda_{max}^{ex}$, nm) and emission maxima ($\lambda_{max}^{em}$, nm) of HPBI in different medium.

| Solvent | Base | $\lambda_{max}^{ex}$ | $\lambda_{max}^{em}$ |
|---|---|---|---|
| Acetonitrile | [Base] = 0 μM | 316, 330 | 460 |
| | [TBAF] = 12 μM | 316, 330 | 460 |
| | | 365 | 412 |
| | [TBAF]= 100 μM | 324, 338 | 421 |
| | | 375 | 421 |
| | | 339, 358 | 380 |
| | Saturated NaOH | 316, 330 | 460 |
| | | 365 | 412 |
| DMSO | [Base] = 0 μM | 320, 334 | 464 |
| | [TBAF]= 100 μM | 330, 344 | 422 |
| | | 375 | 422[a] |
| | [NaOH] = 0.37 mM | 328, 344 | 422 |
| | | 375 | 422 |
| | | 362 | 380 |
| | Saturated NaOH | 328, 344 | 422 |
| | | 375 | 422 |
| | | 365 | 404 |

[a]Matches with ref. 102

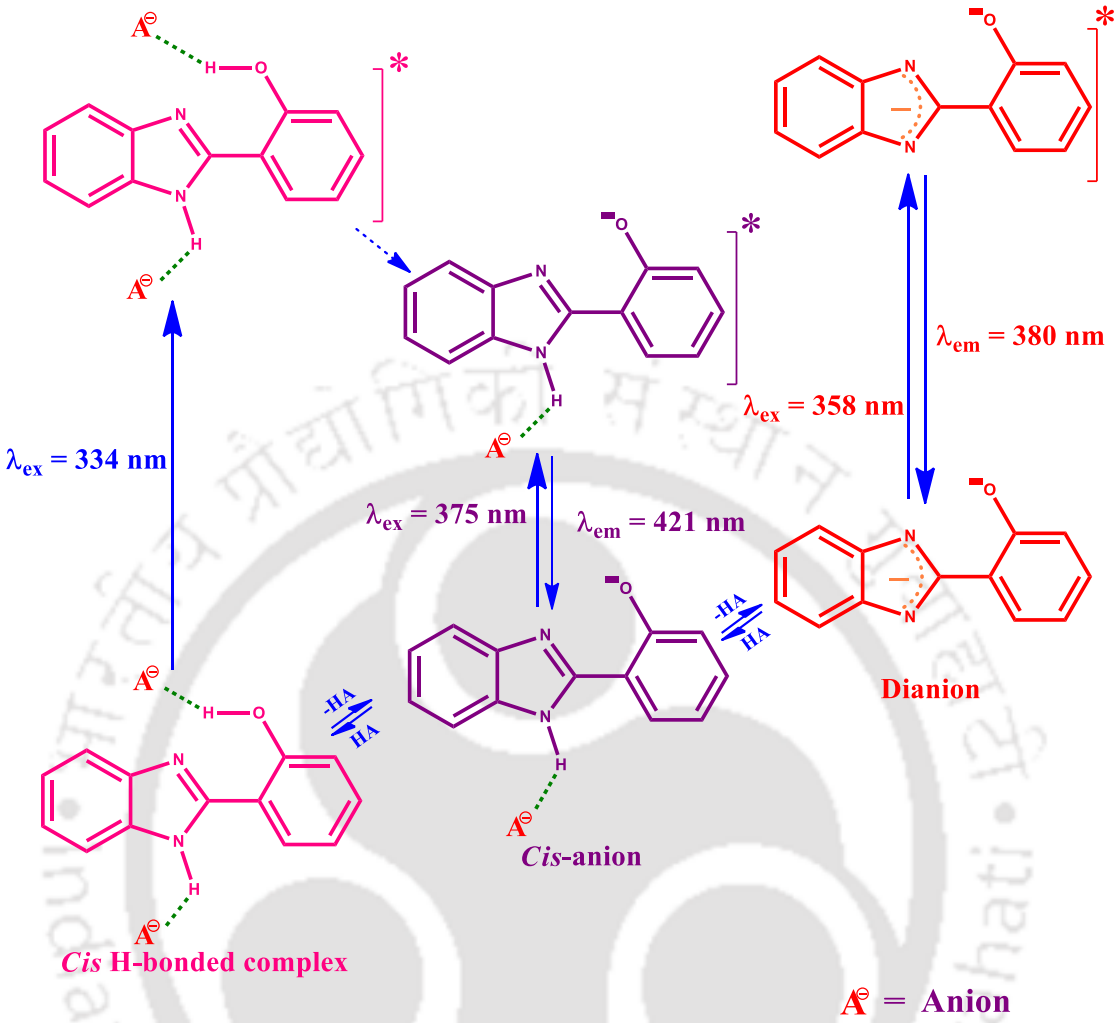


**Scheme 3.1.1.** The different species those exist in the ground state and the excited state at higher concentrations of fluoride in acetonitrile.

the charge flow from the phenolate ring to the benzimidazole ring, which causes a bathochromic shift.[72, 73, 111] The observed red shift in the excitation and the emission spectra suggests that the absorption band at 375 nm and the corresponding emission band at 421 nm are due to the anion formed by deprotonation of the 'OH' group rather than the 'NH' group. Further, the 'OH' proton is more acidic than the 'NH' proton. The $pK_a$ for the 'OH' group and the 'NH' group are ~ 9 and ~12, respectively.[72, 112] Therefore, the 'OH' group is expected to get deprotonated prior to the 'NH' group. The excitation of the *cis* H-bond complex also results in 421 nm emission. This suggests that the 'OH' proton which becomes more acidic upon excitation, transfers the acidic proton to the fluoride ion and generates the same anion in the excited state. The formation of the new 358 nm absorption band at higher concentration suggests the formation of a dianion by the deprotonation of both 'OH' and 'NH' protons. Dogra et al. also reported the

formation of dianion in the ground state at H- 16.[72] As expected, the absorption and emission spectra of the dianion is blue shifted compared to those of anion due to the deprotonation of the 'NH' proton. The corresponding emission spectrum at 380 nm can be assigned to the dianion emission. The emission from the di-anionic species is very similar to the emission from the anion of 2-(2'-methoxyphenyl)benzimidazole, which is formed by the deprotonation of the 'NH' proton.[72] Dogra et al. reported the presence of only *trans*-anion in aqueous medium.[72] Under normal conditions, the *trans*-anion is more stable than the *cis*-anion due to the intramolecular hydrogen bond (Chart 3.1.1). However, the 375 nm absorption and the 421 nm emission bands were assigned to the *cis*-anion rather than the *trans*-anion. The following evidences substantiate this assignment: (i) the absorption and the emission spectra of the anion are more red shifted than those in aqueous medium where *trans*–anion was detected.[20] Theoretical calculations also predict that the spectral maxima of *cis*-anion are red shifted compared to the *trans*-anion. (ii) According to the non-equilibrium of excited rotamers (NEER) principle, due to the exchange of single bond and double bond character in lowest excited state, the equilibrium between the conformers of conjugated polyenes is not feasible in the lowest excited state.[113] The potential energy diagram also shows that the barrier for rotation increases substantially in the excited state (Figure 3. 1.1). Consequently, unlike in the ground state, the rotation of the *cis*-anion is not feasible in the excited state (Figure 3.1.1.). Therefore, the anion that is formed upon excitation of the *cis* H-bond complex should be the *cis*-anion. The excitation of *cis* H-bond complex also produces the 421 nm anionic emission. Thus, the 421 nm anionic emission corresponds to the *cis*-anion. The excitation at the 375 nm anionic absorption band also results in 421 nm emission. Hence, the 375 nm absorption band can be attributed to the *cis*-anion. (iii) Dogra et al. reported the absence of dianion in the excited state even at H-16. They attributed this to the strong intramolecular hydrogen bond between the 'NH' proton and the phenolate oxygen in the excited *trans*-anion whose basicity enhances in the excited state. Such a hydrogen bond does not exist in the *cis*-anion. Therefore, the dianion formation in the excited state is only possible for the existence of the *cis*-anion but not for the *trans*-anion in solution. Experimentally the dianionic emission was observed at 380 nm along with the 421 nm emission. This further substantiates, the existing anion is the *cis*-anion and not the *trans*-anion. Equilibrium between the different species in acetonitrile at higher concentration of fluoride ion are summarized in Scheme 3.1.1. However, at lower concentration (12 μM) of TBAF, the observed bathochromic

shift in absorption spectrum and its corresponding emission spectrum are smaller in comparison to those of *cis*-anion. This 365 nm excitation spectrum and the 412 nm emission spectrum may be attributed to the *trans*-anion. As predicted by the theoretical calculation the absorption and emission spectrum of the *trans*-anion are red shifted compared to neutral HPBI, but blue shifted with respect to the *cis*-anion. The theoretically predicted transition energies of the anions agree with the experimental values. At this concentration (12 μM), no shift in the absorption band of the neutral *cis*-enol is detected. Upon excitation at 320 nm, only the tautomer band is observed from the solution, and no anionic emission band is found. This shows the weaker interactions and the absence of the *cis* H-bond complex.

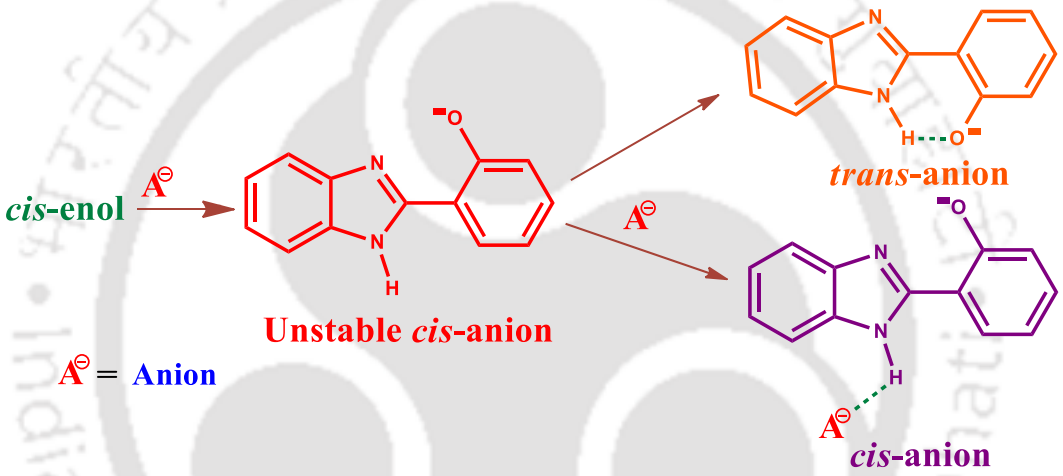


**Scheme 3.1.2.** Formation of stable *trans*-anion (at lower [A$^-$]) and *cis*-anion (at higher [A$^-$]) from *cis*-enol.

The most interesting aspect of the present experimental finding is the observation of the *cis*-anion. The key factor in the existence of the *cis*- or *trans*-anion relies on the stabilization of the 'NH' proton. As mentioned earlier, existence of the intramolecular hydrogen bond provides an extra stability for the *trans*-anion over the *cis*-anion. Not only the phenolate is negatively charged, but the fluoride ion is also negatively charged. In aprotic solvents where the stabilization of the ions is feasible only by dipolar stabilization, there will be competition between the negatively charged phenolate ion and fluoride ion to form a hydrogen bond with the 'NH' proton of the fluorophore. HPBI in neutral form exists predominantly as the *cis*-enol. The formation of the *cis*- and *trans*-anions from the *cis*-enol are explained in Scheme 3.1.2. For initial addition of TBAF, the amount of the fluoride ion may not be sufficient enough to form hydrogen bond with NH proton. Hence the phenolate ion of the initially formed unstable *cis*-anion rotates to form hydrogen bond with the 'NH' proton. This generates a more stable *trans*-

anion. The energy barrier for the rotation of *cis*-anion in the ground state is also found to be very low (Figure 3.1.1). Conversely, at higher concentration when sufficient amount of fluoride is present, they form strong hydrogen bond with the 'NH' proton (Scheme 3.1.2). Since no free 'NH' proton is available for hydrogen bonding the rotation is averted and the molecule exists as the *cis*-anion. Furthermore, the theoretical calculations predict that upon interaction with fluoride ion the *cis*-anion is more stabilized than the *trans*-anion by 3.6 $kJmol^{-1}$ (Figure 3.1.10, Annexure-B). The fluorescence quantum yield for the *cis*-anion is 0.74.

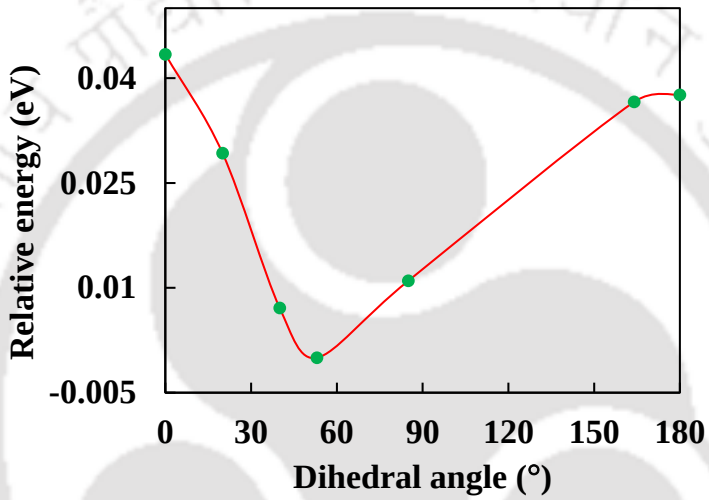


**Figure 3.1.10.** Simulated ground state potential energy diagram of HPBI anions in the presence of fluoride at different preset dihedral angles. The relative energy is plotted with respect to the *cis*-anion energy (-21380.9895 eV).

### 3.1.6. Effect of NaOH

In alkaline acetonitrile, an enhancement in absorbance is observed at 316 nm and 330 nm. However, upon excitation at 320 nm only the tautomer emission is observed. It confirms the weaker interaction between the hydroxyl ion and HPBI same as at 12 μM of TBAF. On the other hand, excitation at longer wavelength results in the 412 nm emission, which corresponds to the *trans*-anion (like as in 12 μM of TBAF). Since NaOH is a strong electrolyte it dissolves in very low quantity in acetonitrile. The dissociation of NaOH is also less in acetonitrile which has a moderate dielectric constant (ε = 37.5). The major difference between the interaction of TBAF and NaOH with HPBI lies in the stabilization of the free 'NH' proton. TBAF is a highly soluble salt and it dissociates enough in acetonitrile. As shown earlier, at higher concentration of TBAF fluoride forms a strong H-bond complex with 'OH' as well as 'NH' groups (Scheme 3.1.1.).

The scenario is different in higher dielectric DMSO solvent (ε = 46.7). In DMSO, the solubility of the base is higher and its dissociation is also higher. Below the saturation limit of NaOH, HPBI behaves similarly as observed with TBAF in acetonitrile (Table 3.1.1). Different excitation spectra observed for 422 nm and 380 nm emission in alkaline DMSO medium, establishes the existence of two different excited species, *cis*-anion and dianion. Two different ground state precursors are found for 422 nm emission. They matche with the *cis* H-bond complex and *cis*-anion. The excitation band of the 380 nm emission also agrees with the dianion excitation band (Table 3.1.1.). In the NaOH saturated solution, the blue shifted band, appeared in the emission and the excitation spectra in addition to those of *cis*-anion, match with the respective bands of the *trans*-anion. The waning of dianion emission (Figure 3.1.7.B) in NaOH saturated DMSO also confirms the formation of *trans*-anion. It may be that in the saturated solution ion pair formation might have led to decrease in relative amount of the free hydroxyl ion. Consequently, the stabilization of the 'NH' proton by the anion decreases and this leads to the decline in the population of stable *cis*-anion. Therefore, significant amount of *cis*-anions are converted into *trans*-anions.

### 3.1.7. Interpretation of NMR spectra

**Table 3.1.2.** NMR peak shifts for different protons of HPBI in presence of different bases with respect to that of HPBI before addition of base.

| | H-6′ | H-5′ | H-4′ | H-3′ |
|---|---|---|---|---|
| HPBI : TBAF (1:10) | -0.01 | 0.43 | 0.39 | 0.37 |
| HPBI in saturate NaOH | 0.005 | 0.9 | 0.61 | 0.595 |

The disappearance of 'NH' and 'OH' peaks with increasing fluoride concentration infers the formation of strong hydrogen bonds by the fluoride anion with HPBI. Increasing separation between the spectral lines of H-3′ and H-5′ indicates that the extent of influence of the hydrogen bond (at the phenolic center) on the *ortho* and *para* hydrogen of the phenol ring is different. Gradual increase in the fluoride anion population around the 'NH' group causes a through space interaction between the fluoride and the H-6′ proton, which leads to the downfield shift.[114] Moreover, the phenomenon indicates a planar *cis* geometry of HPBI with strong hydrogen bonding at H-1, H-6′ and H-7′. This indicates the formation of the *cis* H-bond complex. The strong interaction between the fluoride ion and the 'NH' proton weakens the N-H bond. As a consequence, the symmetric nature between the H-4 and H-7 protons increases. This generates a plane of symmetry in benzimidazole moiety which causes the peaks of H-4 and H-7 protons to merge. As the $pK_a$ for the 'OH' proton is lower than the 'NH' proton, the deprotonation

of 'OH' proton occurs first. Simultaneously, strong hydrogen bond with the 'NH' proton stabilizes the molecule enough and prevents the torsional rotation to form a *trans*-anion. The theoretical calculations predict a twisted geometry for the *cis* anion (Section 3.1.1, Annexure-B). The up field shift of H-6' spectra observed at higher fluoride concentration indicates the formation of anion and is attributed to the non-planarity of the molecule where through space interaction is hindered.

A clear distinction is noticed between the NMR spectral data of HPBI in saturated NaOH and in the presence of ten equivalents of TBAF (Table 3.1.2.). The observed downfield shift in the peak of H-6' proton in TBAF (10 equivalent) suggests that it is de-shielded by interaction with fluoride ion. However, the observed upfield shift in the peak of the same proton in NaOH saturated solution indicates a shielding effect which is consistent with non-interaction of hydroxyl ion due to the *trans*-geometry of the anion. The difference in the chemical shifts of H-3', H-4' and H-5' protons in both media are much higher. Thus, the NMR spectra confirm the formation of two different anions in NaOH and TBAF (Figure 3.1.9.). In presence of ten equivalents of TBAF *cis*-anion is formed, whereas, in NaOH saturated solution, *trans*-anion is generated via the rotation of inter-annular bond rotation.

### 3.1.8. Conclusion

The intermolecular proton transfer between HPBI and different anions were investigated in the ground and excited state in polar aprotic solvents. The intermolecular proton transfer leads to the anion formation; and HPBI exists not only as *trans*-anion, but also as *cis*-anion. The apparent extinction of the conformers relies on the stabilization of the azole 'NH' proton. Unstable *cis*-anion which is prone to rotation to form a more stable *trans*-anion can be stabilized by a strong chemical interaction with the NH proton. It is found that the *cis*-anion absorbs and emits at longer wavelength than the *trans*-anion. The theoretical calculations also substantiate the same. The calculations also predict that the torsional rotation barrier of *cis*-anion to *trans*-anion conversation is less in the ground state but increases significantly in the excited state. At low concentration of TBAF, HPBI exists in neutral and *trans*-anionic forms in both the ground and the excited states. However, at higher concentration, three different species are present, *cis* H-bond complex, *cis*-anion and dianion in the ground state. Upon excitation the *cis* H-bond complex undergoes proton transfer to form *cis*-anion. In the excited state, HPBI exists as *cis*-anion as well as dianion at higher concentration of TBAF. On the other hand, in NaOH saturated acetonitrile solution the equilibrium is

established between neutral and *trans*-anion due to low solubility and low dissociation of NaOH. The weakly interacting HPBI complex in NaOH solution shows a tautomer emission and the *trans*-anion exhibits a higher energy emission than that of the *cis* anion. However, in more polar DMSO both the *cis*-anion and *trans*-anion are found in NaOH saturated solution. When the NaOH amount is less the results are similar to those of TBAF addition.

## 3.2. Effect of nitrogen substitution on anion sensitivity and deprotonation of HPBI

A nitrogen substitution on the benzene ring of the benzimidazole moiety drastically changes the characteristics of the molecule.[115, 116] In water HPBI exists as a Zwitterion, whereas the pyridyl nitrogen substituted analogues, HPIP-b and HPIP-c (Chart 3.0) do not present in the Zwitter ionic form.[72, 117, 118] The pyridyl group which has a higher electron withdrawing ability, weakens the intramolecular hydrogen bond which is a major stabilizer of the *cis*-conformer. As a result the ground state *cis-trans* equilibrium is disturbed, and the relative population of the *cis*-enol of HPIP-b and HPIP-c is less than that of HPBI.[119] The quantum yields of nitrogenous analogues are also less than that of HPBI due to higher stabilization of the non-emissive charge transfer state in nitrogenous analogues.[72, 107, 116-118, 120, 121] On the other hand, the enhancement in the tautomer emission upon encapsulation in cyclodextrin or proteins is much higher for the nitrogenous analogues than that for HPBI.[35, 111, 122, 123] The sensitivity towards the

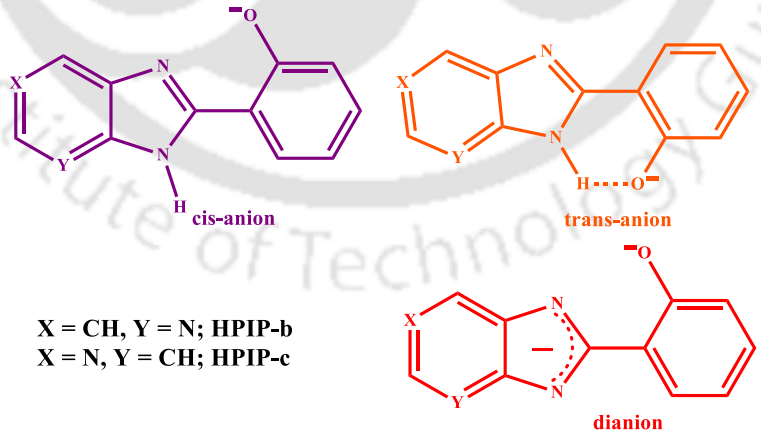


**Chart 3.2.1.** Structures of different anions.

metal ions also differs substantially on the nitrogen substitution.[42] HPBI is most sensitive towards Cu(II) ion whereas HPIP-b and HPIP-c molecule were most sensitive towards Co(II) and Pd(II) ions, respectively. As expected, with increasing electron

accepting capability of the acceptor moiety by nitrogen substitution, the deprotonation of the phenol in alkaline aqueous medium become easier. Therefore, $pK_a$ values for the neutral-anion equilibrium of HPIP-b (8.6) and HPIP-c (9.3) are lesser than that of HPBI (10).[72, 117, 118, 123] In this section, the effect of nitrogen substitution (i) on the existence of anions (Chart 3.2.1) and (ii) the anionic sensing ability are explored. Contrary to the expectation that the formation of anion would be facilitated in nitrogenous analogues as compared to HPBI, a different trend is observed in the formation of anion in polar aprotic solvent. However, the anion sensing abilities of the nitrogenous molecules are higher compared to HPBI.

### 3.2.1. Absorption nature of the fluorophores in presence of different anions

The absorption spectra of HPIP-b at different fluoride concentrations are shown in Figure 3.2.1.A. A moderate bathochromic shift with an additional tail at longer wavelength is found with increasing fluoride concentration. In contrary to fluoride, for initial addition of acetate, the main absorption band of HPIP-b does not change much but a new band appears at longer wavelength (Figure 3.2.1.B). Further increase in acetate concentration produces a moderate shift in the main absorption band of HPIP-b as observed in presence of fluoride. But the spectral changes due to the interaction of anions like hydrogen phosphate, chloride, bromide, iodide, thiocyanate, nitrate and sulfate are found too small (Figure 3.2.2.).

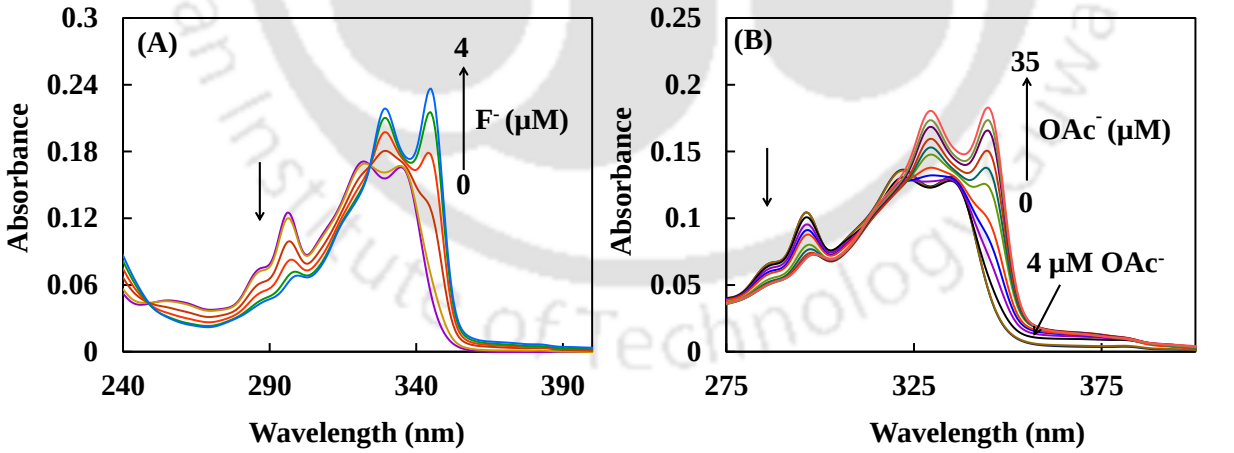


**Figure 3.2.1.** Absorption spectra of HPIP-b with increasing (A) fluoride and (B) acetate concentration in acetonitrile.

When the position of the pyridyl nitrogen is changed the effects of anions are different. The absorption spectra of HPIP-c at different fluoride concentration are depicted in Figure 3.2.3.A. Upon increasing fluoride concentration, unlike those of HPBI

and HPIP-b, no bathochromic shift is observed in the main absorption band of HPIP-c. Instead, an enhancement in absorbance is observed in the absorption spectra of HPIP-c with increasing fluoride concentration. At longer wavelength only a negligible increase is noticed in the absorbance. But same as in HPIP-b, the saturation limit for the fluoride anion is very low (5 μM). The molecule shows almost a similar sensitivity towards the acetate ion as that of fluoride. With other anions, such as hydrogen phosphate, hydrogen sulfate, chloride, bromide, iodide, thiocyanate and nitrate HPIP-c exhibits a low sensitivity (Figure 3.2.2.). The histogram in Figure 3.2.2 shows that the enhancement in absorbance depends on the presence and position of the substituted nitrogen.

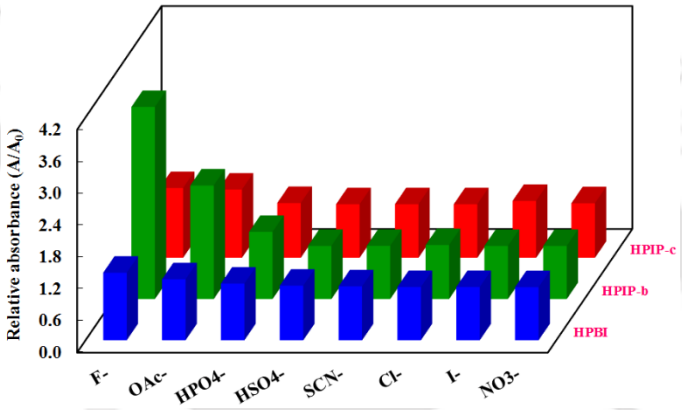


**Figure 3.2.2.** The relative absorbance (with respect to the absorbance in absence of anion) of HPBI (at 338 nm), HPIP-b (at 345 nm) and HPIP-c (at 316 nm) in presence of different anions (5 μM).

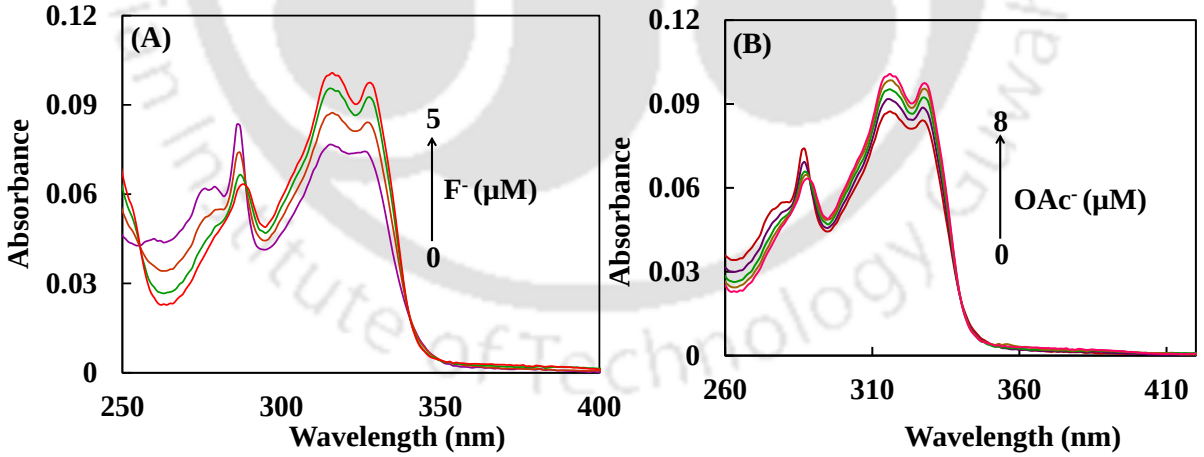


**Figure 3.2.3.** Absorption spectra of HPIP-c with increasing (A) fluoride and (B) acetate concentration in acetonitrile.

### 3.2.2. Emission nature of different species

HPIP-b exhibits a normal enol emission at 352 nm and a keto emission at 485 nm.[120] With increasing fluoride concentration, the normal as well as the tautomer emission decrease, and a new band appears at 455 nm (Figure 3.2.4.A). Upon excitation at 370 nm, the 455

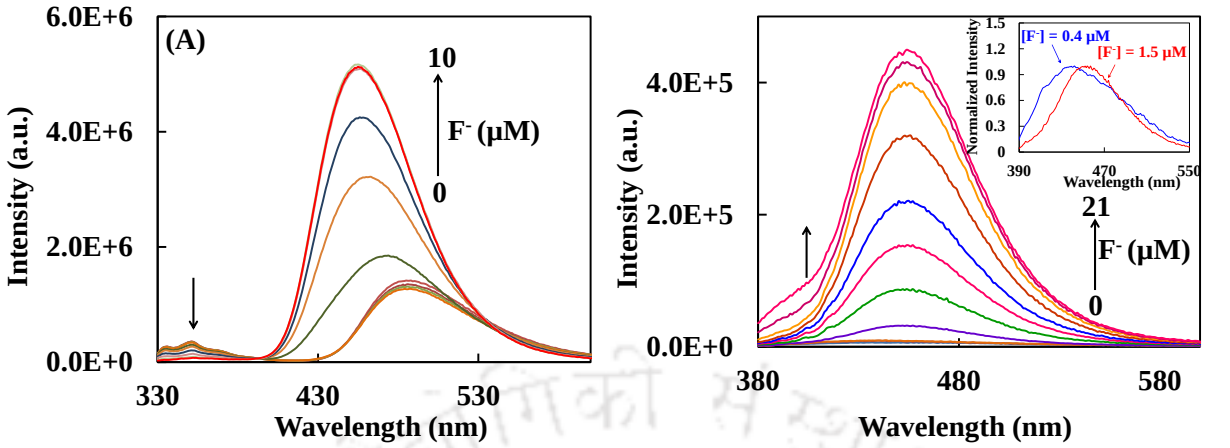


**Figure 3.2.4.** Emission spectra of HPIP-b with increasing fluoride concentration (A) $\lambda_{ex}$ = 320 nm, (B) $\lambda_{ex}$ = 370 nm. Normalized emission spectra of HPIP-b at different fluoride concentration is displayed in inset.

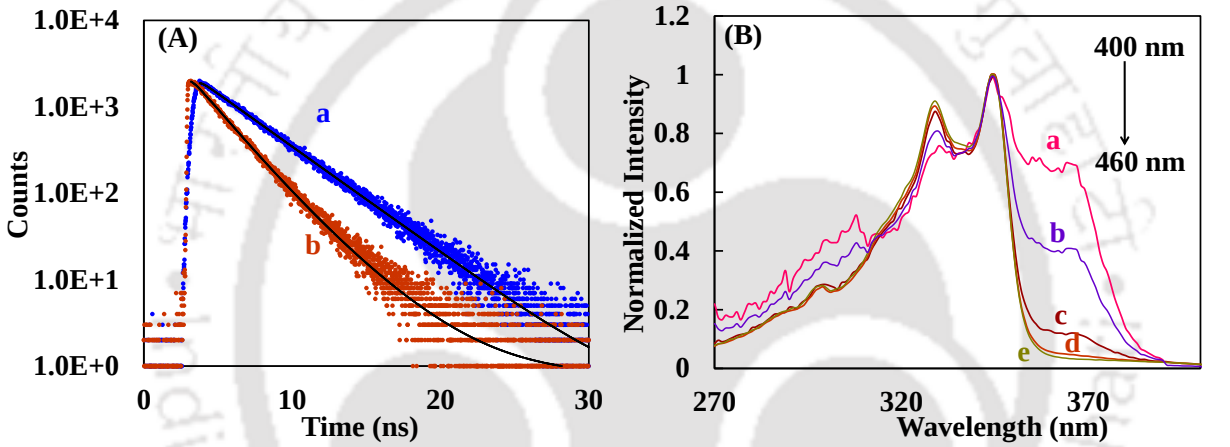


**Figure 3.2.5.** (A) Fluorescence decay of HPIP-b ($\lambda_{ex}$ = 336 nm) in presence of 10 μM of fluoride (a) $\lambda_{em}$ = 455 nm, (b) $\lambda_{em}$ = 410 nm. (B) Excitation spectra of the same solution monitored at different wavelengths (a) 400 nm, (b) 407 nm, (c) 415 nm, (d) 430 nm and (e) 460 nm.

nm emission emerges slowly with addition of fluoride (Figure 3.2.4.B). However, for the initial addition of fluoride (0.4 μM), a new band arises at 440 nm (Figure 3.2.4.B inset). At higher concentration the band position shifts to 455 nm. An additional band also appears as a shoulder at ~ 410 nm along with the 455 nm emission at high fluoride concentration. The intensities of both emissions increase with fluoride concentration. Since, the ~ 410 nm band is not very clear to substantiate the presence of additional emitting species, the fluorescence decays were measured at different emission wavelength (Figure 3.2.5.A). The fluorescence decays of HPIP-b in presence of saturated fluoride anion at 455 nm is monoexponential with lifetime 3.5 ns. However, the decay measured at 410 nm is biexponential with lifetimes 3.5 ns (18 %) and 2.0 ns (82 %). The observation of the second lifetime confirms the presence of an additional emission band which is buried under the 455 nm band. The excitation spectra of HPIP-b recorded in 10

μM of fluoride is shown in Figure 3.2.5.B. When monitored at shorter wavelengths, a new band appears at 365 nm. The band intensity decreases when monitored at longer wavelength. It infers that the species with band maximum at 365 nm is responsible for the shorter wavelength emission at ~ 410 nm. HPIP-b in presence of the acetate anion also exhibits identical changes in the emission spectra when excited at 320 nm. On contrary, the excitation at 370 nm results in an emission band maximum at 440 nm up to 1.2 μM of acetate (Figure 3.2.6.A). The 455 nm band appears only at higher acetate concentration. The 410 nm emission band also emerges at higher anion concentration. The normalized excitation spectra ($\lambda_{em}$ = 440 nm) of HPIP-b at low and high acetate concentrations are displayed in Figure 3.2.6.B. Though the band maxima of the both excitation spectra match with each other, a new band is observed at longer wavelength region at lower acetate concentration.

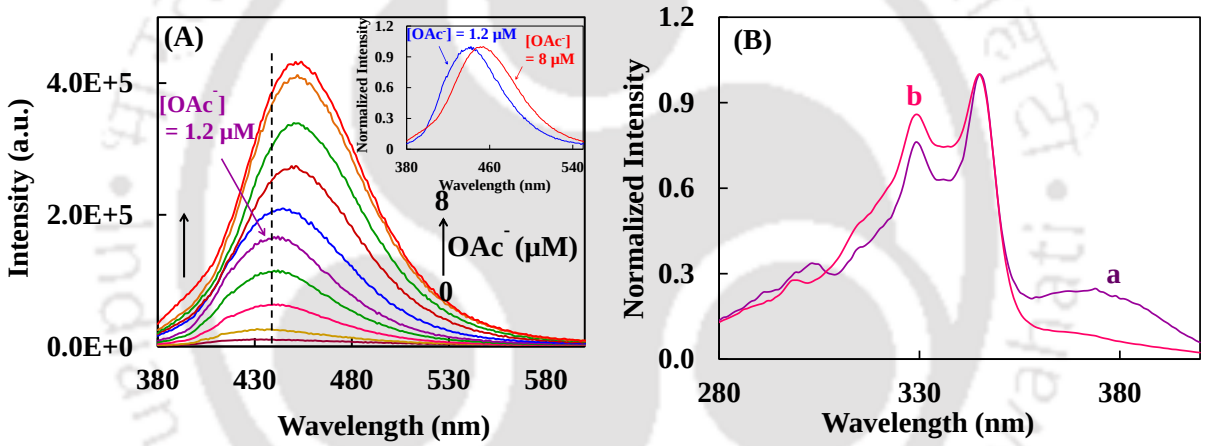


**Figure 3.2.6.** (A) Emission spectra of HPIP-b with increasing acetate concentration, $\lambda_{ex}$ = 370 nm. Normalized emission spectra of HPIP-b at low and high acetate concentration is shown in inset. (B) Normalized excitation spectra of HPIP-b at (a) low and (b) high acetate concentration, $\lambda_{em}$ = 440 nm.

On the other hand, HPIP-c exhibits a normal enol emission at 342 nm and a tautomer emission at 475 nm.[118] With increasing fluoride or acetate concentration the keto emission as well as normal emission decreases and a new band appears at 438 nm upon excitation at 320 nm (Figure 3.2.7.A). The normalized excitation spectra monitored at 430 nm at different fluoride concentration are shown in Figure 3.2.7.B. A new band at 370 nm is observed for HPIP-c at low fluoride concentration. On the other hand, at high fluoride concentration a very low intensity is observed at longer wavelength (370 nm). The excitation at 370 nm results in the emergence of a new band at 427 nm which gradually shifts to 438 nm with increasing anion concentration (Figure 3.2.8.A). Unlike, in HPIP-b no shoulder appears at shorter wavelength. But still a weak emission may be

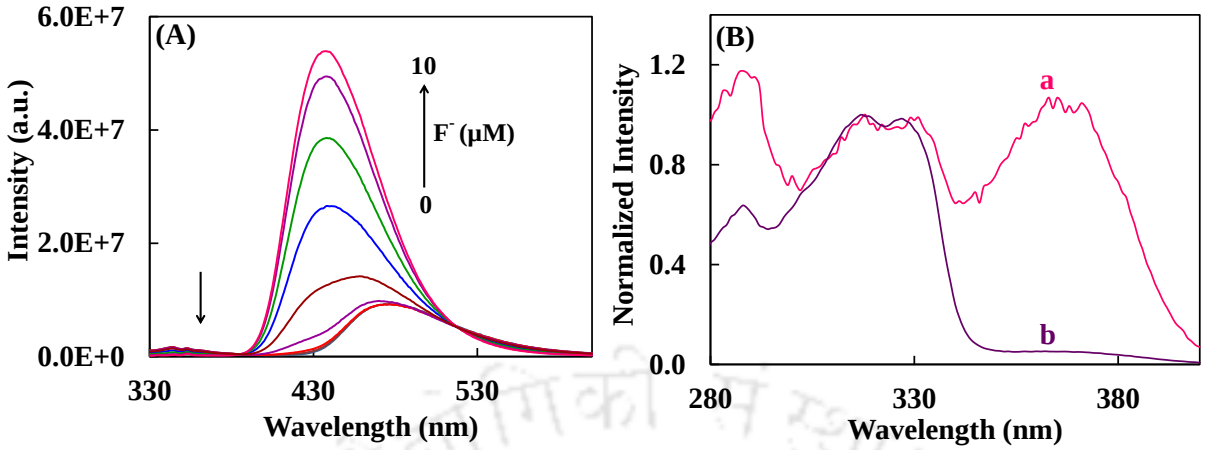


**Figure 3.2.7.** (A) Emission spectra of HPIP-c with increasing fluoride concentration, $\lambda_{ex}$ = 320 nm. (B) Normalized excitation spectra of HPIP-c at (a) low and (b) high fluoride concentration, $\lambda_{em}$ = 430 nm.

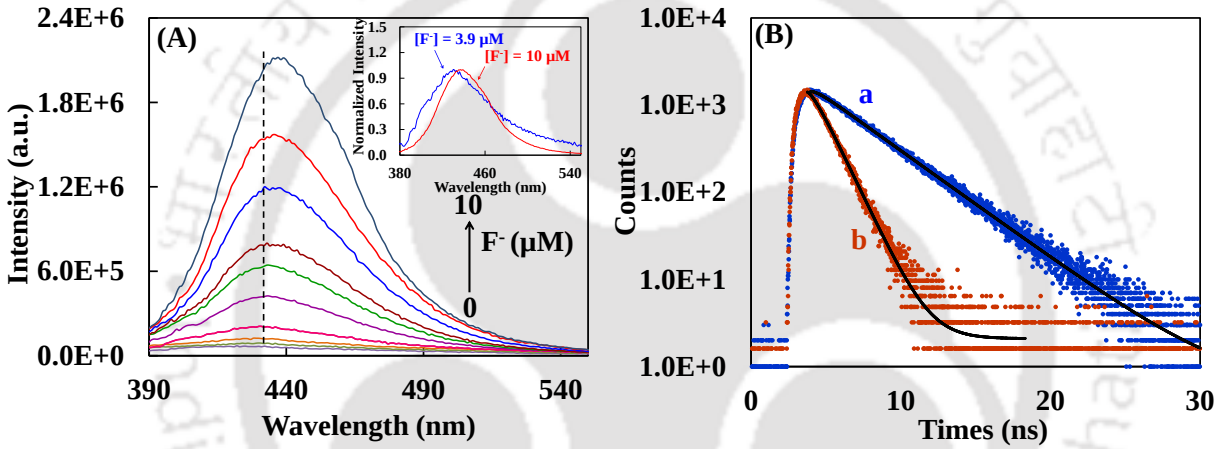


**Figure 3.2.8.** (A) Emission spectra of HPIP-c with increasing fluoride concentration, $\lambda_{ex}$ = 370 nm. Normalized emission spectra of HPIP-c at low and high fluoride concentration is shown in inset. (B) Fluorescence decay of HPIP-c in presence of 10 μM of fluoride; (a) $\lambda_{em}$ = 438 nm, (b) $\lambda_{em}$ = 390 nm.

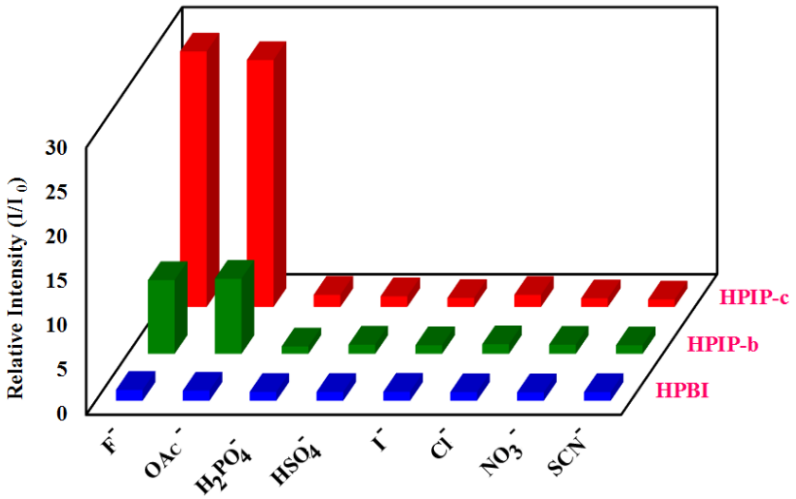


**Figure 3.2.9.** The relative emission intensities of HPBI (at 421 nm), HPIP-b (at 455 nm) and HPIP-c (at 438 nm) in presence of different anions (10 μM).

buried underneath. Therefore, the fluorescence decays of HPIP-c were also measured in presence of 10 μM of fluoride (Figure 3.2.8.B). Like HPIP-b, HPIP-c also exhibits only single exponential decay with 3.4 ns lifetime when monitored at 438 nm, and two different lifetimes, 3.4 ns (10 %) and 1.2 ns (90 %) when monitored at 390 nm.

The sensing ability of HPBI and its nitrogen substituted analogues towards other anions were investigated. The comparative bar diagram of fluorescence intensities of the fluorophores in presence of different anions is depicted in Figure 3.2.9. This advocates that the nitrogen substituted molecules are more sensitive to the presence of anions than HPBI.

### 3.2.3. Theoretical calculation

**Table 3.2.1.** Theoretically predicted relative ground state energy (ΔE, eV)[a], absorption maximum ($\lambda_{max}^{abs}$, nm) and emission maximum ($\lambda_{max}^{em}$, nm), and ground state dipole moment ($\mu_g$, D) of different anions of HPIP-b and HPIP-c.

| | | ΔE | $\lambda_{max}^{abs}$ | $\lambda_{max}^{em}$ | $\mu_g$ |
|---|---|---|---|---|---|
| HPIP-b | *trans*-anion | 0 | 386 | 442 | 6.2 |
| | *cis*-anion | 0.50 | 410 | 468 | 9.9 |
| HPIP-c | *trans*-anion | 0 | 371 | 426 | 1.0 |
| | *cis*-anion | 0.51 | 392 | 447 | 12.9 |

[a] Relative energy is calculated with respect to respective *trans*-anion. Energy of the *trans*-anion of HPIP-b and HPIP-c are -19096.6599 and -19096.5737 eV, respectively.

Like HPBI, the intermolecular proton transfer of phenolic proton would lead to the formation of monoanion in HPIP-b and HPIP-c. Those species can also exist as *cis*- and *trans*- conformers (Chart 3.2.1). Due to electrostatic repulsion between the phenolate anion and the azole nitrogen, the *cis*-anion of HPBI is twisted (43°, Section 3.1.1). Surprisingly, same as the *trans*-anions, the *cis*-anions of both the nitrogenous analogues possess a planar geometry with a negligible dihedral angle (0.05° and 0.01° for HPIP-b and HPIP-c, respectively, Annexure-B) between the phenoxide ion and the pyridylimidazole moiety. Nonetheless, same as the *trans*-anion of HPBI, the *trans*-anion of the nitrogenous analogues are also found to be more stable than the respective *cis*-anions (Table 3.2.1.). The calculated absorption and emission transition energies of *cis*-anions are red shifted compared to the respective *trans*-anions. The dipole moment of the *cis*-anion is found to be higher than the respective *trans*-anion for both the molecules.

### 3.2.4. NMR spectra

Due to low solubility of the fluorophores in deuterated acetonitrile the NMR titrations were carried out in DMSO-$d_6$. The assignment of peaks to protons in the absence of fluoride was already reported.[35] Now in presence of fluoride, the assignment is made based on 2D NMR (Annexure-A). The NMR spectra of HPIP-b and HPIP-c with varying fluoride concentration are depicted in Figure 3.2.10 and Figure 3.2.11, respectively. Up to a certain fluoride concentration, the peak corresponded to the H-6′ proton of HPIP-b and HPIP-c exhibit a downfield shift. Whereas all other proton peaks undergo an upfield shift. Further increase in fluoride concentration causes a reverse shift in the peak corresponded to the H-6′ proton. However, the shift is negligible.

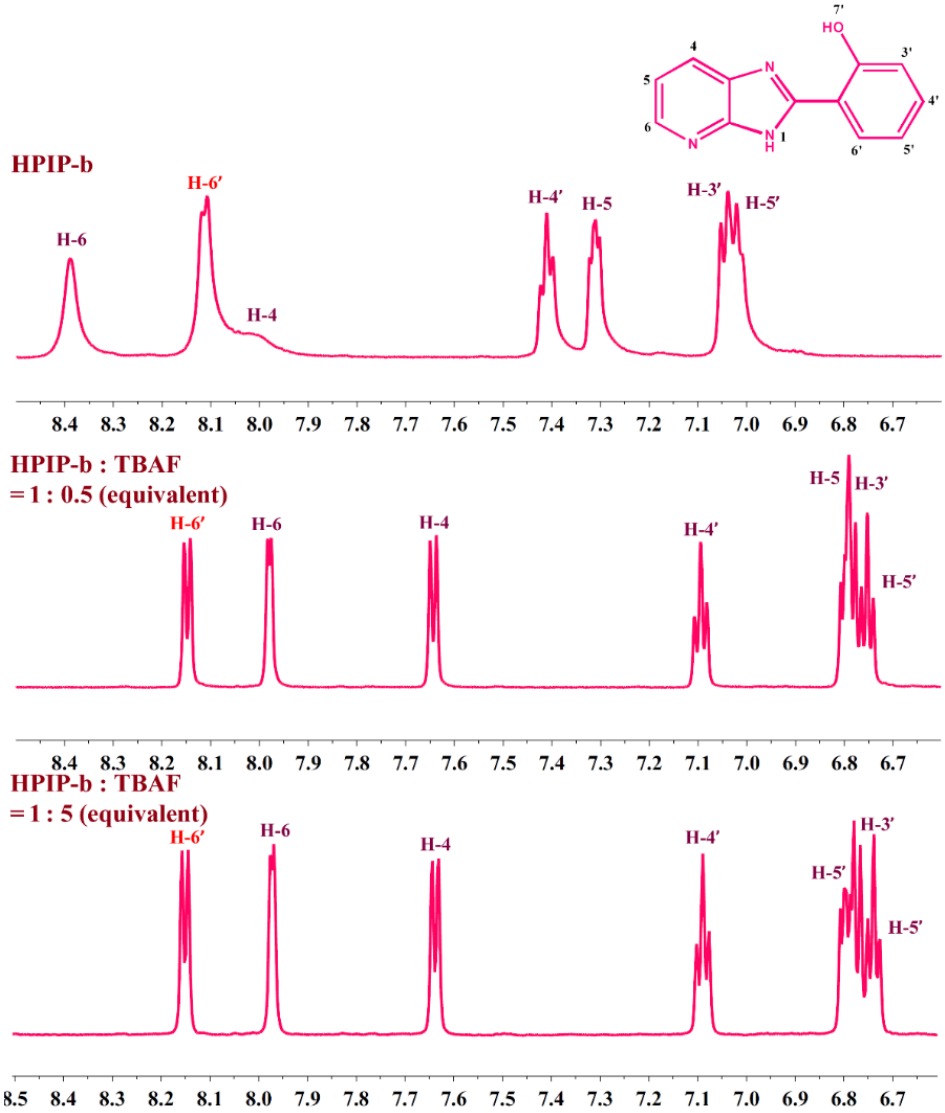


**Figure 3.2.10.** $^1$H NMR spectra of HPIP-b at different fluoride concentration in DMSO-$d_6$.

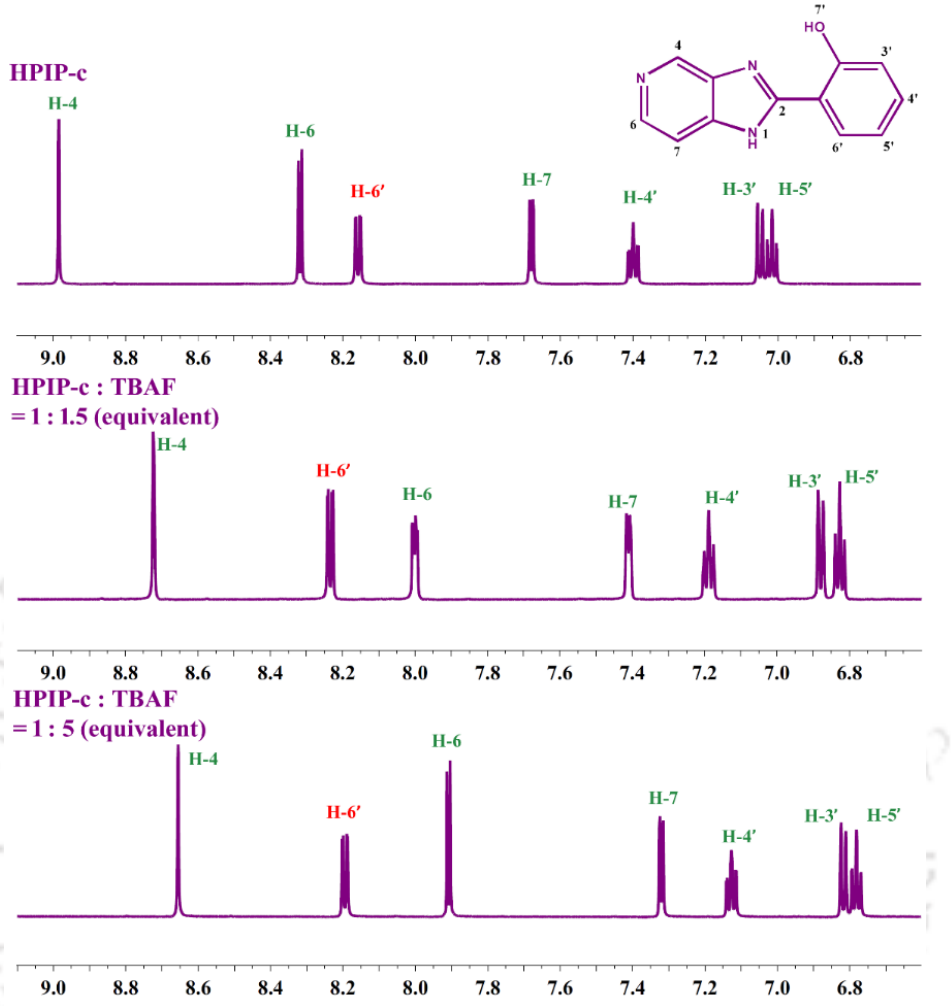


**Figure 3.2.11.** $^{1}$H NMR spectra of HPIP-c at different fluoride concentration in DMSO-$d_6$.

### 3.2.5 Existence of *cis*-H bond complex and different anions of HPIP-b and HPIP-c

The main absorption bands of the imidazopyridines derivatives correspond to their *cis*-enol conformer.[72, 118, 120] The bathochromic shift in the main absorption band of HPIP-b upon addition of fluoride ion is similar to that observed in the absorption spectra of HPBI upon addition of fluoride due to the formation of *cis*-H-bond complex. The vibrational structure is also much resolved in the presence of fluoride. These changes indicate a stronger hydrogen bonding interaction between the *cis*-enol and the added anion, and it is labeled as *cis*-H-bond complex. On the other hand, the absence of similar shift in the main absorption band of HPIP-c clearly indicates a weaker interaction between HPIP-c and the added anions in the ground state.

In presence of fluoride, when excited at 320 nm, the normal and the tautomer emissions of HPIP-b disappear to form a single emission spectrum at 455 nm. The new band is red shifted as compare to the tautomer emission and blue shifted as compare to

the normal emission. This is consistent with the formation of the anion by intermolecular proton transfer of the phenolic proton.[117] The excitation spectrum corresponding to the 455 nm emission matches with the absorption spectra of the *cis*-H-bond complex (Figure 3.2.5.B). Upon excitation, due to enhancement in the acidity of the phenolic group, the *cis*-H-bond complex donates the proton to the nearby hydrogen bonded fluoride ion to generate the anion in the excited state. Since, the *cis*-H-bond complex can produce the *cis*-anion but not the *trans*-anion, the 455 emission should correspond to the emission from the *cis*-anion. This is similar to the emission from the *cis*-anion, observed upon excitation of *cis*-H-bond complex of HPBI in presence of fluoride ion (Section 3.1.5). The theoretically predicted emission energy of the *cis*-anion (Table 3.2.1) is also in agreement with the experimental emission energy. The calculated absorption maximum for the *cis*-anion is 410 nm. A very low intensity at the longer wavelength region of the excitation spectra monitored at 455 nm suggests that the *cis*-anion is present in very small quantity in the ground state (Figure 3.2.5.B). However, excitation at 370 nm indicates that at very low fluoride concentration (0.4 μM) HPIP-b yields a different species which emits at 440 nm. The species can be assigned to the *trans*-anion. The theoretical calculations also predicted such blue shift in the emission maximum of the *trans*-anion compared to that of the *cis*-anion (Table 3.2.1.). The agreement of calculated emission energy of the *trans*-anion with the experimental value substantiates the assignment. The biexponential decay observed at 410 nm ratifies the presence of an additional ~ 410 nm blue shifted emission with 2.0 ns lifetime at higher concentration of fluoride. This indicates the formation of dianion. As the second deprotonation takes place at the azole 'NH' of the *cis*-anion, the emission band is blue shifted.[8] The excitation spectrum corresponded to the dianionic species has a band maxima at 365 nm (Figure 3.2.5.B). It explains the little enhancement in the absorbance at 365 nm at very high anion concentration (Figure 3.2.1.). On the other hand, HPIP-b exhibits *trans*-anion emissions up to 1.2 μM of acetate concentration. The *cis*-anion emission appears at higher acetate concentration. The dissimilarity in the interactions of fluoride and acetate with the fluorophore is due to the difference in their relative strengths. Fluoride is a stronger base than acetate. Under isolated condition, the *trans*-anion is more stable than the *cis*-anion due the intramolecular hydrogen bond between the phenolate ion and the 'NH' proton (Chart 3.2.1.). Therefore, as mentioned in the previous section, the existence of *trans*- or *cis*- anion depends on this intramolecular hydrogen bond. If the external anion cannot interact with the 'NH' proton efficiently,

the unstable *cis* anion rotates to form the *trans*-anion. Due to higher basicity, fluoride effectively stabilizes the 'NH' proton even at low concentration. This prevents the formation of intramolecular hydrogen bond by rotation. But comparatively weaker (lower strength) acetate anion is inefficient to stabilize the 'NH' proton in sufficient extent at lower concentration. As a consequence, the *trans*-anion of HPIP-b is observed at very low fluoride concentration and low acetate concentration. At higher anion concentration, the 'NH' proton is stabilized by the external anion, and the *cis*-anion is detected.

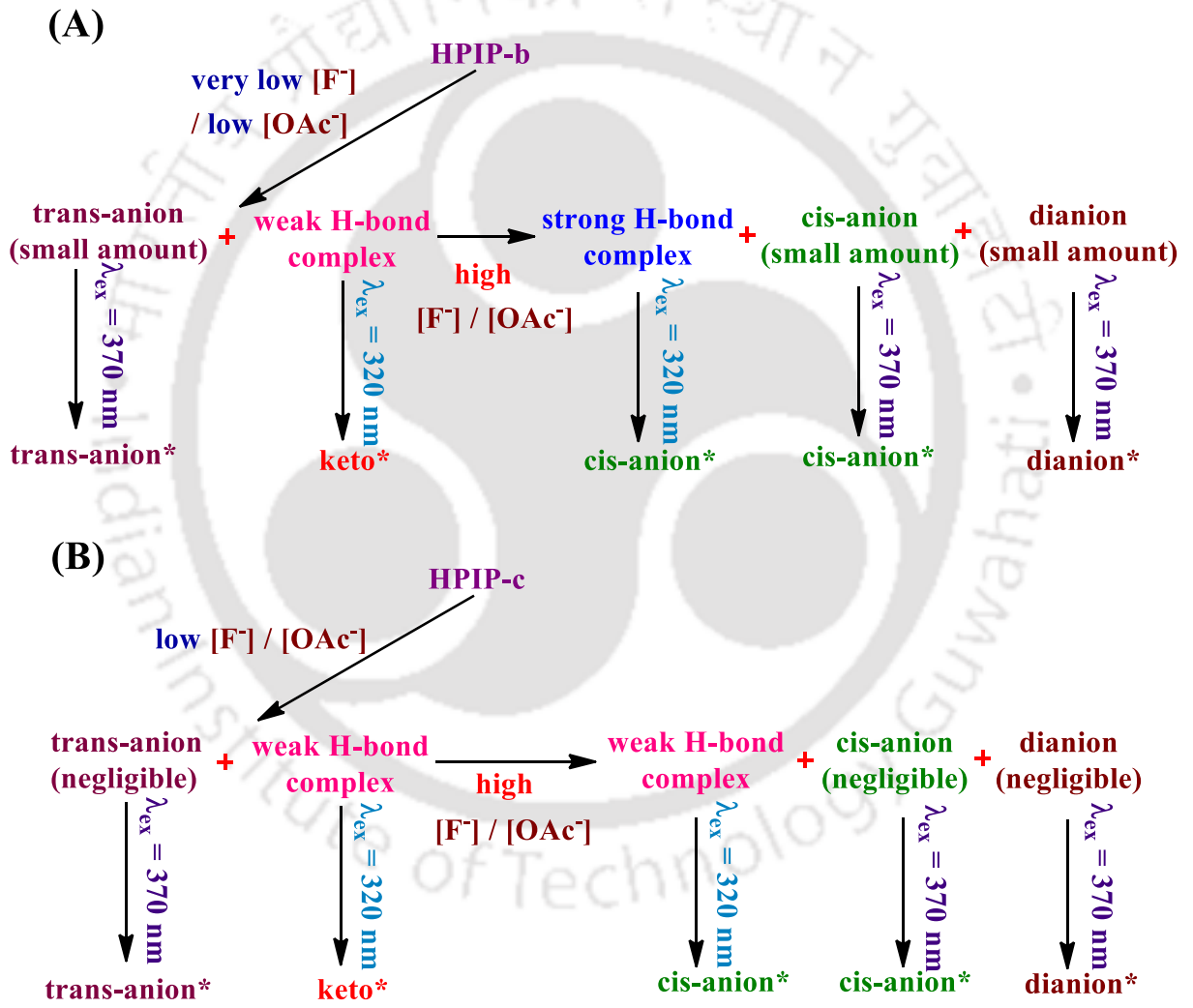


**Scheme 3.2.1.** Formation of different anions of (A) HPIP-b and (B) HPIP-c in the ground and excited state in presence of fluoride and acetate in acetonitrile.

Conversely, HPIP-c has weaker interaction even with fluoride. At low concentration of fluoride and acetate, the excitation at longer wavelength results in the 427 nm emission. The high concentration yields the 438 nm emission. The 427 nm and 438 nm

emissions from HPIP-c should correspond to the *trans*-anionic and *cis*-anionic forms, respectively. This assignment is based on the relative shift of the absorption and emission spectra of *cis*- and *trans*- anion. The calculated emission energies also agree well with the experimental values (Table 3.2.1). Accordingly, the excitation spectral maximum at 368 nm which is obtained at low fluoride concentration can be attributed to the *trans*-anion. The main band of the excitation spectra at high fluoride concentration matches with the absorption spectrum of the weak *cis*-H-bond complex. This further confirms that the anion that formed at higher concentration is the *cis*-anion and therefore the 438 nm emission corresponds to *cis*-anion. Simultaneously, a low intensity at longer wavelength region indicates the existence of negligible amount of the *cis*-anion in ground state. The second 1.2 ns fluorescence lifetime obtained at very high concentration is due to the dianion.

The transformations of HPIP-b and HPIP-c in presence of different anions are summarized in Scheme 3.2.1. The absorption spectra and the excitation spectra suggest the presence of very small amount of *cis*- or *trans*- anion in the ground state. However, in the excited state the emissions are observed from the anions. As mentioned earlier, this is due to the enhanced acidity in the excited state, which facilitates the intermolecular proton transfer. In the excited state, depending on the concentration of fluoride and acetate, HPIP-b and HPIP-c exists as *cis*- and *trans*-anion.

The NMR titration of HPIP-b and HPIP-c with fluoride anion also reveals the formation of *cis*-H-bond complex. The observed upfield shift of proton peaks upon addition of anion indicates the shielding effect due to the presence of negatively charged ions near the molecule. The downfield shift of the H-6′ proton peak suggests a through space interaction between this proton and the fluoride ion which is accumulated near the 'NH' proton.[114] Such shifts were also observed when HPBI forms *cis*-H-bond complex (Figure 3.1.9). The negative charge accumulates on the oxygen atom either due to the hydrogen bonding interaction of the negatively charged ion or by the formation of anionic form. This charge generates a high shielding effect. The extent of this effects on H-3′ (ortho to hydroxyl group) and H-5′ (para to hydroxyl group) must be different. It should depend on the strength of the negative charge generated on the oxygen atom. Hence, the peaks of these protons (H-3′ & H-5′) which were close to each other before the interaction with the external anion, started to move apart from each other after the interaction. The separation between the peaks of H-3′ and H-5′ are 0.040 ± 0.005 for nitrogen substituted molecules (Figure 3.2.9. and 3.2.10.). Whereas, it was 0.085 ppm

for HPBI upon deprotonation of 'OH' proton (Figure 3.1.9). The large difference observed in the NMR spectrum of HPBI in presence of fluoride was the result of accumulation of more negative charge due to the deprotonation of 'OH' proton. Since, the anion formation is less in HPIP-b and HPIP-c, this difference is small. The initially observed downfield shift in the peak of H-6' in *cis*-H-bond complex was shifted upfield considerably upon formation of anion in HPBI (Figure 3.1.9). Such an upfield shift in the H-6' proton peak at high concentration of fluoride is negligible for HPIP-b and HPIP-c. This further suggests that the formation of anion in the ground state is less in nitrogen substituted analogs.

### 3.2.6. Sensitivity and ease of deprotonation

The major differences in the interaction of external anions with nitrogenous analogues and HPBI are found in their sensitivity towards the external anions and in the conversion to the anionic form in presence of the external anions. The fluoride ion detection limit of HPBI, HPIP-b and HPIP-c are 6.25 μM, 0.32 μM and 0.28 μM, respectively. This indicates that substitution of nitrogen enhances the sensitivity of the molecules by nearly 20 times. In contrast, in the ground state the nitrogenous analogues exist in anionic form in a lower quantity than HPBI.[124]

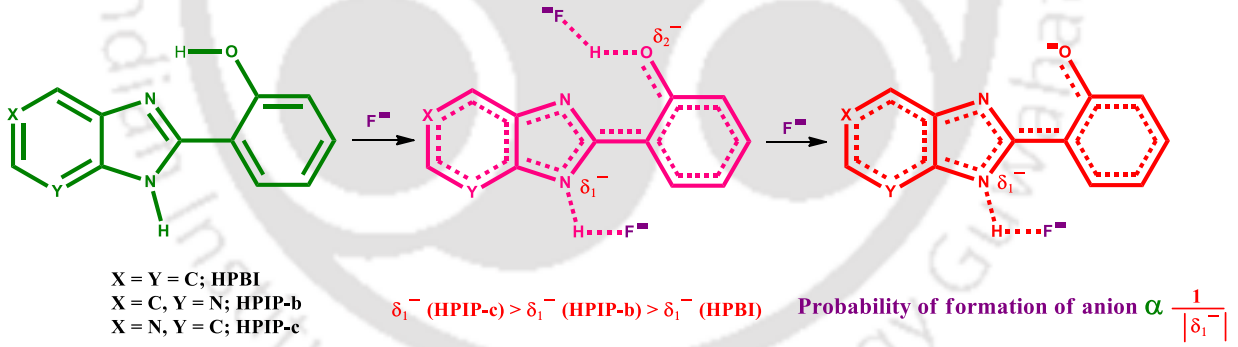


**Scheme 3.2.2.** Feasibility of formation of anion in HPBI and its nitrogenous analogs.

The apparent contrast relies on the higher electron accepting capability of the pyridylimidazole than the benzimidazole moiety. Theoretical calculation predicted a twisted structure for the *cis*-anion of HPBI (Section 3.1.1). This is due to the strong electrostatic repulsion between the $sp^2$ azole nitrogen and the negative charge of the phenoxide anion. But the theoretical calculation predicts a planar geometry for the *cis*-anion of HPIP-b and HPIP-c. This result indicates that due to the strong electron withdrawing nature of the pyridylimidazole group, the negative charge delocalizes over the whole molecule. In solvents, like acetonitrile where solvation of external anions

is relatively less, the anions are more attracted towards the fluorophores. Since the imidazopyridines can delocalize the negative charge more than HPBI, they attract the negatively charged (external) anions more than HPBI. As a result, more partial negative charge delocalizes on nitrogen substituted analogues. Therefore, the deprotonation of the 'OH' proton to generate a negative charge on the flurophore in the ground state is less favored in nitrogenous analogues (Scheme 3.2.2). However, in aqueous medium the $pK_a$ values of the nitrogenous analogues are lower than that of HPBI.[123] Unlike in actetonitrile, in aqueous medium the anions are well solvated by the water molecule, and the accumulation of negative charged ion around the fluorophore is relatively less. Therefore, the deprotonation is more favored in pyridoimidazoles than HPBI.

Not only the substitution of nitrogen but also the position of nitrogen affects the electron accepting ability of imdazopyridines. This can infer the different behavior of HPIP-b and HPIP-c toward the fluoride anion. It appears that the 'NH' proton of HPIP-b is more acidic compared to that of HPIP-c. The pyridylimidazole unit of HPIP-b and HPIP-c are comparable with 7-azaindole and 5-azindole molecule. The calculated neutral-monoanion $pK_a$ value for 7-azaindole and 5-azindole are 13.9±0.3, 15.2±0.3.[125] Therefore, fluoride anions are attracted more towards the 'NH' proton of HPIP-b in comparison to that of HPIP-c, even at low fluoride concentration also. As a result, at low fluoride concentration, the formation of hydrogen bond between the 'NH' proton and the fluoride anion stabilizes the *cis*-anion of HPIP-b. The weaker interaction between the 'NH' proton and fluoride anion fails to stabilize the *cis*-anion of HPIP-c at low fluoride concentration (up to 4 μM of fluoride), and the *cis*-anion rotates to provide a *trans*- HPIP-c anion. On the other hand, HPIP-b forms *trans*-anion only at very low fluoride concentration (0.4 μM). At that concentration, the fluoride amount is substantially low and not available to form hydrogen bond with the 'NH' proton of HPIP-b.

### 3.2.7. Conclusion

The nitrogenous analogues show a higher sensitivity towards the anions than HPBI. The detection limit is enhanced upon nitrogen substitution due to higher electron accepting nature of the pyridylimidazole group. HPIP-b forms *cis*-anion in the presence of fluoride and at high concentration of acetate. Only at very low concentration of fluoride, the *trans*-anion is observed. At low concentration of fluoride or acetate, initially only the *trans*-anion is formed from HPIP-c and only at higher concentrations the *cis*-anion is observed. At very high anion concentrations, both the fluorophores form very little

amount dianion along with little *cis*-anion. In contrary to the expectation, the nitrogenous analogues produce significantly lesser anion than HPBI in the ground state. The HPIP-b forms a strong *cis*-H-bond complex with fluoride and acetate in the ground state. On the other hand, HPIP-c forms a weak complex in the ground state. HPIP-c forms *trans*-anion at low concentration of both fluoride and acetate. In the excited state, the *cis*-anions are formed from the *cis*-H-bond complex due to intermolecular proton transfer.

# Chapter 4

# Intramolecular Proton Transfer and Conformer Specific Aggregation Induced Enhanced Emission of 1,4-bis(2-(2′-Hydroxyphenyl)benzimidazol-1-ylmethyl)-benzene

## 4.0. Introduction

As mentioned earlier, HPBI exhibits normal and tautomer emission, due to equilibrium between the *trans*-enol and *cis*-enol conformers.[72, 73] However, distinct normal and tautomer emissions can make the molecule efficient to display two different emission colors. It is only possible if the ground state equilibrium can be perturbed to end up with a desired conformer. In addition, highly Stokes' shifted emissions are desirable to avoid self-quenching. Though the keto emission of ESIPT molecules are highly Stokes' shifted, the normal emission is less Stokes' shifted. To achieve separate enol and keto emission, a derivative of HPBI, BHPBI is chosen and investigated.[78] BHPBI possesses two HPBI units connected in a non-conjugative manner via a spacer (Chart 4.1). The photophysical characteristics of BHPBI are studied. The possibility of dual tautomer emission from two different HPBI units is also investigated. At the end of the chaper, it is shown that by controlling the molecular solubility and modifying the intra/inter molecular H-bond, different conformers can be separated as different aggregates.

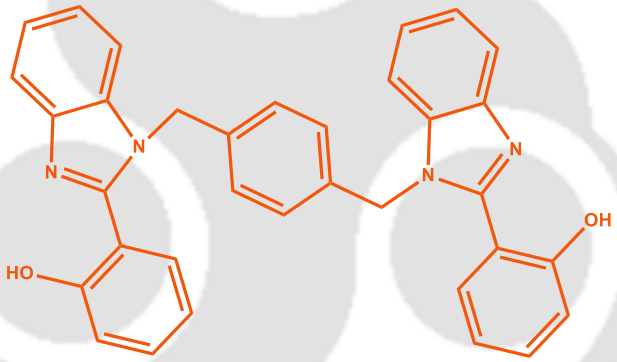


**Chart 4.1.** Molecular structure of 1,4-bis(2-(2'-hydroxyphenyl)benzimidazol-1-ylmethyl)-benzene (BHPBI).

### 4.1. Planar and twisted conformer

BHPBI exhibits absorption bands at ~ 290 nm and ~ 320 nm (Figure 4.1.A and Table 4.1). The absorbance of both the bands are nearly equal in solvents such as cyclohexane, ethylacetate, acetonitrile etc. However, in both hydrogen bond donating and hydrogen bond accepting solvents, the absorbance of the 320 nm band decreases relative to that of the 290 nm band. The absorbance ratios of the longer wavelength band maximum to the shorter wavelength band maximum ($A_{320}/A_{290}$) are 1.2, 0.6, 0.3 and 0.2 in acteronitrile, DMF, methanol and DMSO, respectively. The unsubstituted benzimidazole exhibits the longer wavelength absorption at ~ 280 nm.[126] In HPBI, the substituted benzimidazole molecule shows the longer wavelength absorption band at

**Table 4.1.** Absorption maxima ($\lambda_{max}^{abs}$, nm), emission maxima ($\lambda_{max}^{em}$, nm) and excited state lifetime (τ, ns) of BHPBI in different solvents.

| Solvent | $\lambda_{max}^{abs}$ [a] | $\lambda_{max}^{em}$ | τ (monitored at shorter $\lambda_{max}^{em}$) | τ (monitored at longer $\lambda_{max}^{em}$) |
|---|---|---|---|---|
| Cyclohexane | 321, 285 | 503 | | 3.8 (100 %) |
| Ethylacetate | 323 (2.37), 293 (2.33) | 356, 488 | | 0.4 (90.8 %)<br>3.1 (9.2 %) |
| Dioxane | 324 (2.58), 293 (2.52) | 356, 493 | | 0.4 (82.6 %)<br>3.6 (17.4 %) |
| THF | 320 (2.44), 295 (2.33) | 356, 497 | | 0.3 (47.7 %)<br>3.9 (52.3 %) |
| Methanol | 286 (2.42) | 357, 460 | 0.8 (100.0) | 0.8 (53.8 %)<br>3.4 (46.2 %) |
| 1-Propanol | 339 (1.64), 294 (2.34) | 355, 470 | 1.0 (100.0) | 0.7 (46.7 %)<br>3.4 (53.3 %) |
| Acetonitrile | 325 (2.40), 294 (2.34) | 356, 485 | 1.1 (91.0)<br>3.3 (9.0) | 0.4 (19.8 %)<br>3.4 (80.2 %) |
| DMSO | 340 (1.68), 290 (2.69) | 358, 476 | 0.9 (100) | 0.7 (38.3 %)<br>2.3 (61.7 %) |
| DMF | 322 (2.15), 287 (2.32) | 356, 478 | 0.9 (100) | 0.9 (15.7 %)<br>3.6 (84.3 %) |
| Water | 326, 296 | 479 | | 1.3 (30.9 %)<br>3.5 (69.1 %) |

[a]log value of molar extinction coefficient (ε) at the particular absorption wavelength is given in the parenthesis.

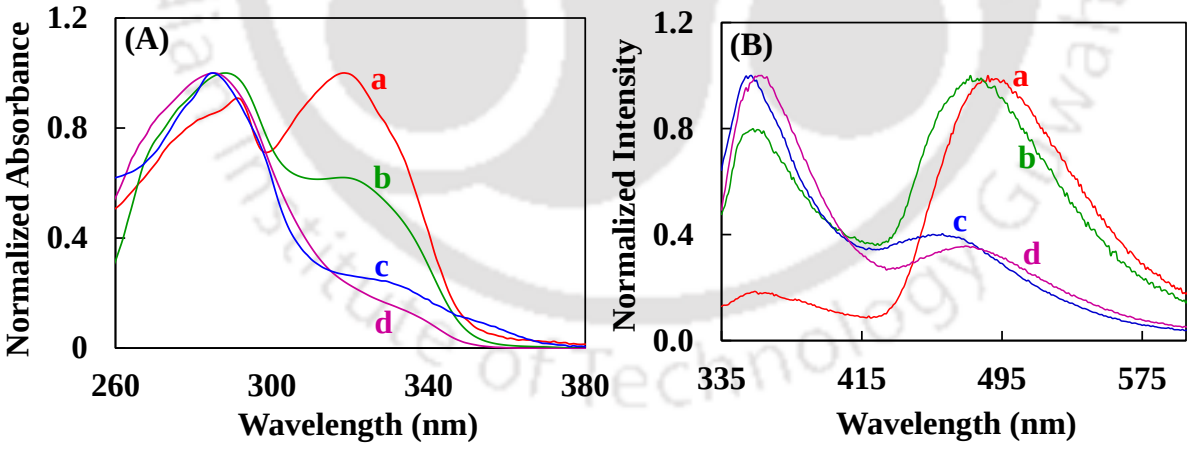


**Figure 4.1.** Absorption (A) and emission (B) spectra of BHPBI in different solvents. (a) ethylacetate, (b) DMF, (c) methanol, (d) DMSO. $\lambda_{ex}$ = 315 nm.

320 nm due to enhanced conjugation with the phenolic ring. [72, 112] The absorption spectra of BHPBI indicate the existence of different ground state conformers which exhibit different absorptions. Moreover, the equilibrium strongly depends on solvents factors. In contrast to the absorption spectrum of HPBI, the well resolved vibrational structures

are not observed in the 320 nm band of BHPBI. This indicates that the benzimidazole moiety and the phenol ring do not hold a complete planar structure. Instead, the HPBI units of BHPBI possess a quasi-planar structure where strong intramolecular hydrogen bond persists between the azole nitrogen and the phenolic 'OH'. In hydrogen bond forming solvents, the intramolecular hydrogen bond is broken and the phenolic ring undergoes a torsional rotation. In HPBI, the breaking of intramolecular hydrogen bond shifts the equilibrium toward the trans-enol.[73] In BHPBI due to the steric hindrance between the bulky spacer unit and the phenol moiety, the torsional rotation does not yield a planar *trans*-enol instead it produces a twisted-enol conformer. As a consequence, the conjugation between the two rings is reduced considerably, and the absorption spectral maximum shifts toward the unsubstituted benzimidazole (~ 290 nm).

### 4.2. Photoinduced planarization and proton transfer

**Figure 4.2.** Excitation spectra (A) $\lambda_{em}$ = 500 nm, (B) $\lambda_{em}$ = 355 nm of BHPBI in different solvents, (a) cyclohexane, (b) dioxane, (c) acetonitrile, (d) DMSO and (e) methanol.

BHPBI exhibits an UV emission around 355 nm and a visible emission at a longer wavelength (Figure 4.1.B and Table 4.1.). In hydrogen bond forming solvents the shorter wavelength emission predominates. Whereas in other solvents, the longer wavelength emission is more intense than the shorter wavelength emission. The longer wavelength emission is highly sensitive to the solvent polarity. With increasing solvent polarity the emission band is shifted to the shorter wavelength. The excitation spectra recorded at the longer emission wavelength have a band maximum around 320 nm (Figure 4.2.A). The high Stokes' shifted nature (> 10000 $cm^{-1}$) and a gradual hypsochromic shift with increasing solvent polarity substantiate that the visible emission appears from a new

excited state species whose excited sate is less stabilized than the ground state upon increasing polarity. The excitation spectra indicate that the quasi-planar HPBI unit which predominates in nonpolar solvents is responsible for the visible emission. The results infer that due to the close proximity of the azole nitrogen and the phenolic 'OH', upon photo excitation, proton transfer occurs to produce an amine-keto tautomer. The excitation spectrum of the shorter wavelength emission matches with the 290 nm absorption band (Figure 4.2.B). It indicates that the twisted conformer which cannot undergo proton transfer in the excited state exhibits the enol emission. The results also support the high intensity of the enol emission in strong hydrogen bond forming solvents. The Stokes' shift for the enol emission is quite high (~ 6400 $cm^{-1}$) compared to HPBI and related molecules.[37, 72, 127] The unusually high Stokes' shift infers the large difference in geometries of the molecule in the ground and the excited states. It indicates that the molecule attains a more planar geometry in the excited state from the initial twisted geometry. Thus, it is clear that the electron redistribution in the excited state assists the planarization process.

### 4.3. Triple fluorescence

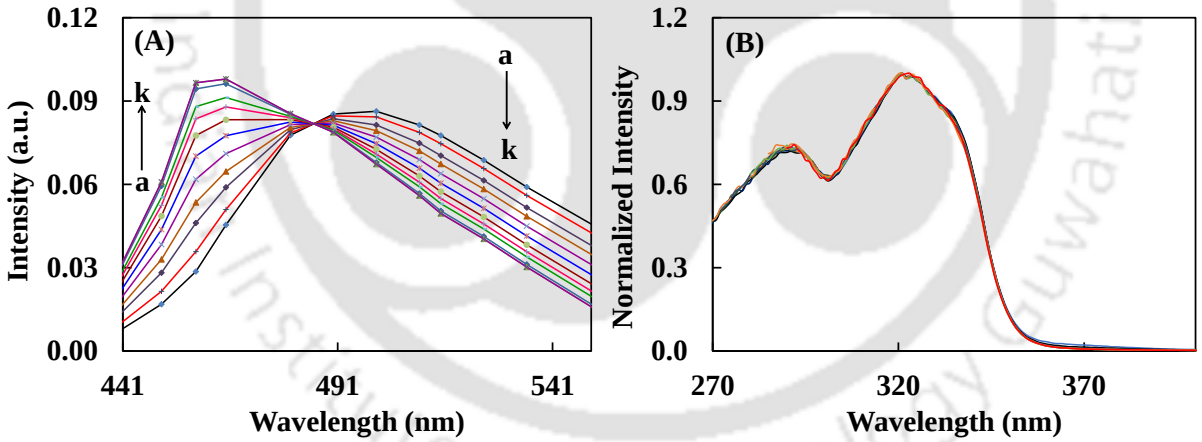


**Figure 4.3.** (A) Time-resolved area normalized emission spectra of BHPBI in dioxane. The delay times are (a) 0 ns, (b) 0.8 ns, (c) 1.2 ns, (d) 1.4 ns, (e) 1.6 ns, (f) 1.8 ns, (g) 2 ns, (h) 2.2 ns, (i) 2.4 ns, (j) 3.0 ns (k) 45 ns. $\lambda_{ex}$ = 308 nm. (B) Normalized excitation spectra of BHPBI in dioxane recorded at different emission wavelengths (460 nm to 530 nm).

The emission nature of two different bands are further investigated by monitoring the fluorescence lifetime at the different emission maxima. The fluorescence decays at different emission maxima in different solvents are displayed in Table 4.1. The enol emission shows a short lifetime (≤ 1 ns, Table 4.1.). On the other hand, the tautomer emission exhibits a biexponential decay (lifetimes ~ 0.5 and ~ 3.6 ns) in all the solvents,

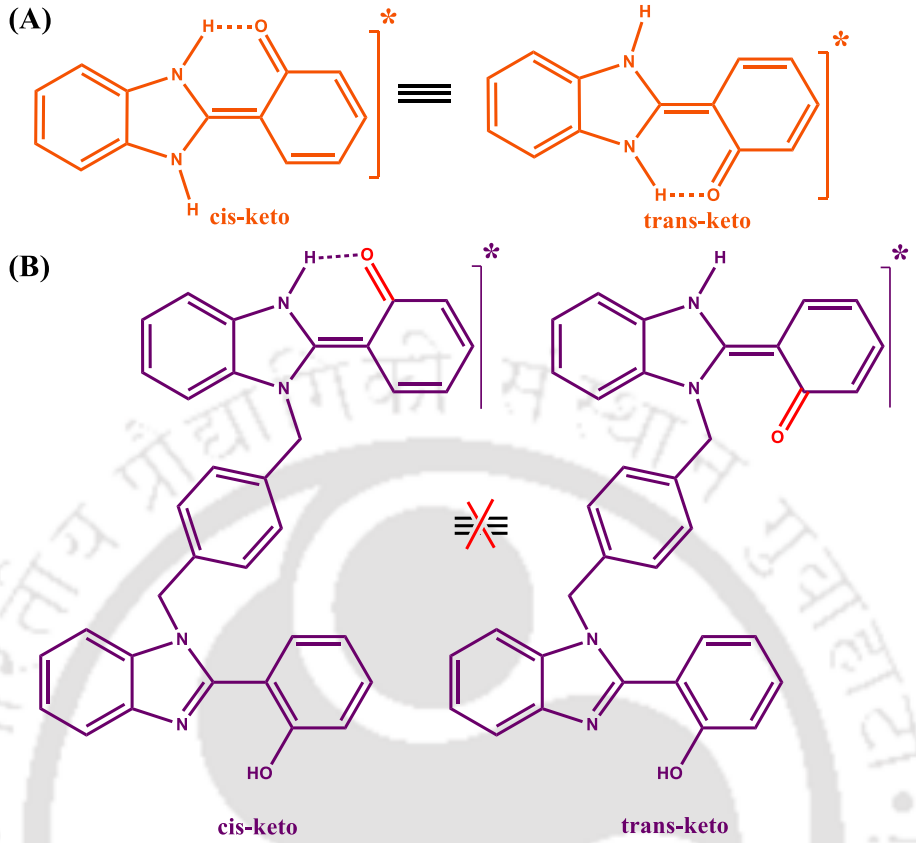


**Chart 4.2.** *Cis-* and *trans-* keto isomer of (A) HPBI and (B) BHPBI.

except cyclohexane (Table 4.1.). The relative amplitude of the short lifetime species is higher when monitored at longer wavelength. The emission spectra of the visible fluorescence emitting species are resolved by Time-resolved fluorescence method. The Time-resolved area normalized emission spectra (TRANES) of BHPBI in dioxane were constructed from the decay profiles obtained from 440 nm to 560 nm (Figure 4.3.A). The emission maxima of the long lifetime and the short lifetime species in dioxane are 460 nm and 495 nm, respectively. But, the excitation spectra recorded at different wavelengths are independent of monitoring wavelength (Figure 4.3.B). This demonstrates that both the species originate from the same ground state precursor. In contrary, the tautomer emission of HPBI exhibits a single exponential decay in all the solvents, and the lifetime of the emitting species is close to 3.5 ns. *Cis-trans* isomerization of the keto tautomer in the excited state via a nonemissive twisted intramolecular charge transfer state is reported as one of the major nonradiative process in HPBI and its analogues.[116, 128-130] But, the torsional rotation of the keto tautomer of HPBI will not yield a new isomer. However, that of BHPBI keto would result in a different isomer due to the substitution at azole ring (Chart 4.2.). Since, the emission maximum and the lifetime

of the 460 nm band are close to that of HPBI, it can be assigned to the initially formed *cis*-keto tautomer. Accordingly, the other band can be assigned to a *trans*-keto.

### 4.4. Prototropic study

BHPBI molecule possesses two phenolic 'OH' and two azole nitrogen. The phenol moiety can be deprotonated in presence of base and the azole nitrogen can be protonated in acidic medium. Therefore, the spectral characteristics of BHPBI were studied over a range of pH. At pH 6.5, BHPBI exists in neutral form and exhibits only keto emission (Figure 4.4). At pH 10.4, it appears as monoanion. The monoanion is formed by the deprotonation of the 'OH' of one of the HPBI units. Since, the other HPBI unit exists as neutral form and takes part in ESIPT, the BHPBI monoanion also exhibits keto emission along with the anionic emission (Figure 4.4). However, when both the 'OH' are deprotonated to form anion at pH 12.5, ESIPT is not feasible from either of the units. Therefore, a single emission corresponding to the anion is observed at 430 nm (Figure 4.4). As expected, the anion emission is blue shifted compared to the tautomer emission and red shifted compared to the normal emission (Figure 4.4, Figure 4.1B). Similarly, when monocation is formed at pH 1.0, the tautomer emission appears from the free HPBI unit in addition to the cationic emission (Figure 4.4). On the other hand, the dication emits only the cationic emission ($H_0$ -4.5) as both the azole nitrogens are protonated and not available for ESIPT (Figure 4.4B). The cationic emission also blue shifted compared to the tautomer emission and red shifted compared to the normal emission (Figure 4.4, Figure 4.1B).

**Figure 4.4.** Normalized emission spectra of (a) neutral (pH 6.5), (b) monocation (pH 1.0), (c) dication ($H_0$ -4.5), (d) monoanion (pH 10.4) and (e) dianion (pH 12.5) of BHPBI. $\lambda_{ex}$ = 290 nm.

The lifetime of BHPBI at different acid base concentration are depicted in Table 4.2. At pH -4.5, when both the azole nitrogen are protonated, single exponential decay is observed with lifetime 1.5 ns. At pH 1.0, when azole nitrogen of one of the HPBI units is protonated, triexponential decays are observed when monitored at 388 nm and 470 nm. The three different lifetimes are 0.6 ns, 1.5 ns and 3.5 ns. The relative amplitude of the species with 1.5 ns lifetime is more when monitored at 388 nm emission than when monitored at 470 nm. This indicates that the 1.5 ns excited state lifetime corresponds to the azole nitrogen protonated species. As expected, the lifetime matches with the lifetime observed at pH -4.5 where the azole nitrogen of both the units are protonated. The other two lifetimes can be assigned to the *cis*- and the *trans*-keto tautomer of the unprotonated HPBI unit of BHPBI monocation. The relative population of the species with 0.6 ns lifetime enhances at 470 nm compared to that at 388 nm. But the most interesting aspect is that it is having higher relative amplitude than the 3.5 ns lifetime species. This shows that the relative population of the *trans*-keto isomer is higher than that of *cis*-keto isomer. This may be attributed to the greater stabilization of *trans*-keto by hydrogen bonding interaction of the carbonyl group with acid proton (Chat 4.3).

**Table 4.2.** Lifetime of BHPBI at different pH, $\lambda_{ex}$ = 290 nm.

| pH | $\lambda_{em}$ (nm) | τ (ns) |
|---|---|---|
| -4.5 | 388 | 1.5 (100%) |
| 1.0 | 470 | 0.6 (77.5%) |
| | | 1.5 (19.4%) |
| | | 3.5 (3.1%) |
| | 388 | 0.6 (55.2%) |
| | | 1.5 (36.5%) |
| | | 3.5 (8.7%) |
| 6.5 | 475 | 1.4 (30.4%) |
| | | 3.8 (70.6%) |
| | 420 | 1.3 (85.5%) |
| | | 3.8 (14.5%) |
| 9.7 | 475 | 1.4 (28.9%) |
| | | 3.7 (71.1%) |
| 12.5 | 430 | 1.6 (100%) |

At pH 12.5 and 9.7, a monoexponential decay with 1.6 ns and a biexponential decay with 1.4 ns and 3.7 ns are observed, respectively. Since at pH 12.5, both the hydroxyl groups are deprotonated to form anion, both the HPBI units behave in the same way, and therefore, only one lifetime is observed. As one of the HPBI unit is not deprotonated at pH 9.7, it can undergo ESIPT. Thus, the keto emission with 3.7 ns also appears along with the 1.4 ns lifetime of the deprotonated species. At pH 6.5, when monitored at 475 nm a biexponential decay with lifetime 1.4 ns and 3.8 ns are found. When monitored at 420 nm, the relative amplitude of the 1.4 ns species increases and that of 3.8 ns species

decreases. Though the *trans*-keto has shorter lifetime than *cis*-keto, it emits at longer wavelength (Figure 4.3). Therefore, the short lifetime 1.4 ns species is not the *trans*-keto isomer. Since its lifetime matches with the lifetime of deprotonated species, it can be assigned to the emission from the deprotonated HPBI unit. Such a deprotonation due to intermolecular proton transfer upon excitation is feasible in HPBI (Section 3.1). The absence of *trans*-keto may be due to the aggregation of HPBI in water due to the low solubility of the molecule (Section 4.5). Only emission from the *cis*-keto is observed from the aggregates due to the restricted rotation (Section 4.5).

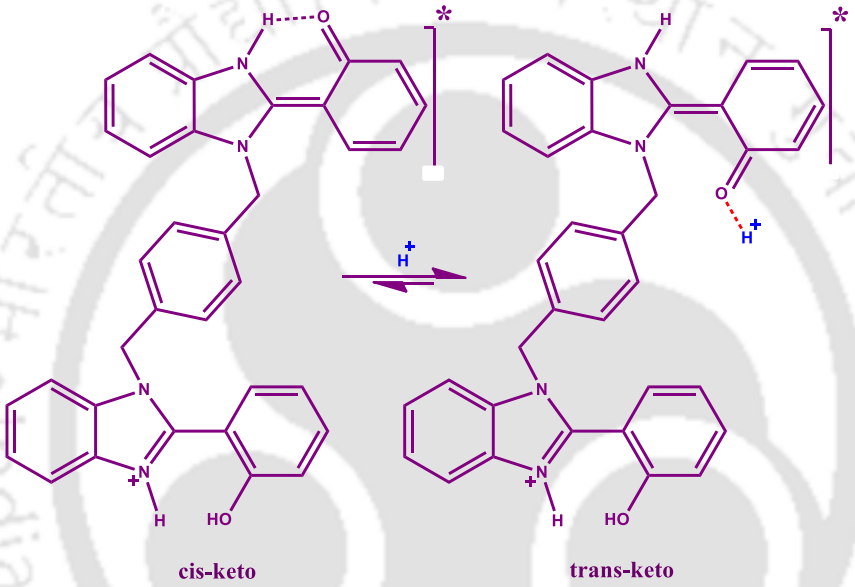


**Chart 4.3.** *Cis*- and *trans*- keto emission from unprotonated HPBI unit of BHPBI monoanion.

## 4.5. Conformer specific aggregation induced enhanced emission

**Figure 4.5.** (A) Fluorescence and (B) absorbance spectra of BHPBI in different water-THF (v/v) mixture (a) 0% (b) 70% (c) 90% and (d) 100% water. $\lambda_{ex}$ = 290 nm [BHPBI] = 5 μM.

BHPBI shows a weak tautomer emission in THF (Figure 4.5.A). Upon addition of water to the THF solution the emission spectrum is blue shifted and the enol emission also emerges. At 70% water, the emission intensities at 355 nm and 430 nm are enhanced by eleven times and twenty times, respectively than those in THF. At 90% water, the enol emission completely disappears, and the 430 nm band is also replaced by the keto emission at 478 nm. The fluorescence quantum yield is also enhanced by ~ 30 times than that in THF. But in neat water, though no shift is observed, the emission intensity appears very low compared to that of 90% water. The emission intensities in THF and in water are found almost comparable though there is a huge difference in their absorbance (Figure 4.5.B).

The absorption patterns of BHPBI at different water fractions also differ from that in THF (Figure 4.5.B). In THF like other nonpolar solvents two absorption bands are observed. Conversely, at 70% water a very sharp band appears at 294 nm along with a long tailing. The band maxima is little red shifted as compared to the shorter wavelength absorption of BHPBI in THF. The longer wavelength absorbance at 322 nm in THF is diminished and buried completely underneath the 290 nm band in 70% water. At 90% water, again two absorption bands appear with very low absorbance and a level off tailing is observed at onset. In neat water, the absorbance is found much lower though no spectral shift is observed with respect to that in 90% water. Due to the low absorbance the level of tailing is not visible but it persists in neat water also. The long tailing in 70%, 90% water and in neat water are due to Mie scattering which indicates the formation of aggregates.[131]

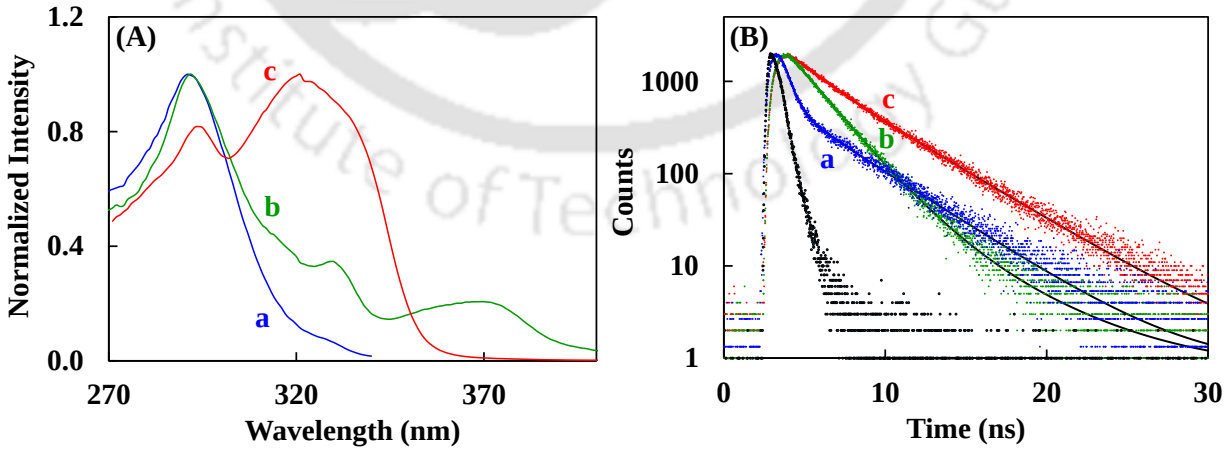


**Figure 4.6.** (A) Fluorescence excitation spectra of BHPBI in (a) 70% water, $\lambda_{em}$ = 360 nm, (b) 70% water, $\lambda_{em}$ = 430 nm, (c) 90% water, $\lambda_{em}$ = 478 nm. (B) Fluorescence decay of BHPBI in (a) THF, $\lambda_{em}$ = 490 nm, (b) 70% water, $\lambda_{em}$ = 400 nm, (c) 90% water, $\lambda_{em}$ = 478 nm. $\lambda_{ex}$ = 290 nm.

The excitation spectra corresponding to the different emission of different aggregated structures are depicted in Figure 4.6.A. In 90% water, the excitation spectra recorded at 478 nm shows a similar nature as those of the keto emission in nonpolar solvent. The absorption band at 320 nm suggests that in 90% water, the aggregates are developed with the quasi planar conformer. The complete absence of the enol emission and the presence of only tautomer emission can be attributed to the nonexistence of the twisted conformer in these aggregates (in 90% water solution). The fluorescence decay of the aggregated tautomer emission is monoexponential with 4.2 ns lifetime and it is little longer than that in other solvents (Figure 4.6.B). The absence of short lifetime keto tautomer indicates that the torsional rotation, one of the major nonradiative decay channel of the excited keto, is prevented in the aggregates. Therefore, the enhanced emission is observed from the aggregates. In 70% water, the excitation spectral maxima recorded at 356 nm and 430 nm appear at 294 nm. This indicates that 294 nm absorbing species is a ground state precursor for both the emissions. The band at 294 nm advocates that those aggregated structures are formed with the twisted conformer in this solution. The twisted conformer does not possess the intramolecular hydrogen bond which is a prerequisite for the ESIPT. Therefore, it emits enol emission in the aggregated state. The additional band at 430 nm matches with the anionic emission observed at higher pH in aqueous solution (Section 4.4). Therefore, it can be assigned to the anionic emission. The lifetime of the enol emission and the anionic emission in 70% water solution are 0.56 ns and 2.1 ns, respectively. Aggregation provides the restricted environment for molecules which reduce the intramolecular rotation of the molecules. This enhances the radiative

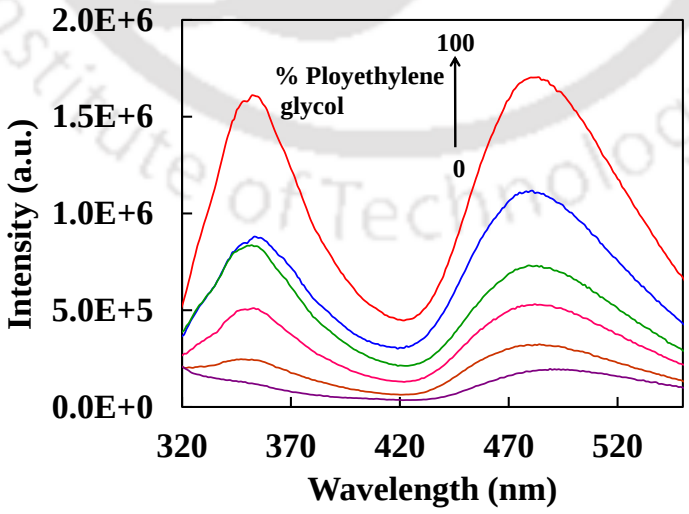


**Figure 4.7.** Emission spectra of BHPBI in THF with gradual increase of polyethylene glycol, $\lambda_{ex}$ = 290 nm. [BHPBI] = 5 μM.

emission. The enhancement of the normal and the tautomer emission with increase of polyethylene glycol concentration in THF solution further supports this (Figure 4.7.).

FESEM images suggest that the blue color emitting aggregates in 70% water are of rod shape with length of 0.5-1.5 μm (Figure 4.8.A). On the other hand, cyan color emitting aggregates in 90% water solution are 10-15 μm long needles (Figure 4.8.B). The longer needles infer the lesser interaction of BHPBI with solvent molecules. Hence, the intramolecular hydrogen bonding between the azole nitrogen and 'OH' proton are more favored. Thus, the molecules possess quasi-planar structure in the aggregate which produces the tautomer emission. The higher solvation energy in 70% water breaks the intramolecular hydrogen bond and produces the twisted conformers. Upon aggregation, this conformer formed much smaller rods. The excitation of the twisted conformer results in the enol emission as observed in other solvents. The photoexcitation also increases the acidity of the phenolic proton. Unlike in the quasi planar conformer, in the twisted conformer azole nitrogen is not in proximity to accept the proton. Therefore, the molecule transfers the proton to the solvent and produces the deprotonated HPBI unit. It results in the anionic emission along with the enol emission. This is same as observed for the *cis*-H-bond complex of HPBI and its analogues, which undergoes intermolecular proton transfer to form anion in the excited state (Chapter 3).

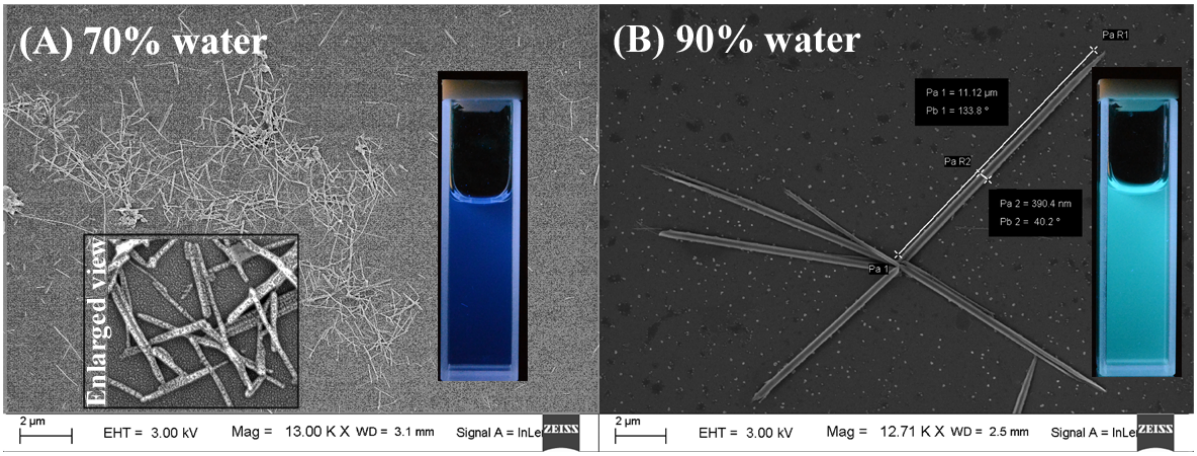


**Figure 4.8.** FESEM images and fluorescence emission of different aggregated forms of BHPBI in (A) 70% and (B) 90% water-THF mixture. [BHPBI] = 5 μM.

## 4.6. Conclusion

The spectral characteristics of BHPBI molecule are studied using the absorption, fluorescence and fluorescence lifetime experiments. The HPBI units in BHPBI can persist in a quasi-planar or a twisted structure. The switching between the quasi planar

and the twisted conformer depends on the environment. In presence of strong hydrogen bond donating and accepting solvents, the twisted conformer predominates. On the other hand, in non-polar solvents the quasi planar structure prevails. The twisted structure produces a normal enol emission whereas the planar structure produces the tautomer emission. Two different keto structures, *cis*-keto and *trans*-keto are responsible for the keto emission. The *trans*-keto emits at longer wavelength than the *cis*-keto. The fluorescence lifetime of the *trans*-keto is smaller than the *cis*-keto. BHPBI molecule is also exploited to produce aggregates in different fashions based on the solvent polarity and hydrogen bonding ability of the solution. In 90% water, the quasi planar structure forms the aggregates which exhibits strong cyan emission. In 70% water, the twisted structure forms aggregates to produce deep blue emission. Thus, the different conformers of a single ESIPT molecule are used to exhibit aggregation induced multicolor enhanced emission. The prototropic study reveals the existence of monoanion, dianion, monocation and dication. The monocation and monoanion undergo ESIPT due to the presence of free HPBI unit.

# Chapter 5

# Proton Transfer Induced Proton Transfer in (3,5-bis(2′-Hydroxyphenyl)-1H-1,2,4-triazole

## 5.0 Introduction

In the last chapter the transfer of a proton from a donor to an acceptor through an intramolecular hydrogen bond is discussed. Despite, the presence of two proton donor-acceptor pair in BHPBI, the molecule does not undergo double proton transfer in the excited state. Another fluorophore molecule, bis-2,5-(2-benzoxazoyl)hydroquinone, contains two proton accepting benzoxazole group linked to a proton donating hydroquinone system. This conjugated system also exhibits single proton transfer upon photoexcitation.[132] On the other hand, [2,2′-bipyridyl] -3,3′-diol ($BP(OH)_2$) which comprises with two symmetric sites, exhibits an excited state intramolecular double proton transfer (ESIDPT).[133] Recently, relay type intramolecular double proton transfer was reported with 7-hydroxyquinoline-8-carboxylic acid and 1,8-Dihydroxy-2-naphthaldehyde.[26, 134]

In the present chapter, the excited state characteristics of the triazole derivative (Tz) with two acid-base pair connected through intramolecular hydrogen bonds (Chart 5.1) are discussed. The spectral studies of Tz and its monomethylated derivative (MTz) have been performed to elucidate the proton transfer process. Theoretical calculations were used to support the experimental findings.

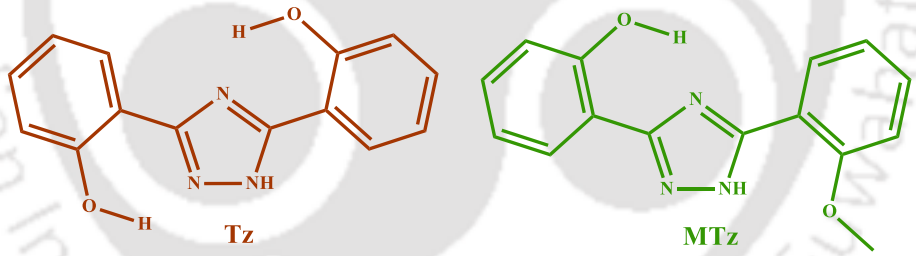


**Chart 5.1.** Molecular structure of Tz and MTz.

## 5.1. Solvatochromic study of MTz molecules

The longer wavelength absorption band of MTz possesses well resolved vibrational structure. The solvent polarity has little effect on the absorption maxima (Figure 5.1.A and Table 5.1). Upon excitation at 308 nm, a less Stokes' shifted UV emission is observed along with a highly Stokes' shifted visible emission. The ratio of the highly Stokes' shifted emission to the normal Stokes' shifted emission gradually decreases with increasing solvent polarity. For instance, in nonpolar solvent like hexane the ratio is 7.5, whereas, it decreases to 0.2 in methanol. With increasing solvent polarity the visible emission gradually shifts to the shorter wavelength. The high Stokes' shifts and the blue solvatochromic shift of the visible emission suggest that it appears from a keto tautomer

**Figure 5.1. (**A) Absorption spectra and (B) emission spectra of MTz in (1) hexane, (2) THF, (3) dioxane, (4) 2-propanol, (5) n-butanol and (6) methanol.

**Figure 5.2.** (A) Excitation spectra of MTz recorded at 340 nm and 440 nm in methanol. (B) Fluorescence lifetime decay of MTz in (a) methanol ($\lambda_{em}$= 440 nm), (b) dioxane ($\lambda_{em}$= 460 nm).

**Table 5.1.** Absorption maxima ($\lambda_{max}^{abs}$, nm) emission maxima ($\lambda_{max}^{em}$, nm) and fluorescence lifetime (τ, ns)[a] of MTz in different solvents.

| Solvents | $\lambda_{max}^{abs}$ | $\lambda_{max}^{em}$ | τ (monitored at shorter $\lambda_{max}^{em}$) | τ (monitored at longer $\lambda_{max}^{em}$) |
|---|---|---|---|---|
| Hexane | 298, 306 | 470 | | |
| Ethyl acetate | 298, 307 | 342, 456 | | 3.8 (100) |
| Chloroform | 299, 308 | 340, 456 | | 2.7 (100) |
| Dioxane | 299, 307 | 340, 450 | | 4.5 (100) |
| THF | 299, 307 | 341, 458 | | 4.1 (100) |
| 1-Butanol | 299, 308 | 340, 435 | 1.2 (100) | 3.5 (100) |
| 2-Propanol | 298, 307 | 340, 436 | 0.9 (93)<br>3.1 (7) | 3.2 (100) |
| Methanol | 298, 307 | 340, 440 | 0.8 (73)<br>1.7 (27) | 0.8 (69)<br>1.7 (31) |

[a] Relative percentage of different emitting species are given in parenthesis.

which is resulted from the ESIPT of the enol tautomer of MTz. The normal Stokes' shifted UV emission appears from the enol tautomer. The excitation spectra corresponded to both the emission in methanol are depicted in Figure 5.2.A. The two spectra does not superimpose on each other. This indicates that the ground state precursors for the different emissions are different. The fluorescence decays were monitored at the emission maxima (Table 5.1). Owing to weak normal emission in all nonpolar and less polar solvents the decays at the shorter wavelength could not be measure. But single exponential decays are observed when monitored at visible emission maximum. In more polar solvents due to the overlap of both the emission, biexpoentential decays are observed in some solvents. The relative amplitude of the short lifetime species is higher when monitored at shorter wavelength, and that of the long lifetime species is higher when monitored at longer wavelength. From this, it can be inferred that normal emission has shorter lifetime than the tautomer emission. Similar behavior was found in several other dyes aslo.[72, 118, 120]

**5.2. The origin of the different emissions in MTz**

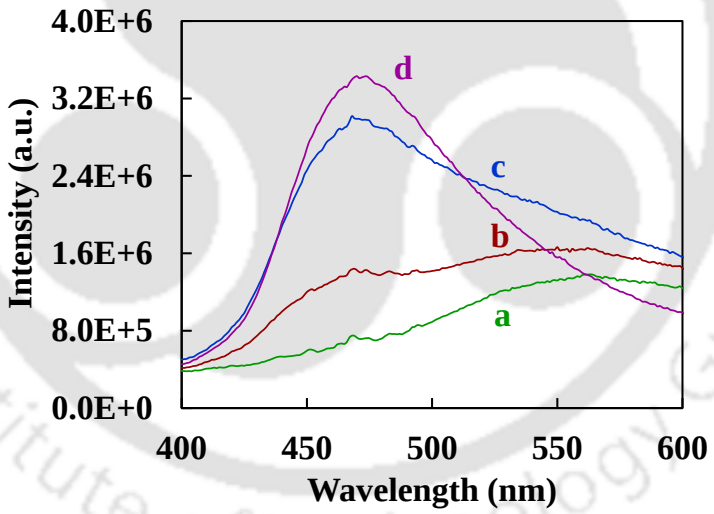


**Figure 5.3.** Emission spectra of MTz powder recorded upon excitation at (a) 320 nm, (b) 325 nm, (c) 330 nm, (d) 336 nm.

The emission spectra of the powder MTz sample are displayed in Figure 5.3. Unlike in solution, two different visible emissions appear at 470 nm and ~ 550 nm for the powder sample. The excitation wavelength dependency of the emission spectra infers the existence of more than one ground state species. Most probably, two different conformers exist in the ground state (Scheme 5.1). A close observation reveals that though the proton donating phenolic group and the proton accepting azole nitrogen are

close to each other, the electronic configuration in the triazole moiety of MTz-I cannot yield a normal keto tautomer structure. The proton transfer would generate either a Zwitter ionic structure or a diradical structure. On the other hand, the proton transfer of MTz-II conformer can produce a normal keto tautomer. Furthermore, the proton transferred species of MTz-II is more conjugated than that of MTz-I. Based on that the longer wavelength emission (~ 550 nm) can be assigned to the keto tautomer of MTz-II conformer. In solution, no visible emission appears around 550 nm, and only a single fluorescence lifetime was detected from the emission of the proton transferred species. It indicates that only the MTz-I conformer but not the MTz-II conformer is ESIPT active in solution. Most probably, the MTz-II conformer produces a normal emission, and the relative percentage of the conformer increases with increasing solvent polarity. Earlier, it was mentioned that the visible emission in solution produces a blue shift with increasing solvent polarity. But, the Zwitter ionic species would be more stable in polar solvent. It would result a bathochromic shift of the visible emission with increasing polarity. [28, 37, 135] However, the opposite results observed with increasing solvent polarity, indicate that MTz-I yields a diradical species after ESIPT (Scheme 5.1). The fluorescence decay of powder MTz are biexponential with lifetime 4.7 ns and 1.2 ns when monitored at 460 nm and 550 nm. The relative percentage of the shorter lifetime species increases at longer wavelength. It indicates that the longer wavelength emitting tautomer species is having the shorter lifetime.

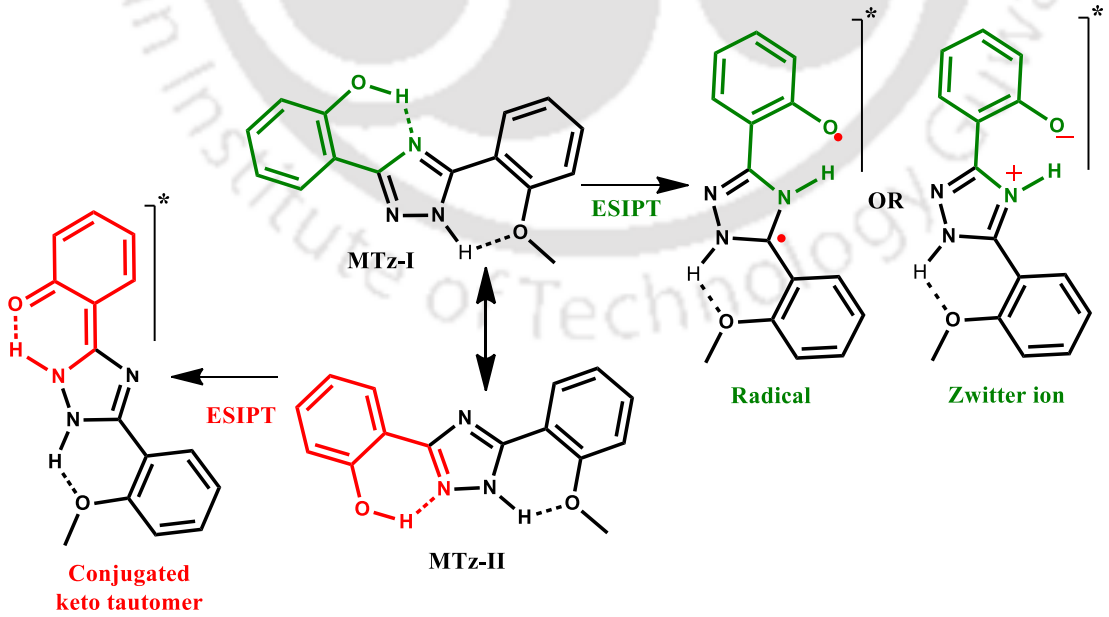


**Scheme 5.1.** Different ground state conformers of MTz and their possible proton transferred species in the excited state.

## 5.3. Solvatochromic study of Tz molecules

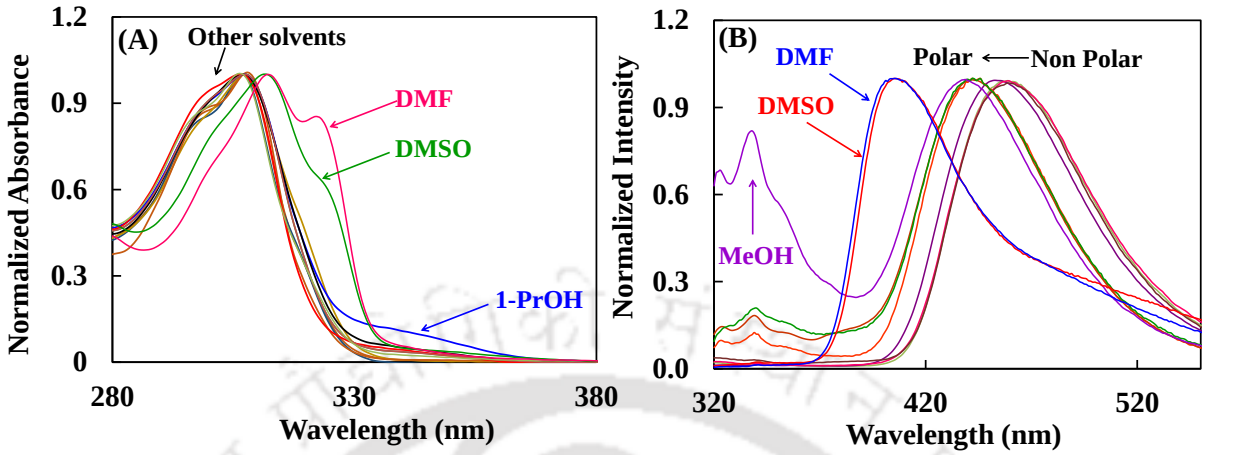


**Figure 5.4.** (A) Absorption spectra of Tz in different solvents. (B) Emission spectra of Tz in different solvents. ($\lambda_{ex}$ = 308 nm).

**Table 5.2.** Absorption maxima ($\lambda_{max}^{abs}$, nm) emission maxima ($\lambda_{max}^{em}$, nm) and fluorescence lifetime (τ, ns)[a] of Tz in different solvents.

| Solvents | $\lambda_{max}^{abs}$ | $\lambda_{max}^{em}$ | τ (monitored at shorter $\lambda_{max}^{em}$) | τ (monitored at longer $\lambda_{max}^{em}$) |
|---|---|---|---|---|
| Ethyl Acetate | 307 | 460 | | 0.7 (72)<br>3.7 (28) |
| Dioxane | 308 | 460 | | 0.8 (61)<br>3.9 (39) |
| THF | 308 | 459 | | 0.8 (62)<br>4.0 (38) |
| Methanol | 307 | 338, 438 | 1.4 (100) | 0.7 (48)<br>3.0 (52) |
| 1-Propanol | 308 | 340, 442 | 1.6 (100) | 1.8 (70)<br>4.1 (30) |
| 1-Butanol | 308 | 340, 444 | 1.6 (100) | 2.4 (68)<br>4.0 (32) |
| DMF | 313, 323 | 406, 480 | 3.0 (66)<br>4.5 (34) | 4.5 (100) |

[a]Relative percentage of different emitting species is given in parenthesis.

Figure 5.4.A depicts the absorption spectra of Tz molecule in different solvents. The absorption spectra of Tz molecule in nonpolar solvents are similar to that of MTz with a maximum at 308 nm. However, in polar protic solvent, a small band is observed around 336 nm along with the main absorption band. In solvents like DMSO, DMF with strong proton accepting character, the absorption band is little red shifted, and band maxima appear at 313 nm and 323 nm. Upon excitation at 308 nm, the emission appears in the UV and the visible region depending on the solvent nature (Figure 5.4.B). Unlike MTz, in less polar medium like hexane, chloroform, THF, dioxane the visible emission

band is only observed (Table 5.2). However, in protic solvents, Tz emits UV emission in addition to the visible emission. The hypsochromic shift of the visible emission with increasing solvent polarity, and the huge Stokes' shift indicate that the emission appears from a keto tautomer which is generated due to the proton transfer from the phenolic unit to the triazole nitrogen of Tz moleule. The UV emission appears from the normal enol tautomer. Similar to MTz, the maximum intensity of the enol emission is observed in methanol. The intensity ratio of the keto to enol emission for Tz in methanol is 1.25, which is six times higher compared to that of MTz. A striking difference is noticed between the fluorescence lifetimes of the visible emission of Tz and MTz. In nonpolar and less polar solvents, the visible emission of MTz decays single exponentially. In contrary, a biexponential decay is observed for the visible emission of Tz molecule in nonpolar and less polar solvents. Along with the longer lifetime species a shorter lifetime also appears. The relative amplitude of the shorter lifetime species increases when monitored at longer wavelength. In polar solvents also, the shorter lifetime obtained at longer wavelength is different from that observed for the UV emission (Table 5.2). This shows the existence of at least two visible emission emitting species. TRANES were constructed using the emission decays recorded at different wavelength of the visible emission in dioxane (Fig. 5.5.A). The emission maxima are 455 nm and 465 nm for 3.9 and 0.8 ns decaying species, respectively. But, the excitation spectra monitored at different visible emissions in dioxane merge with each other (Figure 5.5.B). This indicates that both the visible emissions originate from a single ground state species.

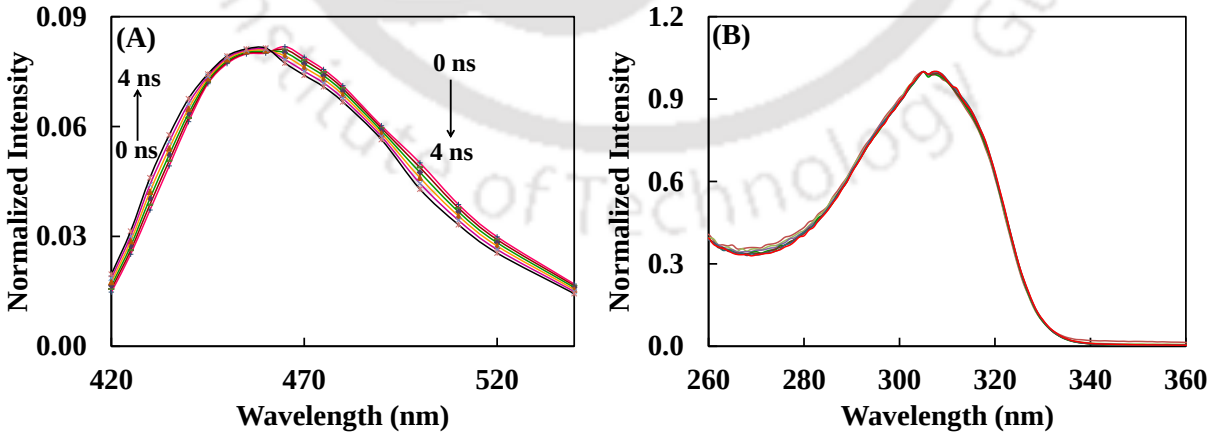


**Figure 5.5.** (A) Time-resolved area normalized emission spectra of Tz in dioxane, $\lambda_{ex}$= 308 nm. (B) Normalized excitation spectra of Tz recorded at different visible emission wavelength ($\lambda_{em}$, 430 nm to 490 nm) in dioxane.

### 5.4. Pathways to generate different tautomer emission in TZ

The results of Tz with MTz suggest that the presence of both 'OH' are essential for the biexponential nature of the visible emission of Tz. The most stable conformer of Tz (referred Section 5.7) is shown in Scheme 5.2. The two phenolic units are labelled as Ph-I and Ph-II for the convenience (Scheme 5.2). Both the units can follow different pathways to generate proton transferred species. The ESIPT of the Ph-I 'OH' produces the keto tautomer, K-I (Scheme 5.2). On the other hand, the ESIPT with the Ph-II unit would produce a more conjugated keto structure, K-II. It should exhibit a longer wavelength keto emission. A similar conjugated keto species of MTz molecule emits at ~ 550 nm in the powder sample. Therefore, the two keto emissions should appear from K-I and diketo (DK) and not form K-II. The keto part of both K-I and DK are structurally closer to each other than that of K-II. This supports the relatively closer band maximum of K-I and DK. The emitting unit of K-I keto tautomer structurally resembles the keto tautomer of 4,5-dimethyl-2-(2'-hydroxyphenyl)imidazole. Furthermore, the keto tautomer of 4,5-dimethyl-2-(2'-hydroxyphenyl)imidazole shows an emission around 450 nm with fluorescence lifetime ~ 4.0 ns.[136] The keto species corresponding to the 455 nm emission of Tz also possesses excited state lifetime 3.9 ns. The theoretical calculation also predicts that DK emits at a longer wavelength than K-I (Section 5.7). Since, DK is expected to emit at longer wavelength, than K-I, the 465 nm emission can be assigned to DK. The other emission at 455 nm can be assigned to K-I.

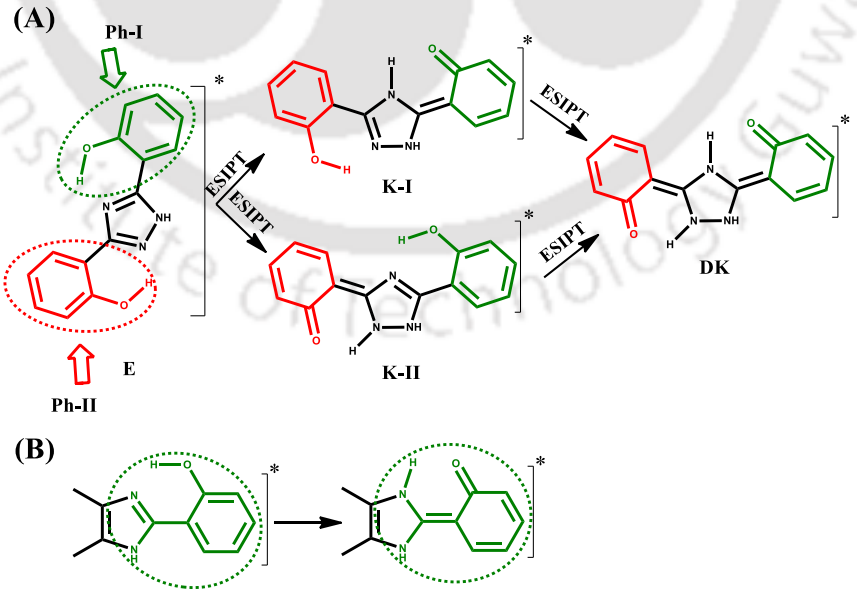


**Scheme 5.2.** (A) Formation of different keto tautomers of Tz molecule in the excited state. (B) Molecular structure of enol and keto tautomer of 4,5-dimethyl-2-(2'-hydroxyphenyl)imidazole.

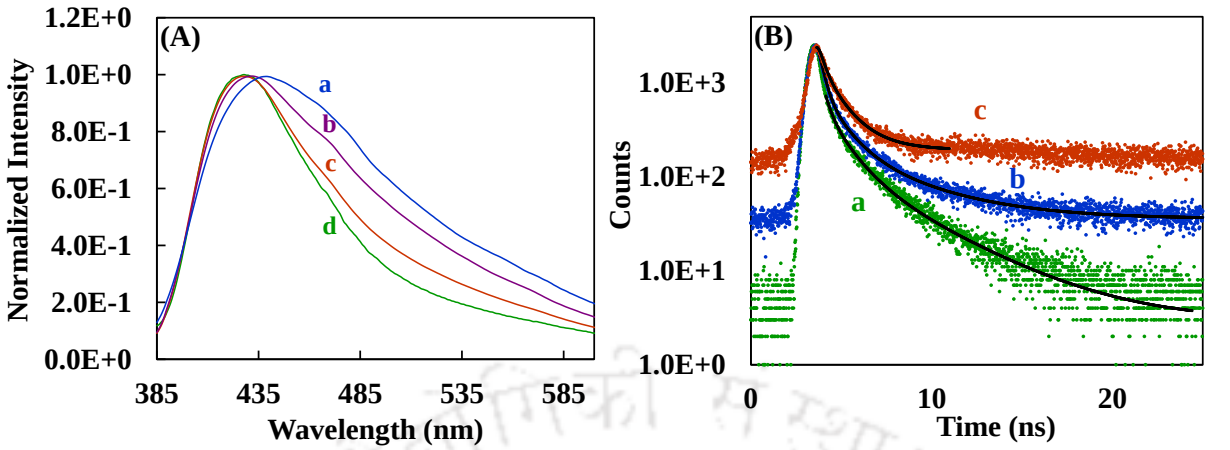


**Figure 5.6.** (A) Emission spectra of Tz powder at different wavelength (a) 340 nm, (b) 350 nm, (c) 360 nm, (d) 370 nm. (B) Fluorescence decay of Tz powder monitored at different emission wavelength, (a) 430 nm, (b) 470 nm and (c) 550 nm.

The emission spectra of Tz molecule were recorded for the powdered sample (Figure 5.6.A) to verify whether the more conjugates keto (K-II) emission appears in the solid state. The normalized emission spectra recorded at different excitation wavelength show the existence of more than one emission. The emission maximum gradually shifts toward the longer wavelength with decreasing the excitation wavelength. A triexponential fluorescence decay is obtained for the emission monitored at 430 nm, 470 nm and 550 nm with lifetime 4.0 ns, 0.3 ns and 1.1 ns (Figure 5.6.B). The relative population of the emitting species with lifetime 4.0 ns, 0.3 ns and 1.1 ns were maximum at 430 nm, 470 nm and 520 nm monitoring wavelength, respectively. However, the longer wavelength emitting species with fluorescence lifetime 1.1 ns is not obtained in solution. Scheme 5.2 shows that three different keto emission is only possible if both the pathways are followed to generate K-I, K-II and diketo (DK) species. It shows that both the paths are followed only in the solid state but not in solution. It appears that in solution, the proton transfer process in Ph-II is not initiated. But, it takes part in ESIPT after the occurrence of the first proton transfer from Ph-I unit. The results indicates that in solution two different keto emissions are due to consecutive proton transfer. This is also substantiated by the fact that both the visible emissions in solution have same ground state precursor.

### 5.5. Emission from different conformers of Tz

Unlike MTz, Tz molecule exhibits only keto emission in nonpolar solvent. It indicates the existence of a single Tz conformer in nonpolar solvent. Most likely, it is Tz-I conformer where both the phenolic 'OH' form strong intramolecular hydrogen bond

with the electron rich $sp^2$ azole nitrogens (Scheme 5.3). Theoretical calculations also reveals that the Tz-I conformer is the most stable conformer in the ground state (Section 5.7). The enol emission appears in polar protic solvents. The excitation spectra recorded at enol and keto emission maxima do not merge with each other (Figure 5.7.A). It indicates that those emissions appear from different ground state species. In polar protic solvents, the intramolecular hydrogen bond in Tz-I is broken and intermolecular hydrogen bond is formed. This leads to the increase in population of the other conformers (Scheme 5.3). The breaking of intramolecular hydrogen bond of *cis*-enol of HPBI in polar protic solvent increases the relative population of *trans*-enol.[72] The trans-enol is formed by 180° torsional rotation of the phenol moiety. The 180° torsional rotation of Ph-II unit provides a sterically hindered conformer Tz-IV, whereas, the torsional rotation of Ph-I unit provides a relatively more stable conformer Tz-II. The excitation spectra, recorded at different wavelengths of the visible emission of Tz in methanol, indicate that the dual tautomer emission in polar protic solvent appears from single ground state precursor/conformer (Figure 5.7). It establishes that Tz-II conformer in polar protic solvent does not undergo ESIPT, and produces only the enol emission. Same as in nonpolar solvent, the visible emission in polar protic solvent also appears from Tz-I conformer. The result indicates that same as Tz-I conformer in Tz-II conformer also Ph-II unit does not undergo ESIPT in solution.

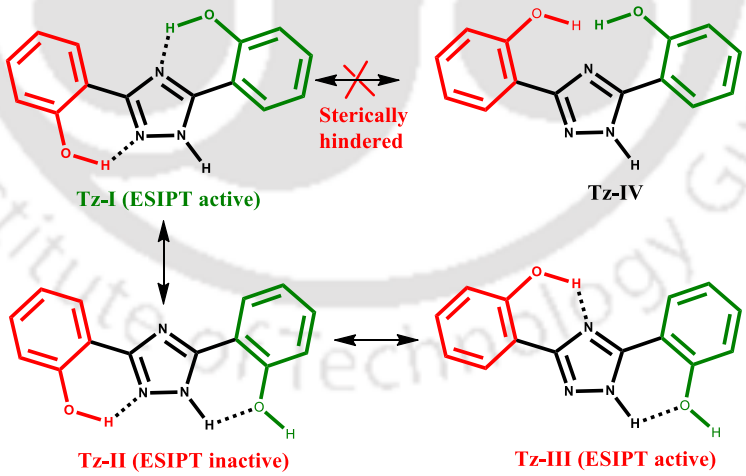


**Scheme 5.3.** Possible switching between different ground state conformers of Tz in solution.

In DMF and DMSO, the absorption spectra of Tz are red shifted compared to that in other solvents (Figure 5.4.A). This suggests a stronger interaction between the solvent and Tz. Similar red shift was observed in the absorption spectra of *cis*-H-bond complexes of HPBI, HPIP-b and HPIP-c in presence of anion (Chapter 3). DMF and

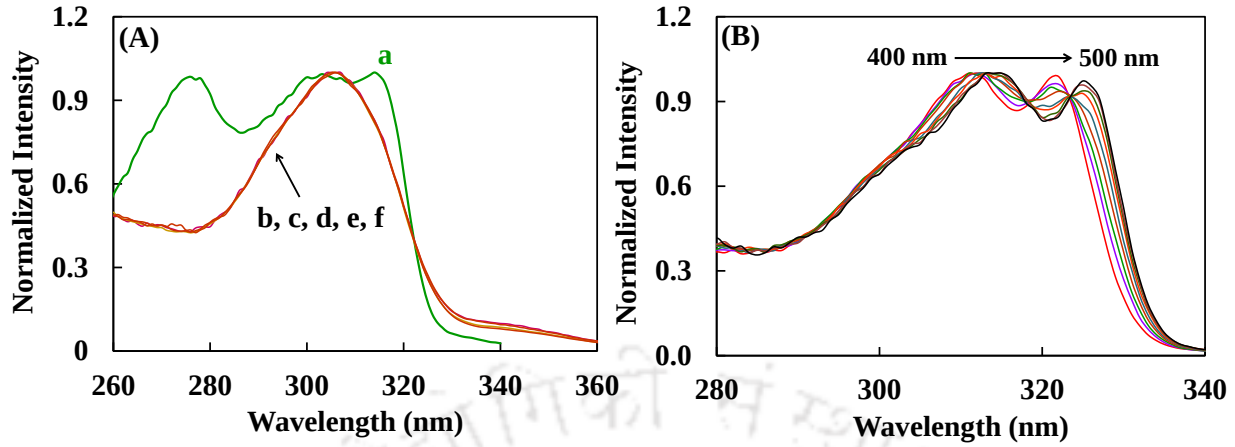


**Figure 5.7.** (A) Excitation spectra of Tz in methanol recorded at different emission wavelength, (a) 350 nm, (b) 430 nm, (c) 440 nm, (d) 460 nm, (e) 480 nm, (f) 500 nm. (B) Excitation spectra of Tz in DMF recorded at different emission wavelength.

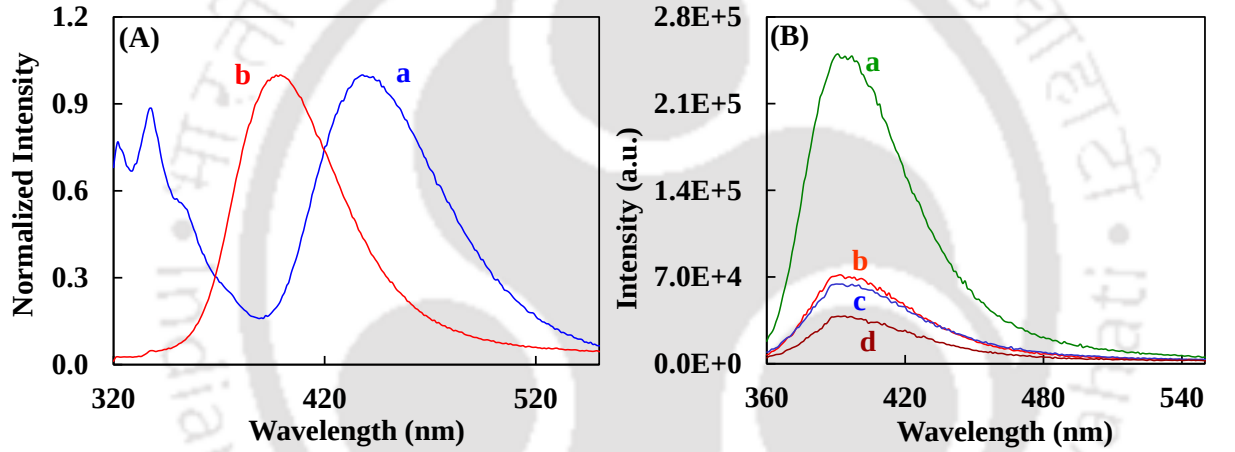


**Figure 5.8.** (A) Emission spectra of Tz in (a) methanol and (b) alkalined methanol, $\lambda_{ex}$= 308 nm. (B) Emission spectra of Tz in different polar protic solvents, (a) propan-1-ol, (b) butan-1-ol, (c) propan-2-ol, (d) methanol, $\lambda_{ex}$= 350 nm.

DMSO are strong proton accepting solvent. Therefore, no surprise they behave similar as external anion. Upon excitation at 308 nm, two different emissions are observed in DMF at 406 nm (major) and a broad band at ~ 480 nm (minor) (Figure 5.4.B). Since, the effect of DMF and DMSO are same, the excitation spectra in DMF are shown in Figure 5.7.B. The excitation spectra, recorded at the two bands possess similar vibration progression though they do not overlap with each other (Figure 5.7.B). It indicates the presence of more than one conformer of Tz exist in these solvents. The excitation spectra of the shorter wavelength emission band is similar to the excitation spectra of the enol emission band observed in polar protic solvents (Figure 5.7.A). But, they are little red shifted than those in polar protic solvents. It indicates that same ground state conformer, Tz-II may be responsible for the 406 nm emission. But it forms strong hydrogen bond

complex with DMF and DMSO. The 406 nm emission is red shifted compared to normal emission and blue shifted compared to tautomer emission. As discussed in earlier chapters, this is due to formation of anion. Due to the high proton accepting nature of these solvents and the enhanced acidity of the phenolic group in the excited state, the intermolecular proton transfer occurs prior to the ESIPT from the 'OH' of Ph-I unit to the solvent molecule, and Tz-II molecule generates anionic emission. In alkaline methanol solution also the anionic emission appears at around 400 nm (Figure 5.8.A). Such an anion emission due to intermolecular proton transfer to solvent is also observed from HPBI in DMSO.[35] The anionic emission is also observed in polar protic solvents upon excitation at 350 nm (Figure 5.8.B). A little absorbance observed for Tz molecule around ~ 340 nm in polar protic solvents explains the existence of anion in the ground state (Figure 5.4.A). The excitation spectra, corresponding to the 480 nm emission in DMF appear in the longer wavelength region as compared to the excitation spectrum obtained for the keto emission of Tz-I conformer in nonpolar and polar protic solvents. This indicate that Tz-I conformer is not responsible for the 480 nm emission in DMF and DMSO. If Tz-II undergoes ESIPT, it would result in more conjugated K-II tautomer. But the emission spectra in DMF and DMSO are substantially blue shifted compared to K-II emission. Other than Tz-I and Tz-II, another possible conformer is Tz-III (Scheme 5.3) which can be generated from Tz-II conformer by 180° torsional rotation of Ph-II unit. This conformer is similar to the MTz-I conformer. Earlier, it was mentioned that MTz-I generates a diradical species after ESIPT. Most probably, the Ph-II unit of Tz-III conformer generates a Zwitter ionic proton transferred species instead of the diradical species. The significant red shifted emission (480 nm) of Tz-III indicates that the proton transferred species is stabilized well in polar DMF and DMSO. In contrary, the visible emission from the proton transferred diradicle species of MTz-I conformer exhibits a hypsochromic shift with increasing solvent polarity. The similar bathochromic shift of Zwitter ionic species upon proton transfer was reported earlier.[28, 37, 135]

**5.6. Annular tautomerism and ESIPT of Tz and MTz**

The two proton donor-acceptor pairs in Tz-I conformer look similar to each other (Scheme 5.3). However, the ESIPT is first initiated only from Ph-I in solution. In contrary to the solution, in powder sample a longer wavelength keto emission appears from K-II tautomer also along with the other two keto emissions (Figure 5.6). It indicates that the proton transfer from the Ph-II unit to 'N2' is not impossible but in solution state the process is unfavorable. This can be explained from the annular tautomerism between

'N1-H' and 'N2'. [137-140] Due to the presence of electron withdrawing $sp^2$ nitrogen ('N2' and 'N4') the 'N1-H' proton in the azole ring is fairly acidic, and it is shared between 'N1' and 'N2'. As a consequence, the intramolecular hydrogen bond between the Ph-II unit and 'N2' is ruptured due to the shuttling nature of the acidic proton. The shifting of the proton from 'N1' to 'N2' would provide a less stable tautomer than Tz-I, which is Tz-III (Scheme 5.3 and Scheme 5.4). However, a torsional rotation of both Ph-I and Ph-II unit of the annular tautomer generates the Tz-I conformer (Scheme 5.4). It further establishes that the acidic proton should be shared equally between the two nitrogens. Due to this, in solution the proton cannot be transferred to 'N2', and Ph-II cannot undergo ESIPT. But in solid state, the torsional rotation and the annular tautomerism are hindered and the molecule exist in the most stable Tz-I conformer. As a result, in the absence of annular tautomerisation in solid state the proton localized on 'N1' nitrogen, and the Ph-II unit finds a suitable proton accepting $sp^2$ azole nitrogen (N2) to undergo ESIPT. However, in solution after the first proton transfer (when the proton is transferred to 'N4'), since the acidity of 'N1-H' decreases the annular tautomerism diminishes. Therefore, ESIPT occurs from Ph-II also.

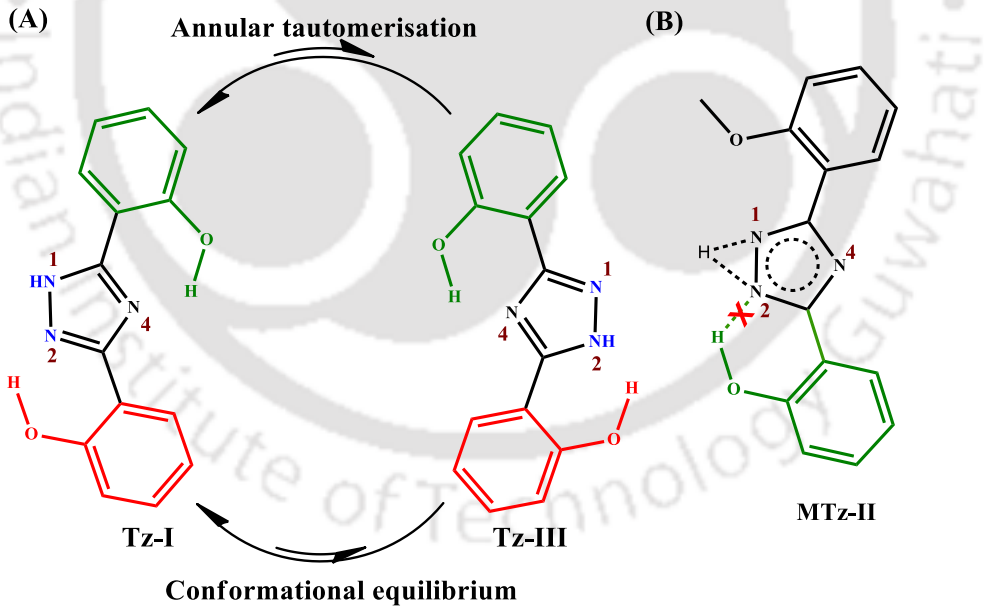


**Scheme 5.4.** (A) Annular tautomerism and conformational equilibrium of Tz-I in solution. (B) Blocking of intramolecular hydrogen bond formation between 'N2' and 'OH' proton due to the annular tautomerism in MTz-II.

MTz molecule also exhibits a similar behavior in solution and solid state. ESIPT from MTz-II conformer is only observed in powder sample but not in solution. Due to the annular tautomerisation the acidic 'NH' proton in MTz-II is shared between 'N1' and

'N2'. The tautomerisation prevents MTz-II conformer to form intramolecular hydrogen bond between 'N2' and phenolic 'OH' proton and averts the ESIPT in solution. In solid state due to the localization of proton the MTz-II conformer exhibit keto emission in the excited state. The variation of the annular tautomerism in solid and solution is reported for different azole derivatives.[137]

### 5.7. Quantum chemical calculations

**Table 5.3.** Relative ground state energy of different Tz conformer with respect to Tz-I in methanol.

| Conformer | Energy (eV) |
|---|---|
| Tz-I | 0 |
| Tz-II | 0.1073 |
| Tz-III | 0.0767 |
| Tz-IV | 0.1164 |

Ground state energy of Tz-I is -23263.159515943 eV.

The DFT optimized ground state energies of different Tz conformers are shown in Table 5.3. Tz-I is the most stable conformer. The lowest energy vertical transition of Tz-I appears at 302 nm in methanol. The calculated enol emission in methanol is found at 364 nm. Both the results agree well with the experimental findings. The 'O-H' bond is stronger in Ph-II (0.98 Å) as compared to that of Ph-I (0.99 Å). The distance of the azole nitrogen 'N4' and the 'OH' proton of Ph-I unit is 1.75 Å, whereas the distance is longer between 'N2' and the 'OH' proton of Ph-II unit (1.80Å). This supports the experimental fact that the proton transfer occurs in solution from Ph-I and not from Ph-II. The calculated emission maxima for K-I is 432 nm. As expected, the K-II tautomer emits at longer wavelength with a maximum at 562 nm. The DK species was optimized with redundant internal coordinates. The calculated emission of DK is 465 nm which is close to the experimental value. The XYZ coordinates of different ground and excited state species are given in Annexure-B.

### 5.8. Conclusion

The monomethyl derivative emits dual emission due to normal emission and proton transferred diradical emission in solution. However, in solid state, only tautomer emissions are observed. Tz molecule undergoes excited state single and double proton transfer and generates a monoketo and a diketo species. The process is initiated with a particular phenol unit. The other phenol unit cannot commence the ESIPT process due to the annular tautomerism. After the first proton transfer, the acidity of 'N1-H' proton decreases and the second proton transfer takes place. However, in solid sample, due to the structural rigidity annular tautomerism is not efficient, and both the phenol unit

undergoes ESIPT. In strong proton accepting solvents like DMF and DMSO Tz forms strong hydrogen bond complex and exhibit anionic emission. In addition, the visible emission of Tz in these solvents appears from Zwitter ionic species which is yielded from the ESIPT.

# Chapter 6

# Construction of Molecular Logic Gates by Perturbing the Emission Behaviors of a Few Azole Derivatives

## 6.0. Introduction

The spectral properties of a molecule can be perturbed using different chemical and optical stimuli.[141-143] External stimuli may produce different stable or quasi stable states which absorb or emit light at different wavelengths. Similar to the high and low output in Boolean system, the spectral changes in different states can be used to mimic the functions of electronic circuits.[66, 144, 145] Although in past few years, molecular interactions have been used extremely to develop molecular OR, AND, XOR, INHIBIT, NOT logic circuits, the alluring idea is, to use the molecular system as a more complex multitask performer device.

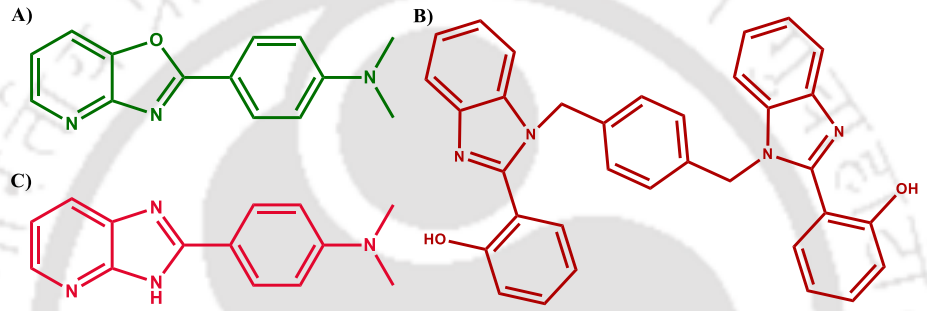


**Chart 6.0.** Molecules used to construct logic gates (A) DMAPOP, (B) BHPBI and (C) DMAPIP-b.

In this chapter, construction of simple logic gate to complex logic operation are shown to miniaturize the operation of silicon chips. Three different azole derivatives, DMAPOP, BHPBI and DMAPIP-b (Chart 6.0) have been used to construct molecular logic gates in presence of different inputs. Accordingly, the chapter is divided in three different sections. In section 6.1, the controlled binding of metal ions with the fluorophore in presence of micelle is exploited to construct simple Boolean logic gates. In section 6.2, the construction of similar Boolean logic gates are shown but rather than using two chemical inputs, one optical and one chemical inputs were used. The molecule is also shown to function as a memory device. Section 6.3 describes not only binary molecular logic systems but also ternary and multiple valued logic systems. The mapping of emission output with different chemical inputs are presented by constructing Fuzzy Interference System (FIS).

## 6.1. Specific site binding of metal ions in presence of anionic micelle and construction of molecular logic gates

DMAPOP possesses three different metal ion binding sites. It was reported that $Cu^{2+}$and $Cd^{2+}$ form two different types of complexes with DMAPOP. $Cu^{2+}$ binding sites are

pyridyl nitrogen and dimethylamino nitrogen, and $Cd^{2+}$ binding sites are azole nitrogen and dimethylamino nitrogen (Chart 6.1.1).[146] In the present section, a surfactant is effectively used to control the metal ion binding site on DMAPOP. The interactions of $Cu^{2+}$, $Cd^{2+}$ in presence and in absence of micelle are utilized to develop different logic functions.

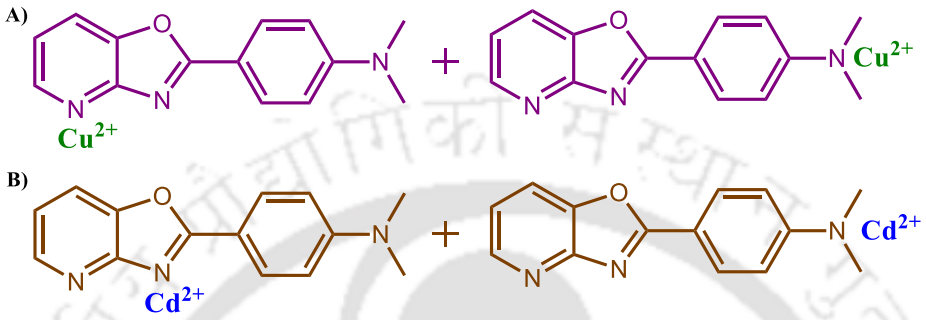


**Chart 6.1.1.** Different metal complexes of DMAPOP in presence of A) $Cu^{2+}$, B) $Cd^{2+}$ in acetonitrile.

### 6.1.1. Metal ion binding in micellar medium

In presence of SDS (surfactant) the absorption spectrum of DMAPOP is red shifted and the fluorescence spectrum is blue shifted compared to those in aqueous medium (Figure 6.1.1). The results are consistent with the encapsulation of DMAPOP inside the micelle. Figure 6.1.2 depicts the absorption spectra of DMAPOP in 8.2 mM of SDS at different concentrations of $Cu^{2+}$ and $Cd^{2+}$ metal ions. The pH of the solutions were kept at 6.1 ± 0.1. The addition of metal ion produce a little red shift in the absorption spectrum of DMAPOP. The fluorescence spectra of DMAPOP with increasing metal concentration is shown in Figure 6.1.3. In presence of $Cu^{2+}$ the emission intensity gradually decreases. It indicates that the excited $Cu^{2+}$ complex of DMAPOP follows a non-radiative decay pathway. The binding constant of the molecule with the metal ion was obtained from the quenching equation (eq. 6.1.1.).[147]

$$I_0/I = 1 + K[Q] \qquad \textbf{(eq. 6.1.1.)}$$

where I and $I_0$ are the fluorescence intensities in presence and absence of quencher, respectively. *K* is the binding constant and [Q] is the concentration of quencher. On the other hand, with gradual increase of $Cd^{2+}$ a new red shifted band emerges at 463 nm (Figure 6.1.3.B).The binding constant of $Cd^{2+}$ with DMAPOP was measured using Benesi-Hildebrand equation (eq. 6.1.2).[148]

$$1/(I - I_0) = 1/(I_\infty - I_0) + 1/((K[M])(I_\infty - I_0)) \qquad \textbf{(eq. 6.1.2.)}$$

where $I_0$, $I_\infty$, I are the intensities of DMAPOP in micelle at zero, maximum and any

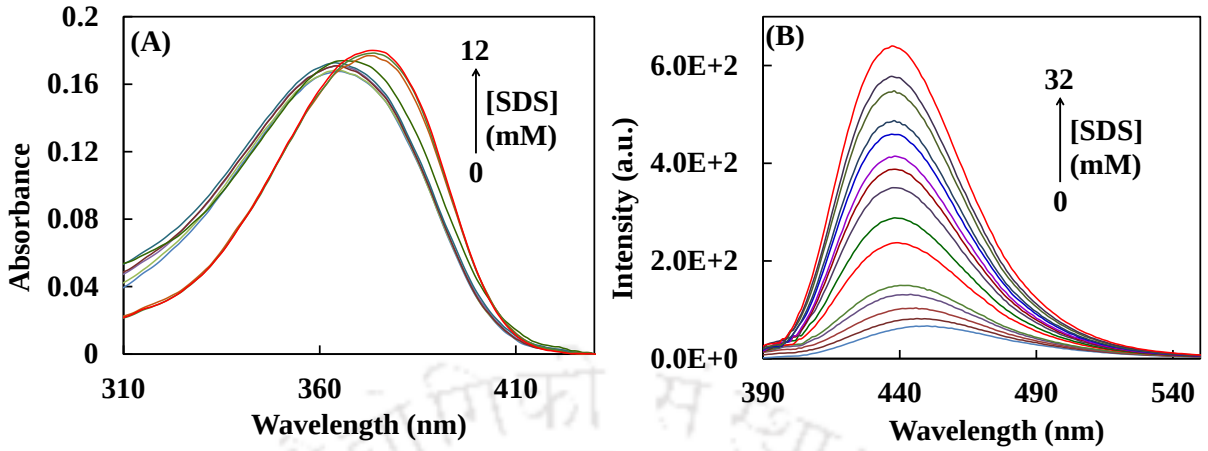


**Figure 6.1.1.** (A) Absorption spectra, (B) emission spectra of DMAPOP with increasing SDS concentration in aqueous medium.

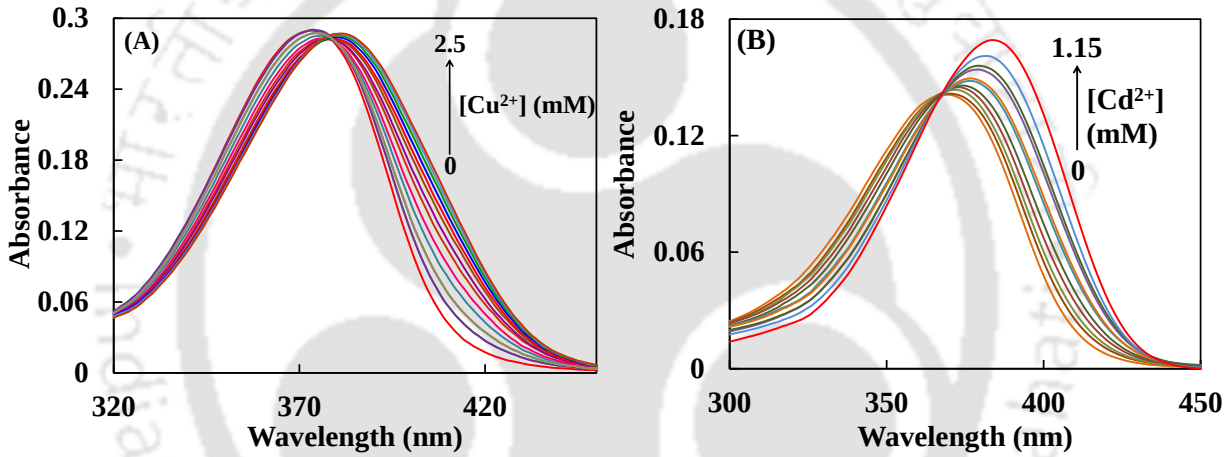


**Figure 6.1.2.** Absorption spectra of DMAPOP in 8.2 mM of SDS solution with gradual increase of (A) $[Cu^{2+}]$ and (B) $[Cd^{2+}]$.

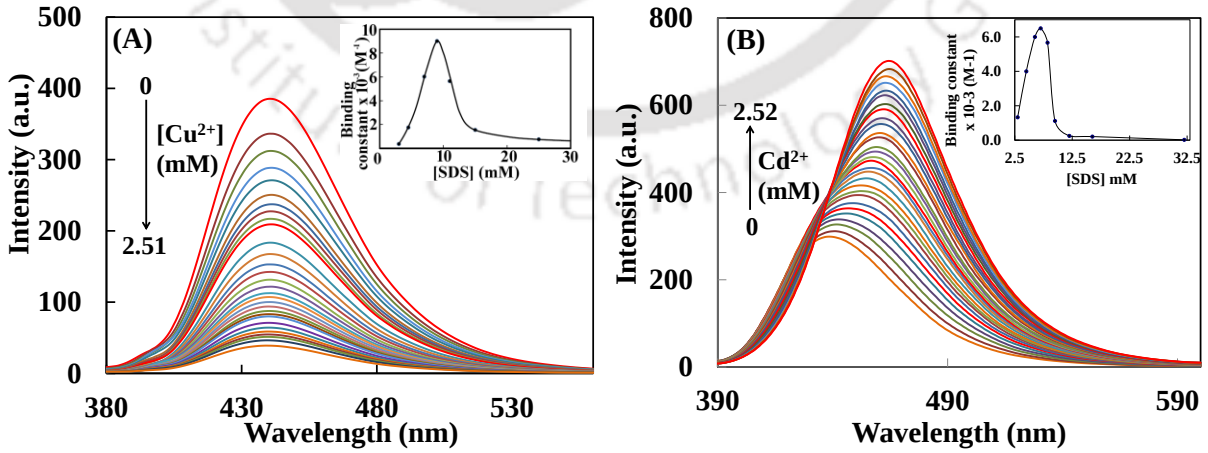


**Figure 6.1.3.** Emission of DMAPOP in 8.2 mM of SDS solution with gradual increase of (A) $[Cu^{2+}]$, (B) $[Cd^{2+}]$, $\lambda_{ex}$ = 378 nm. In both cases the inset shows the binding constant of DMAPOP with the metal ion at different SDS concentration.

intermediate concentration of $Cd^{2+}$, respectively. [M] and *K* are metal ion concentration and the binding constant, respectively. The binding constants for both the metal ion are maximum in 8.2 mM of SDS concentration, which is close to the critical micellar concentration of SDS (Figure 6.1.3. insets). In 8.2 mM of SDS solution the K obtained for $Cu^{2+}$and $Cd^{2+}$ were $9x10^3$ and $6.5x10^3$ $M^{-1}$, respectively.

The molecule has three basic centers pyridyl nitrogen, oxazole nitrogen and dimethylamino nitrogen. The binding of cations through the dimethylamino group results in a blue shift, and those through the ring nitrogen produces a red shift (Table 6.1.1). It is also expected that higher conjugation would provide more bathochromic shift in the absorption spectrum upon binding at the pyridyl nitrogen than at the azole nitrogen.[149] In acetonitrile, the metal complex through the pyridyl nitrogen produces 66 nm bathochromic shift.[146, 150] Whereas the metal complex using the oxazole nitrogen exhibits less (only 16 nm) bathochromic shift in the absorption spectrum (Table 6.1.1.).[146] In micellar medium, the bathochromic shift is just about 12 nm for both $Cd^{2+}$ and $Cu^{2+}$ complexes. Again, neither $Cd^{2+}$ nor $Cu^{2+}$ generates any hypsochromic shift in the absorption spectra of DMAPOP in presence of SDS. The results not only indicate that both the metal ions bind only at one basic center but also suggests that not only $Cd^{2+}$ but also $Cu^{2+}$ bind through the oxazole nitrogen to form the complex with DMAPOP in micellar medium.

**Table 6.1.1.**Absorption band maxima ($\lambda_{max}^{abs}$, nm) and fluorescence band maxima ($\lambda_{max}^{em}$, nm) in different media.

| Medium | In absence of metal ion | | In Presence of $Cu^{2+}$ | | In Presence of $Cd^{2+}$ | |
|---|---|---|---|---|---|---|
| | $\lambda_{max}^{abs}$ | $\lambda_{max}^{em}$ | $\lambda_{max}^{abs}$ | $\lambda_{max}^{em}$ | $\lambda_{max}^{abs}$ | $\lambda_{max}^{em}$ |
| Acetonitrile[a] | 359 | 418 | 310, 425 | 380 | 300, 375 | 370, 470 |
| Water | 364 | 447 | 364 | 447 | 364 | 447 |
| SDS | 372 | 438 | 384 | | 385 | 463 |

[a] reference 146.

## 6.1.2. Mode of encapsulation and metal ion binding at selective site

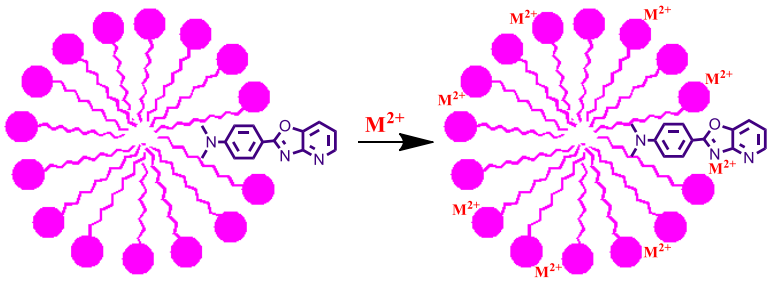


**Scheme 6.1.1.** Encapsulation of DMAPOP in micelle and controlled metal ion binding.

The molecule can go inside the micelle either partially or completely. The fluorescence decay experiment suggests the partial encapsulation of the fluorophore. In acetonitrile medium the fluorescence lifetime of the molecule is ~1.56 ns.[81] DMAPOP has shorter lifetime (1.12 ns) in micellar medium compared to acetonitrile, this may be due to the quenching of the fluorophore by water. To substantiate further, that the decrease in the lifetime is due to the quenching by water, the lifetime of DMAPOP in water was measured. The lifetime thus obtained, 0.43 ns, is shorter than that in micelle. Thus, the results suggest that DMAPOP is not completely buried inside the micelle but partially exposed to water. The other important concern is the orientation of the molecule inside the micelle and site of binding. The molecule can enter inside the micelle either with its dimethylamino group or its pyridyl group. The encapsulation of the dimethylamino group leads to the removal of the solvation shell around the dimethylamino group. Therefore, the lone pair of the dimethylamino nitrogen does not take part in hydrogen bonding anymore. Instead, it delocalizes over the entire molecule. This leads to the red shift in the absorption spectra. The bathochromic shift in the absorption spectrum of DMAPOP in micelle indicates that the molecule enters inside the micelles through the dimethylamino group (Scheme 6.1.1.). Similar red shifts were also observed for analogues of DMAPOP when dimethylamino group enters inside the micelle.[151, 152] Since, the dimethylamino group is present inside the micelle, despite the fact both $Cu^{2+}$ and $Cd^{2+}$ bind at dimethylamino nitrogen of DMAPOP in acetonitrile, the micelle effectively prevents the binding at dimethylamino nitrogen. The controlled binding of $Cu^{2+}$ and $Cd^{2+}$ suggests that the oxazole nitrogen is present near the anionic head of the surfactant. Consequently, not only $Cd^{2+}$ but also $Cu^{2+}$ binds with DMAPOP through the oxazole nitrogen. Since, the strong electrostatic interaction between the anionic head of the micelle and the metal ions increases the metal ion concentration near the azole nitrogen, both the metal ions bind at azole nitrogen (Scheme 6.1.1). At higher micellar concentration, due to the deformation of spherical micellar shape, the fluorophore goes inside the micellar core.[153] But the metal ions reside at the stern layer of the micelle. This restricts the metal ions to interact with the probe molecule, and the binding efficiency gradually decreases at higher micellar concentration.[154]

### 6.1.3. Construction of molecular logic gates

In presence of micelle, the sensitivity of the molecule towards the metal ion in aqueous medium enhances. Even in presence of micelle, the non-radiative decay rate of DMAPOP decreases significantly, which results in enhanced emission of DMAPOP in

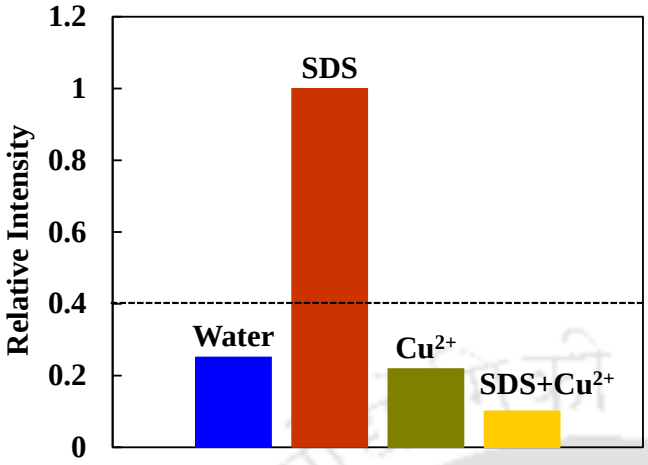


**Molecular INH gate**

| $Cu^{2+}$ | Micelle | Output |
|---|---|---|
| 0 | 0 | 0 |
| 0 | 1 | 1 |
| 1 | 0 | 0 |
| 1 | 1 | 0 |

**Output = 438 nm emission**

**Figure 6.1.4.** Relative intensities of DMAPOP at 438 nm in presence and absence of $Cu^{2+}$ and micelle. Corresponding truth table of molecular INH gate is shown at the right.

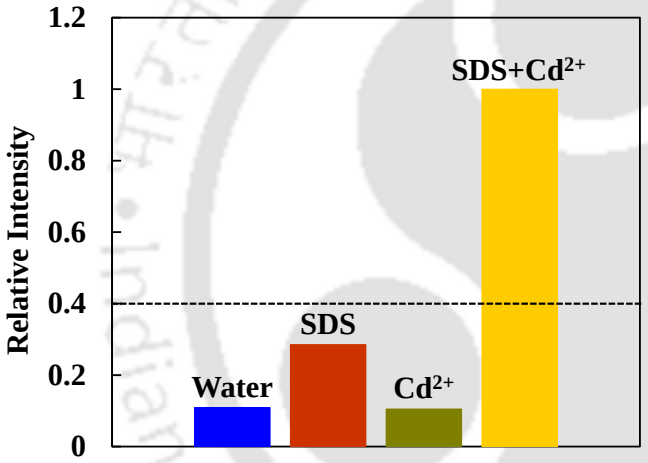


**Molecular AND gate**

| $Cd^{2+}$ | Micelle | Output |
|---|---|---|
| 0 | 0 | 0 |
| 0 | 1 | 0 |
| 1 | 0 | 0 |
| 1 | 1 | 1 |

**Output = 465 nm emission**

**Figure 6.1.5.** Relative intensities of DMAPOP at 465 nm in presence and absence of $Cd^{2+}$ and micelle. Corresponding truth table of molecular AND gate is shown at the right.

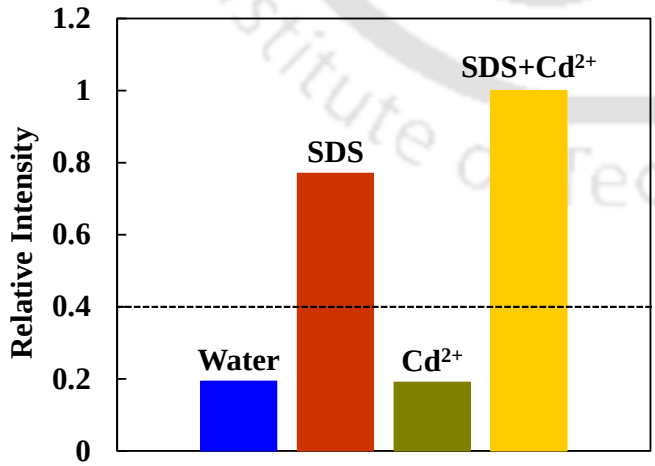


**Molecular TRANSFER gate**

| $Cd^{2+}$ | Micelle | Output |
|---|---|---|
| 0 | 0 | 0 |
| 0 | 1 | 1 |
| 1 | 0 | 0 |
| 1 | 1 | 1 |

**Output = 438 nm emission**

**Figure 6.1.6.** Relative intensities of DMAPOP at 438 nm in presence and absence of $Cd^{2+}$ and micelle. Corresponding truth table of molecular TRANSFER gate is shown at the right.

micellar medium as compared to neat aqueous medium. The results can be correlated with different logic operations. DMAPOP shows a weak emission in aqueous medium. The addition of $Cu^{2+}$ metal ion does not change the fluorescence intensity much. In presence of 8.2 mM SDS micelle, the emission intensity of DMAPOP enhanced almost ten times. The addition of $Cu^{2+}$ in micellar solutions quenches the emission of the fluorophore nearly to one-tenth. It shows that the high emission at 438 nm in presence of micelle is inhibited by the other input ($Cu^{2+}$). Considering the strong emission as logically one and low intensity as logically zero, an INHIBIT (INH) gate can be constructed (Figure 6.1.4). Instead of quenching, $Cd^{2+}$ metal ion enhances the fluorescence intensity of the micellar solution. However, the extent of enhancement at 438 nm and 465 nm are different. The changes in emission behavior of DMAPOP at 465 nm can be correlated with an AND logic operation (Figure 6.1.5). On the other hand the emission intensity at 438 nm is low in not only aqueous medium but also in presence of $Cd^{2+}$ in non-micellar medium. The micellar medium shows high emission from DMAPOP at 438 nm irrespective of the presence of $Cd^{2+}$. The result can be correlated with a TRANSFER logic operation (Figure 6.1.6). The TRANSFER logic operation is a basic logic operation where the state of one input directly transfer to the output ignoring the other input. The truth table in Figure 6.1.6 shows that the input values corresponding to the micelle is transferred to the output value without any change.

### 6.1.4. Conclusion

The metal ion binding increases in SDS as compared to the aqueous medium. The binding constant is maximum near critical micelle concentration. DMAPOP enters the micelle through the dimethylamino group. As a consequence, SDS prevents the binding of metal ions at the dimethylamino nitrogen of DMAPOP. In presence of micellar medium, metal ion binds with DMAPOP at a specific binding site. The strong interaction between the anionic head of the SDS micelle and the metal ion, ensures the metal ions to bind only through the oxazole nitrogen of DMAPOP. Thus, in presence of micellar medium metal ion binds with DMAPOP at a specific binding center. The $Cu^{2+}$ complex is non-emissive in nature. Whereas, the $Cd^{2+}$ complex exhibits an enhanced emission at a longer wavelength. The changes in emission characteristics in presence and absence of the metal ion and micelle are used to construct INHIBIT, TRANSFER and AND molecular logic gates.

## 6.2. Construction of molecular logic gate and keypad lock system by inducing the inter molecular proton transfer

Upon excitation, the basicity of the azole nitrogen and the acidity of the 'OH' group of HPBI are enhanced, and it results in ESIPT.[72] An intermolecular proton transfer from the phenolic 'OH' to the anion results a deprotonated species in the excited state (Section 3.1.1). If the photoacidity is high enough, and the solvent is sufficiently basic, the proton can be transferred from the fluorophore to the solvent. Similarly, the protonation of the azole nitrogen may also take place in excited state by intermolecular proton transfer in presence of suitable proton donating solvent. In this present section the excited state intermolecular proton transfer from solvent to BHPBI (Chart 4.1) is shown upon photoirradiation. The interaction of fluoride ion before and after the irradiation is applied to construct different logic gates. The input sequence dependent output is used to construct a molecular keypad lock system.[155] Rather than two chemical inputs as discussed in earlier section, only one chemical input is used along with photoirradiation.

### 6.2.1. Photoirradiation triggered protonation of BHPBI

As shown in Chapter 4, BHPBI emits both normal and tautomer emission depending on polarity and hydrogen bonding capacity of the solvent. The emission spectrum of BHPBI in chloroform is dominated by the 485 nm visible emission from the tautomer (Figure 6.2.1). The 355 nm ultraviolet emission from the excited enol is very weak. Upon irradiation with 270 nm ultraviolet light, the tautomer emission gradually decreases, and a new band emerges at 390 nm (Figure 6.2.1.A). The emission intensity ratio ($I_{390}/I_{485}$) changes from 0.04 to 2.78 after eight minutes of irradiation. The 390 nm emission band is excitation wavelength independent. However, irradiation with a longer wavelength light (320 nm, where the quasi planar conformer absorbs) decreases the rate of the reaction. Even after 2 hours of irradiation with 320 nm light, the $I_{390}/I_{485}$ ratio changes only to 1.93 (Figure 6.2.1.B). The normalized excitation spectra monitored at 485 nm (before irradiation) and 390 nm (after irradiation) are depicted in Figure 6.2.2.A. The absorption spectra of BHPBI in chloroform upon irradiation with 270 nm light are shown in Figure 6.2.2.B. The absorbance gradually decreases with a hypsochromic shift of both 320 nm and 290 nm band of BHPBI. The absorbance ratio of longer to shorter wavelength band maxima changes from 1.12 to 0.69. The result indicates the formation of a new species upon irradiation, which does not undergo ESIPT. The excitation

wavelength independent emission spectrum infers the existence of the single ground state precursor. The higher absorbance of the shorter wavelength band indicates a decrease in conjugation. Before the irradiation, BHPBI shows two different emissive keto species with lifetime 0.7ns and 2.9 ns in chloroform. The two emission appear from *cis*-keto and *trans*-keto species (Section 4.3). Whereas, after the irradiation the 390 nm species shows a mono-exponential decay with excited state lifetime of 1.5 ns ($\lambda_{ex}$ = 290 nm).

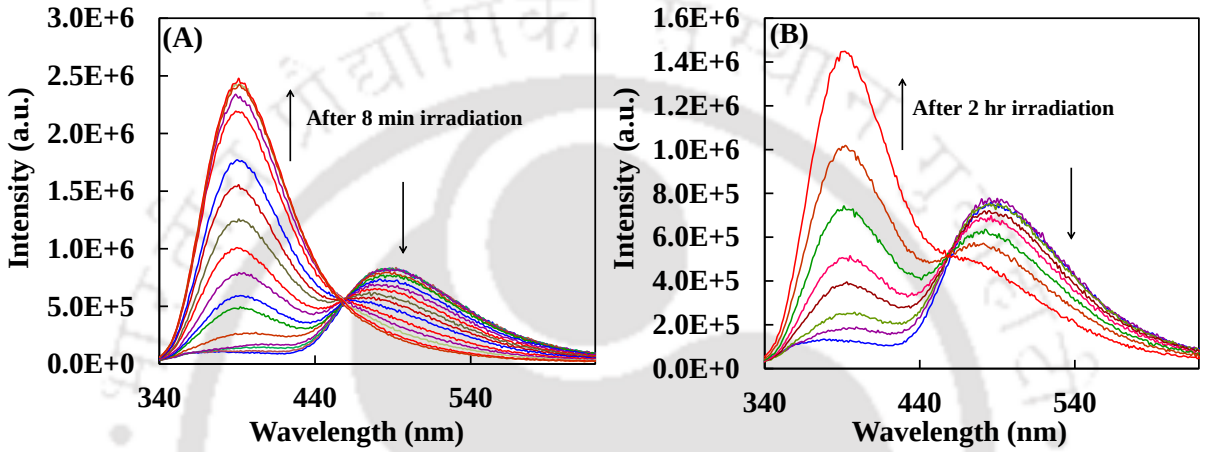


**Figure 6.2.1.** Emission spectra of BHPBI in chloroform upon irradiation with (A) 270 nm light, (B) 320 nm light, $\lambda_{ex}$ = 290 nm.

**Figure 6.2.2.** (A) Excitation spectra of BHPBI before (a) and after (b) irradiation with 270 nm light. $\lambda_{em}$ are 490 nm and 390 nm respectively. (B) Absorption spectra of BHPBI in chloroform with increasing irradiation time with 270 nm light. [BHPBI] = 5 μM.

The new emission band is red shifted with respect to the normal emission of BHPBI, and the ESIPT process is prevented in the new species. Such a shift is observed due to the protonation of the azole nitrogen or deprotonation of the hydroxyl proton (Section

4.5). Both the processes preclude the ESIPT. Though chloroform cannot accept proton, it can donate proton. The irradiation experiment was also performed in deuterated chloroform to find the isotope effect on the photoreaction. The generation of the new species upon irradiation was slowed down in deuterated chloroform as compared to the normal chloroform. After eight minutes of irradiation, the $I_{390}/I_{485}$ ratio increases to 1.82 which is much less than in the undeuterated chloroform. This indicates that the proton from chloroform assists to generate the new species upon irradiation of BHPBI. A comparison with the prototropic study in the acidic medium further confirms the formation of cationic species (Section 4.5). In acidic medium, different emissions were observed for monocation and dication. The monocationic species shows emission from protonated HPBI unit as well as from unprotonated HPBI unit, whereas the dicationic species shows the emission at 388 nm only. The irradiated BHPBI molecule shows a single emission at 390 nm. The absence of keto emission infers that both the HPBI units are protonated upon irradiation. The fluorescence lifetime at 390 nm also matches with the fluorescence lifetime of the dicationic species (1.4 ns, Table 4.2). These results confirm the formation of dicationic species in chloroform upon irradiation. Here, the intermolecular proton transfer from the solvent to BHPBI results in the cation. In solvents like propanol, methanol, DMSO the formation of the dication was not detected.

### 6.2.2. Construction of molecular logic gate

The anionic emission of BHPBI appears at 415 – 430 nm region in alkaline medium (Figure 4.8). HPBI is deprotonated to form anion in presence of fluoride (Section 3.1.6). However, even 50 μM of fluoride produces only a little change in the emission spectrum of BHPIP in chloroform medium (Figure 6.2.3). On the other hand, it was observed that the addition of fluoride to the irradiated BHPBI reverts back the dication to the neutral BHPBI (Figure 6.2.3.). The results can be correlated to construct two different logic gates at 390 nm and 490 nm. The high emission intensity at 390 nm appears only after the irradiation. Addition of fluoride leads to the low emission at 390 nm due to the proton transfer from the cation to the fluoride anion. The emission at 390 nm in presence of 270 nm light and fluoride anion describes an INH logic operation. Except in case of irradiation, in all other circumstances the output signal remain slow (= 0). The logic operation for the INH function is shown in Figure 6.2.4.A. On contrary, at 490 nm high outputs were observed in all cases except upon 270 nm irradiation. The logic operation is just opposite to the previous one (Figure 6.2.4.B). This result explains a molecular IMP logic operation which is complementary to an INH gate.

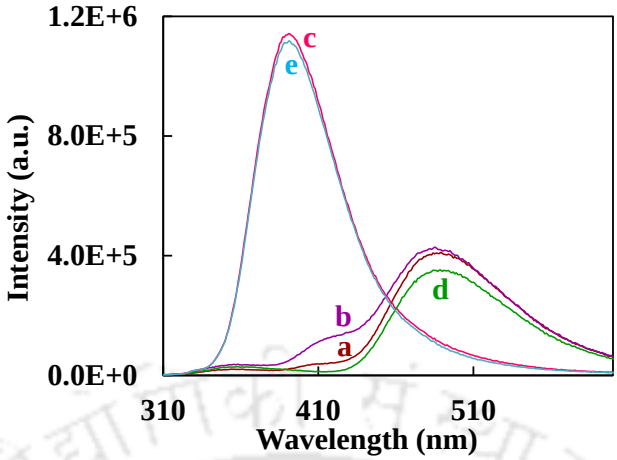


**Figure 6.2.3.** Emission spectra of BHPBI ($\lambda_{ex}$ = 290 nm) in presence of (a) no input, (b) 50 μM of fluoride, (c) irradiation, (d) irradiation followed by addition of 50 μM of fluoride, (e) addition 50 μM of fluoride followed by irradiation.

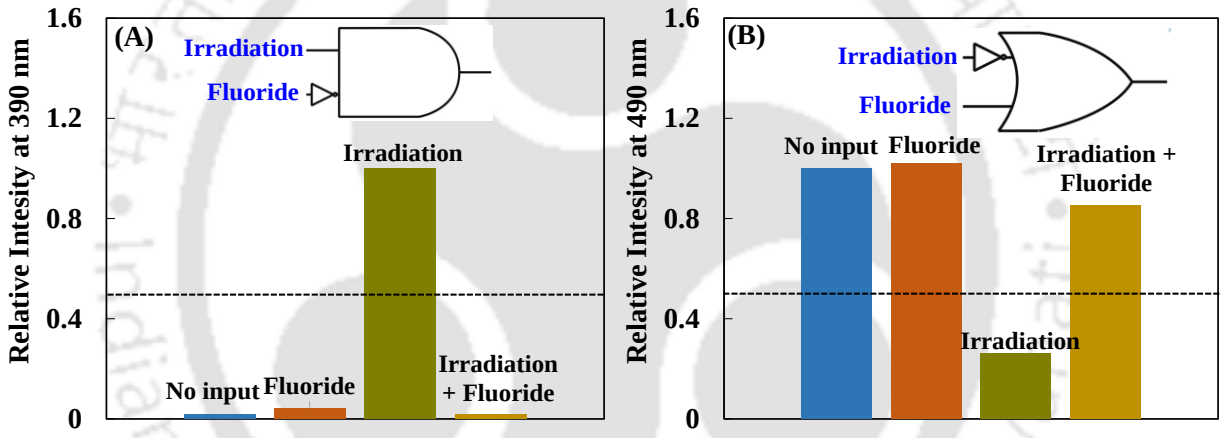


**Figure 6.2.4.** Change in relative intensity at (A) 390 nm (INH) and (B) 490 nm (IMP) in presence of different input. Respective logic operations are shown inside the corresponding graph.

**Table 6.2.1.** Truth table for molecular (A) TRANSFER, (B) INVERTER logic gate of BHPBI in presence of fluoride and 270 nm light.

(A)

| Fluoride (50 μM) | Irradiation | Output |
|---|---|---|
| 0 | 0 | 0 |
| 0 | 1 | 1 |
| 1 | 0 | 0 |
| 1 | 1 | 1 |

Output = emission at 390 nm, $\lambda_{ex}$ = 290 nm.

(B)

| Fluoride (50 μM) | Irradiation | Output |
|---|---|---|
| 0 | 0 | 1 |
| 0 | 1 | 0 |
| 1 | 0 | 1 |
| 1 | 1 | 0 |

Output = emission at 490 nm, $\lambda_{ex}$ = 290 nm.

Instead of the addition of fluoride to the irradiated BHPBI solution, the reverse process exhibits different output results. The irradiation of BHPBI in presence of 50 μM of fluoride shows a high emission at 390 nm, i.e. the output is input sequence dependent. Again, using this sequence order another two other logic gates can be constructed at 390

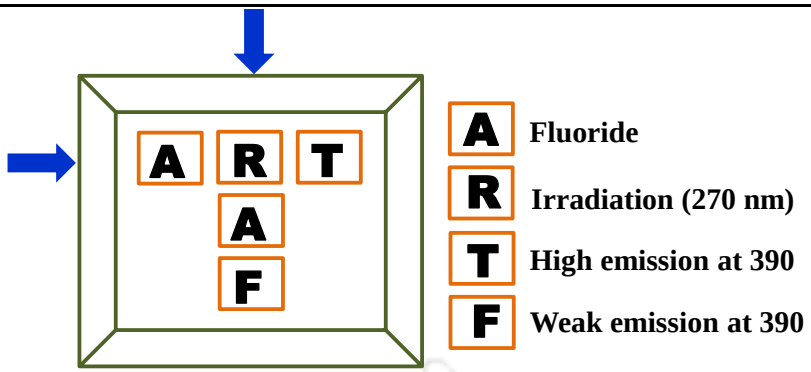


**Figure 6.2.5.** Molecular keypad lock system based on the sequence dependent output at 390 nm.

nm and 490 nm. The truth tables corresponding to the logic operations are displayed in Table 6.2.1. The 390 nm output represents a TRANSFER logic gate. Here, the state (high or low value) of a particular input (Irradiation) is directly transferred to the output irrespective of the second input. On the other hand, the emission behavior at 490 nm can be correlated with a molecular INVERTER. The INVERTER logic operation requires an input that produces an inverted digital output of the other input states. In absence of irradiation, the high output appears at 490 nm. Whereas, upon irradiation the intensity at 490 nm diminishes significantly, irrespective of the presence of fluoride. The input sequence dependency of the output was used to construct a molecular password entry system. The memory of the proper input sequence to obtain a high emission at 380 nm can be assumed as a molecular memory. As described in Figure 6.2.5, the input anion (fluoride) is labelled as A and the irradiation is labelled as R. The high and low outputs at 390 nm are considered as true (T) and false (F) outcome. The keypad would be unlocked only for the password ART. The other sequence would generate a wrong password, RAF.

### 6.2.3. Conclusion

The ESIPT of BHPBI is inhibited in chloroform upon photoirradiation. The intermolecular proton transfer from chloroform leads to the formation of cataonic species which prevents the intramolecular proton transfer. The emergence of cataonic emission upon irradiation and its disappearance upon addition of fluoride anion are employed to mimic the logic operation of INH gate and IMP gate. The sequence dependency of the output, makes the molecule efficient to behave as a password entry system. Molecular INVERTER and TRASFER logic gates are also developed with a reversed input sequence.

## 6.3. Single fluorophore to address multiple logic gates

Earlier two sections describe the construction of simple molecular logic gates by perturbing molecular emission. However, a combinatorial logic circuit constructed with simple logic functions of a single molecule can be developed to mimic the functioning of silicon chip based logic gate. An advantage of molecular logic system is its switching ability between more than two outcomes, upon addition of inputs. The information density is also increased with higher radix number.[63, 64] However, the Boolean logic system can hold only two states either 'On' or 'Off'. But more than two states in molecular logic system can be generated easily using different external stimuli.[60, 65, 156]

In this section, the construction of different logic gates with different radixes are shown with a single molecule DMAPIP-b which is having multiple binding sites. The subtraction between two binary numbers are shown using a molecular full subtractor. Construction of ternary systems are depicted by considering three defined fluorescence intensities at a particular wavelength. At the end the mapping of output emission with respect to the different input concentrations are shown by constructing fuzzy interference system (FIS).[157, 158] The fuzzy logic system is further coupled with neuro adaptation method to predict the dependency of molecular intensity with external inputs more accurately.

### 6.3.1. Interaction of DMAPIP-b with different analyte

DMAPIP-b has an absorption maximum at 345 nm in acetonitrile. With gradual addition of $Fe^{3+}$, a new band maxima appears at 390 nm at the expense of 345 nm band (Figure 6.3.1.A). The red shift in the spectrum confirms the binding of metal ions at pyridyl and/or imidazo ring nitrogen.[159] It is due to the increase of charge flow from the

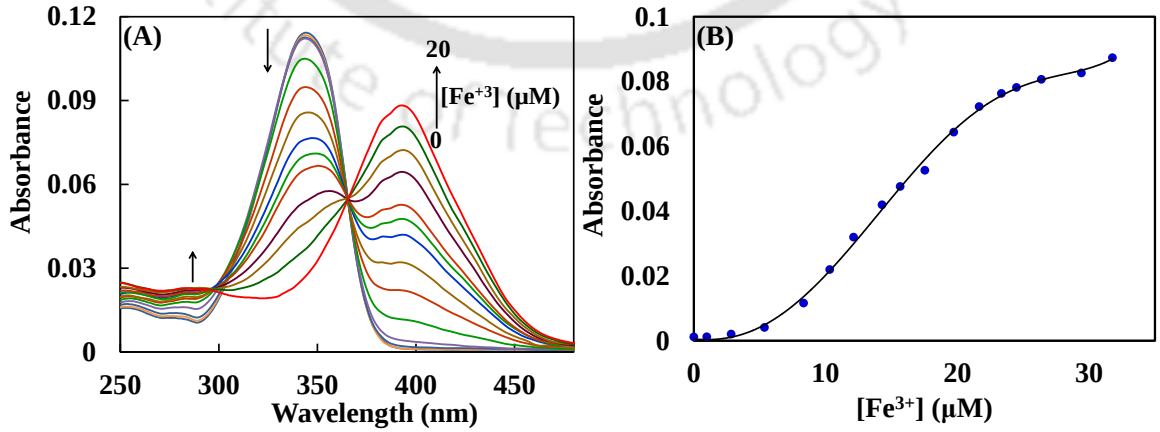


**Figure 6.3.1.** (A) Absorption spectra of DMAPIP-b in acetonitrile with increasing $Fe^{3+}$ concentration. (B) Increase in absorbance of DMAPIP-b at 390 nm with addition of $Fe^{3+}$.

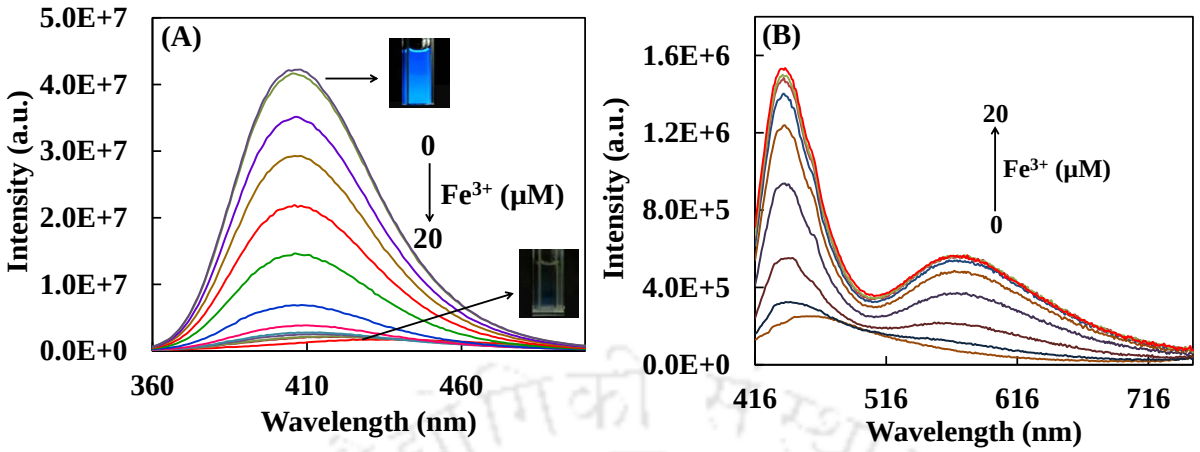


**Figure 6.3.2.** Emission spectra of DMAPIP-b with gradual increase of $Fe^{3+}$ concentration,(A) $\lambda_{ex}$ = 345 nm and (B) $\lambda_{ex}$ = 406 nm.

donor dimethylamino group to the acceptor moiety. The binding constant of the receptor is determined from the nonlinear curve fitting analysis of the titration curve using the equation 6.3.1 (Figure 6.3.1.B).

$$A = A_0 + \frac{(A_f - A_0)}{2C_h}\left[ C_h + C_g + \frac{1}{Ka} - \left[(C_h + C_g + \frac{1}{Ka})^2 - 4C_hC_g\right]^{\frac{1}{2}}\right] \qquad \textbf{(eq. 6.3.1.)}$$

where $A_0$, $A_f$ and $A$ refer the absorbance of DMAPIP-b, $Fe^{3+}$-DMAPIP-b complex and any intermediate $Fe^{3+}$ concentration with DMAPIP-b. $K_a$ refers the $Fe^{3+}$ binding constant of DMAPIP-b. $C_h$ and $C_g$ indicate the concentration of DMAPIP-b and $Fe^{3+}$, respectively. The binding constant for the complex is 9.1 x $10^6$ $M^{-1}$. Along with the longer wavelength band a blue shifted band at 285 nm is also observed with a quasi isobestic point at 300 nm (Figure 6.3.1.A). Binding of metal ion with dimethylamino group decreases the charge flow. Accordingly, the hypsochromic band can be assigned to the complex formed due to the binding of metal ion at dimethyl amino group. The saturation limit is observed at around 20 μM of [$Fe^{3+}$].

Upon excitation at 345 nm the molecular emission appears at 406 nm, but the intensity of the 406 nm emission band gradually decreases with the addition of $Fe^{3+}$ (Figure 6.3.2.A). In presence of 20 μM of metal ion, the quantum yield of DMAPIP-b decreases from 0.76 to 0.02. However, upon excitation at 406 nm, two new emission bands of fluorophore-metal ion complexes appear at 432 nm and 560 nm (Figure 6.3.2.B). The fluorescence decay measurements also suggest the emission from two different complexes when monitored at 432 nm (Table 6.3.1.). To find out the stoichiometric ratio of $Fe^{3+}$ and DMAPIP-b in the complex, Job's plot was constructed with the 432 nm emission of the complex. It confirms the 1:1 binding nature (Figure 6.3.3.).

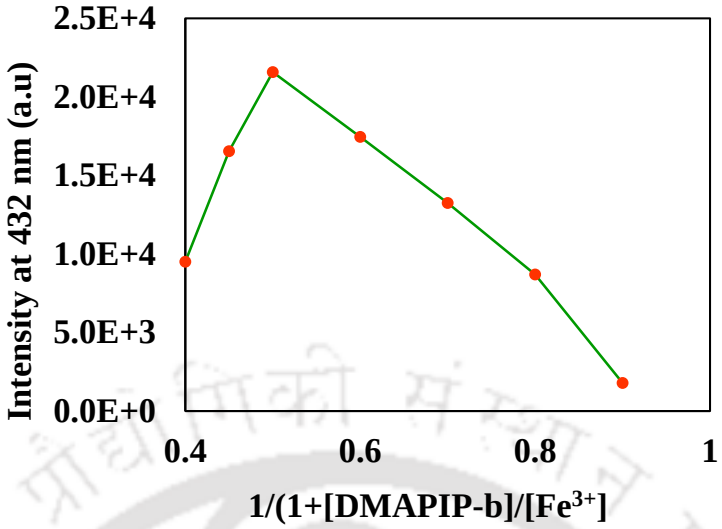


**Figure 6.3.3.** Job's plot for $Fe^{3+}$-DMAPIP-b complex. Due to the interference of the DMAPIP-b emission at low mole fraction of [$Fe^{3+}$], those points were not included in the plot).

**Table 6.3.1.** Fluorescence lifetime (τ, ns) of DMAPIP-b in presence of different substrate.

| Species | τ | χ2 |
|---|---|---|
| DMAPIP-b[a] | 1.53 | 1.05 |
| $Fe^{3+}$-DMAPIP-b[b] | 0.33 (70.25 %)<br>1.86 (29.75 %) | 1.09 |
| $F^-$-$Fe^{3+}$-DMAPIP-b[a] | 1.53 | 1.01 |

$\lambda_{ex}$= 375 nm, [a]$\lambda_{em}$= 406 nm, [b]$\lambda_{em}$= 432 nm. The relative amplitudes of two different complexes have been shown in parenthesis.

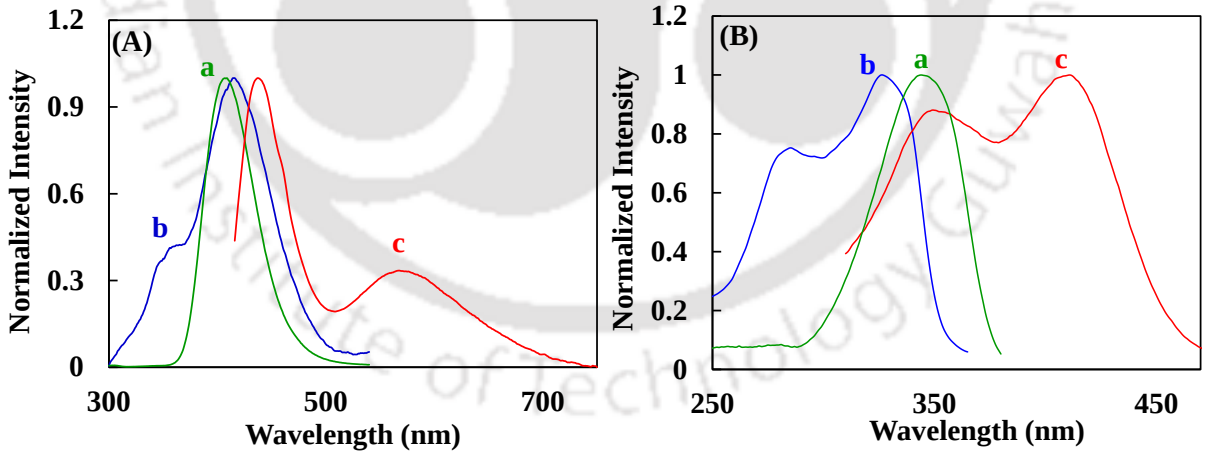


**Figure 6.3.4.** (A) Normalized emission spectra of (a) DMAPIP-b, $\lambda_{ex}$= 280 nm, (b) DMAPIP-b with 20 μM of $Fe^{3+}$, $\lambda_{ex}$= 280 nm, (c) DMAPIP-b with 20 μM of $Fe^{3+}$, $\lambda_{ex}$= 406 nm. (B) Normalized excitation spectra of (a) DMAPIP-b, $\lambda_{em}$ = 406 nm, (b) DMAPIP-b with 20 μM of $Fe^{3+}$, $\lambda_{em}$ = 350 nm, (c) DMAPIP-b with 20 μM of $Fe^{3+}$, $\lambda_{em}$ = 560 nm.

The prototropic studies of DMAPIP-b and analogues molecules established that the protonation might occur at the imidazole and pyridyl nitrogens to form two different kind of monocations.[109, 159] The emission spectrum of the monocation formed by the

protonation of the pyridyl nitrogen is more red-shifted than that of the monocation formed by the protonation of the imidazole nitrogen.[149] Accordingly, the band at 432 nm and 560 nm can be assigned to the complexes formed by the binding of ferric ion at imidazole nitrogen and pyridyl nitrogen, respectively. The larger bathochromic shift in the spectra of pyridyl complex are due to the higher conjugation in this complex (as in this complex metal binds at the terminal (pyridyl) nitrogen which increases the charge flow from the dimethylamino group to the pyridyl ring). However, excitation at 280 nm shows the emergence of a new band in addition to the main band at ~350 nm. This is due to the emission from the complex formed by the binding of $Fe^{3+}$ at dimethylamino nitrogen of DMAPIP-b (Figure 6.3.4.A). This assignment is based on the fact that the binding of the metal ion at dimethylamino nitrogen decreases the charge flow from the dimethylamino group to the acceptor, which causes a blue shift compared to the uncomplexed molecule. The excitation spectra corresponding to all three new bands corroborate the existence of three different $Fe^{3+}$-complexes in the ground state (Figure 6.3.4.B).

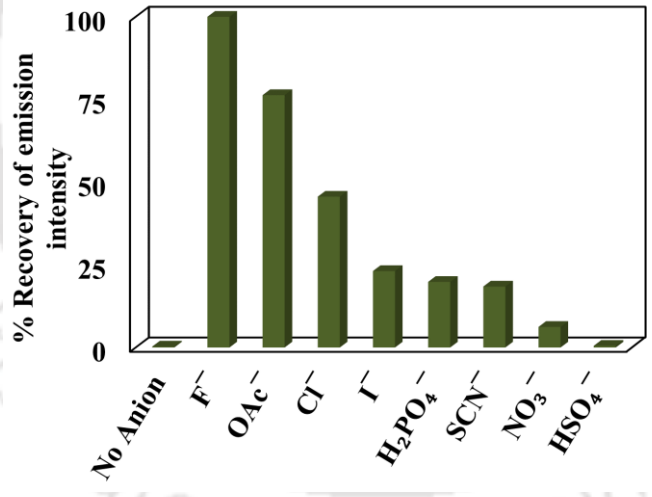


**Figure 6.3.5.** Regaining of fluorescence of DMAPIP-b by different anions in presence of 20 μM of $Fe^{3+}$, $\lambda_{ex}$ = 345 nm.

The molecular fluorescence at 406 nm can be recovered by the addition of anion to the complex. The process occurs more efficiently with increasing the anionic strength (basicity). The efficiency of different anions follows the order $F^- > OAc^- > Cl^- > I^- > SCN^- \sim H_2PO_4^- > NO_3^- >> HSO_4^-$ (Figure 6.3.5.). The fluorescence of the molecule is completely regained in presence of equivalent amount of fluoride anion (20 μM). The fluorescence lifetime obtained at 406 nm (Table 6.3.1) exactly matches with the earlier reported

fluorescence lifetime of DMAPIP-b.[159] This confirms that the addition of anions to the complex solution liberates the free fluorophore in solution.

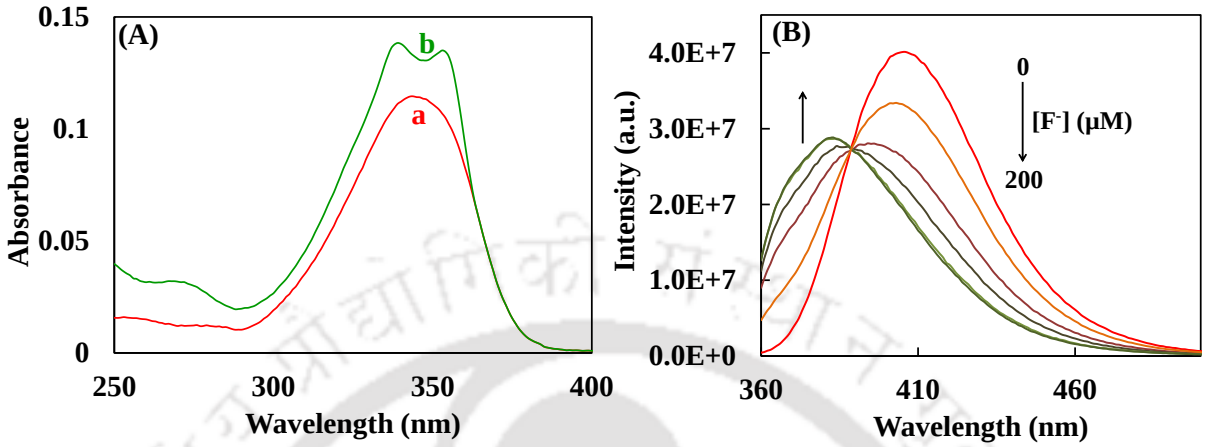


**Figure 6.3.6.** (A) Absorption spectra of (a) DMAPIP-b, (b) DMAPIP-b with 200 μM of fluoride. (B) Emission spectra of DMAPIP-b with increasing fluoride concentration, $\lambda_{ex}$ = 345 nm.

The absorption spectra of DMAPIP-b with increasing fluoride concentration is shown in Figure 6.3.6.A. Unlike $Fe^{3+}$, little amount of fluoride ([$F^-$] < 20 μM) does not affect the absorption spectrum of DMAPIP-b. Only at higher concentrations changes are observed in the absorption spectrum. Same as absorption spectrum, up to 20 μM of fluoride, the emission spectrum of DMAPIP-b exhibits negligible change but upon further increase in anion concentration, a new blue shifted band appears at the cost of the 406 nm emission band with an isoemissive point at 389 nm (Figure 6.3.6.B). As reported earlier, the absorption spectrum and the emission spectrum of DMAPIP-b undergo a blue shift when the hydrogen of the imidazole >NH group is deprotonated to form anion.[82] The formation of negative charge on the imidazole ring increases the electron density on the acceptor moiety, which decreases the charge transfer from donor to acceptor moiety.[109] Therefore the new blue shifted emission band is attributed to the deprotonated DMAPIP-b anion which generates in the excited state.

### 6.3.2. Binary logic gate, full-subtractor and molecular keypad lock

**Table 6.3.2.** One input molecular logic gates, (A) NOT, (B) PASS 1, (C) YES.

(A)

| Input ($Fe^{3+}$, 20 μM) | Output (406 nm) |
|---|---|
| 0 | 1 |
| 1 | 0 |

$\lambda_{ex}$ = 345 nm.

(B)

| Input ($F^-$, 20 μM) | Output (406 nm) |
|---|---|
| 0 | 1 |
| 1 | 1 |

$\lambda_{ex}$ = 345 nm.

(C)

| Input ($Fe^{3+}$, 200 μM) | Output (432 / 560 nm) |
|---|---|
| 0 | 0 |
| 1 | 1 |

$\lambda_{ex}$ = 406 nm.

**Table 6.3.3.** Two input molecular logic gates.

| $F^-$ | $Fe^{3+}$ | IMP[a‡] | INH[b†‡] | INH[c†] | XNOR[a†] | OR[d†] | XOR[e] |
|---|---|---|---|---|---|---|---|
| 0 | 0 | 1 | 0 | 0 | 1 | 0 | 0 |
| 0 | 1 | 0 | 1 | 0 | 0 | 1 | 1 |
| 1 | 0 | 1 | 0 | 1 | 0 | 1 | 1 |
| 1 | 1 | 1 | 0 | 0 | 1 | 1 | 0 |

[a] $\lambda_{ex}$ = 345 nm, $\lambda_{em}$ = 406 nm; [b] $\lambda_{ex}$ = 406 nm, $\lambda_{em}$ = 560 nm; [c] $\lambda_{ex}$ = 345 nm, $\lambda_{em}$ = 378 nm; [d] $\lambda_{ex}$ = 280 nm, $\lambda_{em}$ = 352 nm, [e] considering a negative logic of the XNOR operation. ‡ input concentration 20 μM, †input concentration 200 μM.

Several one input Boolean molecular logic gates can be implemented based on the emission intensities at different wavelengths (Table 6.3.2). At low fluoride concentration (< 20 μM) the emission intensity of DMAPIP-b at 406 nm shows a negligible change. A PASS 1 logic gate can be implemented depending on the emission intensity at 406 nm. A molecular NOT logic gate can be constructed with 20 μM of $Fe^{3+}$ and DMAPIP-b at 406 nm. Two YES logic gate can be developed at 430 nm and 560 nm with addition of 20 μM of $Fe^{3+}$ to DMAPIP-b. However, considering both the inputs together an OR, an IMP, an XNOR and two INH molecular logic gate can be constructed (Table 6.3.3.). The molecular emission at 406 nm with two inputs $F^-$ (20 μM) and $Fe^{3+}$ (20 μM) executes an IMP logic behavior. The emission is OFF in presence of $Fe^{3+}$ only, in all other cases the high outputs are observed (Table 6.3.3.). Schiller et al. has reported the importance of the IMP logic gate toward the functional completeness.[160] At high (200 μM) concentration of inputs, the molecule describes a XNOR logic operation at the same

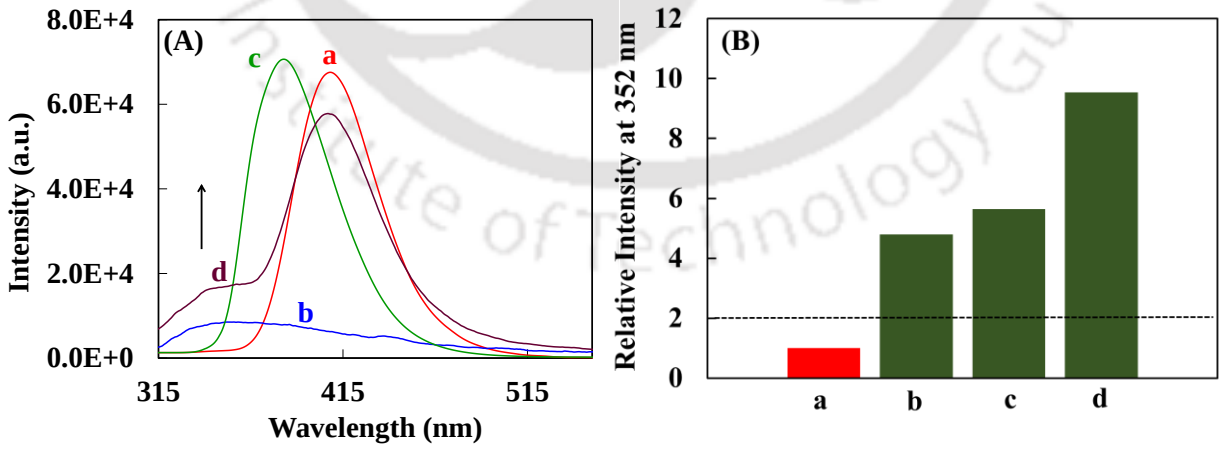


**Figure 6.3.7.** (A) Emission spectra of (a) DMAPIP-b, (b) DMAPIP-b with 200 μM of $Fe^{3+}$, (c) DMAPIP-b with 200 μM of $F^-$, (d) DMAPIP-b with 200 μM of $Fe^{3+}$ and $F^-$. $\lambda_{exc}$ = 280 nm. (B) Relative emission intensity at 352 nm (a) DMAPIP-b, (b) DMAPIP-b with 200 μM of $Fe^{3+}$, (c) DMAPIP-b with 200 μM of $F^-$, (d) DMAPIP-b with 200 μM of $Fe^{3+}$ and $F^-$.

wavelength (Table 6.3.3.). Both inputs lead to the low emission output at 406 nm. But simultaneous presence of equimolar amount (200 μM each) of the inputs leads to a high emission at 406 nm. Based on the new bands at 378 nm in presence of 200 μM $F^-$ (upon excitation at 345 nm), or the 560 nm band appeared for high (200 μM) and low (20 μM) concentration of $Fe^{3+}$ (upon excitation at 406 nm), three INH logic gates can been constructed (Table 6.3.3.). INH gate is basically an AND gate concatenated with a NOT operation at one input. Here, the output is inhibited at the particular wavelength when the second input is present in the solution. At 352 nm, the fluorophore exhibits a weak emission. However, at high concentration (200 μM) of metal ion or fluoride or both, the emission intensity at 352 nm increases. The relative intensities of DMAPIP-b at 352 nm in presence of different stimuli are depicted in Figure 6.3.7. If a threshold value is considered at intensity ratio 2, the higher values can be treated as high output, and the lower ratio can be considered as low output. The result can be correlated with a two input OR logic operation (Table 6.3.3.). Since the XNOR operation is the complementary of a XOR logic operation, the change in the intensity at 406 nm can be compared with a negative XOR operation (Table 6.3.3.). Basically the assignments of the high output as logic 1 and low output as logic 0 are arbitrary. Even it does not worry much to run a negative logic in one channel and a positive logic in other output channel because both the outputs are independent to each other though it is a combinatorial logic operation.

Thus, the XNOR logic operation correspond to the 406 nm can be correlated with a XOR logic gate and can be combined with the INH gate to compose a half subtractor. The change in the emission intensity at 560 nm can be considered as borrower and the change of emission intensity at 406 nm can be correlated with the difference to construct the combined operation (Table 6.3.3.). A half subtractor can find the difference and borrowing for the subtraction of two single bits (Table 6.3.3.), though for multibit subtraction, the borrow value should be accounted as an input during the subtraction of next two bits. A full subtractor which is consisted with two half subtractors and an OR gate, batches the previous borrow value as an input value with the other two binary inputs and results two output, one difference value and a borrow value. The borrow value again performs as an input for the next subtraction. The OR logic gate obtained at 352 nm emission can be combined with two half subtractor to build a molecular full subtractor. The subtraction of binary numbers 100 and 011 is shown in Chart 6.3.1 using the molecular logic gate.

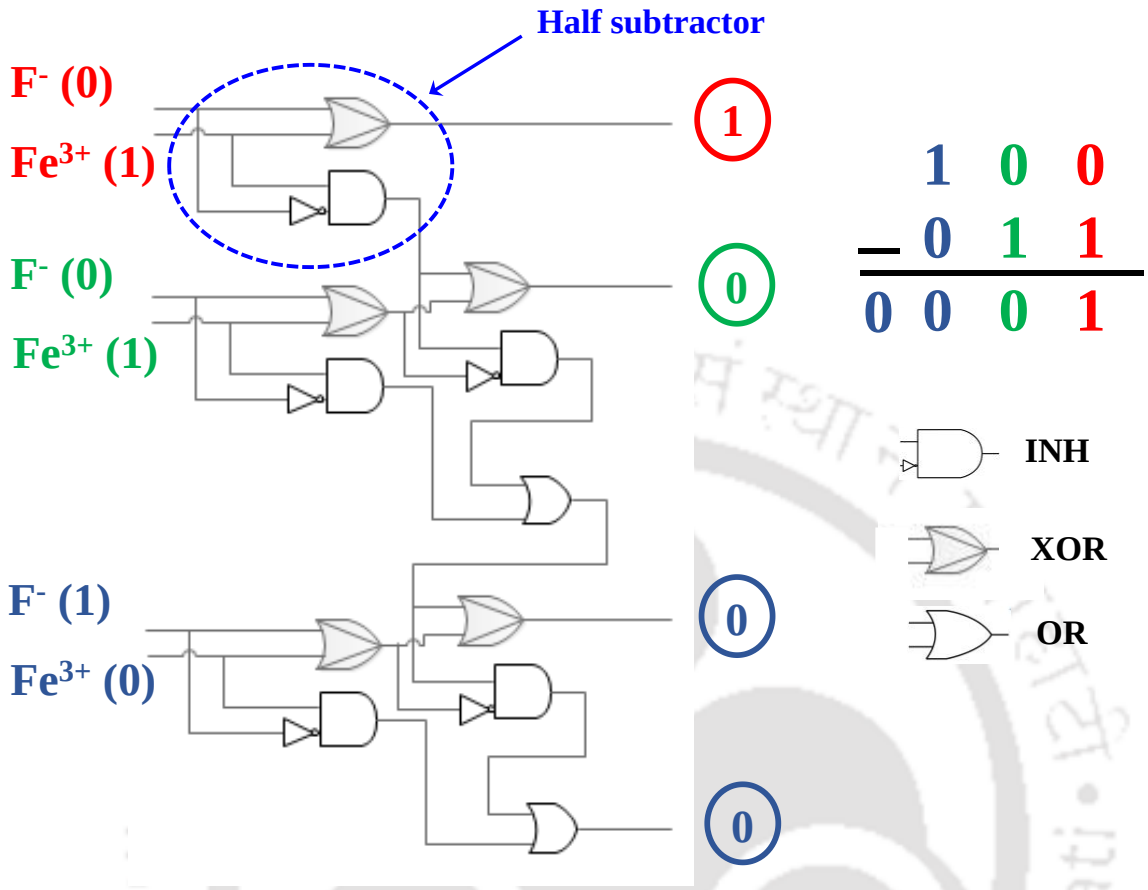


**Chart 6.3.1.** Construction of molecular full subtractor with the emission outputs of DMAPIP-b in presence of $Fe^{3+}$ and $F^-$. The subtraction between two binary numbers 100 and 011 is performed.

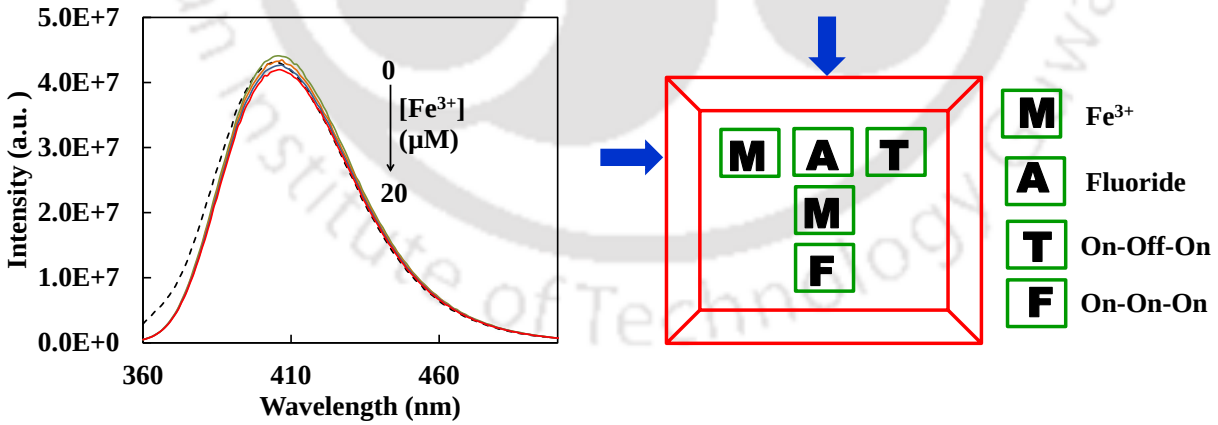


**Figure 6.3.8.** Emission spectra of DMAPIP-b with $F^-$ in acetonitrile with increasing [$Fe^{+3}$]. [$F^-$] = 20 μM. $\lambda_{exc}$ = 345 nm. Dotted line represents the emission spectra for DMAPIP-b with 20 μM $F^-$. Construction of molecular keypad lock system is shown on the right hand side.

Using the Boolean logic system a keypad lock device was proposed at low concentration (20 μM) of $Fe^{3+}$ and $F^-$. The addition of metal ion to the fluorophore quenches the emission intensity at 406 nm ($\lambda_{ex}$ = 345 nm). The emission is regained by

the addition of fluoride. The change in fluorescence follows an 'ON-OFF-ON' switching state. On the other hand, if the input sequence is altered i.e., addition of the fluoride is followed by the metal ion addition, the fluorescence intensity does not go via this switching phenomenon (Figure 6.3.8.A). Here a data storage capability can be imagined, which depends on the input sequence. The switching phenomenon can represent a true outcome (T) and the other state, 'ON-ON-ON' represents a false outcome (F). A password entry system or keypad lock system can be built based on the storage capability. The addition of metal ion (M) followed by the anion (A) generates the T state and it would create the correct password 'MAT'. On the other hand, 'AM' input sequence which generates F outcome, would result the wrong password 'AMF'. The entry system can only be accessed only for the three letter correct password 'MAT' (displayed at the right hand side of Figure 6.3.8.). The other input sequence will provide the wrong password due to the incorrect entry.

### 6.3.3. Ternary system

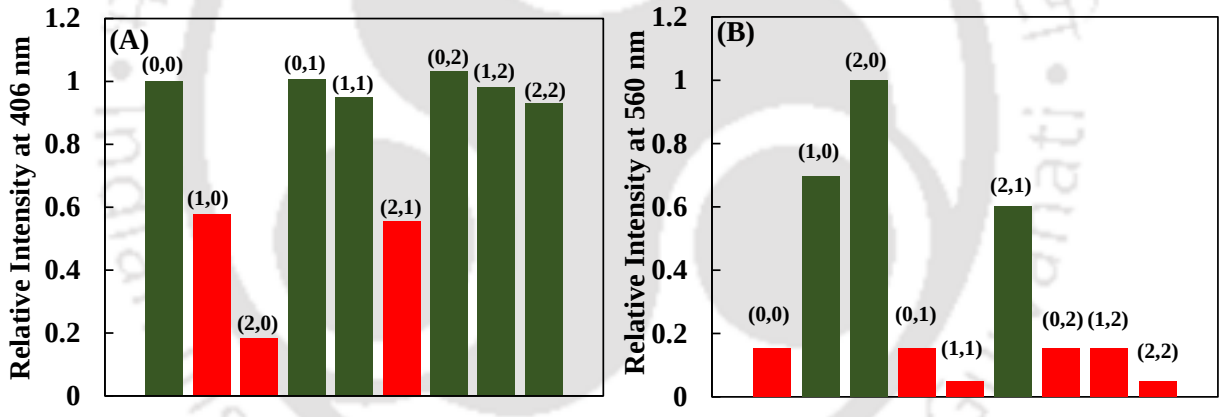


**Figure 6.3.9.** (A) Ternary IMP logic gate based on the emission output at 406 nm. $\lambda_{ex}$= 345 nm. Input concentrations are 0 μM, 6 μM, 20 μM. (B) Ternary INH logic gate based on the emission output at 560 nm, $\lambda_{ex}$= 406 nm. Input concentrations are 0 μM, 10 μM, 20 μM.

Ternary system holds higher information density. In DMAPIP-b system it can be achieved by considering three different well distinct emission intensities at 406 nm. Along with the binary system, an intermediate state is considered in addition for output as well as for inputs. The three states are defined to the intensity ratio at 406 nm with respect to the maximum intensity values as low (0), medium (1) and high (2). The logic values for both the inputs are 0 μM (low), 6 μM (medium) and 20 μM (high). Different combinations of two inputs generate different emission ratios (Figure 6.3.9). The ternary logic output can be correlated with an IMP logic function (Figure 6.3.9.A, Table 6.3.4).

The high output (logically 2) comes only for equal or higher concentration of fluoride. Similarly, upon excitation at 406 nm a ternary INH gate can be constructed at 560 nm emission (Figure 6.3.9.B). Three different input concentrations are 0 μM, 10 μM, 20 μM. Truth table for the INH operation is depicted in Table 6.3.4. Nonzero outputs are observed for the relatively higher input values of $Fe^{3+}$ than $F^-$.

**Table 6.3.4.** Truth table for ternary IMP and INH logic gate.

| $Fe^{3+}$ | $F^-$ | Output at 406 nm (IMP) | Output at 560 nm (INH) |
|---|---|---|---|
| 0 | 0 | 2 (1) | 0 (0.15) |
| 1 | 0 | 1 (0.58) | 1 (0.69) |
| 2 | 0 | 0 (< 0.18) | 2 (1) |
| 0 | 1 | 2 (1) | 0 (0.15) |
| 1 | 1 | 2 (0.95) | 0 (0.05) |
| 2 | 1 | 1 (0.55) | 1 (0.6) |
| 0 | 2 | 2 (1) | 0 (0.15) |
| 1 | 2 | 2 (0.98) | 0 (0.15) |
| 2 | 2 | 2 (0.92) | 0 (<0.5) |

Parenthesis values are the intensity ratio with respect to the maximum intensity at the particular wavelength.

### 6.3.4. Multivalued logic with fuzzy interference system

The addition of different analyte to DMAPIP-b leads to a continuous change in emission intensity. The light intensity at 406 nm can be controlled by maintaining the certain ratio of anion and cation. These can be correlated with a multiple trigger which generate infinite number of outputs. Using different concentration ratio of $Fe^{3+}$ and $F^-$ with respect to a fixed fluorophore concentration (5 μM), a continuous multivalued logic system was constructed (Table 6.3.5.).

Different normalized intensities at 406 nm are monitored as different logic outputs. The result was correlated with an infinite fuzzy logic system. In contrast to the finite numerical data, the fuzzy logic deals with linguistic variables and fuzzy linguistic rules. The values of linguistic variables are words or sentences which are less specific than numerical value. Very often these values are different partially overlapped sets with infinite number of elements. The ambiguity comes on existence of the same element in more than one set. A fuzzy restriction is being implemented by associating each value with a particular compatibility function or so called membership function. It covers all of its elements with a membership function value (a real number) within a limit of [0, 1]. A FIS was constructed using Mamdani method. The input variables are $c_m/c_s$ and $c_a/c_s$, and the output variable is $I/I_0$, where $c_m$, $c_a$, $c_s$ refer to the concentration of $Fe^{3+}$, $F^-$ and DMAPIP-b molecule. $I_0$ refers to the intensity of the fluorophore at 406 nm without any input and I refers to the intensity at different input values. Three different type of membership functions were chosen zmf, trimf and smf (Annexure D). The input $c_m/c_s$

was fragmented in five different sets as follows i) very low, with an asymmetric polynomial function open to the left (μVL, zmf [0.205 0.856]), ii) low, a triangle shaped membership function (μL, trimf [0.403 0.658 4.4]), iii) medium, associated with a triangular membership function (μM, trimf [2.063 7.61 21.3]), iv) high, also a triangular membership function (μH, trimf [12.1 17.9 28.31]), v) very high, associated with an asymmetric polynomial open to the right (μvH, smf [22 24.9]) (Figure 6.2.10). In a similar way, $c_a/c_s$ and $I/I_0$ were split into four different sets (Figure 6.2.10). The four different sets for $c_a/c_s$ are i) low (μL, zmf [0.238 2.923]), ii) medium (μM, trimf [0.0001867 2.769 8.469]), iii) high (μH, trimf [4.51 15.55 39]), iv) very high (μVH, smf [22.6 35.4]). The output $I/I_0$ was split as follow i) very low (μVL, zmf [0.03791 0.1629]), ii) low (μL, trimf [0.041 0.258 0.398]), iii) medium (μM, trimf [0.287 0.641 0.893]), iv) high (μH, smf [0.6628 0.8298]) (Figure 6.3.10).

**Table 6.3.5.** Construction of Infinite valued logic system with fuzzy logic.

| Sl. No. | $C_m/C_s$ | $C_a/C_s$ | $I/I_0$ (Experimental) | $I/I_0$ (Mamdani's FIS) | $I/I_0$ (ANFIS) |
|---|---|---|---|---|---|
| 1 | 0 | 0.74 | 0.96 | 0.873 | 1 |
| 2 | 0 | 5.66 | 0.95 | 0.821 | 0.996 |
| 3 | 0 | 28.57 | 0.73 | 0.607 | 0.687 |
| 4 | 0.4 | 1.23 | 0.76 | 0.873 | 0.817 |
| 5 | 0.4 | 4.05 | 0.79 | 0.873 | 0.804 |
| 6 | 0.4 | 24.24 | 0.6 | 0.607 | 0.517 |
| 7 | 2.8 | 0.74 | 0.67 | 0.614 | 0.658 |
| 8 | 2.8 | 9.09 | 0.9 | 0.801 | 0.949 |
| 9 | 2.8 | 28.57 | 0.94 | 0.837 | 0.883 |
| 10 | 4 | 0.74 | 0.33 | 0.393 | 0.176 |
| 11 | 4 | 5.66 | 0.6 | 0.548 | 0.67 |
| 12 | 4 | 24.24 | 0.68 | 0.686 | 0.775 |
| 13 | 10 | 3.62 | 0.04 | 0.232 | 0.006 |
| 14 | 10 | 7.41 | 0.39 | 0.497 | 0.418 |
| 15 | 10 | 9.09 | 0.59 | 0.607 | 0.57 |
| 16 | 10 | 28.57 | 0.74 | 0.728 | 0.805 |
| 17 | 16 | 0.0.74 | 0.04 | 0.097 | 0.017 |
| 18 | 16 | 20.63 | 0.36 | 0.418 | 0.251 |
| 19 | 20 | 28.57 | 0.23 | 0.519 | 0.249 |
| 20 | 40 | 1.23 | 0.03 | 0.0508 | 0.012 |
| 21 | 40 | 4.05 | 0.02 | 0.0508 | 0.012 |
| 22 | 40 | 28.57 | 0.03 | 0.164 | 0.094 |

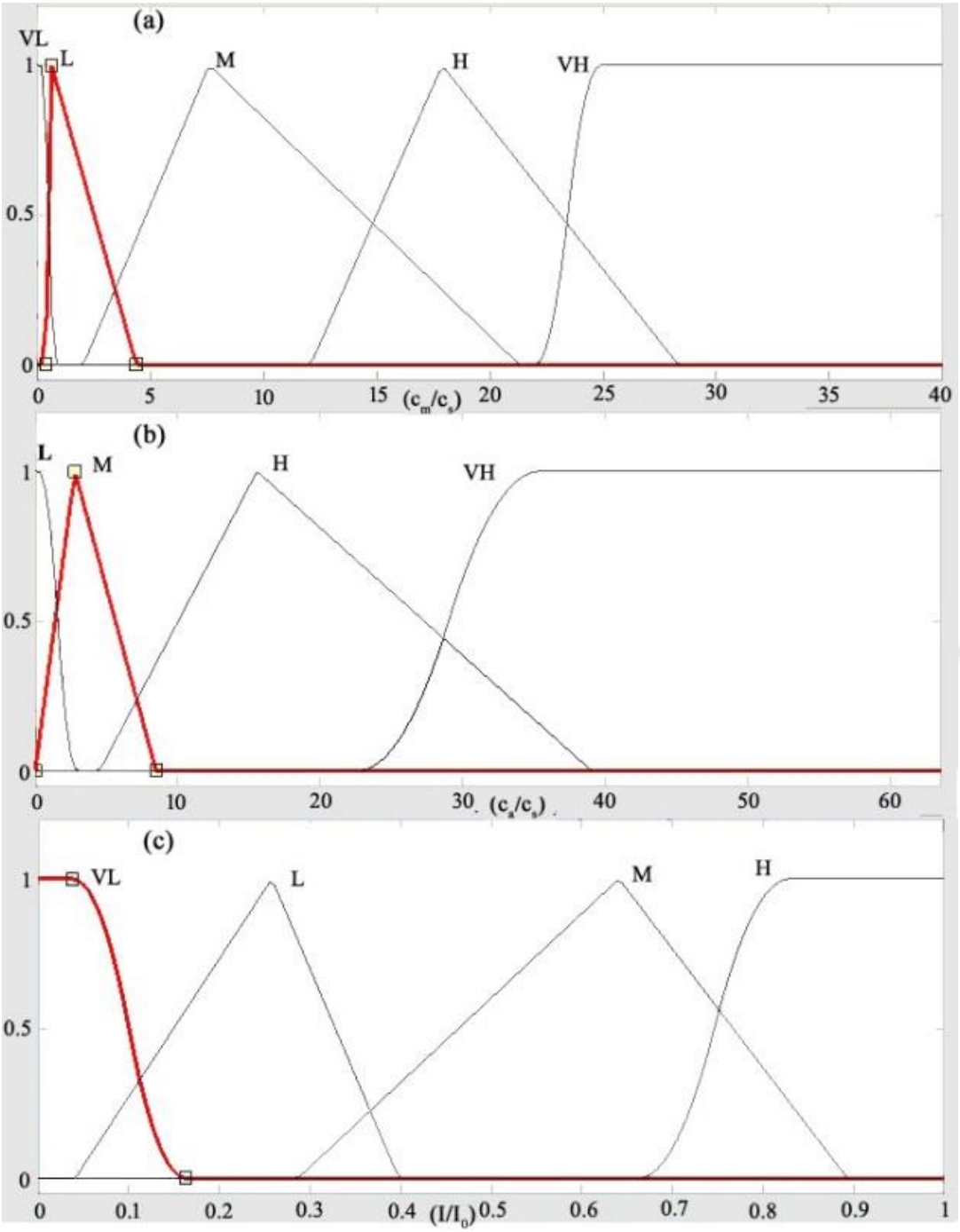


**Figure 6.3.10.** (a) Membership functions of $c_m/c_s$. (b) Membership functions of $c_a/c_s$. (c) Membership functions of $I/I_0$.

Next, the linguistic fuzzy rules were figured out. It basically consists of a few IF-THEN statements. IF part is called antecedent and THEN part is called consequence. Two or more antecedents can be connected with OR or AND or NOT fuzzy operator. In contrast to Boolean operator, in fuzzy system the union operator (OR) refers not only to

the maximum but also the algebraic sum in which one is called s-norm or t-conorm.[158] Similarly, the intersection operator (AND) also refers to either a minimum or a product called t-norm operator.[158] Using the minimum operator, twenty Fuzzy rules were implemented (Table 6.3.6). Each rule is applicable to the particular fuzzy set which holds the highest membership function. The centroid method was chosen for defuzzyfication of fuzzy output to crisp output.

**Table 6.3.6.** Fuzzy IF-THEN rules to construct Mamdani's FIS.

| Sl. No. | IF-THEN rules |
|---|---|
| 1 | If $c_m/c_s$ is very low and $c_a/c_s$ is low then $I/I_0$ is high. |
| 2 | If $c_m/c_s$ is very low and $c_a/c_s$ is medium then $I/I_0$ is high. |
| 3 | If $c_m/c_s$ is very low and $c_a/c_s$ is high then $I/I_0$ is medium. |
| 4 | If $c_m/c_s$ is very low and $c_a/c_s$ is very high then $I/I_0$ is medium. |
| 5 | If $c_m/c_s$ is low and $c_a/c_s$ is low then $I/I_0$ is medium. |
| 6 | If $c_m/c_s$ is low and $c_a/c_s$ is medium then $I/I_0$ is high. |
| 7 | If $c_m/c_s$ is low and $c_a/c_s$ is high then $I/I_0$ is high. |
| 8 | If $c_m/c_s$ is low and $c_a/c_s$ is very high then $I/I_0$ is high. |
| 9 | If $c_m/c_s$ is medium and $c_a/c_s$ is low then $I/I_0$ is very low. |
| 10 | If $c_m/c_s$ is medium and $c_a/c_s$ is medium then $I/I_0$ is low. |
| 11 | If $c_m/c_s$ is medium and $c_a/c_s$ is high then $I/I_0$ is medium. |
| 12 | If $c_m/c_s$ is medium and $c_a/c_s$ is very high then $I/I_0$ is high. |
| 13 | If $c_m/c_s$ is high and $c_a/c_s$ is low then $I/I_0$ is very low. |
| 14 | If $c_m/c_s$ is high and $c_a/c_s$ is medium then $I/I_0$ is very low. |
| 15 | If $c_m/c_s$ is high and $c_a/c_s$ is high then $I/I_0$ is low. |
| 16 | If $c_m/c_s$ is high and $c_a/c_s$ is very high then $I/I_0$ is medium. |
| 17 | If $c_m/c_s$ is very high and $c_a/c_s$ is low then $I/I_0$ is very low. |
| 18 | If $c_m/c_s$ is very high and $c_a/c_s$ is medium then $I/I_0$ is very low. |
| 19 | If $c_m/c_s$ is very high and $c_a/c_s$ is high then $I/I_0$ is very low. |
| 20 | If $c_m/c_s$ is very high and $c_a/c_s$ is very high then $I/I_0$ is low. |

Once all rules and methods are fixed, Mamdani fuzzy interference engine can be put in work to predict complex molecular behavior. Based on the different rules it perceives the nonlinear behavior of the outputs with different inputs. A correlation coefficient 0.95 was obtained for the employed Mamdani fuzzy logic system (Figure 6.3.11.A). The emission of the fluorophore can be changed in a controlled manner with predetermined values of fuzzy logic system. It is observed that up to 50 μM of $[Fe^{3+}]$ and $[F^-]$ a complete regaining of fluorescence intensity can be achieved. Based on the resetting ability of the system, using a low concentration of the inputs a molecular attenuator can be constructed for 406 nm radiation. Considering the emission of DMAPIP-b molecule as 100%, a particular lower intensity can be achieved by addition of premeasured $[Fe^{3+}]$, obtained from FIS input-output mapping. Again the attenuation can work in a continuous way. The resetting can be achieved by the addition of equivalent amount of $[F^-]$. The change of emission intensity with different $Fe^{3+}$ and $F^-$ concentration is pictorially depicted in Figure 6.3.11.B.

**(B)**

**Figure 6.3.11.** (A) Correlation between the normalized fluorescence intensity obtained from the experimental data (-▲-) with the FIS output data from Mamdani method (-◆-) and ANFIS method (-●-). (B) Three dimension plotting of the emission intensity of DMAPIP-b (406 nm) with $Fe^{3+}$ and $F^-$ as predicted from Mamdani FIS.

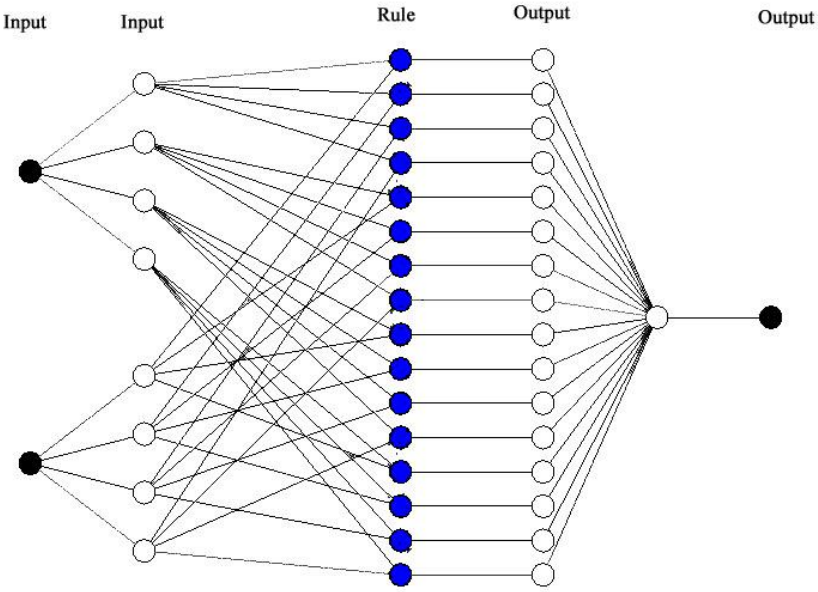


**Figure 6.3.12.**Schematic diagram of ANFIS using Sugeno's method to map the normalized intensity of DMAPIP-b with [$Fe^{3+}$] and [$F^-$].

However, the fuzzy logic system using Mamdani method is a coarse one and not good enough to map the input-output relation efficiently. The advance approach is a neuro computing blended fuzzy logic system. The adaptive neuro fuzzy interference system (ANFIS) is a supreme fuzzy system which not only considers the linguistic variable but also adapts itself with the experimentally observed input-output data set. A FIS obtained by Sugeno's method is combined with neural adaptation technique.[161-163] In Sugeno's method, the output membership functions are either constants or linear

combinations of inputs. Both inputs $c_m/c_s$ and $c_a/c_s$ were fragmented in four different values with trapezoidal and triangular membership functions. The data set was parted into two fractions, training data and checking data. The ANFIS was trained with the training data and the accuracy of the input-output mapping was verified with the experimental checking data. Sixteen different rules were generated (4 x 4) by back propagation-least square method. A schematic diagram of input-output mapping for the constructed ANFIS is represented in Figure 6.3.12. The correlation coefficient for the ANFIS is 0.98 (Figure 6.3.11.A). The ANFIS result is enough accurate to calculate any of the input concentrations for different emissions intensity over a fixed concentration of another input (Table 6.3.5).

| | L | M | H | VH |
|---|---|---|---|---|
| VL | H | H | M | M |
| L | M | H | H | H |
| M | VL | L | M | H |
| H | VL | VL | L | M |
| VH | VL | VL | VL | L |

**Chart 6.3.2.** Molecular keypad lock system based on fluorescence switching at 406 nm using Mamdani FIS.

The limitation of the binary keypad lock system with molecular logic is the insufficient number of keys. A binary keypad lock system possesses only two different choices. The only way to increase the choices in molecular binary keypad lock system is to increase the input numbers. However in Boolean system it is really difficult to find more suitable inputs which allow the ON/OFF switching for a sequential order of additions. On the other hand with the advance of radix number, the number of choices also increases. An infinite valued fuzzy logic system would be the best choice to perform the molecular keypad lock system. For the mentioned Mamdani fuzzy system, a four letter keypad lock can be constructed (Chart 6.3.2). For a particular combination of two different inputs would generate one of the four different keys. If a particular order of the four letters is considered as a true output and a limitation is applied on the reuse of same input keys, it is evident that only a few ways are there to access the correct four letter code. For example a code L-M-H-VL can be generated only by seven different ways from more than thousand combinations (Chart 6.3.2). Rather than using a same

probe solution, for generating different code letter new probe molecule has to be used. The password entry device can be improved by using an efficient resettable fluorescent probe.

### 6.3.5. Conclusion

Construction of binary, ternary and infinite valued logic system based on the switching of emission intensity of the ligand upon interaction with a metal ion and an anion are presented in this section. In Boolean system single input YES, NOT, PASS 1 and two input OR, IMPLICATION, XOR, INHIBIT logic gates were constructed. Synergistic performance of the XOR and the INHIBIT function were combined to build a molecular half subtractor. A molecular full subtractor was also developed by use of the half subtractor and a molecular OR logic gate to subtract binary digits. By assigning three states for inputs and output, a ternary IMPLICATION and a ternary INHIBIT gates were developed. A continuous multivalued system was developed using soft computing. A fuzzy interference engine was generated using Mamdani method and the correlation of the FIS with the real system was improved using an ANFIS model. The fuzzy approach draws an outline for molecular recognition process which one is a difficult task for a binary logic system. Thus, the implementation of a binary, a ternary and a multivalued fuzzy logic within a single molecular platform makes the molecule suitable for versatile use in molecular computing.

# Chapter 7

# Summary and Scope for Future Work

## 7.1. Summary

In the present thesis, the intermolecular proton transfer, intramolecular proton transfer, excites state double proton transfer are investigated with different molecular systems. The studies reveal that how the proton transfer processes yield different end products like different tautomer, anion, cationic, zwitterion etc. The thesis also describes molecular switches, binary subtraction, keypad lock system with simple cation anion interaction with different azole systems. The construction of fuzzy interference system is represented with an azole system to follow the stimuli response of the fluorophore.

In Chapter 3, the intermolecular proton transfer between the fluorophores and different anions were studied. Despite the fact that HPBI exists as *cis*-enol (major) and *trans*- enol (minor) in neutral form, it was reported to exist only in the *trans*-form upon deprotonation in aqueous medium.[72] It was also stated that the dianion formed in the ground state was reprotonated to form the *trans*-anion in the excited state.[72] In the first section, of chapter three, it is shown that the *cis*-anion and dianion can be obtained upon proper stabilization in suitable environments. It is also demonstrated that switching between *cis*- and *trans*- anion is possible by changing the environment. Theoretical calculations are also performed to substantiate the existence of *cis*-anion and dianion. In converse to the literature report,[102] it is also shown that not only in protic solvents but also in aprotic solvents 'OH' group is deprotonated before the 'NH' group to form monoanion.

In the second section of chapter three, the anion sensitivity and the deprotonation nature of the nitrogenous analogues of HPBI are investigated in a polar aprotic medium. It is observed that the substitution of pyridyl nitrogen enhances the anion sensitivity. However, despite the enhanced sensitivity of the nitrogenous analogues the deprotonation of these molecules in presence of strong anion is less favored as compared to HPBI. The anomalous trend observed for the nitrogenous analogs are discussed and explained with theoretical calculations and experimental findings. It is also found that the sensitivity towards anion and the formation of anion depends also on the position of the pyridyl nitrogen.

Most of the excited state proton transfer molecule shows a dual emission. In chapter four, the intra and inter molecular proton transfer of a HPBI derivative, BHPBI is demonstrated. The highly Stokes' shifted normal emission is obtained by photoinduced planarization, and the tautomer emission occurs due to the phtotoinduced proton transfer. In the excited state, the tautomer undergoes torsional rotation induced

isomerization to generate one more tautomer emission. The ground state conformers of the molecule are separated from each other and exploited to produce aggregation induced enhanced emission with different emission color. Thus, a single molecule is used as two distinct color emitting fluorophore. The intermolecular proton transfer between solvent and BHPBI at different pH produces different cations and anions.

In chapter five, the consecutive proton transfer process was investigated with Tz molecule. The studies reveals that Tz molecule undergoes excited state single and double proton transfer, and generates a monoketo and a diketo species. The process is initiated with a particular phenol unit. The other phenol unit cannot commence the ESIPT process in solution due to the annular tautomerism. However, in the solid state ESIPT occurs through other phenol unit also to produce three different tautomers in the excited state.

The binding interactions of $Cu^{2+}$ and $Cd^{2+}$ with DMAPOP were studied in acetonitrile. The studies revealed that the binding of metal ions occurs through more than one site. In the first section of chapter six, it is established that anionic micelle can formulate the metal ion binding at a specific site. In presence of SDS both the metal ion binds at oxazole nitrogen. However, $Cu^{2+}$ quenches the fluorescence and $Cd^{2+}$ enhances the fluorescence of DMAPOP. The different emission nature of DMAPOP in presence and abscence of micelle and metal ions are exploited to construct different logic gates.

Construction of different molecular logic gates with BHPBI are shown in section 6.2. BHPBI exhibits tautomer emission from the quasi planar conformer upon photoexcitation. However, in chloroform, upon photoirradiation the ESIPT is inhibited due to the formation of dication species. Here, solvent act as a proton donor. The interaction of the molecule with fluoride before and after the irradiations are different. This alters the emission characteristics of the molecule, and this is used to construct molecular INH, IMP, TRANSFER, INVERTER logic gates. The input sequence dependency of the emission output was used to construct molecular keypad lock system.

In the section three of chapter six, logic gates with different radixes have been constructed within DMAPIP-b. Taking the advantage of multiple binding sites of the fluorophore, a series of different molecular logic gates have been developed using fluorescence intensities at different wavelengths. The high emission of the molecule is drastically quenched in presence of $Fe^{3+}$. It regains back by addition of equivalent amount of $F^-$. The fluorescence On-Off nature was used to construct molecular full

subtractor and molecular keypad lock system with Boolean logic. Ternary system is generated by considering three defined fluorescence intensities at particular wavelength. The smooth dependency of emission intensities with analyte concentration has been utilized to construct infinite valued fuzzy logic system. The fuzzy logic system has been further coupled with neuro adaptation method to predict more accurately the dependency of molecular intensity in presence of external inputs more accurately.

### 7.2. Scope for future work

The existence of the *cis*-anion of HPBI is proved in polar aprotic solvent. In NaOH saturated DMSO, a mixture of *cis*- and *trans*- anion are observed. Their existence completely depend on their relative stability in presence of the external anion. It would be interesting to find out a suitable perturbing factor which can control the equilibrium and would be able to lead the equilibrium to a specific desired conformer. For the nitrogenous analogues also the study in DMSO can be performed. These processes can be studied in microheterogeneous system such as micelles and proteins and in other similar system for better understanding.

The *cis*- and *trans*- keto isomer of BHPBI produce two different emission in the excited state. The transition absorption spectra of the species may provide more detail information about the absorption nature of the keto species. Theoretical calculations can be performed to follow the excited state process. The conformers of BHPBI are separated by molecular aggregation and AIEE is obtained. Simulation study can be performed to further understand the influence of polarity and hydrogen bonding in the separation of conformers as molecular aggregates.

Due to limitation of instrument time, the evolution of tautomer species could not be followed. Such a study will be interesting particularly for Tz in different medium where ESIPT triggered ESIPT takes place.

Construction of different molecular logic gates are shown in chapter 6. Using combinatorial logic circuit molecular subtractor has been designed. It can subtract two binary numbers. Similarly, a molecular adder, multiplexer, demultiplexer can be constructed by designing organic molecule with proper receptor unit and choosing appropriate stimuli. Azole molecules with multi receptor unit can be synthesized to construct multi logic system with single fluorophore probe. Furthermore, use of reversible optical input instead of chemical input can be designed to resolve the resetting issue which is the most common problem for the chemical inputs.

## References

### Primary Sources

### Secondary Sources

### Uncategorized References


1. A. Kotlyar, N. Borovok, S. Kiryati, E. Nachliel and M. Gutman, *Biochemistry*, 1994, **33**, 873-879.
2. M. S. Celej, W. Caarls, A. P. Demchenko and T. M. Jovin, *Biochemistry*, 2009, **48**, 7465-7472.
3. A. Müller, H. Ratajczak, W. Junge and E. Diemann, *Electron and Proton Transfer in Chemistry and Biology*, 1992.
4. T. Gensch, J. Heberle and C. Viappiani, *Photochemical & Photobiological Sciences*, 2006, **5**, 529-530.
5. H. Ishikita and K. Saito, *Journal of The Royal Society Interface*, 2014, **11**, 20130518.
6. K. Weber, *Z. Physik. Chem. B*, 1931, **15**, 18.
7. T. Förster, *Naturwissenschaften*, 1949, **36**, 186-187.
8. L. G. Arnaut and S. J. Formosinho, *Journal of Photochemistry and Photobiology A: Chemistry*, 1993, **75**, 1-20.
9. M. Kondo, *Bulletin of the Chemical Society of Japan*, 1978, **51**, 3027-3029.
10. R. G. Brown, N. Entwistle, J. D. Hepworth, K. W. Hodgson and B. May, *The Journal of Physical Chemistry*, 1982, **86**, 2418-2420.
11. J. F. Ireland and P. A. H. Wyatt, in *Advances in Physical Organic Chemistry*, ed. V. Gold, Academic Press, 1976, vol. Volume 12, pp. 131-221.
12. F. Rodriguez Prieto, M. Mosquera and M. Novo, *The Journal of Physical Chemistry*, 1990, **94**, 8536-8542.
13. M. Mosquera, M. C. Ríos Rodríguez and F. Rodríguez-Prieto, *The Journal of Physical Chemistry A*, 1997, **101**, 2766-2772.
14. C. A. Taylor, M. A. El-Bayoumi and M. Kasha, *Proceedings of the National Academy of Sciences of the United States of America*, 1969, **63**, 253-260.
15. J. Catalán, P. Pérez, J. C. del Valle, J. L. G. de Paz and M. Kasha, *Proceedings of the National Academy of Sciences of the United States of America*, 2004, **101**, 419-422.
16. J. Catalan and P. Perez, *Physical Chemistry Chemical Physics*, 2005, **7**, 94-99.
17. H. Sekiya and K. Sakota, *Journal of Photochemistry and Photobiology C: Photochemistry Reviews*, 2008, **9**, 81-91.
18. J. Catalán and M. Kasha, *The Journal of Physical Chemistry A*, 2000, **104**, 10812-10820.
19. S. Takeuchi and T. Tahara, *Chemical Physics Letters*, 2001, **347**, 108-114.
20. M. Itoh, T. Adachi and K. Tokumura, *Journal of the American Chemical Society*, 1984, **106**, 850-855.
21. P. J. Thistlethwaite and P. J. Corkill, *Chemical Physics Letters*, 1982, **85**, 317-321.
22. B. Kang, K. C. Ko, S.-Y. Park, D.-J. Jang and J. Y. Lee, *Physical Chemistry Chemical Physics*, 2011, **13**, 6332-6339.
23. A. Weller, *Naturwissenschaften*, 1955, **42**, 175-176.
24. M. Lukeman and P. Wan, *Chemical Communications*, 2001, DOI: 10.1039/B100817J, 1004-1005.
25. N. Basarić, N. Došlić, J. Ivković, Y.-H. Wang, J. Veljković, K. Mlinarić-Majerski and P. Wan, *The Journal of Organic Chemistry*, 2013, **78**, 1811-1823.
26. C.-Y. Peng, J.-Y. Shen, Y.-T. Chen, P.-J. Wu, W.-Y. Hung, W.-P. Hu and P.-T. Chou, *Journal of the American Chemical Society*, 2015, **137**, 14349-14357.

27. W.-S. Yu, C.-C. Cheng, Y.-M. Cheng, P.-C. Wu, Y.-H. Song, Y. Chi and P.-T. Chou, *Journal of the American Chemical Society*, 2003, **125**, 10800-10801.
28. N. Suzuki, A. Fukazawa, K. Nagura, S. Saito, H. Kitoh-Nishioka, D. Yokogawa, S. Irle and S. Yamaguchi, *Angewandte Chemie International Edition*, 2014, **53**, 8231-8235.
29. F. G. Bordwell, G. E. Drucker, N. H. Andersen and A. D. Denniston, *Journal of the American Chemical Society*, 1986, **108**, 7310-7313.
30. B. L. McDowell and H. Rapoport, *The Journal of Organic Chemistry*, 1972, **37**, 3261-3265.
31. T. Mutai, H. Tomoda, T. Ohkawa, Y. Yabe and K. Araki, *Angewandte Chemie*, 2008, **120**, 9664-9666.
32. F. Rodriguez-Prieto, J. Carlos Penedo and M. Mosquera, *Journal of the Chemical Society, Faraday Transactions*, 1998, **94**, 2775-2782.
33. B. W. Clare, D. Cook, E. C. F. Ko, Y. C. Mac and A. J. Parker, *Journal of the American Chemical Society*, 1966, **88**, 1911-1916.
34. G. Köbrich, *Angewandte Chemie*, 1966, **78**, 786-786.
35. F. A. S. Chipem, S. K. Behera and G. Krishnamoorthy, *The Journal of Physical Chemistry A*, 2013, **117**, 4084-4095.
36. W. Klöpffer and G. Naundorf, *Journal of Luminescence*, 1974, **8**, 457-461.
37. A. Douhal, F. Amat-Guerri and A. U. Acuna, *The Journal of Physical Chemistry*, 1995, **99**, 76-80.
38. K. Inuzuka and A. Fujimoto, *Spectrochimica Acta Part A: Molecular Spectroscopy*, 1986, **42**, 929-937.
39. H. Ishikawa, K. Iwata and H.-o. Hamaguchi, *The Journal of Physical Chemistry A*, 2002, **106**, 2305-2312.
40. F.-T. Hung, W.-P. Hu, T.-H. Li, C.-C. Cheng and P.-T. Chou, *The Journal of Physical Chemistry A*, 2003, **107**, 3244-3253.
41. Q. Chu, D. A. Medvetz and Y. Pang, *Chemistry of Materials*, 2007, **19**, 6421-6429.
42. F. A. S. Chipem, S. K. Behera and G. Krishnamoorthy, *Sensors and Actuators B: Chemical*, 2014, **191**, 727-733.
43. M. M. Henary and C. J. Fahrni, *The Journal of Physical Chemistry A*, 2002, **106**, 5210-5220.
44. A. Helal and H.-S. Kim, *Tetrahedron Letters*, 2009, **50**, 5510-5515.
45. S. Dalapati, S. Jana and N. Guchhait, *Spectrochimica Acta Part A: Molecular and Biomolecular Spectroscopy*, 2014, **129**, 499-508.
46. J. Zhao, S. Ji, Y. Chen, H. Guo and P. Yang, *Physical Chemistry Chemical Physics*, 2012, **14**, 8803-8817.
47. Y. Wu, X. Peng, J. Fan, S. Gao, M. Tian, J. Zhao and S. Sun, *The Journal of Organic Chemistry*, 2007, **72**, 62-70.
48. G.-Y. Li and T. Chu, *Physical Chemistry Chemical Physics*, 2011, **13**, 20766-20771.
49. K. C. Gross and P. G. Seybold, *International Journal of Quantum Chemistry*, 2000, **80**, 1107-1115.
50. S.-i. Nagaoka, A. Nakamura and U. Nagashima, *Journal of Photochemistry and Photobiology A: Chemistry*, 2002, **154**, 23-32.
51. T. Mutai, H. Sawatani, T. Shida, H. Shono and K. Araki, *The Journal of Organic Chemistry*, 2013, **78**, 2482-2489.
52. A. O. Doroshenko, E. A. Posokhov, A. A. Verezubova, L. M. Ptyagina, V. T. Skripkina and V. M. Shershukov, *Photochemical & Photobiological Sciences*, 2002, **1**, 92-99.
53. Z. Song, W. Zhang, M. Jiang, H. H. Y. Sung, R. T. K. Kwok, H. Nie, I. D. Williams, B. Liu and B. Z. Tang, *Advanced Functional Materials*, 2015, DOI: 10.1002/adfm.201503788, n/a-n/a.
54. K. R. Phatangare, V. D. Gupta, A. B. Tathe, V. S. Padalkar, V. S. Patil, P. Ramasami and N. Sekar, *Tetrahedron*, 2013, **69**, 1767-1777.
55. R. Wei, P. Song and A. Tong, *The Journal of Physical Chemistry C*, 2013, **117**, 3467-3474.

56. Y. Qian, S. Li, G. Zhang, Q. Wang, S. Wang, H. Xu, C. Li, Y. Li and G. Yang, *The Journal of Physical Chemistry B*, 2007, **111**, 5861-5868.
57. R. Hu, S. Li, Y. Zeng, J. Chen, S. Wang, Y. Li and G. Yang, *Physical Chemistry Chemical Physics*, 2011, **13**, 2044-2051.
58. S. Kumar, V. Luxami, R. Saini and D. Kaur, *Chemical Communications*, 2009, DOI: 10.1039/B900131J, 3044-3046.
59. P. Singh, H. Singh, G. Bhargava and S. Kumar, *J. Mater. Chem. C*, 2015, **3**, 5524-5532.
60. G. de Ruiter, L. Motiei, J. Choudhury, N. Oded and M. E. van der Boom, *Angewandte Chemie*, 2010, **122**, 4890-4893.
61. I. Gallardo, G. Guirado, J. Hernando, S. Morais and G. Prats, *Chemical Science*, 2016, **7**, 1819-1825.
62. S. Park, J. Seo, S. H. Kim and S. Y. Park, *Advanced Functional Materials*, 2008, **18**, 726-731.
63. K. S. Menger, *IEEE Transactions on Computers*, 1969, **C-18**, 241-250.
64. S. L. Hurst, *IEEE Transactions on Computers*, 1984, **C-33**, 1160-1179.
65. S. Stockinger and O. Trapp, *Chemical Science*, 2014, **5**, 2677-2682.
66. K. Szaciłowski, *Chemical Reviews*, 2008, **108**, 3481-3548.
67. J. Andreasson and U. Pischel, *Chemical Society Reviews*, 2010, **39**, 174-188.
68. G. McSkimming, J. H. R. Tucker, H. Bouas-Laurent and J.-P. Desvergne, *Angewandte Chemie International Edition*, 2000, **39**, 2167-2169.
69. P. A. de Silva, N. H. Q. Gunaratne and C. P. McCoy, *Nature*, 1993, **364**, 42-44.
70. A. Credi, V. Balzani, S. J. Langford and J. F. Stoddart, *Journal of the American Chemical Society*, 1997, **119**, 2679-2681.
71. R. Ferreira, P. Remón and U. Pischel, *The Journal of Physical Chemistry C*, 2009, **113**, 5805-5811.
72. H. K. Sinha and S. K. Dogra, *Chemical Physics*, 1986, **102**, 337-347.
73. M. Mosquera, J. C. Penedo, M. C. Ríos Rodríguez and F. Rodríguez-Prieto, *The Journal of Physical Chemistry*, 1996, **100**, 5398-5407.
74. R. Wortmann, S. Lebus, H. Reis, A. Grabowska, K. Kownacki and S. Jarosz, *Chemical Physics*, 1999, **243**, 295-304.
75. C. M. Orlando, J. G. Wirth and D. R. Heath, *The Journal of Organic Chemistry*, 1970, **35**, 3147-3149.
76. R. W. Middleton and D. G. Wibberley, *Journal of Heterocyclic Chemistry*, 1980, **17**, 1757-1760.
77. D. W. Hein, R. J. Alheim and J. J. Leavitt, *Journal of the American Chemical Society*, 1957, **79**, 427-429.
78. B. Shankar, S. Sahu, N. Deibel, D. Schweinfurth, B. Sarkar, P. Elumalai, D. Gupta, F. Hussain, G. Krishnamoorthy and M. Sathiyendiran, *Inorganic Chemistry*, 2014, **53**, 922-930.
79. S. Stucky, N. J. Koch, U. Heinz and K. Hegetschweiler, *Chemical Papers*, 2008, **62**, 388-397.
80. A. Einhorn, E. Bischkopff, B. Szelinski, G. Schupp, E. Spröngerts, C. Ladisch and T. Mauermayer, *Justus Liebigs Annalen der Chemie*, 1905, **343**, 207-305.
81. A. Mishra and G. Krishnamoorthy, *Photochemical & Photobiological Sciences*, 2012, **11**, 1356-1367.
82. A. Mishra, S. Sahu, N. Dash, S. K. Behera and G. Krishnamoorthy, *The Journal of Physical Chemistry B*, 2013, **117**, 9469-9477.
83. G. A. Crosby and J. N. Demas, *The Journal of Physical Chemistry*, 1971, **75**, 991-1024.
84. C. Wohlfarth, *Handbook of Chemistry and Physics*, 2004.
85. M. Lechner, *Landolt Börnstein*, 2008, **47**.
86. A. S. R. Koti, M. M. G. Krishna and N. Periasamy, *The Journal of Physical Chemistry A*, 2001, **105**, 1767-1771.

87. M. J. Frisch, G. W. Trucks, H. B. Schlegel, G. E. Scuseria, M. A. Robb, J. R. Cheeseman, G. Scalmani, V. Barone, B. Mennucci, G. A. Petersson, H. Nakatsuji, M. Caricato, X. Li, H. P. Hratchian, A. F. Izmaylov, J. Bloino, G. Zheng, J. L. Sonnenberg, M. Hada, M. Ehara, K. Toyota, R. Fukuda, J. Hasegawa, M. Ishida, T. Nakajima, Y. Honda, O. Kitao, H. Nakai, T. Vreven, J. A. Montgomery Jr., J. E. Peralta, F. Ogliaro, M. J. Bearpark, J. Heyd, E. N. Brothers, K. N. Kudin, V. N. Staroverov, R. Kobayashi, J. Normand, K. Raghavachari, A. P. Rendell, J. C. Burant, S. S. Iyengar, J. Tomasi, M. Cossi, N. Rega, N. J. Millam, M. Klene, J. E. Knox, J. B. Cross, V. Bakken, C. Adamo, J. Jaramillo, R. Gomperts, R. E. Stratmann, O. Yazyev, A. J. Austin, R. Cammi, C. Pomelli, J. W. Ochterski, R. L. Martin, K. Morokuma, V. G. Zakrzewski, G. A. Voth, P. Salvador, J. J. Dannenberg, S. Dapprich, A. D. Daniels, Ö. Farkas, J. B. Foresman, J. V. Ortiz, J. Cioslowski and D. J. Fox, *Journal*, 2009.
88. R. Dennington, *Inc., Wallingford, CT*, 2008.
89. P. Hohenberg and W. Kohn, *Physical Review*, 1964, **136**, B864-B871.
90. W. Kohn and L. J. Sham, *Physical Review*, 1965, **140**, A1133-A1138.
91. M. E. CASIDA, in *Recent Advances in Density Functional Methods*, WORLD SCIENTIFIC, 2011, DOI: doi:10.1142/9789812830586_0005, pp. 155-192.
92. A. D. Becke, *The Journal of Chemical Physics*, 1993, **98**, 5648-5652.
93. C. Lee, W. Yang and R. G. Parr, *Physical Review B*, 1988, **37**, 785-789.
94. E. K. U. Gross, J. F. Dobson and M. Petersilka, in *Density Functional Theory II*, ed. R. F. Nalewajski, Springer Berlin Heidelberg, 1996, vol. 181, ch. 2, pp. 81-172.
95. J. B. Foresman, M. Head-Gordon, J. A. Pople and M. J. Frisch, *The Journal of Physical Chemistry*, 1992, **96**, 135-149.
96. J. R. Lakowicz, *Principles of fluorescence spectroscopy*, Springer Science & Business Media, 2013.
97. B. Valeur and M. N. Berberan-Santos, *Molecular fluorescence: principles and applications*, John Wiley & Sons, 2012.
98. S. SMART, *Siemens Analytical X-ray Instruments Inc.: Madison, Wisconsin, USA*, 1995.
99. G. Sheldrick, *University of Göttingen*, 1996.
100. G. Sheldrick, *Inc., Madison, WI*, 1996.
101. C. F. Macrae, I. J. Bruno, J. A. Chisholm, P. R. Edgington, P. McCabe, E. Pidcock, L. Rodriguez-Monge, R. Taylor, J. v. Streek and P. A. Wood, *Journal of Applied Crystallography*, 2008, **41**, 466-470.
102. Y. Zheng, Q. Wang and C. Tan, *Luminescence*, 2012, **27**, 302-306.
103. O. K. Abou-Zied, *Chemical Physics*, 2007, **337**, 1-10.
104. N. Alarcos, B. Cohen and A. Douhal, *The Journal of Physical Chemistry C*, 2014, **118**, 19431-19443.
105. T. Elsaesser and B. Schmetzer, *Chemical Physics Letters*, 1987, **140**, 293-299.
106. A. Helal, N. Thao, S. Lee and H.-S. Kim, *J Incl Phenom Macrocycl Chem*, 2010, **66**, 87-94.
107. F. A. S. Chipem, N. Dash and G. Krishnamoorthy, *The Journal of Chemical Physics*, 2011, **134**, 104308.
108. K. Das, N. Sarkar, A. K. Ghosh, D. Majumdar, D. N. Nath and K. Bhattacharyya, *The Journal of Physical Chemistry*, 1994, **98**, 9126-9132.
109. G. Krishnamoorthy and S. K. Dogra, *The Journal of Organic Chemistry*, 1999, **64**, 6566-6574.
110. S. K. Behera and G. Krishnamoorthy, *Photochemical & Photobiological Sciences*, 2015, **14**, 2225-2237.
111. E. L. Roberts, J. Dey and I. M. Warner, *The Journal of Physical Chemistry A*, 1997, **101**, 5296-5301.
112. A. K. Mishra and S. K. Dogra, *Spectrochimica Acta Part A: Molecular Spectroscopy*, 1983, **39**, 609-611.
113. H. J. C. Jacobs and E. Havinga, in *Advances in Photochemistry*, John Wiley & Sons, Inc., 2007, DOI: 10.1002/9780470133415.ch4, pp. 305-373.
114. N. Kaur, G. Dhaka and J. Singh, *Tetrahedron Letters*, 2015, **56**, 1162-1165.

115. A. Brenlla, M. Veiga, J. L. Pérez Lustres, M. C. Ríos Rodríguez, F. Rodríguez-Prieto and M. Mosquera, *The Journal of Physical Chemistry B*, 2013, **117**, 884-896.
116. F. A. S. Chipem and G. Krishnamoorthy, *The Journal of Physical Chemistry A*, 2009, **113**, 12063-12070.
117. G. Krishnamoorthy and S. K. Dogra, *Journal of Luminescence*, 2000, **92**, 103-114.
118. M. M. Balamurali and S. K. Dogra, *Journal of Photochemistry and Photobiology A: Chemistry*, 2002, **154**, 81-92.
119. F. A. S. Chipem and G. Krishnamoorthy, *The Journal of Physical Chemistry B*, 2013, **117**, 14079-14088.
120. G. Krishnamoorthy and S. K. Dogra, *Journal of Luminescence*, 2000, **92**, 91-102.
121. H.-H. G. Tsai, H.-L. S. Sun and C.-J. Tan, *The Journal of Physical Chemistry A*, 2010, **114**, 4065-4079.
122. E. L. Roberts, J. Dey and I. M. Warner, *The Journal of Physical Chemistry*, 1996, **100**, 19681-19686.
123. F. A. S. Chipem, S. K. Behera and G. Krishnamoorthy, *Photochemical & Photobiological Sciences*, 2014, **13**, 1297-1304.
124. S. Sahu, M. Das and G. Krishnamoorthy, *Physical Chemistry Chemical Physics*, 2016, **18**, 11081-11090.
125. K. L. Geremia, Wright State University, 2015.
126. M. Krishnamurthy, P. Phaniraj and S. K. Dogra, *Journal of the Chemical Society, Perkin Transactions 2*, 1986, DOI: 10.1039/P29860001917, 1917-1925.
127. D. LeGourriérec, V. A. Kharlanov, R. G. Brown and W. Rettig, *Journal of Photochemistry and Photobiology A: Chemistry*, 2000, **130**, 101-111.
128. T. Iijima, A. Momotake, Y. Shinohara, T. Sato, Y. Nishimura and T. Arai, *The Journal of Physical Chemistry A*, 2010, **114**, 1603-1609.
129. J. S. Stephan and K. H. Grellmann, *The Journal of Physical Chemistry*, 1995, **99**, 10066-10068.
130. M. Ikegami and T. Arai, *J. Chem. Soc., Perkin Trans. 2*, 2002, DOI: 10.1039/b202559k, 1296-1301.
131. J. Luo, Z. Xie, J. W. Y. Lam, L. Cheng, H. Chen, C. Qiu, H. S. Kwok, X. Zhan, Y. Liu, D. Zhu and B. Z. Tang, *Chemical Communications*, 2001, DOI: 10.1039/B105159H, 1740-1741.
132. A. Mordziński, A. Grabowska, W. Kühnle and A. Kröwczyński, *Chemical physics letters*, 1983, **101**, 291-296.
133. H. Bulska, *Chemical Physics Letters*, 1983, **98**, 398-402.
134. K.-C. Tang, C.-L. Chen, H.-H. Chuang, J.-L. Chen, Y.-J. Chen, Y.-C. Lin, J.-Y. Shen, W.-P. Hu and P.-T. Chou, *The Journal of Physical Chemistry Letters*, 2011, **2**, 3063-3068.
135. S.-Y. Park, H. Jeong, H. Yu, S. Y. Park and D.-J. Jang, *Photochemistry and Photobiology*, 2010, **86**, 1197-1201.
136. A. Douhal, F. Amat-Guerri, M. P. Lillo and A. U. Acuña, *Journal of Photochemistry and Photobiology A: Chemistry*, 1994, **78**, 127-138.
137. P. Cornago, P. Cabildo, R. M. Claramunt, L. Bouissane, E. Pinilla, M. R. Torres and J. Elguero, *New Journal of Chemistry*, 2009, **33**, 125-135.
138. F. Tomas, J. L. M. Abboud, J. Laynez, R. Notario, L. Santos, S. O. Nilsson, J. Catalan, R. M. Claramunt and J. Elguero, *Journal of the American Chemical Society*, 1989, **111**, 7348-7353.
139. F. C. Teixeira, H. Ramos, I. F. Antunes, M. J. M. Curto, M. T. Duarte and I. Bento, *Molecules*, 2006, **11**, 867-889.
140. E. D. Raczyńska, W. Kosińska, B. Ośmiałowski and R. Gawinecki, *Chemical Reviews*, 2005, **105**, 3561-3612.
141. J. Wu, W. Liu, J. Ge, H. Zhang and P. Wang, *Chemical Society Reviews*, 2011, **40**, 3483-3495.

142. J. Wu, B. Kwon, W. Liu, E. V. Anslyn, P. Wang and J. S. Kim, *Chemical Reviews*, 2015, **115**, 7893-7943.
143. A. J. McConnell, C. S. Wood, P. P. Neelakandan and J. R. Nitschke, *Chemical Reviews*, 2015, **115**, 7729-7793.
144. A. P. De Silva, *Molecular Logic-based Computation*, Royal Society of Chemistry, Cambridge, UK, 2013.
145. E. Katz, *Molecular and Supramolecular Information Processing: From Molecular Switches to Logic Systems*, 2012.
146. S. Sahu, A. Mishra and G. Krishnamoorthy, *Analyst*, 2013, **138**, 5942-5948.
147. XXX and Xx, *Blank Reference*, 2015, **00**, 00-xx.
148. H. A. Benesi and J. H. Hildebrand, *Journal of the American Chemical Society*, 1949, **71**, 2703-2707.
149. N. Dash, F. A. S. Chipem and G. Krishnamoorthy, *Photochemical & Photobiological Sciences*, 2009, **8**, 1708-1715.
150. N. Dash, A. Malakar, M. Kumar, B. B. Mandal and G. Krishnamoorthy, *Sensors and Actuators B: Chemical*, 2014, **202**, 1154-1163.
151. N. Dash and G. Krishnamoorthy, *Journal of Fluorescence*, 2010, **20**, 135-142.
152. G. Krishnamoorthy and S. K. Dogra, *Chemical Physics Letters*, 2000, **323**, 234-242.
153. J. Gao, W. Ge and J. Li, *Science in China Series B: Chemistry*, 2005, **48**, 470-475.
154. A. Mallick, M. C. Mandal, B. Haldar, A. Chakrabarty, P. Das and N. Chattopadhyay, *Journal of the American Chemical Society*, 2006, **128**, 3126-3127.
155. J. Andréasson, U. Pischel, S. D. Straight, T. A. Moore, A. L. Moore and D. Gust, *Journal of the American Chemical Society*, 2011, **133**, 11641-11648.
156. F. Pu, J. Ren, X. Yang and X. Qu, *Chemistry – A European Journal*, 2011, **17**, 9590-9594.
157. L. A. Zadeh, *IEEE Software*, 1994, **11**, 48-56.
158. J. M. Mendel, *Proceedings of the IEEE*, 1995, **83**, 345-377.
159. N. Dash, F. A. S. Chipem, R. Swaminathan and G. Krishnamoorthy, *Chemical Physics Letters*, 2008, **460**, 119-124.
160. M. Elstner, J. Axthelm and A. Schiller, *Angewandte Chemie International Edition*, 2014, **53**, 7339-7343.
161. M. Sugeno and T. Yasukawa, *IEEE Transactions on fuzzy systems*, 1993, **1**, 7-31.
162. J.-S. R. Jang, *Systems, Man and Cybernetics, IEEE Transactions on*, 1993, **23**, 665-685.
163. J.-S. R. Jang and C.-T. Sun, *Proceedings of the IEEE*, 1995, **83**, 378-406.

## References


1. A. Kotlyar, N. Borovok, S. Kiryati, E. Nachliel and M. Gutman, *Biochemistry*, 1994, **33**, 873-879.
2. M. S. Celej, W. Caarls, A. P. Demchenko and T. M. Jovin, *Biochemistry*, 2009, **48**, 7465-7472.
3. A. Müller, H. Ratajczak, W. Junge and E. Diemann, *Electron and Proton Transfer in Chemistry and Biology*, 1992.
4. T. Gensch, J. Heberle and C. Viappiani, *Photochemical & Photobiological Sciences*, 2006, **5**, 529-530.
5. H. Ishikita and K. Saito, *Journal of The Royal Society Interface*, 2014, **11**, 20130518.
6. K. Weber, *Z. Physik. Chem. B*, 1931, **15**, 18.
7. T. Förster, *Naturwissenschaften*, 1949, **36**, 186-187.
8. L. G. Arnaut and S. J. Formosinho, *Journal of Photochemistry and Photobiology A: Chemistry*, 1993, **75**, 1-20.
9. M. Kondo, *Bulletin of the Chemical Society of Japan*, 1978, **51**, 3027-3029.
10. R. G. Brown, N. Entwistle, J. D. Hepworth, K. W. Hodgson and B. May, *The Journal of Physical Chemistry*, 1982, **86**, 2418-2420.
11. J. F. Ireland and P. A. H. Wyatt, in *Advances in Physical Organic Chemistry*, ed. V. Gold, Academic Press, 1976, vol. Volume 12, pp. 131-221.
12. F. Rodriguez Prieto, M. Mosquera and M. Novo, *The Journal of Physical Chemistry*, 1990, **94**, 8536-8542.
13. M. Mosquera, M. C. Ríos Rodríguez and F. Rodríguez-Prieto, *The Journal of Physical Chemistry A*, 1997, **101**, 2766-2772.
14. C. A. Taylor, M. A. El-Bayoumi and M. Kasha, *Proceedings of the National Academy of Sciences of the United States of America*, 1969, **63**, 253-260.
15. J. Catalán, P. Pérez, J. C. del Valle, J. L. G. de Paz and M. Kasha, *Proceedings of the National Academy of Sciences of the United States of America*, 2004, **101**, 419-422.
16. J. Catalan and P. Perez, *Physical Chemistry Chemical Physics*, 2005, **7**, 94-99.
17. H. Sekiya and K. Sakota, *Journal of Photochemistry and Photobiology C: Photochemistry Reviews*, 2008, **9**, 81-91.
18. J. Catalán and M. Kasha, *The Journal of Physical Chemistry A*, 2000, **104**, 10812-10820.
19. S. Takeuchi and T. Tahara, *Chemical Physics Letters*, 2001, **347**, 108-114.
20. M. Itoh, T. Adachi and K. Tokumura, *Journal of the American Chemical Society*, 1984, **106**, 850-855.
21. P. J. Thistlethwaite and P. J. Corkill, *Chemical Physics Letters*, 1982, **85**, 317-321.
22. B. Kang, K. C. Ko, S.-Y. Park, D.-J. Jang and J. Y. Lee, *Physical Chemistry Chemical Physics*, 2011, **13**, 6332-6339.
23. A. Weller, *Naturwissenschaften*, 1955, **42**, 175-176.
24. M. Lukeman and P. Wan, *Chemical Communications*, 2001, DOI: 10.1039/B100817J, 1004-1005.
25. N. Basarić, N. Došlić, J. Ivković, Y.-H. Wang, J. Veljković, K. Mlinarić-Majerski and P. Wan, *The Journal of Organic Chemistry*, 2013, **78**, 1811-1823.
26. C.-Y. Peng, J.-Y. Shen, Y.-T. Chen, P.-J. Wu, W.-Y. Hung, W.-P. Hu and P.-T. Chou, *Journal of the American Chemical Society*, 2015, **137**, 14349-14357.
27. W.-S. Yu, C.-C. Cheng, Y.-M. Cheng, P.-C. Wu, Y.-H. Song, Y. Chi and P.-T. Chou, *Journal of the American Chemical Society*, 2003, **125**, 10800-10801.
28. N. Suzuki, A. Fukazawa, K. Nagura, S. Saito, H. Kitoh-Nishioka, D. Yokogawa, S. Irle and S. Yamaguchi, *Angewandte Chemie International Edition*, 2014, **53**, 8231-8235.
29. F. G. Bordwell, G. E. Drucker, N. H. Andersen and A. D. Denniston, *Journal of the American Chemical Society*, 1986, **108**, 7310-7313.
30. B. L. McDowell and H. Rapoport, *The Journal of Organic Chemistry*, 1972, **37**, 3261-3265.
31. T. Mutai, H. Tomoda, T. Ohkawa, Y. Yabe and K. Araki, *Angewandte Chemie*, 2008, **120**, 9664-9666.
32. F. Rodriguez-Prieto, J. Carlos Penedo and M. Mosquera, *Journal of the Chemical Society, Faraday Transactions*, 1998, **94**, 2775-2782.
33. B. W. Clare, D. Cook, E. C. F. Ko, Y. C. Mac and A. J. Parker, *Journal of the American Chemical Society*, 1966, **88**, 1911-1916.
34. G. Köbrich, *Angewandte Chemie*, 1966, **78**, 786-786.
35. F. A. S. Chipem, S. K. Behera and G. Krishnamoorthy, *The Journal of Physical Chemistry A*, 2013, **117**, 4084-4095.
36. W. Klöpffer and G. Naundorf, *Journal of Luminescence*, 1974, **8**, 457-461.
37. A. Douhal, F. Amat-Guerri and A. U. Acuna, *The Journal of Physical Chemistry*, 1995, **99**, 76-80.
38. K. Inuzuka and A. Fujimoto, *Spectrochimica Acta Part A: Molecular Spectroscopy*, 1986, **42**, 929-937.
39. H. Ishikawa, K. Iwata and H.-o. Hamaguchi, *The Journal of Physical Chemistry A*, 2002, **106**, 2305-2312.
40. F.-T. Hung, W.-P. Hu, T.-H. Li, C.-C. Cheng and P.-T. Chou, *The Journal of Physical Chemistry A*, 2003, **107**, 3244-3253.
41. Q. Chu, D. A. Medvetz and Y. Pang, *Chemistry of Materials*, 2007, **19**, 6421-6429.
42. F. A. S. Chipem, S. K. Behera and G. Krishnamoorthy, *Sensors and Actuators B: Chemical*, 2014, **191**, 727-733.
43. M. M. Henary and C. J. Fahrni, *The Journal of Physical Chemistry A*, 2002, **106**, 5210-5220.
44. A. Helal and H.-S. Kim, *Tetrahedron Letters*, 2009, **50**, 5510-5515.
45. S. Dalapati, S. Jana and N. Guchhait, *Spectrochimica Acta Part A: Molecular and Biomolecular Spectroscopy*, 2014, **129**, 499-508.
46. J. Zhao, S. Ji, Y. Chen, H. Guo and P. Yang, *Physical Chemistry Chemical Physics*, 2012, **14**, 8803-8817.

47. Y. Wu, X. Peng, J. Fan, S. Gao, M. Tian, J. Zhao and S. Sun, *The Journal of Organic Chemistry*, 2007, **72**, 62-70.
48. G.-Y. Li and T. Chu, *Physical Chemistry Chemical Physics*, 2011, **13**, 20766-20771.
49. K. C. Gross and P. G. Seybold, *International Journal of Quantum Chemistry*, 2000, **80**, 1107-1115.
50. S.-i. Nagaoka, A. Nakamura and U. Nagashima, *Journal of Photochemistry and Photobiology A: Chemistry*, 2002, **154**, 23-32.
51. T. Mutai, H. Sawatani, T. Shida, H. Shono and K. Araki, *The Journal of Organic Chemistry*, 2013, **78**, 2482-2489.
52. A. O. Doroshenko, E. A. Posokhov, A. A. Verezubova, L. M. Ptyagina, V. T. Skripkina and V. M. Shershukov, *Photochemical & Photobiological Sciences*, 2002, **1**, 92-99.
53. Z. Song, W. Zhang, M. Jiang, H. H. Y. Sung, R. T. K. Kwok, H. Nie, I. D. Williams, B. Liu and B. Z. Tang, *Advanced Functional Materials*, 2015, DOI: 10.1002/adfm.201503788, n/a-n/a.
54. K. R. Phatangare, V. D. Gupta, A. B. Tathe, V. S. Padalkar, V. S. Patil, P. Ramasami and N. Sekar, *Tetrahedron*, 2013, **69**, 1767-1777.
55. R. Wei, P. Song and A. Tong, *The Journal of Physical Chemistry C*, 2013, **117**, 3467-3474.
56. Y. Qian, S. Li, G. Zhang, Q. Wang, S. Wang, H. Xu, C. Li, Y. Li and G. Yang, *The Journal of Physical Chemistry B*, 2007, **111**, 5861-5868.
57. R. Hu, S. Li, Y. Zeng, J. Chen, S. Wang, Y. Li and G. Yang, *Physical Chemistry Chemical Physics*, 2011, **13**, 2044-2051.
58. S. Kumar, V. Luxami, R. Saini and D. Kaur, *Chemical Communications*, 2009, DOI: 10.1039/B900131J, 3044-3046.
59. P. Singh, H. Singh, G. Bhargava and S. Kumar, *J. Mater. Chem. C*, 2015, **3**, 5524-5532.
60. G. de Ruiter, L. Motiei, J. Choudhury, N. Oded and M. E. van der Boom, *Angewandte Chemie*, 2010, **122**, 4890-4893.
61. I. Gallardo, G. Guirado, J. Hernando, S. Morais and G. Prats, *Chemical Science*, 2016, **7**, 1819-1825.
62. S. Park, J. Seo, S. H. Kim and S. Y. Park, *Advanced Functional Materials*, 2008, **18**, 726-731.
63. K. S. Menger, *IEEE Transactions on Computers*, 1969, **C-18**, 241-250.
64. S. L. Hurst, *IEEE Transactions on Computers*, 1984, **C-33**, 1160-1179.
65. S. Stockinger and O. Trapp, *Chemical Science*, 2014, **5**, 2677-2682.
66. K. Szaciłowski, *Chemical Reviews*, 2008, **108**, 3481-3548.
67. J. Andreasson and U. Pischel, *Chemical Society Reviews*, 2010, **39**, 174-188.
68. G. McSkimming, J. H. R. Tucker, H. Bouas-Laurent and J.-P. Desvergne, *Angewandte Chemie International Edition*, 2000, **39**, 2167-2169.
69. P. A. de Silva, N. H. Q. Gunaratne and C. P. McCoy, *Nature*, 1993, **364**, 42-44.
70. A. Credi, V. Balzani, S. J. Langford and J. F. Stoddart, *Journal of the American Chemical Society*, 1997, **119**, 2679-2681.
71. R. Ferreira, P. Remón and U. Pischel, *The Journal of Physical Chemistry C*, 2009, **113**, 5805-5811.
72. H. K. Sinha and S. K. Dogra, *Chemical Physics*, 1986, **102**, 337-347.
73. M. Mosquera, J. C. Penedo, M. C. Ríos Rodríguez and F. Rodríguez-Prieto, *The Journal of Physical Chemistry*, 1996, **100**, 5398-5407.
74. R. Wortmann, S. Lebus, H. Reis, A. Grabowska, K. Kownacki and S. Jarosz, *Chemical Physics*, 1999, **243**, 295-304.
75. C. M. Orlando, J. G. Wirth and D. R. Heath, *The Journal of Organic Chemistry*, 1970, **35**, 3147-3149.
76. R. W. Middleton and D. G. Wibberley, *Journal of Heterocyclic Chemistry*, 1980, **17**, 1757-1760.
77. D. W. Hein, R. J. Alheim and J. J. Leavitt, *Journal of the American Chemical Society*, 1957, **79**, 427-429.
78. B. Shankar, S. Sahu, N. Deibel, D. Schweinfurth, B. Sarkar, P. Elumalai, D. Gupta, F. Hussain, G. Krishnamoorthy and M. Sathiyendiran, *Inorganic Chemistry*, 2014, **53**, 922-930.
79. S. Stucky, N. J. Koch, U. Heinz and K. Hegetschweiler, *Chemical Papers*, 2008, **62**, 388-397.
80. A. Einhorn, E. Bischkopff, B. Szelinski, G. Schupp, E. Spröngerts, C. Ladisch and T. Mauermayer, *Justus Liebigs Annalen der Chemie*, 1905, **343**, 207-305.
81. A. Mishra and G. Krishnamoorthy, *Photochemical & Photobiological Sciences*, 2012, **11**, 1356-1367.
82. A. Mishra, S. Sahu, N. Dash, S. K. Behera and G. Krishnamoorthy, *The Journal of Physical Chemistry B*, 2013, **117**, 9469-9477.
83. G. A. Crosby and J. N. Demas, *The Journal of Physical Chemistry*, 1971, **75**, 991-1024.
84. C. Wohlfarth, *Handbook of Chemistry and Physics*, 2004.
85. M. Lechner, *Landolt Börnstein*, 2008, **47**.
86. A. S. R. Koti, M. M. G. Krishna and N. Periasamy, *The Journal of Physical Chemistry A*, 2001, **105**, 1767-1771.
87. M. J. Frisch, G. W. Trucks, H. B. Schlegel, G. E. Scuseria, M. A. Robb, J. R. Cheeseman, G. Scalmani, V. Barone, B. Mennucci, G. A. Petersson, H. Nakatsuji, M. Caricato, X. Li, H. P. Hratchian, A. F. Izmaylov, J. Bloino, G. Zheng, J. L. Sonnenberg, M. Hada, M. Ehara, K. Toyota, R. Fukuda, J. Hasegawa, M. Ishida, T. Nakajima, Y. Honda, O. Kitao, H. Nakai, T. Vreven, J. A. Montgomery Jr., J. E. Peralta, F. Ogliaro, M. J. Bearpark, J. Heyd, E. N. Brothers, K. N. Kudin, V. N. Staroverov, R. Kobayashi, J. Normand, K. Raghavachari, A. P. Rendell, J. C. Burant, S. S. Iyengar, J. Tomasi, M. Cossi, N. Rega, N. J. Millam, M. Klene, J. E. Knox, J. B. Cross, V. Bakken, C. Adamo, J. Jaramillo, R. Gomperts, R. E. Stratmann, O. Yazyev, A. J. Austin, R. Cammi, C. Pomelli, J. W. Ochterski, R. L. Martin, K. Morokuma, V. G. Zakrzewski, G. A. Voth, P. Salvador, J. J. Dannenberg, S. Dapprich, A. D. Daniels, Ö. Farkas, J. B. Foresman, J. V. Ortiz, J. Cioslowski and D. J. Fox, Gaussian 09, Revision D.01, *Gaussian, Inc., Wallingford CT, 2013*.
88. D. Roy; K. Todd; M. John. GaussView, Version 5, *Semichem Inc*., Shawnee Mission, KS, 2009.

89. P. Hohenberg and W. Kohn, *Physical Review*, 1964, **136**, B864-B871.
90. W. Kohn and L. J. Sham, *Physical Review*, 1965, **140**, A1133-A1138.
91. M. E. CASIDA, in *Recent Advances in Density Functional Methods*, WORLD SCIENTIFIC, 2011, DOI: doi:10.1142/9789812830586_0005, pp. 155-192.
92. A. D. Becke, *The Journal of Chemical Physics*, 1993, **98**, 5648-5652.
93. C. Lee, W. Yang and R. G. Parr, *Physical Review B*, 1988, **37**, 785-789.
94. E. K. U. Gross, J. F. Dobson and M. Petersilka, in *Density Functional Theory II*, ed. R. F. Nalewajski, Springer Berlin Heidelberg, 1996, vol. 181, ch. 2, pp. 81-172.
95. J. B. Foresman, M. Head-Gordon, J. A. Pople and M. J. Frisch, *The Journal of Physical Chemistry*, 1992, **96**, 135-149.
96. J. R. Lakowicz, *Principles of fluorescence spectroscopy*, Springer Science & Business Media, 2013.
97. B. Valeur and M. N. Berberan-Santos, *Molecular fluorescence: principles and applications*, John Wiley & Sons, 2012.
98. S. SMART, *Siemens Analytical X-ray Instruments Inc.: Madison, Wisconsin, USA*, 1995.
99. G. Sheldrick, *University of Göttingen*, 1996.
100. G. Sheldrick, *Inc., Madison, WI*, 1996.
101. C. F. Macrae, I. J. Bruno, J. A. Chisholm, P. R. Edgington, P. McCabe, E. Pidcock, L. Rodriguez-Monge, R. Taylor, J. v. Streek and P. A. Wood, *Journal of Applied Crystallography*, 2008, **41**, 466-470.
102. Y. Zheng, Q. Wang and C. Tan, *Luminescence*, 2012, **27**, 302-306.
103. O. K. Abou-Zied, *Chemical Physics*, 2007, **337**, 1-10.
104. N. Alarcos, B. Cohen and A. Douhal, *The Journal of Physical Chemistry C*, 2014, **118**, 19431-19443.
105. T. Elsaesser and B. Schmetzer, *Chemical Physics Letters*, 1987, **140**, 293-299.
106. A. Helal, N. Thao, S. Lee and H.-S. Kim, *J Incl Phenom Macrocycl Chem*, 2010, **66**, 87-94.
107. F. A. S. Chipem, N. Dash and G. Krishnamoorthy, *The Journal of Chemical Physics*, 2011, **134**, 104308.
108. K. Das, N. Sarkar, A. K. Ghosh, D. Majumdar, D. N. Nath and K. Bhattacharyya, *The Journal of Physical Chemistry*, 1994, **98**, 9126-9132.
109. G. Krishnamoorthy and S. K. Dogra, *The Journal of Organic Chemistry*, 1999, **64**, 6566-6574.
110. S. K. Behera and G. Krishnamoorthy, *Photochemical & Photobiological Sciences*, 2015, **14**, 2225-2237.
111. E. L. Roberts, J. Dey and I. M. Warner, *The Journal of Physical Chemistry A*, 1997, **101**, 5296-5301.
112. A. K. Mishra and S. K. Dogra, *Spectrochimica Acta Part A: Molecular Spectroscopy*, 1983, **39**, 609-611.
113. H. J. C. Jacobs and E. Havinga, in *Advances in Photochemistry*, John Wiley & Sons, Inc., 2007, DOI: 10.1002/9780470133415.ch4, pp. 305-373.
114. N. Kaur, G. Dhaka and J. Singh, *Tetrahedron Letters*, 2015, **56**, 1162-1165.
115. A. Brenlla, M. Veiga, J. L. Pérez Lustres, M. C. Ríos Rodríguez, F. Rodríguez-Prieto and M. Mosquera, *The Journal of Physical Chemistry B*, 2013, **117**, 884-896.
116. F. A. S. Chipem and G. Krishnamoorthy, *The Journal of Physical Chemistry A*, 2009, **113**, 12063-12070.
117. G. Krishnamoorthy and S. K. Dogra, *Journal of Luminescence*, 2000, **92**, 103-114.
118. M. M. Balamurali and S. K. Dogra, *Journal of Photochemistry and Photobiology A: Chemistry*, 2002, **154**, 81-92.
119. F. A. S. Chipem and G. Krishnamoorthy, *The Journal of Physical Chemistry B*, 2013, **117**, 14079-14088.
120. G. Krishnamoorthy and S. K. Dogra, *Journal of Luminescence*, 2000, **92**, 91-102.
121. H.-H. G. Tsai, H.-L. S. Sun and C.-J. Tan, *The Journal of Physical Chemistry A*, 2010, **114**, 4065-4079.
122. E. L. Roberts, J. Dey and I. M. Warner, *The Journal of Physical Chemistry*, 1996, **100**, 19681-19686.
123. F. A. S. Chipem, S. K. Behera and G. Krishnamoorthy, *Photochemical & Photobiological Sciences*, 2014, **13**, 1297-1304.
124. S. Sahu, M. Das and G. Krishnamoorthy, *Physical Chemistry Chemical Physics*, 2016, **18**, 11081-11090.
125. K. L. Geremia, Wright State University, 2015.
126. M. Krishnamurthy, P. Phaniraj and S. K. Dogra, *Journal of the Chemical Society, Perkin Transactions 2*, 1986, DOI: 10.1039/P29860001917, 1917-1925.
127. D. LeGourriérec, V. A. Kharlanov, R. G. Brown and W. Rettig, *Journal of Photochemistry and Photobiology A: Chemistry*, 2000, **130**, 101-111.
128. T. Iijima, A. Momotake, Y. Shinohara, T. Sato, Y. Nishimura and T. Arai, *The Journal of Physical Chemistry A*, 2010, **114**, 1603-1609.
129. J. S. Stephan and K. H. Grellmann, *The Journal of Physical Chemistry*, 1995, **99**, 10066-10068.
130. M. Ikegami and T. Arai, *J. Chem. Soc., Perkin Trans. 2*, 2002, DOI: 10.1039/b202559k, 1296-1301.
131. J. Luo, Z. Xie, J. W. Y. Lam, L. Cheng, H. Chen, C. Qiu, H. S. Kwok, X. Zhan, Y. Liu, D. Zhu and B. Z. Tang, *Chemical Communications*, 2001, DOI: 10.1039/B105159H, 1740-1741.
132. A. Mordziński, A. Grabowska, W. Kühnle and A. Kröwczyński, *Chemical physics letters*, 1983, **101**, 291-296.
133. H. Bulska, *Chemical Physics Letters*, 1983, **98**, 398-402.
134. K.-C. Tang, C.-L. Chen, H.-H. Chuang, J.-L. Chen, Y.-J. Chen, Y.-C. Lin, J.-Y. Shen, W.-P. Hu and P.-T. Chou, *The Journal of Physical Chemistry Letters*, 2011, **2**, 3063-3068.
135. S.-Y. Park, H. Jeong, H. Yu, S. Y. Park and D.-J. Jang, *Photochemistry and Photobiology*, 2010, **86**, 1197-1201.
136. A. Douhal, F. Amat-Guerri, M. P. Lillo and A. U. Acuña, *Journal of Photochemistry and Photobiology A: Chemistry*, 1994, **78**, 127-138.

137. P. Cornago, P. Cabildo, R. M. Claramunt, L. Bouissane, E. Pinilla, M. R. Torres and J. Elguero, *New Journal of Chemistry*, 2009, **33**, 125-135.
138. F. Tomas, J. L. M. Abboud, J. Laynez, R. Notario, L. Santos, S. O. Nilsson, J. Catalan, R. M. Claramunt and J. Elguero, *Journal of the American Chemical Society*, 1989, **111**, 7348-7353.
139. F. C. Teixeira, H. Ramos, I. F. Antunes, M. J. M. Curto, M. T. Duarte and I. Bento, *Molecules*, 2006, **11**, 867-889.
140. E. D. Raczyńska, W. Kosińska, B. Ośmiałowski and R. Gawinecki, *Chemical Reviews*, 2005, **105**, 3561-3612.
141. J. Wu, W. Liu, J. Ge, H. Zhang and P. Wang, *Chemical Society Reviews*, 2011, **40**, 3483-3495.
142. J. Wu, B. Kwon, W. Liu, E. V. Anslyn, P. Wang and J. S. Kim, *Chemical Reviews*, 2015, **115**, 7893-7943.
143. A. J. McConnell, C. S. Wood, P. P. Neelakandan and J. R. Nitschke, *Chemical Reviews*, 2015, **115**, 7729-7793.
144. A. P. De Silva, *Molecular Logic-based Computation*, Royal Society of Chemistry, Cambridge, UK, 2013.
145. E. Katz, *Molecular and Supramolecular Information Processing: From Molecular Switches to Logic Systems*, 2012.
146. S. Sahu, A. Mishra and G. Krishnamoorthy, *Analyst*, 2013, **138**, 5942-5948.
147. A. Mishra, *Ph.D Thesis*, IIT Guwahati, 2013.
148. H. A. Benesi and J. H. Hildebrand, *Journal of the American Chemical Society*, 1949, **71**, 2703-2707.
149. N. Dash, F. A. S. Chipem and G. Krishnamoorthy, *Photochemical & Photobiological Sciences*, 2009, **8**, 1708-1715.
150. N. Dash, A. Malakar, M. Kumar, B. B. Mandal and G. Krishnamoorthy, *Sensors and Actuators B: Chemical*, 2014, **202**, 1154-1163.
151. N. Dash and G. Krishnamoorthy, *Journal of Fluorescence*, 2010, **20**, 135-142.
152. G. Krishnamoorthy and S. K. Dogra, *Chemical Physics Letters*, 2000, **323**, 234-242.
153. J. Gao, W. Ge and J. Li, *Science in China Series B: Chemistry*, 2005, **48**, 470-475.
154. A. Mallick, M. C. Mandal, B. Haldar, A. Chakrabarty, P. Das and N. Chattopadhyay, *Journal of the American Chemical Society*, 2006, **128**, 3126-3127.
155. J. Andréasson, U. Pischel, S. D. Straight, T. A. Moore, A. L. Moore and D. Gust, *Journal of the American Chemical Society*, 2011, **133**, 11641-11648.
156. F. Pu, J. Ren, X. Yang and X. Qu, *Chemistry – A European Journal*, 2011, **17**, 9590-9594.
157. L. A. Zadeh, *IEEE Software*, 1994, **11**, 48-56.
158. J. M. Mendel, *Proceedings of the IEEE*, 1995, **83**, 345-377.
159. N. Dash, F. A. S. Chipem, R. Swaminathan and G. Krishnamoorthy, *Chemical Physics Letters*, 2008, **460**, 119-124.
160. M. Elstner, J. Axthelm and A. Schiller, *Angewandte Chemie International Edition*, 2014, **53**, 7339-7343.
161. M. Sugeno and T. Yasukawa, *IEEE Transactions on fuzzy systems*, 1993, **1**, 7-31.
162. J.-S. R. Jang, *Systems, Man and Cybernetics, IEEE Transactions on*, 1993, **23**, 665-685.
163. J.-S. R. Jang and C.-T. Sun, *Proceedings of the IEEE*, 1995, **83**, 378-406.

# Annexure-A

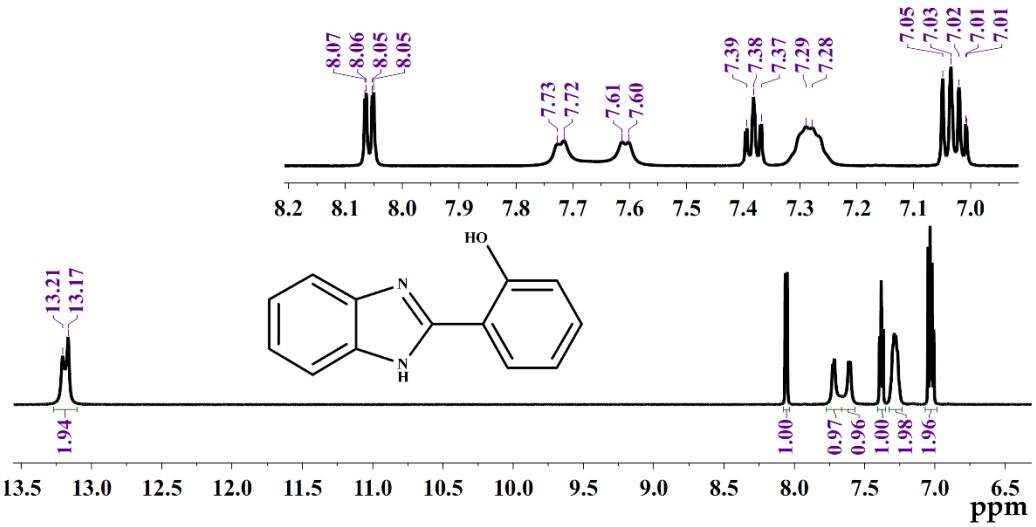


**Figure A1.** [1]HNMR spectra of HPBI in DMSO.

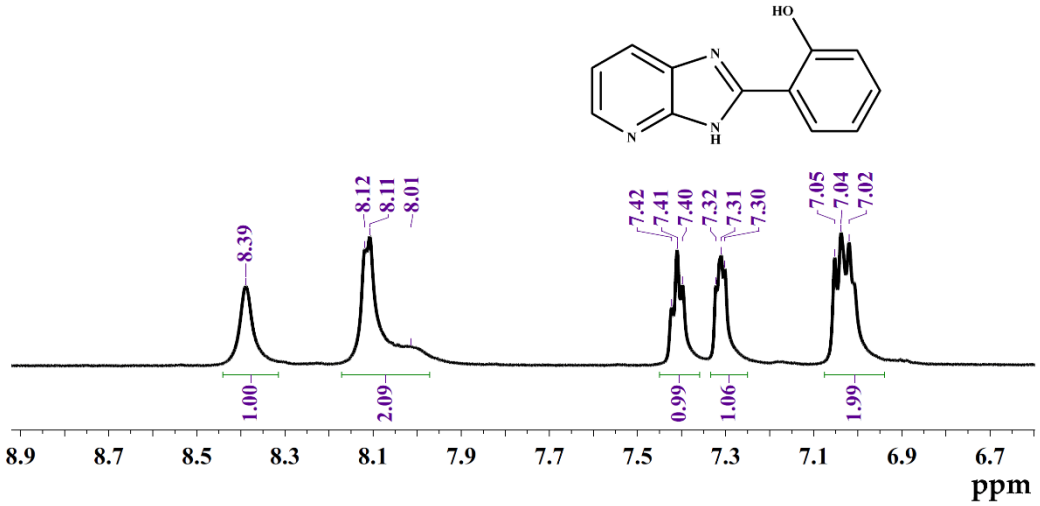


**Figure A2.** [1]HNMR spectra of HPIP-b in DMSO.

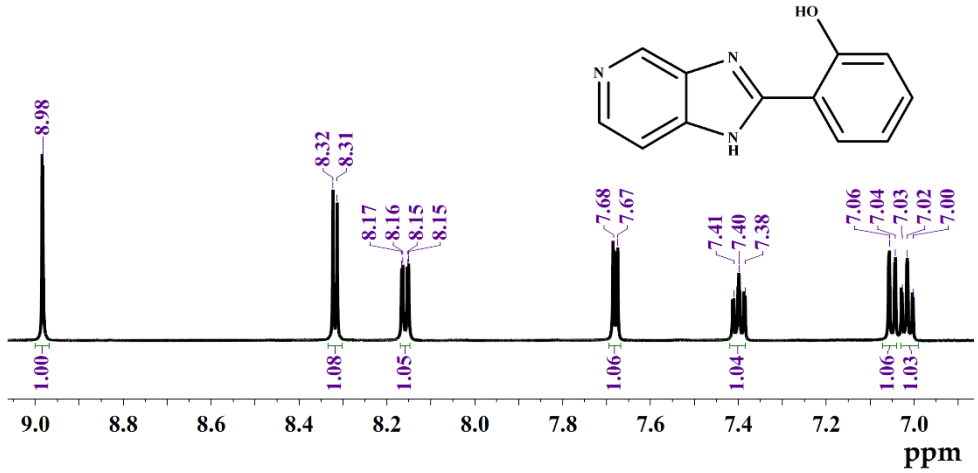


**Figure A3.** [1]HNMR spectra of HPIP-c in DMSO.

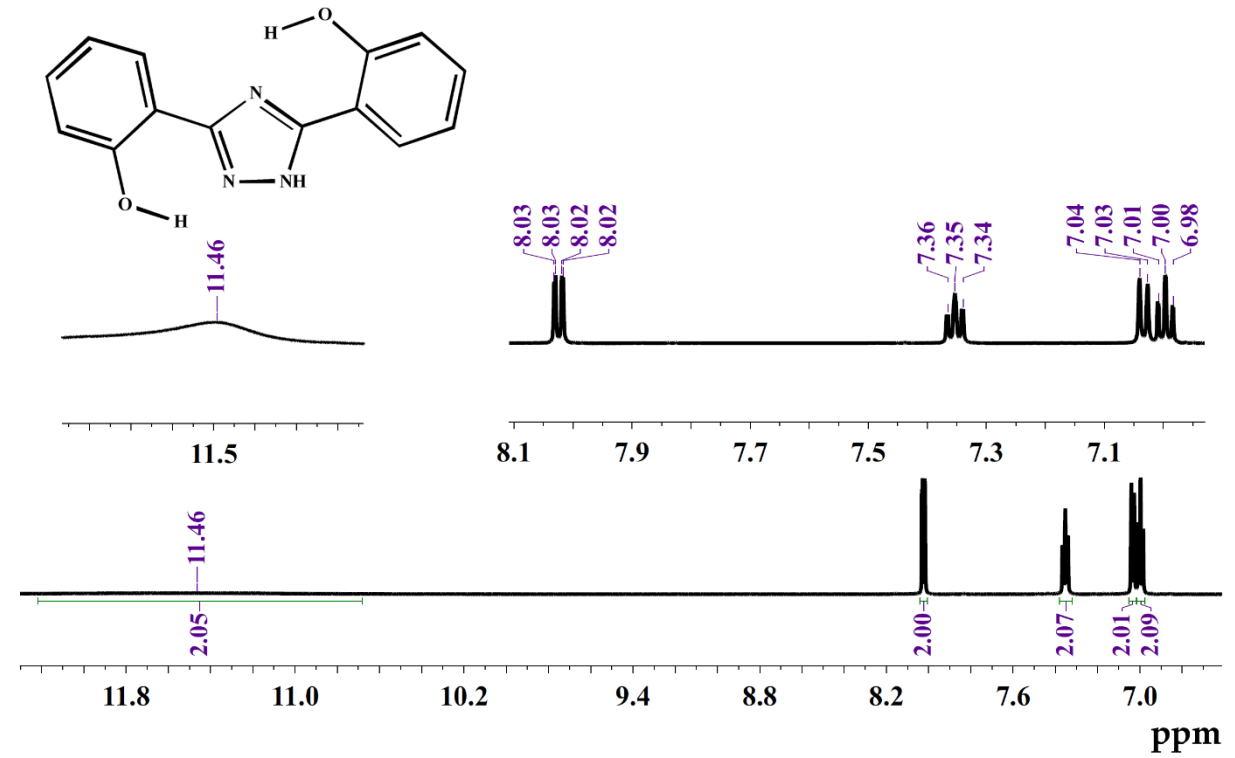


**Figure A4.** [1]HNMR spectra of Tz in DMSO.

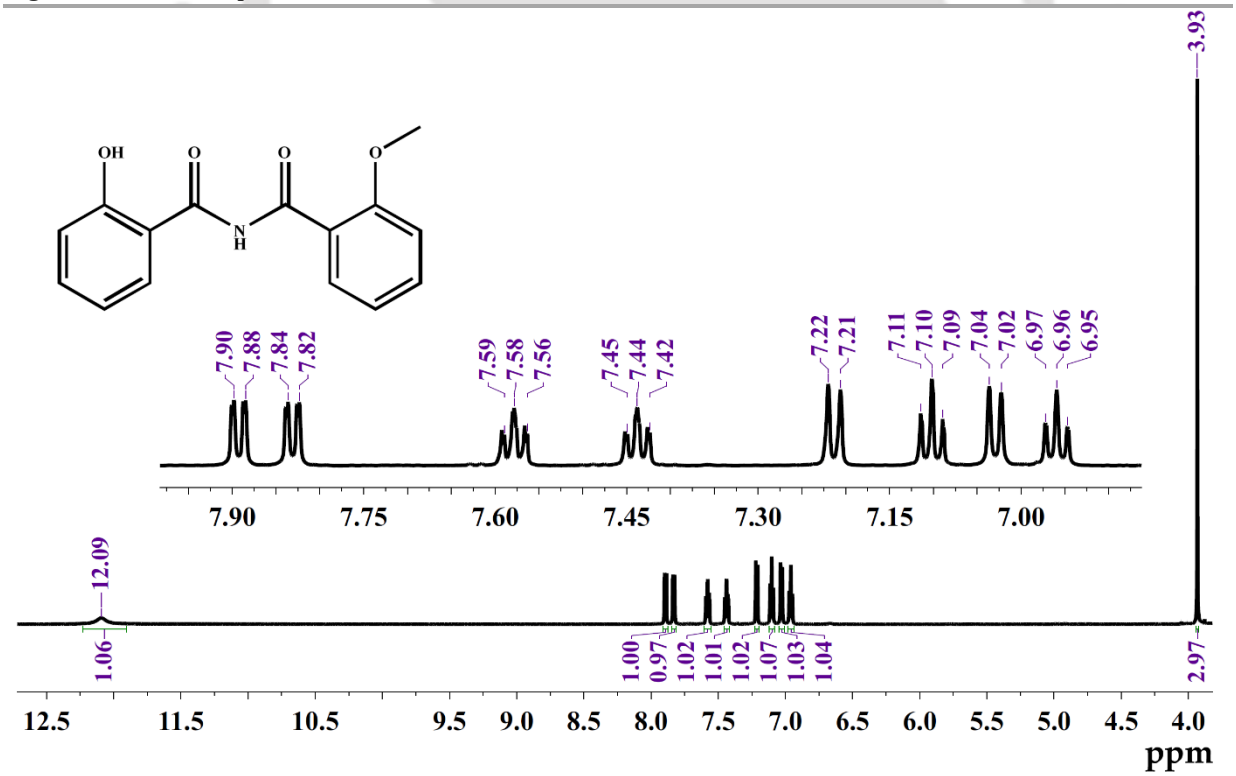


**Figure A5.** [1]HNMR of HMB in DMSO.

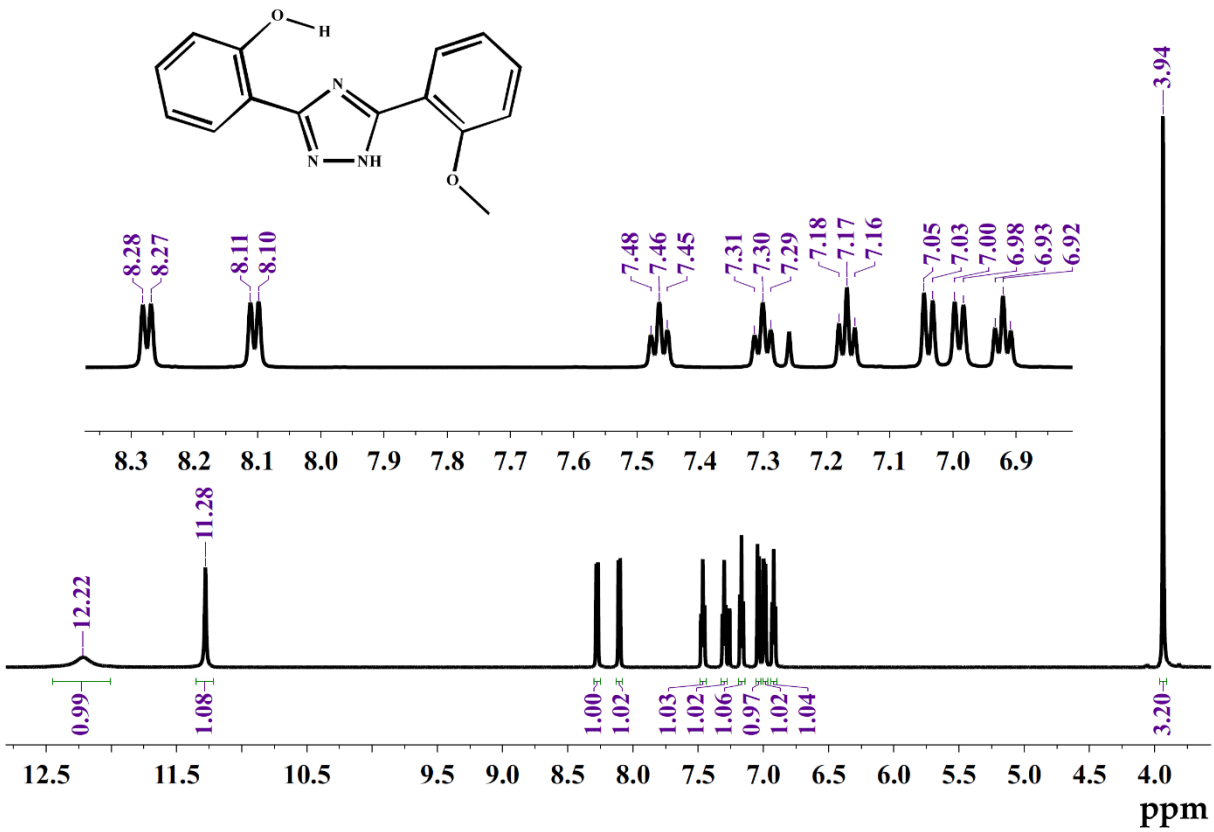


**Figure A6.** $^{1}$HNMR of MTz in $CDCl_3$

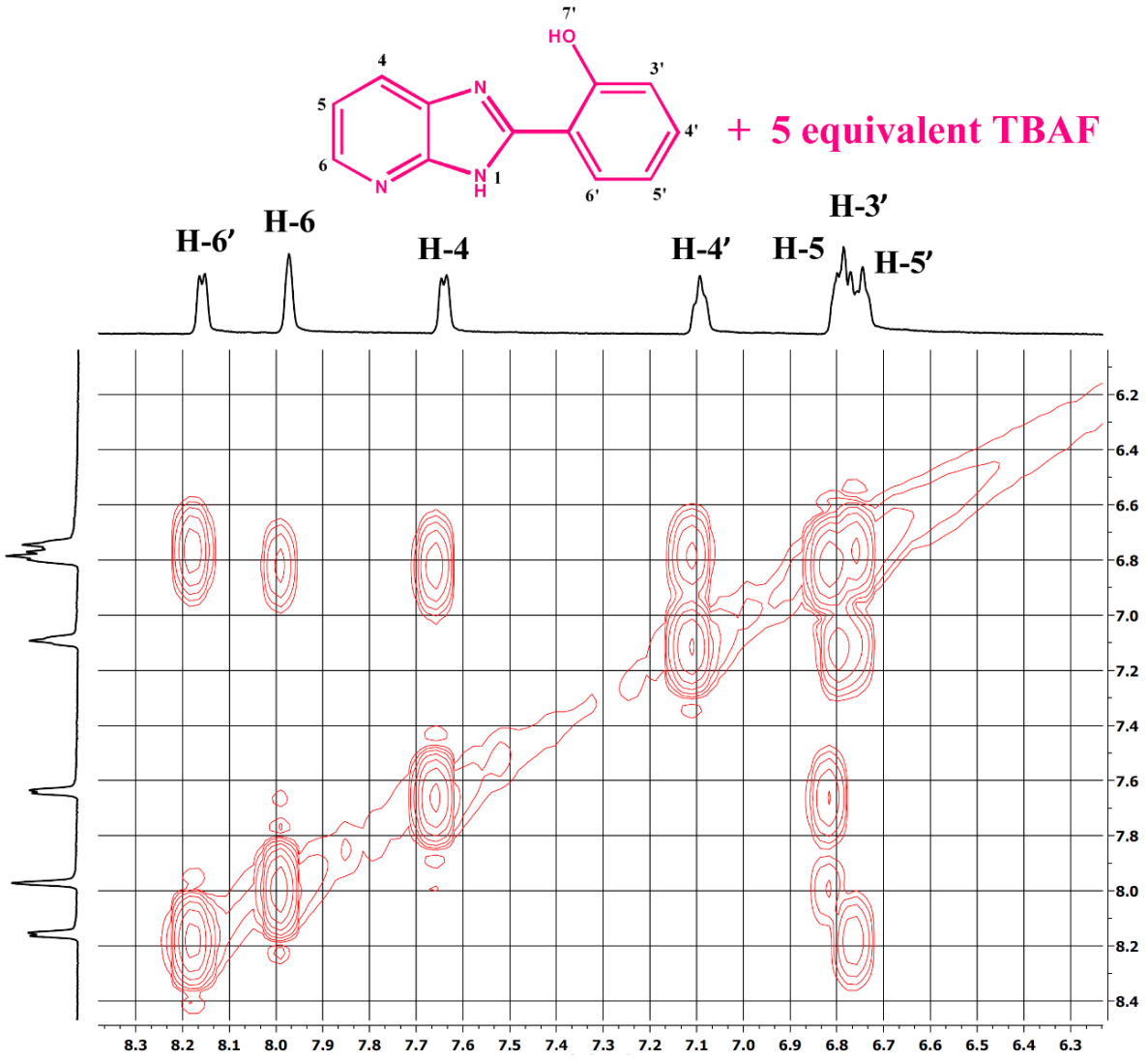


**Figure A7.** 2D-NMR of HPIP-b in presence of 5 equivalent of TBAF.

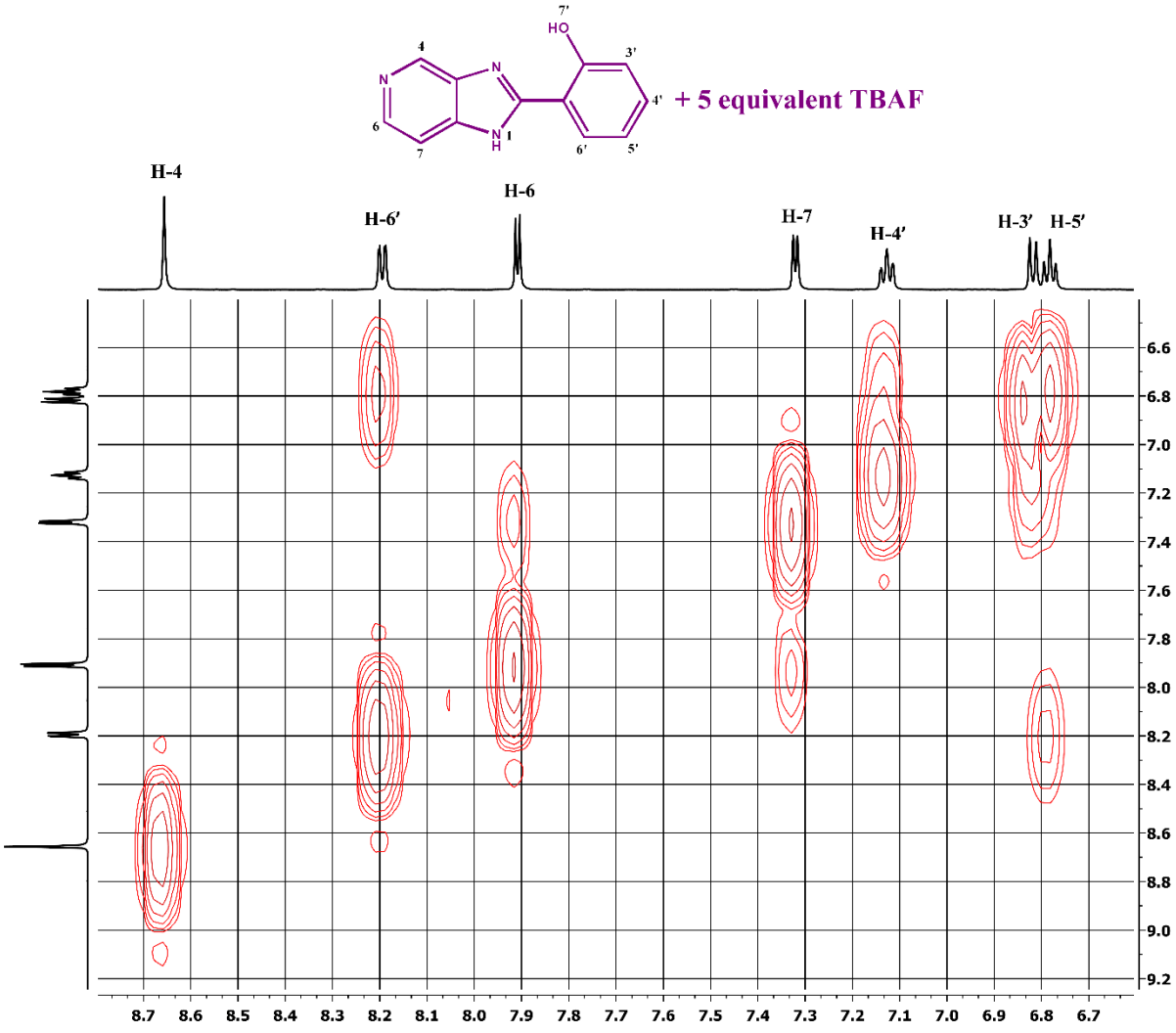


**Figure A8.** 2D-NMR of HPIP-c in presence of 5 equivalent of TBAF.

# Annexure-B

**Table B1.** XYZ coordinate of optimized *cis*- HPBI anion in the ground state. (Optimized geometry is shown below).

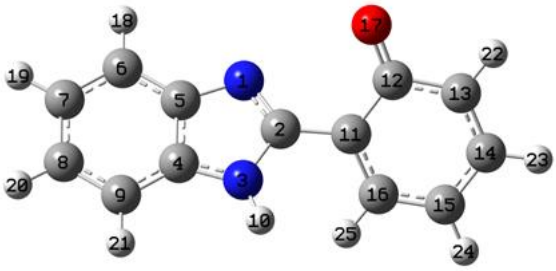

| Center Number | Atomic Number | Coordinates (Angstroms) | | |
|---|---|---|---|---|
| | | X | Y | Z |
| 1 | 7 | -0.6323 | 1.010844 | -0.49686 |
| 2 | 6 | 0.124848 | 0.011786 | -0.0568 |
| 3 | 7 | -0.65216 | -1.04073 | 0.407205 |
| 4 | 6 | -1.98005 | -0.69304 | 0.263478 |
| 5 | 6 | -1.94428 | 0.604206 | -0.30947 |
| 6 | 6 | -3.14633 | 1.267587 | -0.59959 |
| 7 | 6 | -4.34615 | 0.618262 | -0.30326 |
| 8 | 6 | -4.36148 | -0.67016 | 0.272702 |
| 9 | 6 | -3.17579 | -1.34967 | 0.565348 |
| 10 | 1 | -0.2961 | -1.87373 | 0.852765 |
| 11 | 6 | 1.588067 | -0.09489 | -0.07083 |
| 12 | 6 | 2.444668 | 1.022404 | 0.299721 |
| 13 | 6 | 3.859758 | 0.751802 | 0.226187 |
| 14 | 6 | 4.379381 | -0.47965 | -0.14195 |
| 15 | 6 | 3.528665 | -1.55148 | -0.4736 |
| 16 | 6 | 2.152824 | -1.33702 | -0.42901 |
| 17 | 8 | 2.008497 | 2.163358 | 0.693345 |
| 18 | 1 | -3.13699 | 2.260156 | -1.04091 |
| 19 | 1 | -5.28911 | 1.112837 | -0.51837 |
| 20 | 1 | -5.3136 | -1.14418 | 0.492772 |
| 21 | 1 | -3.18744 | -2.34195 | 1.006187 |
| 22 | 1 | 4.525932 | 1.57052 | 0.4906 |
| 23 | 1 | 5.458997 | -0.61657 | -0.17453 |
| 24 | 1 | 3.929457 | -2.51537 | -0.77197 |
| 25 | 1 | 1.487257 | -2.15029 | -0.71326 |

**Table B2.** XYZ coordinate of optimized *cis*- HPBI anion in the excited state. (Optimized geometry is shown below).

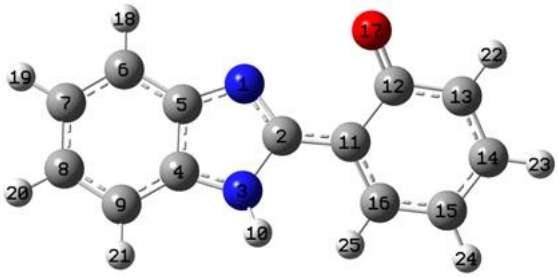

| Center Number | Atomic Number | Coordinates (Angstroms) | | |
|---|---|---|---|---|
| | | X | Y | Z |
| 1 | 7 | -0.64509 | 1.073054 | -0.25599 |
| 2 | 6 | 0.136013 | -0.00833 | 0.019663 |
| 3 | 7 | -0.68366 | -1.14462 | 0.20923 |
| 4 | 6 | -1.99834 | -0.74536 | 0.141914 |
| 5 | 6 | -1.93581 | 0.650054 | -0.17712 |
| 6 | 6 | -3.1468 | 1.371911 | -0.34899 |
| 7 | 6 | -4.35476 | 0.680811 | -0.19123 |
| 8 | 6 | -4.39301 | -0.68895 | 0.132908 |
| 9 | 6 | -3.20311 | -1.4311 | 0.309567 |
| 10 | 1 | -0.36978 | -2.02137 | 0.599105 |
| 11 | 6 | 1.562693 | -0.13315 | -0.02161 |
| 12 | 6 | 2.463564 | 1.031693 | 0.168218 |
| 13 | 6 | 3.879596 | 0.816818 | 0.070661 |
| 14 | 6 | 4.430941 | -0.45649 | -0.12197 |
| 15 | 6 | 3.57043 | -1.55769 | -0.2618 |
| 16 | 6 | 2.172102 | -1.39678 | -0.22958 |
| 17 | 8 | 2.001986 | 2.184099 | 0.454503 |
| 18 | 1 | -3.128 | 2.43157 | -0.58677 |
| 19 | 1 | -5.2924 | 1.217441 | -0.31599 |
| 20 | 1 | -5.35246 | -1.18488 | 0.250772 |
| 21 | 1 | -3.22806 | -2.4874 | 0.560708 |
| 22 | 1 | 4.512736 | 1.687474 | 0.219556 |
| 23 | 1 | 5.507882 | -0.59378 | -0.15616 |
| 24 | 1 | 3.982272 | -2.5515 | -0.41579 |
| 25 | 1 | 1.552045 | -2.27006 | -0.40797 |

**Table B3** XYZ coordinate of optimized *trans*-HPBI anion in the ground state. (Optimized geometry is shown below).

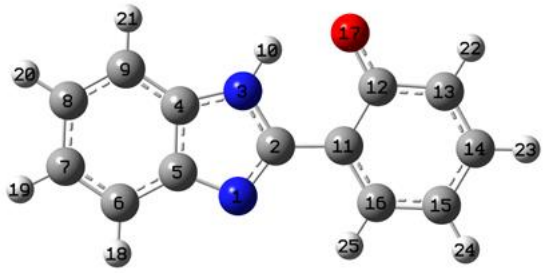

| Center Number | Atomic Number | Coordinates (Angstroms) X | Y | Z |
|---|---|---|---|---|
| 1 | 7 | 0.667966 | -1.33005 | 0.00006 |
| 2 | 6 | -0.13279 | -0.25921 | -0.00005 |
| 3 | 7 | 0.574917 | 0.919872 | -0.00012 |
| 4 | 6 | 1.916028 | 0.606937 | -0.00011 |
| 5 | 6 | 1.953177 | -0.81646 | 0.000086 |
| 6 | 6 | 3.192673 | -1.47628 | 0.000201 |
| 7 | 6 | 4.354702 | -0.70178 | 0.000112 |
| 8 | 6 | 4.298945 | 0.708677 | -0.00008 |
| 9 | 6 | 3.076266 | 1.38634 | -0.0002 |
| 10 | 1 | 0.041234 | 1.800666 | -0.00027 |
| 11 | 6 | -1.58995 | -0.24709 | -7.3E-05 |
| 12 | 6 | -2.30804 | 1.012976 | -2.1E-05 |
| 13 | 6 | -3.73867 | 0.915824 | 0.000085 |
| 14 | 6 | -4.40162 | -0.30288 | 0.000002 |
| 15 | 6 | -3.6838 | -1.51589 | -0.00012 |
| 16 | 6 | -2.29394 | -1.46779 | -0.00012 |
| 17 | 8 | -1.71409 | 2.167844 | 0.000291 |
| 18 | 1 | 3.241061 | -2.56176 | 0.00033 |
| 19 | 1 | 5.323925 | -1.19283 | 0.00019 |
| 20 | 1 | 5.22356 | 1.27878 | -0.00013 |
| 21 | 1 | 3.032533 | 2.471439 | -0.00033 |
| 22 | 1 | -4.29727 | 1.849113 | 0.000232 |
| 23 | 1 | -5.4898 | -0.31972 | 0.000054 |
| 24 | 1 | -4.20396 | -2.46913 | -0.00016 |
| 25 | 1 | -1.71662 | -2.3884 | -0.00018 |

**Table B4** XYZ coordinate of optimized *trans*- HPBI anion in the excited state. (Optimized geometry is shown below).

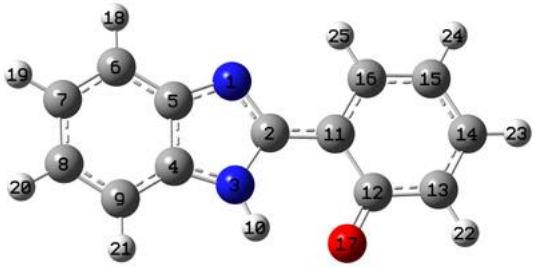

| Center Number | Atomic Number | Coordinates (Angstroms) X | Y | Z |
|---|---|---|---|---|
| 1 | 7 | -0.67717 | -1.28873 | -3.8E-05 |
| 2 | 6 | 0.144534 | -0.19321 | -1.2E-05 |
| 3 | 7 | -0.62193 | 0.977097 | 0.000013 |
| 4 | 6 | -1.94459 | 0.632195 | 0.000011 |
| 5 | 6 | -1.94907 | -0.80487 | -2.2E-05 |
| 6 | 6 | -3.18915 | -1.4932 | -3.5E-05 |
| 7 | 6 | -4.3661 | -0.73179 | -1.3E-05 |
| 8 | 6 | -4.33966 | 0.676484 | 0.000018 |
| 9 | 6 | -3.12224 | 1.389991 | 0.00003 |
| 10 | 1 | -0.18177 | 1.890762 | 0.000025 |
| 11 | 6 | 1.565299 | -0.23279 | -9E-06 |
| 12 | 6 | 2.378071 | 1.009217 | 0.000025 |
| 13 | 6 | 3.80391 | 0.89052 | 0.000032 |
| 14 | 6 | 4.43981 | -0.3578 | 0 |
| 15 | 6 | 3.657091 | -1.53211 | -3.5E-05 |
| 16 | 6 | 2.257776 | -1.47737 | -3.9E-05 |
| 17 | 8 | 1.807832 | 2.157486 | 0.000062 |
| 18 | 1 | -3.21699 | -2.57897 | -0.00006 |
| 19 | 1 | -5.3275 | -1.23962 | -2.2E-05 |
| 20 | 1 | -5.27671 | 1.226806 | 0.000033 |
| 21 | 1 | -3.10123 | 2.475386 | 0.000053 |
| 22 | 1 | 4.372492 | 1.816656 | 0.000062 |
| 23 | 1 | 5.523993 | -0.42487 | 0.000004 |
| 24 | 1 | 4.146913 | -2.5027 | -5.9E-05 |
| 25 | 1 | 1.677721 | -2.39353 | -6.5E-05 |

**Table B5.** XYZ coordinate of optimized HPBI di-anion in the ground state. (Optimized geometry is shown below).

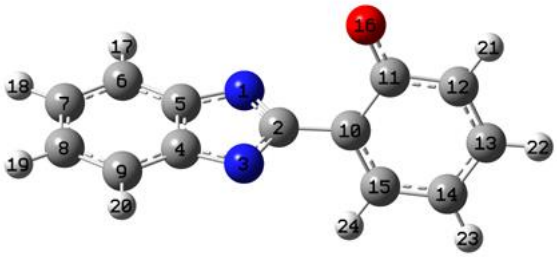

| Center Number | Atomic Number | Coordinates (Angstroms) | | |
|---|---|---|---|---|
| | | X | Y | Z |
| 1 | 7 | -0.62454 | 0.681304 | -0.90675 |
| 2 | 6 | 0.089931 | -0.07882 | -0.03655 |
| 3 | 7 | -0.63201 | -0.82744 | 0.8389 |
| 4 | 6 | -1.93711 | -0.52688 | 0.515891 |
| 5 | 6 | -1.93148 | 0.410852 | -0.56899 |
| 6 | 6 | -3.14155 | 0.885633 | -1.10642 |
| 7 | 6 | -4.34095 | 0.422528 | -0.55735 |
| 8 | 6 | -4.34626 | -0.50131 | 0.514169 |
| 9 | 6 | -3.15166 | -0.98303 | 1.0581 |
| 10 | 6 | 1.578915 | -0.14244 | -0.06736 |
| 11 | 6 | 2.390549 | 0.955308 | 0.420353 |
| 12 | 6 | 3.81198 | 0.764217 | 0.319211 |
| 13 | 6 | 4.38575 | -0.3985 | -0.18978 |
| 14 | 6 | 3.580549 | -1.45667 | -0.637 |
| 15 | 6 | 2.188458 | -1.30261 | -0.56242 |
| 16 | 8 | 1.893016 | 2.035587 | 0.932009 |
| 17 | 1 | -3.14529 | 1.59641 | -1.93074 |
| 18 | 1 | -5.28761 | 0.77751 | -0.95817 |
| 19 | 1 | -5.29673 | -0.8414 | 0.918823 |
| 20 | 1 | -3.16289 | -1.69506 | 1.881322 |
| 21 | 1 | 4.446178 | 1.575019 | 0.674672 |
| 22 | 1 | 5.470856 | -0.48368 | -0.23593 |
| 23 | 1 | 4.018333 | -2.36843 | -1.03409 |
| 24 | 1 | 1.546162 | -2.11176 | -0.90814 |

**Table B6.** XYZ coordinate of optimized NH-stabilized *cis*- HPBI anion in the ground state. (Optimized geometry is shown below).

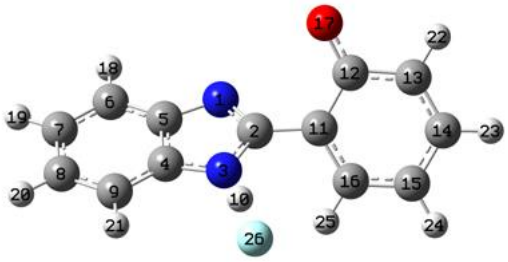

| Center Number | Atomic Number | Coordinates (Angstroms) | | |
|---|---|---|---|---|
| | | X | Y | Z |
| 1 | 7 | 0.615765 | -1.34036 | -0.38884 |
| 2 | 6 | -0.11795 | -0.25614 | -0.12056 |
| 3 | 7 | 0.652075 | 0.853004 | 0.149692 |
| 4 | 6 | 1.968197 | 0.456716 | 0.055088 |
| 5 | 6 | 1.929805 | -0.92344 | -0.28423 |
| 6 | 6 | 3.127738 | -1.63455 | -0.46292 |
| 7 | 6 | 4.333088 | -0.95099 | -0.29199 |
| 8 | 6 | 4.357139 | 0.41908 | 0.052209 |
| 9 | 6 | 3.176039 | 1.143703 | 0.23107 |
| 10 | 1 | 0.325598 | 1.836547 | 0.461476 |
| 11 | 6 | -1.59062 | -0.17315 | -0.16653 |
| 12 | 6 | -2.43251 | -1.11279 | 0.554645 |
| 13 | 6 | -3.84925 | -0.91452 | 0.385429 |
| 14 | 6 | -4.38572 | 0.109347 | -0.3849 |
| 15 | 6 | -3.5489 | 1.020681 | -1.0526 |
| 16 | 6 | -2.16727 | 0.860847 | -0.92541 |
| 17 | 8 | -1.97802 | -2.04583 | 1.31717 |
| 18 | 1 | 3.112329 | -2.68905 | -0.72573 |
| 19 | 1 | 5.272795 | -1.48047 | -0.4245 |
| 20 | 1 | 5.313521 | 0.918726 | 0.180121 |
| 21 | 1 | 3.196175 | 2.196941 | 0.495442 |
| 22 | 1 | -4.50528 | -1.60737 | 0.909292 |
| 23 | 1 | -5.46732 | 0.205668 | -0.46806 |
| 24 | 1 | -3.96054 | 1.823144 | -1.65766 |
| 25 | 1 | -1.50413 | 1.549043 | -1.44556 |
| 26 | 9 | 0.040822 | 3.195118 | 0.919558 |

**Table B7.** XYZ coordinate of optimized NH-stabilized *trans*- HPBI anion in the ground state. (Optimized geometry is shown below).

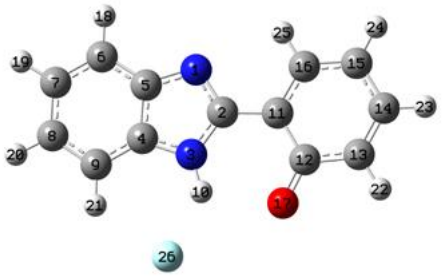

| Center Number | Atomic Number | Coordinates (Angstroms) | | |
|---|---|---|---|---|
| | | X | Y | Z |
| 1 | 7 | -0.47896 | -1.55946 | 0.000086 |
| 2 | 6 | 0.232721 | -0.42058 | -0.00013 |
| 3 | 7 | -0.58319 | 0.691252 | -0.00031 |
| 4 | 6 | -1.88886 | 0.245694 | -0.00016 |
| 5 | 6 | -1.80245 | -1.17078 | 0.000013 |
| 6 | 6 | -2.97914 | -1.93973 | 0.000239 |
| 7 | 6 | -4.20453 | -1.26966 | 0.000244 |
| 8 | 6 | -4.27057 | 0.141853 | 0.000079 |
| 9 | 6 | -3.11182 | 0.923875 | -6.9E-05 |
| 10 | 1 | -0.31683 | 1.687334 | -0.00026 |
| 11 | 6 | 1.694627 | -0.3827 | -0.00014 |
| 12 | 6 | 2.429697 | 0.868104 | 0.000158 |
| 13 | 6 | 3.865787 | 0.748191 | 0.000449 |
| 14 | 6 | 4.51675 | -0.475 | 0.000245 |
| 15 | 6 | 3.781858 | -1.67867 | -0.00025 |
| 16 | 6 | 2.392539 | -1.6096 | -0.00039 |
| 17 | 8 | 1.85583 | 2.019081 | 0.000106 |
| 18 | 1 | -2.93218 | -3.02561 | 0.000396 |
| 19 | 1 | -5.12748 | -1.84375 | 0.00038 |
| 20 | 1 | -5.24271 | 0.627828 | 0.000121 |
| 21 | 1 | -3.12465 | 2.008924 | -0.00017 |
| 22 | 1 | 4.4334 | 1.676573 | 0.000753 |
| 23 | 1 | 5.605145 | -0.5048 | 0.000416 |
| 24 | 1 | 4.28716 | -2.64021 | -0.00059 |
| 25 | 1 | 1.806392 | -2.52384 | -0.00067 |
| 26 | 9 | -1.19329 | 3.397377 | -0.00015 |

**Table B8.** XYZ coordinate of optimized *cis*- HPIP-b anion in the ground state. (Optimized geometry is shown below).

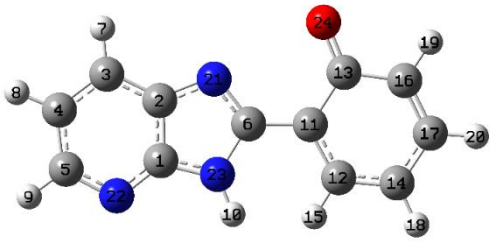

| Center Number | Atomic Number | Coordinates (Angstroms) | | |
|---|---|---|---|---|
| | | X | Y | Z |
| 1 | 6 | -2.01711 | -0.73095 | -3.8E-05 |
| 2 | 6 | -1.95185 | 0.686589 | 0.00005 |
| 3 | 6 | -3.16006 | 1.385911 | 0.000093 |
| 4 | 6 | -4.33177 | 0.617899 | 0.000045 |
| 5 | 6 | -4.26372 | -0.78419 | -4.3E-05 |
| 6 | 6 | 0.106962 | -0.00161 | 0.000007 |
| 7 | 1 | -3.19003 | 2.471545 | 0.000161 |
| 8 | 1 | -5.30492 | 1.098385 | 0.000076 |
| 9 | 1 | -5.17829 | -1.37153 | -8.1E-05 |
| 10 | 1 | -0.4074 | -2.10316 | -0.00014 |
| 11 | 6 | 1.561396 | -0.11097 | 0.000008 |
| 12 | 6 | 2.146446 | -1.40333 | 0.000054 |
| 13 | 6 | 2.435378 | 1.063086 | -3.8E-05 |
| 14 | 6 | 3.516017 | -1.62084 | 0.000059 |
| 15 | 1 | 1.511598 | -2.28512 | 0.000099 |
| 16 | 6 | 3.854689 | 0.777385 | -2.8E-05 |
| 17 | 6 | 4.375394 | -0.50098 | 0.000018 |
| 18 | 1 | 3.911881 | -2.6316 | 0.000099 |
| 19 | 1 | 4.515536 | 1.641453 | -0.00006 |
| 20 | 1 | 5.454238 | -0.64503 | 0.000023 |
| 21 | 7 | -0.63811 | 1.107547 | 0.000074 |
| 22 | 7 | -3.11135 | -1.48712 | -8.7E-05 |
| 23 | 7 | -0.70591 | -1.1402 | -6.4E-05 |
| 24 | 8 | 2.030548 | 2.274414 | -9.5E-05 |

**Table B9.** XYZ coordinate of optimized *trans*- HPIP-b anion in the ground state. (Optimized geometry is shown below)

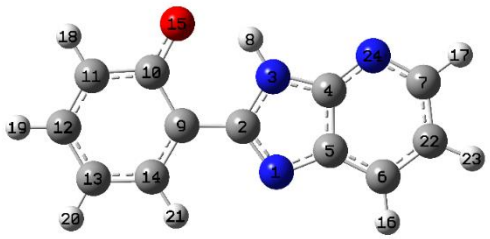

.

| Center Number | Atomic Number | Coordinates (Angstroms) | | |
|---|---|---|---|---|
| | | X | Y | Z |
| 1 | 7 | 0.677149 | -1.35091 | 0.00004 |
| 2 | 6 | -0.1171 | -0.2725 | -0.00009 |
| 3 | 7 | 0.595705 | 0.906359 | -0.00037 |
| 4 | 6 | 1.929576 | 0.583261 | -0.00017 |
| 5 | 6 | 1.95985 | -0.8434 | 0.000039 |
| 6 | 6 | 3.213398 | -1.45994 | 0.000187 |
| 7 | 6 | 4.171639 | 0.778531 | -0.00014 |
| 8 | 1 | 0.064624 | 1.791193 | -0.00068 |
| 9 | 6 | -1.57067 | -0.25121 | -0.00009 |
| 10 | 6 | -2.27934 | 1.014805 | 0.000073 |
| 11 | 6 | -3.71119 | 0.927736 | 0.000242 |
| 12 | 6 | -4.38105 | -0.28601 | 0.000065 |
| 13 | 6 | -3.67175 | -1.50535 | -0.00017 |
| 14 | 6 | -2.28299 | -1.46834 | -0.0002 |
| 15 | 8 | -1.67761 | 2.164175 | 0.000687 |
| 16 | 1 | 3.31664 | -2.54128 | 0.00036 |
| 17 | 1 | 5.046795 | 1.423481 | -0.00022 |
| 18 | 1 | -4.26332 | 1.864691 | 0.000528 |
| 19 | 1 | -5.46922 | -0.29584 | 0.000165 |
| 20 | 1 | -4.19965 | -2.4542 | -0.00027 |
| 21 | 1 | -1.71224 | -2.39292 | -0.00033 |
| 22 | 6 | 4.331153 | -0.61712 | 0.000095 |
| 23 | 1 | 5.33369 | -1.03311 | 0.000197 |
| 24 | 7 | 2.97777 | 1.404801 | -0.00029 |

**Table B10.** XYZ coordinate of optimized *cis*- HPIP-c anion in the ground state. (Optimized geometry is shown below).

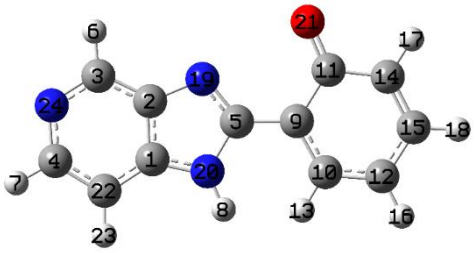

| Center Number | Atomic Number | Coordinates (Angstroms) | | |
|---|---|---|---|---|
| | | X | Y | Z |
| 1 | 6 | -2.00346 | -0.76541 | -0.0003 |
| 2 | 6 | -1.94934 | 0.648189 | 0.000429 |
| 3 | 6 | -3.15454 | 1.358343 | 0.000803 |
| 4 | 6 | -4.36079 | -0.62114 | -0.00026 |
| 5 | 6 | 0.115845 | -0.01315 | 0.000094 |
| 6 | 1 | -3.16367 | 2.446315 | 0.001373 |
| 7 | 1 | -5.34699 | -1.07904 | -0.00051 |
| 8 | 1 | -0.37507 | -2.11758 | -0.00114 |
| 9 | 6 | 1.571279 | -0.11582 | 0.000102 |
| 10 | 6 | 2.163561 | -1.40457 | 0.000611 |
| 11 | 6 | 2.43789 | 1.063467 | -0.00042 |
| 12 | 6 | 3.534534 | -1.61396 | 0.000597 |
| 13 | 1 | 1.534397 | -2.29046 | 0.001176 |
| 14 | 6 | 3.858827 | 0.786396 | -0.00043 |
| 15 | 6 | 4.386985 | -0.489 | 0.00005 |
| 16 | 1 | 3.936544 | -2.62224 | 0.001035 |
| 17 | 1 | 4.514712 | 1.654203 | -0.00084 |
| 18 | 1 | 5.466664 | -0.62669 | 0.000028 |
| 19 | 7 | -0.63834 | 1.085581 | 0.000647 |
| 20 | 7 | -0.6918 | -1.16072 | -0.0005 |
| 21 | 8 | 2.025043 | 2.271858 | -0.00097 |
| 22 | 6 | -3.22661 | -1.43618 | -0.00068 |
| 23 | 1 | -3.31032 | -2.51795 | -0.00125 |
| 24 | 7 | -4.34154 | 0.731655 | 0.000465 |

**Table B11.** XYZ coordinate of optimized *trans*-HPIP-c anion in the ground state. (Optimized geometry is shown below).

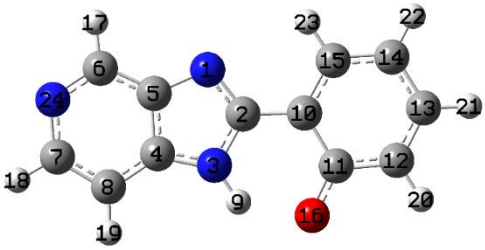

| Center Number | Atomic Number | Coordinates (Angstroms) | | |
|---|---|---|---|---|
| | | X | Y | Z |
| 1 | 7 | 0.677827 | -1.33219 | -9E-06 |
| 2 | 6 | -0.12515 | -0.26461 | -6E-06 |
| 3 | 7 | 0.580928 | 0.922458 | 0.000193 |
| 4 | 6 | 1.914322 | 0.61319 | 0.000106 |
| 5 | 6 | 1.956957 | -0.80787 | -5.3E-05 |
| 6 | 6 | 3.209791 | -1.43257 | -0.00017 |
| 7 | 6 | 4.279174 | 0.62563 | 0.000044 |
| 8 | 6 | 3.092974 | 1.361083 | 0.000157 |
| 9 | 1 | 0.035777 | 1.800067 | 0.000376 |
| 10 | 6 | -1.57946 | -0.24943 | -2.2E-05 |
| 11 | 6 | -2.29197 | 1.013856 | -0.00015 |
| 12 | 6 | -3.72318 | 0.922501 | -5.3E-05 |
| 13 | 6 | -4.38911 | -0.29351 | 0.00006 |
| 14 | 6 | -3.67599 | -1.51045 | 0.000099 |
| 15 | 6 | -2.28726 | -1.46899 | 0.000064 |
| 16 | 8 | -1.69363 | 2.165807 | -0.00022 |
| 17 | 1 | 3.295137 | -2.51754 | -0.00026 |
| 18 | 1 | 5.232819 | 1.148031 | 0.000082 |
| 19 | 1 | 3.103365 | 2.446083 | 0.000283 |
| 20 | 1 | -4.27828 | 1.857676 | -9.3E-05 |
| 21 | 1 | -5.47722 | -0.30682 | 0.000099 |
| 22 | 1 | -4.20085 | -2.46095 | 0.000177 |
| 23 | 1 | -1.71355 | -2.39178 | 0.000126 |
| 24 | 7 | 4.35056 | -0.72659 | -0.00011 |

**Table B12.** XYZ coordinate of optimized Tz-I conformer in the ground state. (Optimized geometry is shown below).

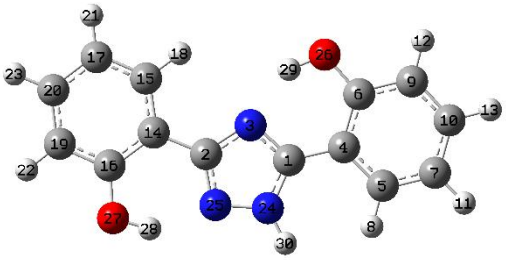

| Center Numbe | Atomic Number | Coordinates (Angstroms) | | |
|---|---|---|---|---|
| | | X | Y | Z |
| 1 | 6 | 1.123769 | -0.5958 | -0.00015 |
| 2 | 6 | -1.01542 | -0.44001 | 0.000045 |
| 3 | 7 | 0.131199 | 0.303601 | 0.000009 |
| 4 | 6 | 2.542899 | -0.2615 | -0.00024 |
| 5 | 6 | 3.54201 | -1.25541 | -0.00042 |
| 6 | 6 | 2.935075 | 1.102911 | -0.00015 |
| 7 | 6 | 4.89042 | -0.92129 | -0.00049 |
| 8 | 1 | 3.261076 | -2.30407 | -0.00049 |
| 9 | 6 | 4.298983 | 1.431807 | -0.00023 |
| 10 | 6 | 5.264803 | 0.431217 | -0.0004 |
| 11 | 1 | 5.643598 | -1.70186 | -0.00062 |
| 12 | 1 | 4.575898 | 2.481102 | -0.00015 |
| 13 | 1 | 6.315941 | 0.703611 | -0.00046 |
| 14 | 6 | -2.37053 | 0.113511 | 0.000204 |
| 15 | 6 | -2.56604 | 1.507212 | 0.000313 |
| 16 | 6 | -3.50652 | -0.73291 | 0.00025 |
| 17 | 6 | -3.84365 | 2.057637 | 0.000464 |
| 18 | 1 | -1.69409 | 2.152586 | 0.000277 |
| 19 | 6 | -4.79208 | -0.17404 | 0.000402 |
| 20 | 6 | -4.95925 | 1.208258 | 0.000508 |
| 21 | 1 | -3.97172 | 3.135161 | 0.000545 |
| 22 | 1 | -5.64639 | -0.84358 | 0.000435 |
| 23 | 1 | -5.96211 | 1.624938 | 0.000625 |
| 24 | 7 | 0.578376 | -1.8333 | -0.0002 |
| 25 | 7 | -0.77658 | -1.75191 | -8.4E-05 |
| 26 | 8 | 2.043014 | 2.121734 | 0.000014 |
| 27 | 8 | -3.41808 | -2.09053 | 0.000151 |
| 28 | 1 | -2.47221 | -2.36039 | 0.000044 |
| 29 | 1 | 1.125976 | 1.743379 | 0.000047 |
| 30 | 1 | 1.026747 | -2.73882 | -0.00033 |

**Table B13.** XYZ coordinate of optimized Tz-II conformer in the ground state. (Optimized geometry is shown below).

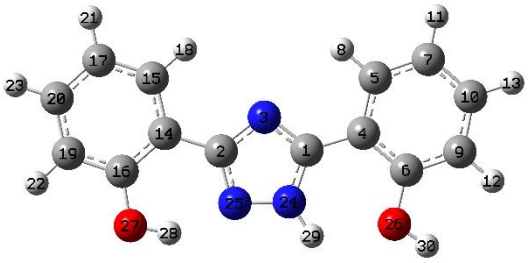

| Center Number | Atomic Number | Coordinates (Angstroms) | | |
|---|---|---|---|---|
| | | X | Y | Z |
| 1 | 6 | 1.053068 | -0.20331 | -0.00011 |
| 2 | 6 | -1.07574 | -0.22442 | 0.000095 |
| 3 | 7 | -0.00304 | 0.615864 | 0.000047 |
| 4 | 6 | 2.455756 | 0.218664 | -0.00021 |
| 5 | 6 | 2.753459 | 1.594274 | -0.00013 |
| 6 | 6 | 3.52897 | -0.69713 | -0.00039 |
| 7 | 6 | 4.06817 | 2.049814 | -0.00022 |
| 8 | 1 | 1.927272 | 2.296408 | 0.000009 |
| 9 | 6 | 4.851374 | -0.24283 | -0.00048 |
| 10 | 6 | 5.11959 | 1.12522 | -0.0004 |
| 11 | 1 | 4.273535 | 3.115134 | -0.00015 |
| 12 | 1 | 5.663806 | -0.96439 | -0.00062 |
| 13 | 1 | 6.150276 | 1.466094 | -0.00047 |
| 14 | 6 | -2.47581 | 0.211062 | 0.00025 |
| 15 | 6 | -2.78999 | 1.582507 | 0.000352 |
| 16 | 6 | -3.53632 | -0.72803 | 0.000294 |
| 17 | 6 | -4.11037 | 2.022728 | 0.00049 |
| 18 | 1 | -1.97274 | 2.296031 | 0.000318 |
| 19 | 6 | -4.86506 | -0.28132 | 0.000436 |
| 20 | 6 | -5.14997 | 1.082049 | 0.000532 |
| 21 | 1 | -4.32979 | 3.085603 | 0.000565 |
| 22 | 1 | -5.65938 | -1.02122 | 0.000467 |
| 23 | 1 | -6.18484 | 1.411709 | 0.00064 |
| 24 | 7 | 0.615413 | -1.48516 | -0.00015 |
| 25 | 7 | -0.73644 | -1.51934 | -2.2E-05 |
| 26 | 8 | 3.22928 | -2.03448 | -0.00047 |
| 27 | 8 | -3.33076 | -2.07381 | 0.000201 |
| 28 | 1 | -2.36253 | -2.25639 | 0.000096 |
| 29 | 1 | 1.175813 | -2.32785 | -0.00026 |
| 30 | 1 | 4.035999 | -2.56995 | -0.0006 |

**Table B14.** XYZ coordinate of optimized Tz-III conformer in the ground state. (Optimized geometry is shown below).

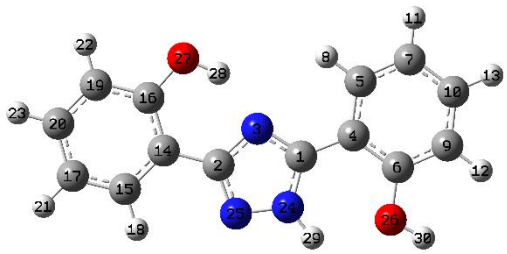

| Center Number | Atomic Number | Coordinates (Angstroms) | | |
|---|---|---|---|---|
| | | X | Y | Z |
| 1 | 6 | 0.996803 | -0.42558 | -0.00011 |
| 2 | 6 | -1.13565 | -0.64415 | 0.000073 |
| 3 | 7 | -0.13402 | 0.290185 | 0.000049 |
| 4 | 6 | 2.355195 | 0.11789 | -0.0002 |
| 5 | 6 | 2.536258 | 1.513738 | -7.1E-05 |
| 6 | 6 | 3.502153 | -0.70413 | -0.00042 |
| 7 | 6 | 3.807992 | 2.078086 | -0.00015 |
| 8 | 1 | 1.657338 | 2.148532 | 0.000098 |
| 9 | 6 | 4.781647 | -0.14038 | -0.0005 |
| 10 | 6 | 4.933564 | 1.245386 | -0.00037 |
| 11 | 1 | 3.92244 | 3.156895 | -4.7E-05 |
| 12 | 1 | 5.651892 | -0.79141 | -0.00067 |
| 13 | 1 | 5.931667 | 1.672152 | -0.00044 |
| 14 | 6 | -2.55495 | -0.2747 | 0.000237 |
| 15 | 6 | -3.55549 | -1.2647 | 0.000336 |
| 16 | 6 | -2.94652 | 1.086784 | 0.000304 |
| 17 | 6 | -4.90578 | -0.92952 | 0.000501 |
| 18 | 1 | -3.25186 | -2.30661 | 0.000286 |
| 19 | 6 | -4.30934 | 1.420524 | 0.000473 |
| 20 | 6 | -5.27978 | 0.42246 | 0.00057 |
| 21 | 1 | -5.6604 | -1.70949 | 0.000577 |
| 22 | 1 | -4.58366 | 2.470898 | 0.000518 |
| 23 | 1 | -6.33038 | 0.698013 | 0.000697 |
| 24 | 7 | 0.658169 | -1.73401 | -0.00017 |
| 25 | 7 | -0.68625 | -1.89981 | -3.9E-05 |
| 26 | 8 | 3.314845 | -2.0612 | -0.00055 |
| 27 | 8 | -2.04957 | 2.108989 | 0.000189 |
| 28 | 1 | -1.13588 | 1.724583 | 0.000023 |
| 29 | 1 | 1.291168 | -2.52357 | -0.00029 |
| 30 | 1 | 4.163446 | -2.52715 | -0.00072 |

**Table B15.** XYZ coordinate of optimized Tz-IV conformer in the ground state. (Optimized geometry is shown below).

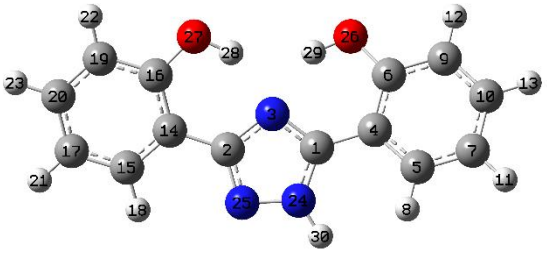

| Center Number | Atomic Number | Coordinates (Angstroms) | | |
|---|---|---|---|---|
| | | X | Y | Z |
| 1 | 6 | 1.070685 | -0.73642 | 0.033937 |
| 2 | 6 | -1.08052 | -0.7814 | -0.02583 |
| 3 | 7 | -0.00116 | 0.070782 | 0.016797 |
| 4 | 6 | 2.467287 | -0.31148 | 0.050494 |
| 5 | 6 | 3.499121 | -1.20453 | 0.403169 |
| 6 | 6 | 2.810067 | 1.013677 | -0.31546 |
| 7 | 6 | 4.831183 | -0.80849 | 0.387696 |
| 8 | 1 | 3.252878 | -2.21621 | 0.710848 |
| 9 | 6 | 4.155317 | 1.406066 | -0.33419 |
| 10 | 6 | 5.155591 | 0.503701 | 0.013645 |
| 11 | 1 | 5.609241 | -1.50993 | 0.669081 |
| 12 | 1 | 4.391852 | 2.424896 | -0.62335 |
| 13 | 1 | 6.192776 | 0.824441 | -0.00114 |
| 14 | 6 | -2.47498 | -0.32441 | -0.03753 |
| 15 | 6 | -3.50814 | -1.218 | -0.37986 |
| 16 | 6 | -2.81786 | 1.002255 | 0.313355 |
| 17 | 6 | -4.8406 | -0.81913 | -0.37764 |
| 18 | 1 | -3.24306 | -2.23405 | -0.65315 |
| 19 | 6 | -4.16174 | 1.401539 | 0.316474 |
| 20 | 6 | -5.16464 | 0.499313 | -0.02654 |
| 21 | 1 | -5.61976 | -1.52377 | -0.6496 |
| 22 | 1 | -4.39581 | 2.424892 | 0.592327 |
| 23 | 1 | -6.20077 | 0.82449 | -0.02265 |
| 24 | 7 | 0.627173 | -2.01017 | -0.0038 |
| 25 | 7 | -0.72858 | -2.06354 | -0.03385 |
| 26 | 8 | 1.885482 | 1.942395 | -0.67152 |
| 27 | 8 | -1.8936 | 1.936471 | 0.673313 |
| 28 | 1 | -0.99835 | 1.548128 | 0.591512 |
| 29 | 1 | 0.988642 | 1.558767 | -0.57478 |
| 30 | 1 | 1.160645 | -2.86819 | -0.03776 |

**Table B16.** XYZ coordinate of optimized Tz-I conformer in the excited state. (Optimized geometry is shown below).

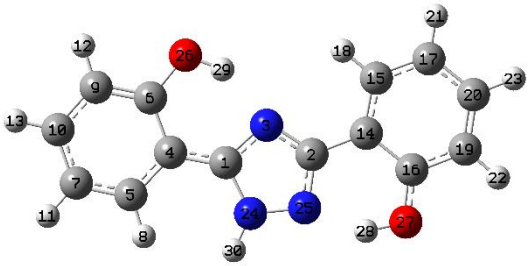

| Center Number | Atomic Number | Coordinates (Angstroms) | | |
|---|---|---|---|---|
| | | X | Y | Z |
| 1 | 6 | -1.14505 | -0.5235 | 0.000218 |
| 2 | 6 | 1.003225 | -0.34964 | 0.000018 |
| 3 | 7 | -0.1165 | 0.393329 | 0.000042 |
| 4 | 6 | -2.52271 | -0.2514 | 0.000266 |
| 5 | 6 | -3.52302 | -1.29002 | 0.000258 |
| 6 | 6 | -3.00315 | 1.114299 | 0.000271 |
| 7 | 6 | -4.87877 | -0.98249 | 0.000248 |
| 8 | 1 | -3.21502 | -2.33125 | 0.000237 |
| 9 | 6 | -4.35797 | 1.394501 | 0.000249 |
| 10 | 6 | -5.31801 | 0.351501 | 0.000244 |
| 11 | 1 | -5.60513 | -1.7914 | 0.000235 |
| 12 | 1 | -4.66752 | 2.43593 | 0.000253 |
| 13 | 1 | -6.37694 | 0.5878 | 0.000235 |
| 14 | 6 | 2.365771 | 0.161509 | -0.0002 |
| 15 | 6 | 2.635751 | 1.527901 | -0.00041 |
| 16 | 6 | 3.491375 | -0.75997 | -0.00024 |
| 17 | 6 | 3.951066 | 1.993309 | -0.00065 |
| 18 | 1 | 1.806777 | 2.225146 | -0.00038 |
| 19 | 6 | 4.827759 | -0.2663 | -0.0005 |
| 20 | 6 | 5.04944 | 1.08801 | -0.0007 |
| 21 | 1 | 4.141203 | 3.06036 | -0.00081 |
| 22 | 1 | 5.636885 | -0.9869 | -0.00052 |
| 23 | 1 | 6.061597 | 1.475618 | -0.00089 |
| 24 | 7 | -0.54854 | -1.79669 | 0.000262 |
| 25 | 7 | 0.804832 | -1.67433 | 0.000192 |
| 26 | 8 | -2.11899 | 2.161797 | 0.000347 |
| 27 | 8 | 3.323158 | -2.06133 | -2.7E-05 |
| 28 | 1 | 2.325935 | -2.27061 | 0.000238 |
| 29 | 1 | -1.1994 | 1.799517 | 0.000465 |
| 30 | 1 | -0.97453 | -2.71038 | 0.000455 |

**Table B17.** XYZ coordinate of optimized K-I tautomer in the excited state. (Optimized geometry is shown below).

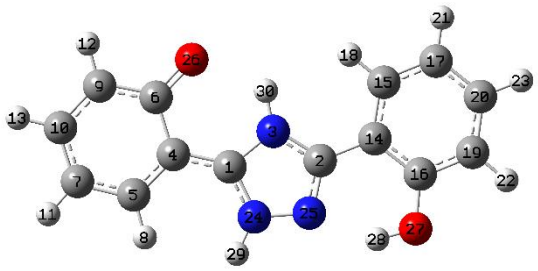

| Center Number | Atomic Number | Coordinates (Angstroms) | | |
|---|---|---|---|---|
| | | X | Y | Z |
| 1 | 6 | -1.17689 | -0.56398 | 0.000138 |
| 2 | 6 | 1.055783 | -0.40808 | -9.4E-05 |
| 3 | 7 | -0.10548 | 0.312282 | -1E-06 |
| 4 | 6 | -2.57213 | -0.25941 | 0.000243 |
| 5 | 6 | -3.55528 | -1.25371 | 0.000355 |
| 6 | 6 | -3.00217 | 1.153612 | 0.000227 |
| 7 | 6 | -4.94508 | -0.92268 | 0.000444 |
| 8 | 1 | -3.28205 | -2.30447 | 0.000372 |
| 9 | 6 | -4.39741 | 1.433303 | 0.000316 |
| 10 | 6 | -5.36536 | 0.402739 | 0.000424 |
| 11 | 1 | -5.6704 | -1.73022 | 0.000526 |
| 12 | 1 | -4.69147 | 2.47866 | 0.000299 |
| 13 | 1 | -6.4229 | 0.646031 | 0.000489 |
| 14 | 6 | 2.40744 | 0.131548 | -0.00025 |
| 15 | 6 | 2.631771 | 1.523927 | -0.00045 |
| 16 | 6 | 3.528095 | -0.74059 | -0.0002 |
| 17 | 6 | 3.919507 | 2.045746 | -0.00058 |
| 18 | 1 | 1.786927 | 2.204948 | -0.00052 |
| 19 | 6 | 4.823318 | -0.20544 | -0.00032 |
| 20 | 6 | 5.017432 | 1.172743 | -0.00051 |
| 21 | 1 | 4.069328 | 3.120066 | -0.00073 |
| 22 | 1 | 5.66356 | -0.89217 | -0.00027 |
| 23 | 1 | 6.028016 | 1.569666 | -0.0006 |
| 24 | 7 | -0.57362 | -1.80035 | 0.00013 |
| 25 | 7 | 0.78763 | -1.70483 | -0.00001 |
| 26 | 8 | -2.11906 | 2.085324 | 0.000135 |
| 27 | 8 | 3.415588 | -2.09217 | -2.7E-05 |
| 28 | 1 | 2.465655 | -2.3488 | 0.00003 |
| 29 | 1 | -1.00701 | -2.71103 | 0.000227 |
| 30 | 1 | -0.28573 | 1.313986 | -4E-06 |

**Table B18.** XYZ coordinate of optimized K-II tautomer in the excited state. (Optimized geometry is shown below).

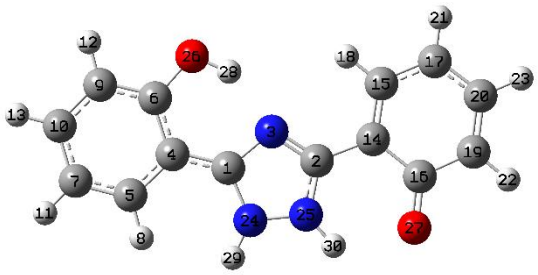

| Center Number | Atomic Number | Coordinates (Angstroms) | | |
|---|---|---|---|---|
| | | X | Y | Z |
| 1 | 6 | -1.15812 | -0.58711 | 0.000152 |
| 2 | 6 | 1.015175 | -0.41032 | -4.2E-05 |
| 3 | 7 | -0.09317 | 0.305106 | -1.5E-05 |
| 4 | 6 | -2.52673 | -0.253 | 0.000234 |
| 5 | 6 | -3.5559 | -1.25076 | 0.000378 |
| 6 | 6 | -2.95309 | 1.12343 | 0.000171 |
| 7 | 6 | -4.90209 | -0.90407 | 0.000454 |
| 8 | 1 | -3.28199 | -2.30155 | 0.000422 |
| 9 | 6 | -4.30142 | 1.447112 | 0.000251 |
| 10 | 6 | -5.29148 | 0.44342 | 0.000394 |
| 11 | 1 | -5.65347 | -1.68883 | 0.00056 |
| 12 | 1 | -4.57517 | 2.498321 | 0.000199 |
| 13 | 1 | -6.34119 | 0.717709 | 0.000453 |
| 14 | 6 | 2.393434 | 0.116633 | -0.00021 |
| 15 | 6 | 2.599608 | 1.479533 | -0.00034 |
| 16 | 6 | 3.540086 | -0.7924 | -0.00024 |
| 17 | 6 | 3.906444 | 2.023392 | -0.0005 |
| 18 | 1 | 1.745917 | 2.147983 | -0.00031 |
| 19 | 6 | 4.859234 | -0.19004 | -0.00041 |
| 20 | 6 | 5.029918 | 1.180615 | -0.00053 |
| 21 | 1 | 4.031643 | 3.100025 | -0.0006 |
| 22 | 1 | 5.704703 | -0.86937 | -0.00043 |
| 23 | 1 | 6.026931 | 1.608138 | -0.00066 |
| 24 | 7 | -0.6187 | -1.87097 | 0.000209 |
| 25 | 7 | 0.750452 | -1.72984 | 0.0001 |
| 26 | 8 | -2.04459 | 2.150466 | 0.000031 |
| 27 | 8 | 3.406941 | -2.05072 | -0.00013 |
| 28 | 1 | -1.13589 | 1.771712 | -0.00002 |
| 29 | 1 | -1.04666 | -2.78285 | 0.000373 |
| 30 | 1 | 1.425909 | -2.488 | 0.000098 |

**Table B19.** XYZ coordinate of optimized DK tautomer in the excited state. (Optimized geometry is shown below).

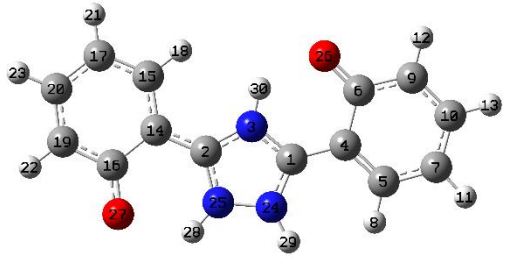

| Center Number | Atomic Number | Coordinates (Angstroms) | | |
|---|---|---|---|---|
| | | X | Y | Z |
| 1 | 6 | 1.158325 | -0.63328 | -8.4E-05 |
| 2 | 6 | -1.08565 | -0.4271 | 0.000227 |
| 3 | 7 | 0.114638 | 0.220544 | 0.000131 |
| 4 | 6 | 2.5593 | -0.26248 | -0.00024 |
| 5 | 6 | 3.56389 | -1.2164 | -0.00037 |
| 6 | 6 | 2.916713 | 1.159875 | -0.00024 |
| 7 | 6 | 4.937012 | -0.83899 | -0.00051 |
| 8 | 1 | 3.327968 | -2.27565 | -0.00035 |
| 9 | 6 | 4.311266 | 1.492924 | -0.00039 |
| 10 | 6 | 5.302119 | 0.506707 | -0.00052 |
| 11 | 1 | 5.693569 | -1.61564 | -0.00062 |
| 12 | 1 | 4.564714 | 2.547984 | -0.0004 |
| 13 | 1 | 6.350084 | 0.78724 | -0.00064 |
| 14 | 6 | -2.39399 | 0.127768 | 0.000309 |
| 15 | 6 | -2.60064 | 1.531769 | 0.00052 |
| 16 | 6 | -3.53278 | -0.78679 | 0.000148 |
| 17 | 6 | -3.87883 | 2.070516 | 0.00056 |
| 18 | 1 | -1.74732 | 2.205586 | 0.000678 |
| 19 | 6 | -4.8262 | -0.1729 | 0.000196 |
| 20 | 6 | -4.9942 | 1.20501 | 0.000391 |
| 21 | 1 | -4.01597 | 3.147153 | 0.000725 |
| 22 | 1 | -5.68671 | -0.83693 | 0.000069 |
| 23 | 1 | -5.99795 | 1.622977 | 0.00042 |
| 24 | 7 | 0.629854 | -1.88421 | -0.00015 |
| 25 | 7 | -0.76365 | -1.76346 | 0.000237 |
| 26 | 8 | 2.01455 | 2.06202 | -0.00011 |
| 27 | 8 | -3.38094 | -2.06672 | -3.7E-05 |
| 28 | 1 | -1.4344 | -2.52605 | -0.00019 |
| 29 | 1 | 1.076955 | -2.78716 | -0.00024 |
| 30 | 1 | 0.316279 | 1.218162 | 0.000115 |

# Annexure-C

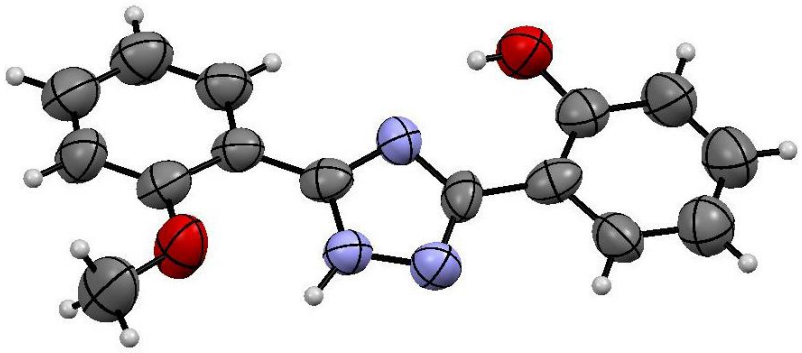

Figure C1. ORTEP view of MTZ.

Crystal data of MTz

| | |
|---|---|
| Formula | $C_{15}H_{13}N_3O_2$ |
| CCDC no. | 1446785 |
| Mol.wt. | 267.28 |
| Space group | P 21/n |
| a/Å | 18.7759(9) |
| b/Å | 14.3560(10) |
| c/Å | 19.8160(12) |
| α/° | 90.00 |
| β/° | 91.407(5) |
| γ/° | 90.00 |
| V/Å3 | 5339.7(6) |
| Density/g cm−3 | 1.330 |
| Abs. coeff./mm−1 | 0.091 |
| F(000) | 2240 |
| Total no. of reflections | 9617 |
| Reflections, I > 2σ(I) | 5032 |
| Max. θ/° | 25.25 |
| Ranges (h, k, l) | −22 ≤ h ≤ 19<br>−13 ≤ k ≤ 17<br>−23 ≤ l ≤ 21 |
| Complete to 2θ (%) | 99.30 |
| Data/restraints/parameters | 9617/0/732 |
| GooF (F2) | 1.094 |
| R indices [I > 2σ(I)] | 0.0623 |
| wR2 [I > 2σ(I)] | 0.1795 |
| R indices (all data) | 0.1325 |
| wR2 (all data) | 0.1795 |

# Annexure-D

**Membership Functions**

A zmf can be represented as

$$f(x;a,b)=\begin{cases}1, x\le a\\ 1-2\left(\frac{x-a}{b-a}\right)^2, a\le x\le\frac{a+b}{2}\\ 2\left(\frac{x-b}{b-a}\right)^2, \frac{a+b}{2}\le x\le b\\ 0, x\ge b\end{cases}$$

A trimf can be represented as follow

$$f(x;a,b,c)=\begin{cases}0, x\le a\\ \frac{x-a}{b-a}, a\le x\le b\\ \frac{c-x}{c-b}, b\le x\le c\\ 0, x\ge c\end{cases}$$

A smf can be represented as follow

$$f(x;a,b)=\begin{cases}0, x\le a\\ 2\left(\frac{x-a}{b-a}\right)^2, a\le x\le\frac{a+b}{2}\\ 1-2\left(\frac{x-b}{b-a}\right)^2, \frac{a+b}{2}\le x\le b\\ 1, x\ge b\end{cases}$$

## List of publication

1) **Sahu, S.**; Mishra, A.; Krishnamoorthy, G., Specific Site Binding of Metal Ions on the Intramolecular Charge Transfer Fluorophore in Micelles. *Analyst* **2013**, *138*, 5942-5948. ‡

2) Mishra, A.; **Sahu, S.**; Dash, N.; Behera, S. K.; Krishnamoorthy, G., Double Proton Transfer Induced Twisted Intramolecular Charge Transfer Emission in 2-(4′-N,N-Dimethylaminophenyl)imidazo[4,5-b]pyridine. *The Journal of Physical Chemistry B* **2013**, *117*, 9469-9477.

3) Mishra, A.; **Sahu, S.**; Tripathi, S.; Krishnamoorthy, G., Photoinduced Intramolecular Charge Transfer in *trans*-2-[4′-(N,N-Dimethylamino)styryl]imidazo[4,5-b]pyridine: Effect of Introducing a C=C Double Bond. *Photochemical & Photobiological Sciences* **2014**, *13*, 1476-1486.

4) Shankar, B.; **Sahu, S.**; Deibel, N.; Schweinfurth, D.; Sarkar, B.; Elumalai, P.; Gupta, D.; Hussain, F.; Krishnamoorthy, G.; Sathiyendiran, M., Luminescent Dirhenium(I)-Double-Heterostranded Helicate and Mesocate. *Inorganic Chemistry* **2014**, *53*, 922-930.

5) **Sahu, S.**; Sil, T. B.; Das, M.; Krishnamoorthy, G., A Single Fluorophore to Address Multiple Logic Gates. *Analyst* **2015**, *140*, 6114-6123. ‡

6) **Sahu, S.**; Das, M.; Krishnamoorthy, G., Switching between *Cis*- and *Trans*- Anions of 2-(2′-Hydroxyphenyl)benzimidazole: A Molecular Rotation Perturbed by Chemical Stabilization. *Physical Chemistry Chemical Physics* **2016**, *18*, 11081-11090. ‡

7) **Sahu, S.**; Dutta, S.; Krishnamooorthy, G., An Unusual Deprotonation Trend in 2-(2′-Hydroxyphenyl)pyrido imidazoles. (Manuscript submitted) ‡

8) **Sahu, S.**; Ila, V.; Shankar, B.; M. Satiydren; Krishnamooorthy, G., Molecular Aggregation to Regulate the Conformational Equilibrium of a Triple Emissive ESIPT molecule. (Manuscript submitted) ‡

9) **Sahu, S.**; Das, M.; Krishnamooorthy, G., Excited State Intramolecular Proton Transfer Induced Proton Transfer: Two Consecutive Self-assisted Intramolecular Proton Transfer. (Manuscript under preparation) ‡

10) **Sahu, S.**; Das, M.; Shankar, B.; M. Satiydren; Krishnamooorthy, G., Solvent Dependent Photochemical Reaction of 1,4-bis(2-(2-Hydroxyphenyl)benzimidazol-1-ylmethyl)-benzene. (Manuscript under preparation) ‡

## Conferences and Proceedings

- Effects of β-Cyclodextrin on Dual Fluorescence of 2-(2'-Hydroxyphenyl)-3H-imidazo[4,5-b]pyridine and 2-(2'-Hydroxyphenyl)-3H-imidazo[4,5-c]pyridine. Saugata Sahu, Francis A. S. Chipem, and G. Krishnamoorthy , Conference on Photochemistry and Luminescence, Guwahati (Assam), March 2012. ‡
- Effective Controlling of Metal ion Binding Site by Surfactant. Saugata Sahu, Anasuya Mishra, G. Krishnamoorthy, International Conference on Emerging Trends in Chemical Science, Vellore (Tamil Nadu), December 2013.
- Inhibition of Excited State Intra molecular Proton Transfer to Detect Different Anions. Saugata Sahu, Sanjay Dutta, G. Krishnamoorty, Chemcon, Guwahati (Assam), April, 2014.
- Fluorescence Based Molecular Keypad Lock Device, Half Subtractor and Anion Sensor. Saugata Sahu, Timiar Baran Sil, Minati Das, G. Krishnamoorthy, Asian Photochemistry Conference (APC 2014), Trivandrum (Kerala), November 2014.
- Subtraction Using Molecular Logic Gate, Saugata Sahu, G. Krishnamoorthy, Research Conclave, Guwahati (Assam), March, 2015.

‡ part of the present thesis.